Observability
of Anomalous Couplings
# of Electroweak Vector-Bosons
at the LHC
and
Improved Formulation of an
Effective Vector-Boson Approximation

Dissertation
von
Ingolf Kuss
aus Osnabrück

vorgelegt der
Fakultät für Physik der Universität Bielefeld
zur Erlangung des
naturwissenschaftlichen Doktorgrades

June 1996

Observability
of Anomalous Couplings
# of Electroweak Vector-Bosons
at the LHC
and
Improved Formulation of an
Effective Vector-Boson Approximation

Dissertation
von
Ingolf Kuss
aus Osnabrück

vorgelegt der
Fakultät für Physik der Universität Bielefeld
zur Erlangung des
naturwissenschaftlichen Doktorgrades

June 1996

Tag der Disputation: 1.7.1996

Mitglieder des Prüfungsausschusses:
Prof. Dr. D. Schildknecht (1. Gutachter)
Priv.-Doz. Dr. H. Spiesberger (2. Gutachter)
Priv.-Doz. Dr. D. Feldmann
Prof. Dr. O. Steinmann (Vorsitzender)

Contents

Danksagung

Ich danke Herrn Prof. Dr. D. Schildknecht und Herrn Priv.-Doz. Dr. H. Spiesberger für ihr stetiges Interesse am Fortkommen meiner Arbeit und für zahlreiche Diskussionen und Anregungen. Ohne die stetige Förderung von Herrn Prof. Schildknecht wäre das zügige Voranschreiten meiner Arbeit nicht möglich gewesen. Herrn Dr. Spiesberger danke ich besonders für die fortdauernde Betreuung meiner Arbeit auch über größere Entfernungen hinweg.

Außerdem danke ich den Mitgliedern der elektroschwachen Arbeitsgruppe, besonders den Drs. S. Dittmaier, C. Grosse-Knetter, Herrn Prof. Dr. R. Kögerler und G. Weiglein, für freundliche Unterstützung, Zusammenarbeit und Anregungen. S. Dittmaier danke ich für zahlreiche Diskussionen und für Unterstützung und Anregungen bei der Erstellung des Manuskriptes dieser Arbeit.

Diese Arbeit wurde zum Teil von der Landesgraduiertenförderung des Landes Nordrhein-Westfalen unterstützt.

Chapter 1

Introduction

This work is about the observable effects of the interactions of the electroweak vector-bosons among each other, which are expected to manifest themselves in experiments at the Large Hadron Collider (LHC) at the CERN.

The determination of the self-interactions of the electroweak vector-bosons is one of the important remaining experimental tasks in the verification of the predictions of the standard model of the electroweak interactions [1]. Definite values of the coupling constants for vector-boson self-interactions are predicted in the standard model. These values are the consequence of an assumed local gauge symmetry principle. This symmetry principle could also explain the origin of the masses of the vector-bosons and their coupling constants to the known fermions. The masses would occur as a consequence of a spontaneous breakdown of the symmetry caused by a non-zero vacuum-expectation value of a so far undiscovered particle, the scalar Higgs boson [2].

The standard model has so far stood all experimental tests and its predictions have been succesively verified. The weak vector-bosons, the mediators of the weak force, have been discovered by the CERN UA2 and UA1 collaborations [3, 4] in 1983. Since then, many experiments have been carried out in order to further test the theory. Particularly remarkable were the recent precision measurements of the LEP 1 collaborations at CERN and the SLD collaboration at SLAC (recent reviews are [5, 6]). With these measurements, the theory was tested at the level of radiative corrections and some parameters of the theory were determined with an unprecedented accuracy. The predictions of the standard model concerning the couplings of the vector-bosons to fermions were confirmed. Recently, evidence for the existence of a sixth quark, the top quark, which is predicted by the theory, has been reported by the CDF collaboration at FNAL [7].

Largely untested so far remained the self-couplings of the electroweak vector-bosons. Also, there is so far no experimental evidence for the existence of a Higgs particle. Recently, first direct experimental limits on the magnitudes of vector-boson self-couplings were obtained [8, 9]. These limits are in agreement with the standard predictions, but a more precise determination of the couplings is necessary in order to draw firm conclusions. In the near future, an inprovement of the limits can be obtained from measurements of the LEP 2 experiment at the CERN [10, 11]. A still more precise determination could come from measurements of vector-boson–pair production in the CERN LHC-experiment [12] of colliding protons. In this work we investigate to what extent possible deviations from the standard model can be ruled out in future measurements, assuming that the measurements will be actually in agreement with the standard model predictions.

We will first have to discuss how to parametrize anomalous (= non–standard-model)

vector-boson self-interactions with minimal model-assumptions. The parametrization of vector-boson self-interactions has been the subject of a number of publications. Let us consider for the moment only the interactions of *three* vector-bosons with each other (trilinear interactions). Let us restrict ourselves to interactions which do not violate the charge-conjugation-symmetry (C) or the parity-symmetry (P). There are two different interactions (vertices), which exist already in the standard model, namely the vertex of a photon (γ) with two charged vector-bosons (W^+ und W^-) and the vertex of a Z-boson with two charged vector-bosons. For each of these vertices there are three different interaction-terms, which are invariant under transformations of the Lorentz group. Two of these terms are already present in the standard model. In the $\gamma W^+ W^-$-vertex, the coefficient of one of these terms is determined by the requirement of electromagnetic gauge invariance. Symmetry considerations lead to the omission of two further free parameters (cf. Chapter 2). With a minimal set of theoretical assumptions, the trilinear interactions can therefore be described by *three* free parameters (to be called anomalous couplings in the following). The couplings can be chosen as coefficients of gauge-invariant terms of mass-dimension six and will be called ϵ_W, $\epsilon_{W\Phi}$ and $\epsilon_{B\Phi}$ here.

Concerning the phenomenology of anomalous vector-boson self-couplings, it was noted that anomalous couplings would manifest themselves in hadron-hadron collisions at large scattering energies. The manifestation would be a modified production rate for pairs of electroweak vector-bosons. This signature will be especially manifest for large invariant masses of those pairs or for large transverse momenta of the produced vector-bosons. Of the possible types of vector-boson pairs with at least one massive vector-boson, $W^+ W^-$, $W^\pm Z$, $W^\pm \gamma$, ZZ and $Z\gamma$, not all pairs are equally relevant for the investigation of anomalous couplings. The production of ZZ- or $Z\gamma$-pairs, proceeding via the dominant $q\bar{q}'$-annihilation process, does not receive a contribution from vector-boson self-interactions. The production of these pairs will therefore not be considered here. The experimental analysis to identify $W^+ W^-$-pairs is problematic, because in the purely leptonic decay of this pair two (not detectable) neutrinos appear, while the hadronic decay modes must be seperated from QCD-background-processes [13] and top-quark-pair production-processes (with a subsequent decay of the top-quarks into a W-boson and a b-quark) [14]. Both background-processes have higher event rates than the signal from vector-boson pair-production, unless one applies sophisticated kinematical cuts. We will therefore not consider $W^+ W^-$-production here. In contrast, the analysis of produced $W^\pm Z$- and $W^\pm \gamma$-pairs will allow for an unbiased test of vector-boson self-interactions at the LHC [15]. With $W^\pm Z$-pairs, one tests the $ZW^+ W^-$-vertex, while through an analysis of $W^\pm \gamma$-pairs, the $\gamma W^+ W^-$-vertex is investigated. An analysis of the $\gamma W^+ W^-$ Vertex will give a bound on the sum $\epsilon_{W\Phi} + \epsilon_{B\Phi}$ and on the parameter ϵ_W, while an analysis of the $ZW^+ W^-$-vertex will allow one to derive bounds on all three anomalous couplings. In this work, we will investigate $W^\pm Z$-production in the process $pp \to WZX$, $W = W^+$ or W^-, at a scattering-energy of $\sqrt{s} = 14$ TeV. This is the scattering-energy for the planned LHC-experiment. Results of similar relevance could be obtained from an investigation of the process $pp \to W\gamma X$.

The production of vector-boson–pairs, $V_3 V_4$, in future multi-TeV proton-proton collisions (i.e. for LHC or SSC energies, $\sqrt{s_{pp}} > 10$ TeV) has been investigated by many authors. Cross-sections for $pp \to V_3 V_4 X$ in the standard model have already been given in [16, 17]. It was assumed that the $V_3 V_4$-pairs are produced in the quark-antiquark annihilation processes $q\bar{q}' \to V_3 V_4$. In analogy to the production-processes of lepton pairs,

$q\bar{q}' \to l^+l^-$, these processes have been called Drell-Yan processes in the recent literature. The Drell-Yan process is the one which receives contributions of lowest order, $\mathcal{O}(\alpha^2)$ in the cross-section, in an expansion in powers of the coupling-constant α. The influence of anomalous couplings on the cross-sections was investigated in the following and upper and lower values (sensitivity limits) for the anomalous couplings were derived, which would, in view of the expected experimental errors, still be consistent with a measurement which is in agreement with the standard predictions [18]-[24]. The initially made simplification, that only one parameter at a time is allowed to deviate from its standard value, was later improved. Sensitivity limits were derived, which made no assumption on the magnitudes of the respective other couplings. Further, $\mathcal{O}(\alpha_s)$ radiative corrections were calculated and included in the analysis of anomalous couplings [25]-[29].

Vector-boson pair production was also investigated in model-scenarios, in which longitudinally polarized $W^{\pm}$- and Z-bosons interact strongly [30]. In these models, another type of reaction for vector-boson–pair production had to be considered in addition to the Drell-Yan processes. In these processes, two quarks q_1 and q_2 (they might also be antiquarks) react with each other and produce two other quarks q_1' and q_2' as well as two vector-bosons V_3 and V_4, $q_1q_2 \to q_1'q_2'V_3V_4$. The cross-sections for these reactions are formally of higher order, $\mathcal{O}(\alpha^4)$, in an expansion in powers of the coupling constant. The calculation of these cross-sections was done at first in the framework of an effective vector-boson aproximation (EVBA) [31, 32, 33]. Such an approximation is based on the observation, that fermions of a high energy (here the quarks q_1 and q_2) can be considered as the source of vector-bosons (V_1 and V_2), which are radiated off in the forward direction. These vector-bosons then initiate a scattering process, in which e.g. a V_3V_4-pair is produced. The approximation is in close analogy to the effective photon approximation (EPA) (Weizsäcker-Williams-approximation) of QED [34].

The concept of the EPA is plausible, since the emission in the forward direction of an on-shell massless vector-boson from a fermion is kinematically enhanced if the mass of the fermion is very small against the energy of the fermion. High-energy fermions can therefore indeed be considered as a source of on-shell photons. In the EVBA, the cross-section for a process $q_1q_2 \to q_1'q_2'V_3V_4$ can be determined from the cross-sections for vector-boson scattering into V_3V_4 and emission probabilities of vector-bosons from fermions. The emission probabilities of a *pair* of vector-bosons from a pair of fermions, as it is the case here, have been called *luminosities*, $\mathcal{L}_{V_1V_2}^{q_1q_2}$. The step from the photon approximation to the vector-boson approximation consists of the additional requirement that also the vector-boson masses have to be very small against the fermion-fermion scattering energy.

Returning to the consideration of the processes $q_1q_2 \to q_1'q_2'V_3V_4$ in proton-proton collisions, we note that the vector-boson–vector-boson scattering processes $V_1V_2 \to V_3V_4$ appear as a subprocess to the subprocess. The vector-boson scattering processes can have very large cross-sections in a strongly-interacting scenario and therefore had to be taken into account. Corresponding investigations have been made in [35, 36, 37, 38]. The application of the EVBA to the WZ-production process $q_1q_2 \to q_1'q_2'WZ$ was at first restricted [35] to the calculation of the *difference* of a cross-section in which a heavy Higgs particle $M_H \simeq 1$ TeV is assumed and a cross-section in which a light Higgs-particle $M_H \simeq 100$ GeV is assumed (This difference shows an interesting behavior in a strongly-interacting scenario and was therefore considered as a signal for strongly interacting vector-bosons.). Only scattering-processes with longitudinally polarized vector-bosons contribute to this

quantity. This is because the dependence of polarized cross-sections on the mass of the Higgs particle is small for cross-sections with at least one transversely polarized particle. In contrast, the dependence is very large if all external particles are in the longitudinal polarization state. Thus, the EVBA was only applied to longitudinally polarized vector-bosons. In [36] the application of the EVBA was extended to the entire cross-section. Thus, the contributions from all polarization states of the intermediate vector-bosons were calculated within the EVBA. Following this calculation, the rate of WZ-production in pp-collisions at the LHC through the processes $q_1q_2 \rightarrow q'_1q'_2WZ$ would amount to about **57%** of the rate from the Drell-Yan processes[1]. A complete perturbative calculation to lowest order $(\mathcal{O}(\alpha^4))$ [37], however, led to a different result, namely that the rate via the $q_1q_2 \rightarrow q'_1q'_2WZ$ production processes is only **17%** of the Drell-Yan rate[2]. The discrepancy between the two calculations thus amounts to a factor of 3. We will see that this discrepancy can be traced back to deficiencies in the conventional formulation of the EVBA. The discrepancy almost disappears if one uses an improved verison of the EVBA. This version will be introduced here. It will become manifest that the conventional version is based on an approximation which overestimates the contribution from *transversely* polarized intermediate vector-bosons.

The EVBA in its conventional form was also applied in investigations about the observability of anomalous couplings. In the framework of chiral perturbation theory, anomalous couplings were investigated in [39]. This theory amounts to the introduction of anomalous couplings in the strongly-interacting scenario.

A simultaneous investigation of Drell-Yan production and of the $q_1q_2 \rightarrow q'_1q'_2V_3V_4$-processes for an $SU(2)_L \times U(1)$-invariant dimension-6 extension of the standard model, as we consider it here, has been made in [40, 41]. The effects of the coupling ϵ_W have been discussed there. The calculations were based on the conventional EVBA, however. Since the authors of [40, 41] were mainly interested in the investigation of ratios of cross-sections for the production processes of different vector-boson pairs, this treatment does not necessarily lead to inconclusive results. Concerning the ratio of $q_1q_2 \rightarrow q'_1q'_2WZ$-processes to Drell-Yan processes, however, the treatment of [40, 41] again leads to a value which is similarly large as the one of [36], namely **52%**[3]. This large value is again not in agreement with the result of the exact calculation in [37].

Concerning the $V_1V_2 \rightarrow WZ$ processes, it is known that the ratios are considerably affected by the presence of anomalous couplings. Similarly, the Drell-Yan rate is also affected. An investigation remaining to be done therefore concerns a more quantitative

---

[1]The calculation [36] was for pp-collisions at $\sqrt{s} = 16$ TeV and the cross-section for the production of WZ-pairs with invariant masses in the interval 0.5 TeV $< M_{WZ} <$ 10 TeV was computed. Cuts were applied to the rapidities y and the transvere momenta p_T of both produced bosons, $|y| < 1.5$ and $p_T > 10$ GeV.

[2]In the calculation [37], the cross-section for W^+Z-production at $\sqrt{s} = 16$ TeV was calculated. The cross-section was integrated for transverse masses $M_T > 0.5$ TeV of the W^+Z pair. Differents cuts than in [36] were applied, namely a rapidity-cut on the decay-products of the vector-bosons, $|y(l)| < 2.5$, and cuts to remove small transverse momenta of the decay products. The exact choice of the cuts, however, does not very much affect the ratio of the rates. As an example I note that the calculation of [36] was also carried out for the case $|y| < 2.5$. Although the Drell-Yan rate increases by a factor of 5.9 with this choice of the cut, the *ratio* of the rates does only change from 57% to 64%.

[3]In [41], the cross-section for W^+Z-production in pp-collisions at $\sqrt{s} = 14$ TeV has been calculated. A rapidity-cut of $Y = 2$ was applied to the produced vector-bosons. The ratio of the rates was not explicitly computed. I have repeated the calculation of [41] and have established agreement with the results of [41]. After that, I carried out the same calculation for WZ-production and used a cut of $\eta = 1.5$. I find that the ratio of the rates is 52% if the cross-section is integrated over the region 0.5 TeV $< M_{WZ} <$ 2 TeV.

comparison of the rates of the $V_1 V_2 \to WZ$-processes and the $q\bar{q}' \to WZ$-processes, including the presence of anomalous couplings. Such an investigation will be carried out here. A necessary ingredient of the investigation is a more precise determination of the rate of the $q_1 q_2 \to q'_1 q'_2 WZ$-processes.

Exposition

This work is organized as follows: In Chapter 2 the parametrization of self-interactions of electroweak vector-bosons is introduced. Chapter 3 contains a discussion of the different mechanisms, by which a vector-boson pair can be produced in hadron-hadron collisions. In Chapter 4 the improved formulation of the effective vector-boson approximation is derived. Also, existing formulations of the method are discussed and compared to the improved treatment. The formalism of the improved EVBA for hadron-hadron collisions is introduced in Chapter 5. Comparisons with exact calculations for $pp \to ZZX$ are presented. In Chapter 6, the cross-sections for the process $pp \to WZX$ and for its sub-processes are discussed. Chapter 7 contains the analysis of anomalous couplings in $pp \to WZX$ at the LHC. Confidence intervals for anomalous couplings are derived and compared to the current experimental limits. Appendix A contains details of the derivation presented in Chapter 4. Approximate analytical formulae for vector-boson scattering cross-sections can be found in Appendix B.

Chapter 2

Parametrization of Vector-Boson Self-Interactions

Vector-boson self-interactions have been parametrized by a number of authors [19],[42]-[52]. The parametrizations differ concerning the theoretical assumptions which have been made. We will follow the treatments of [52].

2.1 Self-Interactions in the Standard Model

We briefly review the bosonic part of the standard model and fix the notation to be used. The part of the Lagrangian of the standard model, which describes the propagation of the free vector-bosons $W^{\pm}, Z, \gamma$, the free (postulated) scalar boson H (Higgs boson) and the triplet of the scalar fields $\phi_i, i = 1, 2, 3$ (Goldstone fields), as well as the interactions of these particles among each other, is given by the expression,

$$\mathcal{L}_{\text{SM,bosonic}} = \mathcal{L}_{WW} + \mathcal{L}_{BB} + \mathcal{L}_{\Phi\Phi}, \tag{2.1}$$

with

$$\begin{aligned} \mathcal{L}_{WW} &= -\frac{1}{2}\text{tr}[W^{\mu\nu}W_{\mu\nu}], \\ \mathcal{L}_{BB} &= -\frac{1}{2}\text{tr}[B^{\mu\nu}B_{\mu\nu}], \\ \mathcal{L}_{\Phi\Phi} &= \frac{1}{2}\text{tr}\left[(D^{\mu}\Phi)^{\dagger}(D_{\mu}\Phi)\right] - \frac{\mu^2}{2}\text{tr}[\Phi^{\dagger}\Phi] - \frac{1}{4}\lambda\left(\text{tr}[\Phi^{\dagger}\Phi]\right)^2. \end{aligned} \tag{2.2}$$

In (2.2),

$$\begin{aligned} W^{\mu\nu} &= \partial^{\mu}W^{\nu} - \partial^{\nu}W^{\mu} + i\,g\,[W^{\mu}, W^{\nu}], \\ B^{\mu\nu} &= \partial^{\mu}B^{\nu} - \partial^{\nu}B^{\mu}, \end{aligned} \tag{2.3}$$

are the field strength tensors for the vector-bosons (written in matrix form) and the expression

$$\Phi = \frac{1}{\sqrt{2}}\left((v + H)\mathbf{1} + i\phi_i\tau_i\right) \tag{2.4}$$

contains the scalar fields. The expression

$$D^{\mu}\Phi = \partial^{\mu}\Phi + i\,g\,W^{\mu}\Phi - i\,g'\Phi B^{\mu} \tag{2.5}$$

9

is the covariant derivative for these fields. The fields W_i^μ, $i = 1, 2, 3$, represent the gauge fields of the weak isospin and are described by the matrix $W^\mu = W_i^\mu \tau_i / 2$. The matrix $B^\mu = B_0^\mu \tau_3 / 2$ contains the field B_0^μ, which is the gauge field of the weak hypercharge Y. Further, g is the coupling constant for the fields of the weak isospin and g' is the coupling constant for the field of the weak hypercharge. The quantities μ and λ are constants, which describe the masses and the self-interactions of the scalar fields. It is assumed that μ^2 is less than zero, so that the Higgs boson acquires a non-zero vacuum-expectation value

$$v = \sqrt{\frac{-\mu^2}{\lambda}}. \tag{2.6}$$

The gauge-bosons acquire their masses as a result of this non-zero value. I point out that the Goldstone fields are unphysical states, i.e., they do not appear in external states, but only as virtual quanta. In the unitary gauge, they disappear completely. The symbols $\tau_i, i = 1, 2, 3$ denote the Pauli matrices, $\mathbf{1}$ is the unity matrix in two dimensions, and i is the imaginary unit. The Lagrangian (2.2) does not change its form under local transformations belonging to the combined group of the weak isospin and the weak hypercharge, $SU(2)_{WI} \times U(1)_Y$. Under such a transformation, the fields transform according to

$$W^\mu \rightarrow S W^\mu S^\dagger - \frac{i}{g} S \partial^\mu S^\dagger, \tag{2.7}$$

with

$$S = \exp\left(i g \alpha_i \frac{\tau_i}{2}\right), \quad \alpha_i = \alpha_i(x), \ i = 1, 2, 3, \tag{2.8}$$

and

$$B^\mu \rightarrow B^\mu - \partial^\mu \beta \frac{\tau_3}{2}, \quad \beta = \beta(x), \tag{2.9}$$

where $\alpha_i, i = 1, 2, 3$, are the parameters of the $SU(2)_{WI}$ gauge transformation and β is the parameter of the $U(1)_Y$ gauge transformation. Under the symmetry transformations (2.7) the field strength tensors transform according to

$$\begin{aligned} W^{\mu\nu} &\rightarrow S W^{\mu\nu} S^\dagger, \\ B^{\mu\nu} &\rightarrow B^{\mu\nu}, \end{aligned} \tag{2.10}$$

and the scalar fields according to

$$\begin{aligned} \Phi &\rightarrow S \Phi \sigma, \quad \sigma = \exp\left(-i g' \beta \frac{\tau_3}{2}\right), \\ D^\mu \Phi &\rightarrow S (D^\mu \Phi) \sigma. \end{aligned} \tag{2.11}$$

In the unitary gauge, in which the Goldstone fields disappear, $\phi_i = 0$, and by resolving the matrix notation, the first and the third term in (2.2) take on the forms

$$\mathcal{L}_{WW} = -\frac{1}{4} \left[(\vec{W}^{\mu\nu})_A \cdot (\vec{W}_{\mu\nu})_A - 2\,g(\vec{W}^{\mu\nu})_A \cdot \left(\vec{W}_\mu \times \vec{W}_\nu\right) + g^2 \left(\vec{W}^\mu \times \vec{W}^\nu\right)^2 \right], \tag{2.12}$$

and

$$\begin{aligned} \mathcal{L}_{\Phi\Phi} &= \frac{1}{2} \partial^\mu H \partial_\mu H - \frac{M_H^2}{2} H^2 + \frac{1}{4} g^2 (v + H)^2 W^{+\mu} W_\mu^- \\ &\quad + \frac{1}{8} (v + H)^2 (W_3^\mu, B_0^\mu) \begin{pmatrix} g^2 & -gg' \\ -gg' & g'^2 \end{pmatrix} \begin{pmatrix} W_\mu^3 \\ (B_0)_\mu \end{pmatrix} \\ &\quad - g \frac{M_H^2}{4\,M_W} H^3 - g^2 \frac{M_H^2}{32\,M_W^2} H^4 + \frac{2\,M_H^2 M_W^2}{g^2}. \end{aligned} \tag{2.13}$$

In (2.13), $\vec{W}$ is the vector composed of the fields $W_i, i = 1, 2, 3$, and $(\vec{W}^{\mu\nu})_A$ is the Abelian part of the vector of field strength tensors, $\vec{W}^{\mu\nu}$. The Abelian and non-Abelian field strength tensors are related through

$$\vec{W}^{\mu\nu} = (\vec{W}^{\mu\nu})_A - g\,\vec{W}^{\mu} \times \vec{W}^{\nu}. \qquad (2.14)$$

The connection to the matrix-valued field strength tensors is given by the relation $W^{\mu\nu} = W_i^{\mu\nu}\tau_i/2$. The quantity $M_W = g\,v/2$ is the mass of the charged vector-bosons $W^{\pm\mu}$, which are defined by

$$W^{\pm\mu} \equiv \frac{1}{\sqrt{2}}\left(W_1^{\mu} \mp i\,W_2^{\mu}\right), \qquad (2.15)$$

and $M_H = \sqrt{2\lambda v}$ is the mass of the Higgs boson. The first two terms in (2.13) describe the free Higgs field, the following two terms the masses of the electroweak vector-bosons as well as interactions of the vector-bosons with the Higgs boson, the fifth and the sixth terms describe self-interactions of Higgs bosons and the last term is a physically meaningless constant.

The removal of the non-diagonal mass-terms in (2.13) is achieved by the transition to the physical, neutral vector-boson fields A^{μ} (the photon) and Z^{μ}, which are linear combinations of B_0^{μ} and W_3^{μ},

$$\begin{aligned} A^{\mu} &\equiv c_W B_0^{\mu} + s_W W_3^{\mu}, \\ Z^{\mu} &\equiv -s_W B_0^{\mu} + c_W W_3^{\mu}. \end{aligned} \qquad (2.16)$$

In these relations, $s_W \equiv e/g$ and $c_W \equiv e/g'$ are the sine and the cosine of the weak mixing angle (Weinberg angle). They are related to each other by $s_W^2 + c_W^2 = 1$. The quantity $e > 0$ is the unit of charge. We also note that $c_W = M_W/M_Z$.

The self-interactions of the vector-bosons are contained in the term $\mathcal{L}_{WW}$, (2.12), and the trilinear interactions containd therein are given by

$$\begin{aligned} \mathcal{L}_{3\text{VB,SM}} &= \frac{1}{2}\,g\,(\vec{W}^{\mu\nu})_A \cdot \left(\vec{W}_{\mu} \times \vec{W}_{\nu}\right) \\ &= -ie\left[A_{\mu}((W^{-\mu\nu})_A W_{\nu}^{+} - (W^{+\mu\nu})_A W_{\nu}^{-}) + (F^{\mu\nu})_A W_{\mu}^{+} W_{\nu}^{-}\right] \\ &\quad -ie\frac{c_W}{s_W}\left[Z_{\mu}((W^{-\mu\nu})_A W_{\nu}^{+} - (W^{+\mu\nu})_A W_{\nu}^{-}) + (Z^{\mu\nu})_A W_{\mu}^{+} W_{\nu}^{-}\right]. \quad (2.17) \end{aligned}$$

The quantities

$$\begin{aligned} (W^{\pm\mu\nu})_A &= \partial^{\mu} W^{\pm\nu} - \partial^{\nu} W^{\pm\mu}, \\ (Z^{\mu\nu})_A &= \partial^{\mu} Z^{\nu} - \partial^{\nu} Z^{\mu}, \\ (F^{\mu\nu})_A &= \partial^{\mu} A^{\nu} - \partial^{\nu} A^{\mu}, \end{aligned} \qquad (2.18)$$

in (2.17) are the Abelian field strength tensors for the physical fields. Concerning trilinear interactions, the standard model thus contains a $\gamma W^+ W^-$ and a $Z W^+ W^-$ interaction, given by (2.17).

2.2 Parametrization of Anomalous Self-Interactions

Anomalous vector-boson self-interactions can be represented as additional terms to the Lagrangian of the standard model. To parametrize such terms, we consider the general

form of a Lorentz-, C- and P- invariant interaction without higher derivatives[1] between a neutral vector-boson V and the charged vector-bosons $W^\pm$. This interaction can be expressed with the help of three free parameters, g_V, κ_V and y_V, [42],

$$
\begin{aligned}
\mathcal{L}_{VWW} &= -ie\, g_V \left[V_\mu ((W^{-\mu\nu})_A W_\nu^+ - (W^{+\mu\nu})_A W_\nu^-) + \kappa_V\, (V^{\mu\nu})_A W_\mu^+ W_\nu^- \right] \\
&\quad + ie\frac{y_V}{M_W^2}(V_\mu{}^\nu)_A (W_\nu^{-\lambda})_A (W_\lambda^{+\mu})_A.
\end{aligned} \tag{2.19}
$$

The general VW^+W^--vertices (2.19) for the vector-bosons $V = \gamma$ or $V = Z$ contain the interaction-terms of mass-dimension-6 (2.17) of the standard model, however with arbitrary coupling constants g_V and κ_V. In addition, they contain a dimension-6 interaction with the coupling strength y_V. The parametrization (2.19), applied to γW^+W^-- and ZW^+W^--interactions, thus contains the six free parameters $g_\gamma, \kappa_\gamma, y_\gamma, g_Z, \kappa_Z$ and y_Z. The coupling g_γ must not deviate from its standard value $g_\gamma = 1$. This follows from the demand of electromagnetic gauge invariance. To see this we note that the kinetic term for the charged vector-bosons contained in (2.12) ,

$$
-\frac{1}{4}\sum_{i=1,2}(W_i^{\mu\nu})_A (W_{\mu\nu}^i)_A = -\frac{1}{2}(W^{+\mu\nu})_A (W_{\mu\nu}^-)_A \tag{2.20}
$$

is not gauge invariant by itself. Only the sum

$$
\begin{aligned}
&-\frac{1}{2}(W^{+\mu\nu})_A (W_{\mu\nu}^-)_A - ie\, A_\mu ((W^{-\mu\nu})_A W_\nu^+ - (W^{+\mu\nu})_A W_\nu^-) \\
&-e^2[A^\mu A_\mu W^{+\nu} W_\nu^- - A^\mu A^\nu W_\mu^+ W_\nu^-]
\end{aligned} \tag{2.21}
$$

exhibits this symmetry.

Another parametrization, equivalent to the one of (2.19), has been given in [47]. The parameters introduced in this reference will be denoted here by $g_1^Z, \kappa^\gamma, \kappa^Z, \lambda^\gamma$ and λ^Z. They are related to the parameters of (2.19) by

$$
\begin{aligned}
g_1^Z &\equiv \frac{s_W}{c_W}g_Z, \\
\kappa^\gamma &\equiv \kappa_\gamma, \\
\kappa^Z &\equiv \frac{s_W}{c_W}g_Z\kappa_Z, \\
\lambda^\gamma &\equiv y_\gamma, \\
\lambda^Z &\equiv \frac{s_W}{c_W}y_Z.
\end{aligned} \tag{2.22}
$$

To clarify the discussion to follow, we elaborate on electromagnetic gauge transformations. These transformations are a special case of the $SU(2)_{WI} \times U(1)_Y$-transformations (2.7), defined through the following choice of the parameters: $\alpha_1 = \alpha_2 = 0, \alpha_3 = \frac{e}{g}\chi, \beta = \frac{e}{g'}\chi$. Under electromagnetic gauge transformations, the physical fields transform according

---

[1]Terms with a second or even higher derivative with respect to the space-time coordinates on the fields are not considered. These terms imply higher divergences in loop-graphs and are therefore theoretically and phenomenologically disfavored. In addition, these terms can be eliminated in the context of an effective Lagrangian theory with the help of the equations of motion [53] if one assumes that the anomalous couplings are small.

to

$$
\begin{aligned}
W^{\pm\mu} &\rightarrow \exp(\pm ie\chi)W^{\pm\mu} \\
W^{\pm\mu\nu} &\rightarrow \exp(\pm ie\chi)W^{\pm\mu\nu} \\
Z^{\mu} &\rightarrow Z^{\mu} \\
Z^{\mu\nu} &\rightarrow Z^{\mu\nu} \\
(Z^{\mu\nu})_A &\rightarrow (Z^{\mu\nu})_A \\
A^{\mu} &\rightarrow A^{\mu} - \partial^{\mu}\chi \\
F^{\mu\nu} &\rightarrow F^{\mu\nu} \\
(F^{\mu\nu})_A &\rightarrow (F^{\mu\nu})_A,
\end{aligned}
\tag{2.23}
$$

where $\chi = \chi(x)$ is the parameter of the electromagnetic gauge transformation. In (2.23),

$$
\begin{aligned}
W^{\pm\mu\nu} &= \frac{1}{\sqrt{2}}(W_1^{\mu\nu} \mp iW_2^{\mu\nu}) = (W^{\pm\mu\nu})_A \pm ig(W_3^{\mu}W^{\pm\nu} - W_3^{\nu}W^{\pm\mu}), \\
Z^{\mu\nu} &= -s_W B_0^{\mu\nu} + c_W W_3^{\mu\nu} = (Z^{\mu\nu})_A + ie\frac{c_W}{s_W}(W^{+\mu}W^{-\nu} - W^{-\mu}W^{+\nu}), \\
F^{\mu\nu} &= c_W B_0^{\mu\nu} + s_W W_3^{\mu\nu} = (F^{\mu\nu})_A + ie(W^{+\mu}W^{-\nu} - W^{-\mu}W^{+\nu}),
\end{aligned}
\tag{2.24}
$$

are the non-Abelian field strength tensors. In (2.24), $B_0^{\mu\nu} = \partial^{\mu}B_0^{\nu} - \partial^{\nu}B_0^{\mu}$.

The difference of the general Lagrangian, obtained from the parametrizations (2.19) with the restriction $g_{\gamma} = 1$, and the standard Lagrangian, (2.17), is given by the expression

$$
\begin{aligned}
\mathcal{L}_{\text{3VB,anom}} =\ & -ie\,x_{\gamma}(F^{\mu\nu})_A W_{\mu}^{+}W_{\nu}^{-} - ie\,x_Z(Z^{\mu\nu})_A W_{\mu}^{+}W_{\nu}^{-} \\
& -ie\delta_Z\left[Z_{\mu}((W^{-\mu\nu})_A W_{\nu}^{+} - (W^{+\mu\nu})_A W_{\nu}^{-}) + (Z^{\mu\nu})_A W_{\mu}^{+}W_{\nu}^{-}\right] \\
& +ie\frac{y_{\gamma}}{M_W^2}(F_{\mu}{}^{\nu})_A(W_{\nu}^{-\lambda})_A(W_{\lambda}^{+\mu})_A \\
& +ie\frac{y_Z}{M_W^2}(Z_{\mu}{}^{\nu})_A(W_{\nu}^{-\lambda})_A(W_{\lambda}^{+\mu})_A.
\end{aligned}
\tag{2.25}
$$

The Lagrangian (2.25) contains five free parameters,

$$
\begin{aligned}
x_{\gamma} &\equiv \kappa_{\gamma} - 1, \\
x_Z &\equiv g_Z(\kappa_Z - 1), \\
\delta_Z &\equiv g_Z - \frac{c_W}{s_W},
\end{aligned}
\tag{2.26}
$$

as well as y_{γ} und y_Z, which each take on the value zero in the standard model. Alternatively, small deviations from the standard values of the couplings in (2.22) have been defined [20] by

$$
\begin{aligned}
\Delta g_1^Z &\equiv g_1^Z - 1 = \frac{s_W}{c_W}\delta_Z, \\
\Delta\kappa^{\gamma} &\equiv \kappa^{\gamma} - 1 = x_{\gamma}, \\
\Delta\kappa^Z &\equiv \kappa^Z - 1 = \frac{s_W}{c_W}(x_Z + \delta_Z), \\
\lambda^{\gamma} &= y_{\gamma}, \\
\lambda^Z &= \frac{s_W}{c_W}y_Z,
\end{aligned}
\tag{2.27}
$$

where also the relations to the parameters of (2.25) have been given in (2.27).

We modify the Lagrangian (2.25) by using the non-Abelian field strength tensors $W^{\pm\mu\nu}$ instead of the Abelian ones, $(W^{\pm\mu\nu})_A$. This brings (2.25) into a manifestly electromagnetically gauge invariant form. If one also uses the non-Abelian forms $F^{\mu\nu}$ and $Z^{\mu\nu}$ instead of the Abelian forms, one obtains from (2.25), after a transformation back to the W_3B-basis, the Lagrangian

$$
\begin{aligned}
\mathcal{L}_{\text{int,anom}} = \ & -2c_1\frac{i}{4}\left[\vec{W}^{\mu\nu}\cdot\left(\vec{W}_\mu\times\vec{W}_\nu\right)+2i\frac{s_W}{c_W}(B_0)_\mu(W^{-\mu\nu}W_\nu^+ - W^{+\mu\nu}W_\nu^-)\right] \\
& +c_2 B_0^{\mu\nu}W_\mu^+ W_\nu^- \\
& +c_3 W_3^{\mu\nu}W_\mu^+ W_\nu^- \\
& -\frac{3}{2}\frac{c_4}{M_W^2}(W_3)_\mu{}^\nu W_\nu^{-\ \lambda}W^{+\mu}_{\ \lambda} \\
& -\frac{c_5}{M_W^2}(B_0)_\mu{}^\nu W_\nu^{-\lambda}W_\lambda^{+\mu},
\end{aligned}
\tag{2.28}
$$

with the coefficients

$$
\begin{aligned}
c_1 &= iec_W\delta_Z \\
c_2 &= -ie(c_W x_\gamma - s_W x_Z - s_W\delta_Z) \\
c_3 &= -ie(c_W x_Z + s_W x_\gamma) \\
c_4 &= -\frac{2}{3}ie(c_W y_Z + s_W y_\gamma) \\
c_5 &= ie(s_W y_Z - c_W y_\gamma).
\end{aligned}
\tag{2.29}
$$

The parameters in (2.29) are imaginary quantities. The Lagrangian (2.28) describes the trilinear interactions (2.25) and in addition self-interactions of four or more vector-bosons. These latter interactions have been introduced by the use of the non-Abelian field strength tensors. The terms described by c_1, c_2 and c_3 are of dimension-4, while the c_4 and c_5 terms are of dimension-6. In matrix notation the Lagrangian (2.28) takes on the form

$$
\begin{aligned}
\mathcal{L}_{\text{int,anom}} = \ & 2c_1\text{tr}\left[\left(W^\mu - \frac{g'}{g}B_\mu\right)W_{\mu\nu}\left(W^\nu - \frac{g'}{g}B^\nu\right)\right] \\
& + 2c_2\text{tr}[B^{\mu\nu}W_\mu W_\nu] \\
& + c_3\text{tr}[\tau_3 W^{\mu\nu}]\text{tr}[\tau_3 W_\mu W_\nu] \\
& + \frac{c_4}{M_W^2}\text{tr}[W_\mu{}^\nu W_\nu{}^\lambda W_\lambda{}^\mu] \\
& + 2\frac{c_5}{M_W^2}\text{tr}[B_\mu{}^\nu W_\nu{}^\lambda W_\lambda{}^\mu].
\end{aligned}
\tag{2.30}
$$

Symmetry arguments make the existence of some of the interactions in (2.30) appear less likely to be realized in nature than others. For the case $c_3 = 0$ there exists a global $SU(2)_{WI}$ weak isospin invariance which is only broken by the presence of the B^μ-field [19, 46]. The corresponding symmetry transformation is given by

$$
W^\mu \xrightarrow{SU(2)_{\text{global}}} SW^\mu S^\dagger,
\tag{2.31}
$$

with

$$
S = \exp\left(ig\omega_i\frac{\tau_i}{2}\right), \quad i = 1,2,3,
\tag{2.32}
$$

where the ω_i are parameters which are no functions of the space-time coordinates. Such a symmetry is being respected by all the known interactions. If one admits, in addition, only those of the dimension-6 terms, which respect the $SU(2)_{WI}$ invariance in an unbroken form, [45], one obtains the restriction $c_5 = 0$. Thus, $SU(2)_{WI}$ symmetry considerations lead to

$$c_3 = c_5 = 0. \tag{2.33}$$

We can bring the Lagrangian (2.30) into a gauge-invariant form by re-introducing the scalar fields. In a first step, the Goldstone fields are introduced into (2.30) in a non-linear form,

$$U = \exp\left(\frac{i}{v}\phi_i\tau_i\right), \tag{2.34}$$

by means of a Stueckelberg transformation [54],

$$
\begin{aligned}
W^\mu &\rightarrow U^\dagger W^\mu U - \frac{i}{g}U^\dagger\partial^\mu U, \\
B^\mu &\rightarrow B^\mu.
\end{aligned}
\tag{2.35}
$$

This transformation brings the Lagrangian (2.30) into an $SU(2)_{WI}\times U(1)_Y$ invariant form. In contrast to the $SU(2)_{WI}\times U(1)_Y$-symmetry of the standard model, this symmetry is realized in a non-linear way. The corresponding symmetry transformations are given by (2.7) and (2.10) for the vector-bosons and

$$U \rightarrow SU\sigma \tag{2.36}$$

for the scalar fields. The introduction of the Higgs boson into the anomalous interaction terms is achieved by the transformation [55]

$$U \rightarrow \frac{\sqrt{2}}{v}\Phi, \tag{2.37}$$

where Φ is the quantity defined in (2.4). The transformation (2.37) implies that instead of the complete polynomial of the exponential function in (2.34) only the constant term and the term *linear* in the Goldstone fields is kept. After the change of normalization from U to Φ, given by (2.37), the constant term of Φ becomes the vacuum-expectation-value of the Higgs field. To this term, the field of the physical Higgs particle, H, is added.

The application of the combined transformations (2.35) followed by (2.37) can be described in a single step by the transformation prescriptions

$$
\begin{aligned}
W^\mu - \frac{g'}{g}B^\mu &\rightarrow -i\frac{g}{2M_W^2}\Phi^\dagger(D^\mu\Phi) = i\frac{g}{2M_W^2}(D^\mu\Phi)^\dagger\Phi, \\
W^{\mu\nu} &\rightarrow \frac{g^2}{2M_W^2}\Phi^\dagger W^{\mu\nu}\Phi, \\
B^\mu &\rightarrow B^\mu, \\
B^{\mu\nu} &\rightarrow B^{\mu\nu}.
\end{aligned}
\tag{2.38}
$$

The transformation of W^μ was only given in the combination $W^\mu - g'/gB^\mu$ in (2.38). The reason for this is that the terms (2.30) de facto only contain this combination. To see this, we note that the c_2- and c_3-terms in (2.30) are invariant under the substitution

$W^\mu W^\nu \rightarrow (W^\mu - \frac{g'}{g}B^\mu)(W^\nu - \frac{g'}{g}B^\nu)$. The application of the transformation (2.38) to the Lagrangian (2.30) leads to the Lagrangian

$$\mathcal{L}_{\text{int,anom,gauge}} = -i\frac{c_1}{M_W^2}\mathcal{L}_{W\Phi} + i\frac{c_2}{M_W^2}\mathcal{L}_{B\Phi} - i\,g^2\frac{c_3}{M_W^4}\mathcal{L}'_{W\Phi}$$
$$+i\frac{3}{2}\frac{c_4}{M_W^2}\mathcal{L}_W + i\,g^2\frac{c_5}{2M_W^4}\mathcal{L}'_W, \qquad (2.39)$$

where the expressions

$$\begin{aligned}
\mathcal{L}_{W\Phi} &= i\text{tr}[(D^\mu\Phi)^\dagger W_{\mu\nu}(D^\nu\Phi)], \\
\mathcal{L}_{B\Phi} &= i\text{tr}[(D^\mu\Phi)B_{\mu\nu}(D^\nu\Phi)^\dagger], \\
\mathcal{L}'_{W\Phi} &= i\text{tr}[\frac{\tau_3}{2}(D^\mu\Phi)^\dagger(D^\nu\Phi)]\text{tr}[\frac{\tau_3}{2}\Phi^\dagger W_{\mu\nu}\Phi], \\
\mathcal{L}_W &= -\frac{2}{3}i\text{tr}[W_\mu{}^\nu W_\nu{}^\lambda W_\lambda{}^\mu], \\
\mathcal{L}'_W &= -2\,i\text{tr}[B_\mu{}^\nu\Phi^\dagger W_\nu{}^\lambda W_\lambda{}^\mu\Phi] \qquad\qquad (2.40)
\end{aligned}$$

are $SU(2)_L \times U(1)_Y$-invariant interaction terms. The Lagramgian (2.39) exhibits a local $SU(2)_{WI}\times U(1)_Y$ symmetry with a linearly realized scalar sector. The corresponding symmetry transformations are (2.7), (2.10) and (2.11). The interaction-terms (2.40) have been discussed by various authors in connection with anomalous vector-boson self-interactions [48, 49, 50, 51, 52].

The Lagrangian (2.39) contains the interactions of the Lagrangian (2.30) and, in addition, interactions of one or more Higgs bosons with the electroweak vector-bosons. Not for all terms in (2.40) the dimensions are the same as the dimensions of the corresponding terms in (2.30); the c_3- and c_5-terms in (2.40) are of dimension-8, while the c_1, c_2- and c_4-terms are of dimension-6.

In summary, the Lagrangian (2.39) is a general extension of the trilinear self-interactions of the standard model if one does not allow for C- or P-violating interactions.

2.3 Small Deviations from the Standard Model

One expects that the magnitudes of the coefficients c_3 and c_5 in (2.39) are small against the one of the coefficients c_1, c_2 and c_4 if one assumes the approximate validity of the standard model. This validity is assumed to be broken only through effects of virtual particles with masses which are very large compared to the masses of the known particles. We assume that the validity of the standard model is given below a certain energy scale, represented by the quantity Λ. An estimate about the magnitudes of the couplings follows from a general consideration about effective Lagrangians [44].

One assumes the validity of a self-consistent, in particular renormalizable, theory, T, below the scale Λ. The paramter Λ can be the scattering energy of a scattering process to be considered. Connected with the theory T is a certain symmetry group and the Lagrangian $\mathcal{L}_0$. Fields, which appear as free fields only above the energy Λ, can, due to their quantum nature, already lead to observable effects below the scale Λ. These effects can be described by interaction-terms $\mathcal{L}_j^{d_j}, j = 1, 2, \ldots$, which have to be added to the Lagrangian $\mathcal{L}_0$,

$$\mathcal{L}_{\text{eff}} = \mathcal{L}_0 + \sum_j \tilde{\alpha}_j \frac{\mathcal{L}_j^{d_j}}{M^{d_j-4}}. \qquad (2.41)$$

In (2.41), d_j is the dimension of the term $\mathcal{L}_j^{d_j}$, M is a mass scale which is typical for the theory T (e.g. the mass of one of the particles of the theory) and the quantities $\tilde{\alpha}_j$ are coefficients for the interaction-terms. We can estimate the order of magnitude of the coefficients if we refine our assumption about the approximate validity of T by demanding that the Lagrangian (2.41) reduces to the Lagrangian $\mathcal{L}_0$ in the limit $\Lambda \to \infty$. In this case it is possible to identify the effective Lagrangian (2.41) with an expansion of the effects of an underlying (unknown) Lagrangian with higher symmetries and additional particles. The expansion is carried out in powers of the parameter M/Λ. The Lagrangian (2.41) is thus of the general form

$$\mathcal{L}_{\text{eff}} = \mathcal{L}_0 + \sum_j \frac{\tilde{g}}{\Lambda} \mathcal{L}_j^{(5)} + \sum_j \frac{\tilde{g}}{\Lambda^2} \mathcal{L}_j^{(6)} + \ldots, \tag{2.42}$$

where $\tilde{g}$ is a coupling constant which is typical for the fields contained in $\mathcal{L}_j^{d_j}$ (for the standard model, $\tilde{g}$ can be g, g' or e). By comparison of (2.41) with (2.42) an order of magnitude estimate for the coefficients $\tilde{\alpha}_j$ can be given,

$$\tilde{\alpha}_j = \mathcal{O}\left[\tilde{g}\left(\frac{M}{\Lambda}\right)^{d_j-4}\right]. \tag{2.43}$$

Further, since the terms $\mathcal{L}_j^{d_j}$ are to contain only the particles of the theory T, we assume the same symmetry for these terms as for the Lagrangian $\mathcal{L}_0$.

Applying now this discussion to the standard model for vector-bosons and their interactions, taken as the model T, one can take for M the masses of the charged vector bosons[2], $M = M_W$. If the sum in (2.41) is identified with the Lagrangian (2.39), one concludes that the coupling strengths $g^2 c_3$ and $g^2 c_5$ in (2.39) are smaller by a factor of the order $\mathcal{O}(M_W^2/\Lambda^2)$ than the couplings c_1, c_2 und c_4 in (2.29)[3]. The couplings c_1, c_2 and c_4 are of the order of magnitude

$$c_1, c_2, c_4 = \mathcal{O}\left(\tilde{g}\frac{M_W^2}{\Lambda^2}\right). \tag{2.44}$$

If Λ is in the range $1 \text{ TeV} \leq \Lambda \leq 2 \text{ TeV}$, the suppression of c_3 and c_5 with respect to c_1, c_2 and c_4 is of the order of magnitude $\mathcal{O}(10^{-2})$. One should not forget that the above considerations assume the approximate validity of the standard model below a certain energy scale Λ. The assumption in turn requires that a Higgs boson with a mass $M_H < \Lambda$ exists.

The neglect of the c_3- and c_5-terms in (2.39) leads to the relations

$$\begin{aligned} x_\gamma &= -\frac{c_W}{s_W} x_Z \\ y_\gamma &= \frac{s_W}{c_W} y_Z, \end{aligned} \tag{2.45}$$

among the parameters in (2.25). We see that we obtain the same two restrictions, $c_3 = 0$ and $c_5 = 0$, as we did previously from $SU(2)_{WI}$-symmetry considerations, Eq. (2.33). For

---

[2]In this context, the difference between the mass of the neutral vector-boson and the one of the charged vector-bosons is not significant.

[3]Note that $g^2 \simeq 0.4$.

the non-suppressed terms in (2.39) we introduce the parameters $\epsilon_W, \epsilon_{W\Phi}$ and $\epsilon_{B\Phi}$ (instead of c_1, c_2 and c_4) and obtain the Lagrangian

$$\mathcal{L}_{\text{int}} = \epsilon_{W\Phi}\frac{g}{M_W^2}\mathcal{L}_{W\Phi} + \epsilon_{B\Phi}\frac{g'}{M_W^2}\mathcal{L}_{B\Phi} + \epsilon_W\frac{g}{M_W^2}\mathcal{L}_W. \tag{2.46}$$

The relations between the parameters $\epsilon_i, i = W, W\Phi, B\Phi$, and the parameters in (2.25) with the restrictions (2.45) are given by

$$\begin{aligned}
\epsilon_W &\equiv \frac{3}{2}i\frac{c_4}{g} = \frac{s_W}{c_W}y_Z, \\
\epsilon_{W\Phi} &\equiv -i\frac{c_1}{g} = s_W c_W \delta_Z, \\
\epsilon_{B\Phi} &\equiv i\frac{c_2}{g'} = -\frac{c_W}{s_W}(x_Z + s_W^2\delta_Z).
\end{aligned} \tag{2.47}$$

The expected order of magnitude of the parameters $\epsilon_W, \epsilon_{W\Phi}, \epsilon_{B\Phi}$ in (2.46), following from (2.44), is given by

$$\epsilon_W, \epsilon_{W\Phi}, \epsilon_{B\Phi} = \mathcal{O}\left(\frac{M_W^2}{\Lambda^2}\right). \tag{2.48}$$

For 1 TeV $\leq \Lambda \leq 2$ TeV the expected order of magnitude is

$$\mathcal{O}(10^{-3}) \leq \epsilon_W, \epsilon_{W\Phi}, \epsilon_{B\Phi} \leq \mathcal{O}(10^{-2}). \tag{2.49}$$

I note that effective interaction-terms are also generated by radiative corrections already in the standard model. The coefficients for such terms are of the order of magnitude $\mathcal{O}(\alpha/\pi)$. They are thus of similar magnitude as the couplings in (2.49).

The independent parameters δ_Z, x_Z and y_Z, with x_γ and y_γ following from (2.45), might be used instead of the parameters $\epsilon_W, \epsilon_{W\Phi}$ and $\epsilon_{B\Phi}$. These parameters are given in terms of the ϵ_i by

$$\begin{aligned}
\delta_Z &= \frac{\epsilon_{W\Phi}}{c_W s_W}, \\
x_Z &= -\frac{s_W}{c_W}(\epsilon_{W\Phi} + \epsilon_{B\Phi}), \\
y_Z &= \frac{c_W}{s_W}\epsilon_W, \\
x_\gamma &= \epsilon_{W\Phi} + \epsilon_{B\Phi}, \\
y_\gamma &= \epsilon_W.
\end{aligned} \tag{2.50}$$

Equivalently, the parameters (2.27) with the restrictions

$$\begin{aligned}
\Delta\kappa^\gamma &= -\frac{c_W^2}{s_W^2}(\Delta\kappa^Z - \Delta g_1^Z), \\
\lambda^\gamma &= \lambda^Z,
\end{aligned} \tag{2.51}$$

which are equivalent to (2.45), might be used. The relations between the parameters (2.27) and the ϵ_i are given by

$$\begin{aligned}
\Delta g_1^Z &= \frac{\epsilon_{W\Phi}}{c_W^2}, \\
\Delta\kappa^\gamma &= \epsilon_{W\Phi} + \epsilon_{B\Phi}, \\
\Delta\kappa^Z &= \epsilon_{W\Phi} - \frac{s_W^2}{c_W^2}\epsilon_{B\Phi}, \\
\lambda^\gamma &= \epsilon_W, \\
\lambda^Z &= \epsilon_W.
\end{aligned} \tag{2.52}$$

For WZ-production via $q\bar{q}'$-anihilation, only the three parameters of the ZWW-coupling, g_Z (or δ_Z), x_Z and y_Z, or, equivalently, $\Delta g_1^Z, \Delta\kappa^Z$ and λ^Z, contribute. As another set of three independent parameters for the ZWW-coupling we might choose the parameters $\epsilon_W, \epsilon_{W\Phi}, \epsilon_{B\Phi}$. From (2.47) one obtains, taking into account the relations (2.45), the relations

$$
\begin{aligned}
g_Z &= \frac{c_W}{s_W}\left(1 + \frac{\epsilon_{W\Phi}}{c_W^2}\right), \\
x_Z &= -\frac{s_W}{c_W}(\epsilon_{W\Phi} + \epsilon_{B\Phi}), \\
y_Z &= \frac{c_W}{s_W}\epsilon_W,
\end{aligned}
\tag{2.53}
$$

which have in part already been given in (2.50). We will refer to (2.53) later. Similarly, following from (2.52), one obtains the relations

$$
\begin{aligned}
\epsilon_W &= \lambda^Z, \\
\epsilon_{W\Phi} &= c_W^2\Delta g_1^Z, \\
\epsilon_{B\Phi} &= \frac{c_W^4}{s_W^2}\Delta g_1^Z - \frac{c_W^2}{s_W^2}\Delta\kappa^Z,
\end{aligned}
\tag{2.54}
$$

which we will also use later. Likewise, in $W\gamma$-production via $q\bar{q}'$-annihilation, only two independent parameters contribute. These parameters might be taken as x_γ and y_γ or $\Delta\kappa^\gamma$ and λ^γ or, equivalently, $\epsilon_{W\Phi} + \epsilon_{B\Phi}$ and ϵ_W.

We note that the Lagrangian (2.46) is a general parametrization of $C-$ and P-conserving self-interactions of vector-bosons (excluding higher derivatives and modifications of the interactions between fermions and vector-bosons) in the framework of an extension of the standard model by gauge invariant dimension-6 terms. This has been discussed in [52, 56]. Due to their gauge invariant forms, the interaction-terms in (2.46) contain various additional interactions, in particular those of four vector-bosons among each other and interactions of vector-bosons with Higgs particles. These interactions, if relevant to vector-boson scattering, have been discussed in [56].

In summary, the vector-boson self-interactions can be parametrized by three independent parameters, $\epsilon_W, \epsilon_{W\Phi}$ and $\epsilon_{B\Phi}$, without making very restrictive theoretical assumptions. These parameters are the coefficients of gauge-invariant dimension-6 interactions. The calculations of this work are based on the Lagrangian (2.46).

Chapter 3

Mechanisms for Vector-Boson Pair-Production in Hadron-Hadron Collisions

In this chapter we will briefly discuss the mechanisms by means of which a vector-boson pair can be produced in hadron-hadron collisions. We will describe hadron-hadron collisions in the quark-parton model [57]. The different parton-processes by means of which a vector-boson pair can be produced are then discussed. The calculational tools employed to evaluate the cross-sections for the parton- and hadron-processes and the results for the cross-sections themselves will be discussed in the following chapters.

3.1 Description of Hadron-Collisions in the Quark-Parton Model

In the quark-parton model, the cross-section for a scattering-process of two hadrons of high energies, p_1 and p_2, (e.g. protons or antiprotons), in which a final state W is produced, is given by a two-dimensional integral over a product of parton distribution-functions in the hadrons and the cross-section for parton-parton scattering processes,

$$\sigma(p_1 p_2 \to WX, s_{pp}) = \sum_{q_1, q_2} \int_0^1 f_{q_1}^{p_1}(x_1, Q_1^2) dx_1 \int_0^1 f_{q_2}^{p_2}(x_2, Q_2^2) dx_2$$
$$\cdot \sigma(q_1 q_2 \to WX', s_{qq}). \tag{3.1}$$

In (3.1), the symbols X and X' represent additional particles in the final state and s_{pp} is the square of the invariant mass of the hadron-pair. The sum in (3.1) extends over all partons (quarks, antiquarks and gluons) q_1 in the hadron p_1 and q_2 in the hadron p_2. The quantity $x_i, i = 1, 2$ is the ratio of the magnitude of the spacelike momentum of the parton q_i and the one of the hadron p_i. In writing down (3.1), we assumed that the partons have no transverse momentum. We will also neglect the masses of the hadrons and partons. Thus, the scale variable x_i is also the ratio of the energies of the parton and the hadron. The quantity $f_{q_i}^{p_i}(x_i, Q_i^2) dx_i, i = 1, 2$ represents the probability that a parton q_i with momentum fraction in the interval $[x_i, x_i + dx_i]$ is found inside the hadron p_i. Further, $\sqrt{Q_i^2}$ is an energy which is of the order of magnitude of a characteristic energy

of the process which is initiated by the parton q_i. It is called a factorization scale. The quantity $\sigma(q_1 q_2 \to W X')$ in (3.1) is the cross-section for the parton-parton subprocess. The quantity s_{qq} is the square of the invariant mass of the parton-pair. It is connected to s_{pp} by the relation $s_{qq} = x_1 x_2 s_{pp}$.

Expressed in terms of the ratio of the invariant masses squared, $\tau \equiv s_{qq}/s_{pp}$, and the rapidity y of the motion of the center-of-mass of the parton-pair in the center-of-mass system of the hadrons, taken along the direction of motion of the hadron p_1, the cross-section (3.1) takes on the form

$$\sigma(p_1 p_2 \to WX, s_{pp}) = \sum_{q_1, q_2} \int_0^1 d\tau \int_{\frac{1}{2}\ln(\tau)}^{-\frac{1}{2}\ln(\tau)} dy \, f_{q_1}^{p_1}\left(\sqrt{\tau}e^y, Q_1^2\right) f_{q_2}^{p_2}\left(\sqrt{\tau}e^{-y}, Q_2^2\right)$$
$$\cdot \sigma(q_1 q_2 \to WX', s_{qq} = \tau s_{pp}). \tag{3.2}$$

The relations between the variables x_1, x_2 in (3.1) and τ, y in (3.2) are given by $\tau \equiv x_1 x_2$, $y \equiv 1/2 \ln(x_1/x_2)$ or, equivalently, $x_1 \equiv \sqrt{\tau}e^y$ and $x_2 \equiv \sqrt{\tau}e^{-y}$.

3.2 Parton-Processes for Vector-Boson Pair Production

There are different mechanisms for the production of a vector-boson pair $V_3 V_4$ in parton-parton collisions.

In lowest order of perturbation theory, the vector-boson pair is produced via the Drell-Yan process, $q\bar{q}' \to V_3 V_4$, where q is a quark and $\bar{q}'$ is an antiquark. This is the dominant process. The three different possible Feynman graphs for the generic process (we did not specify the type of particles) are shown in Figure 3.1a. The parton-parton cross-section in lowest order of perturbation theory is proportional to the square of the fine-structure-constant, $\sigma = \mathcal{O}(\alpha^2)$.

In addition to the lowest order contribution, one might consider the electroweak radiative corrections to the Drell-Yan process. The corrections are $\sigma = \mathcal{O}(\alpha^3)$ (in their lowest order) and consist of virtual corrections and real corrections. The virtual corrections are also indicated in Figure 3.1a. Figure 3.1b shows some diagrams for the real corrections. These latter corrections are due to the process $q_1 q_2 \to V_3 V_4 \gamma$. They are represented by bremsstrahlung-diagrams with a photon being emitted. The real corrections are usually divided into a contribution from soft photons and a contribution from hard photons. Soft photons have such a small energy that they can not be experimentally detected, while hard photons have larger energies. The contribution from hard photons is to be considered only if these photons can not be detected. This is the case if they are produced with their directions of motion near the hadron beam-direction. The contribution from photons produced in these directions, although an $\mathcal{O}(\alpha)$-correction, is in general enhanced by logarithmic factors of $\ln(s_{qq}/m_q^2)$, where m_q is a quark mass. These logarithmic factors can be partially absorbed into the definition of the parton distribution-functions $f_{q_i}^{p_i}$ in (3.1) [60]. The partial absorption of the factor only leads to a negligible change of the values of the parton distributions [60]. The remaining enhancement of the cross-section for $q_1 q_2 \to V_3 V_4 \gamma$ is due to a factor of $\ln(s_{qq}/\mu_0^2)$, where μ_0^2 is a reference scale used in the definition of the parton distribution-function. Typical numerical values for μ_0^2 are
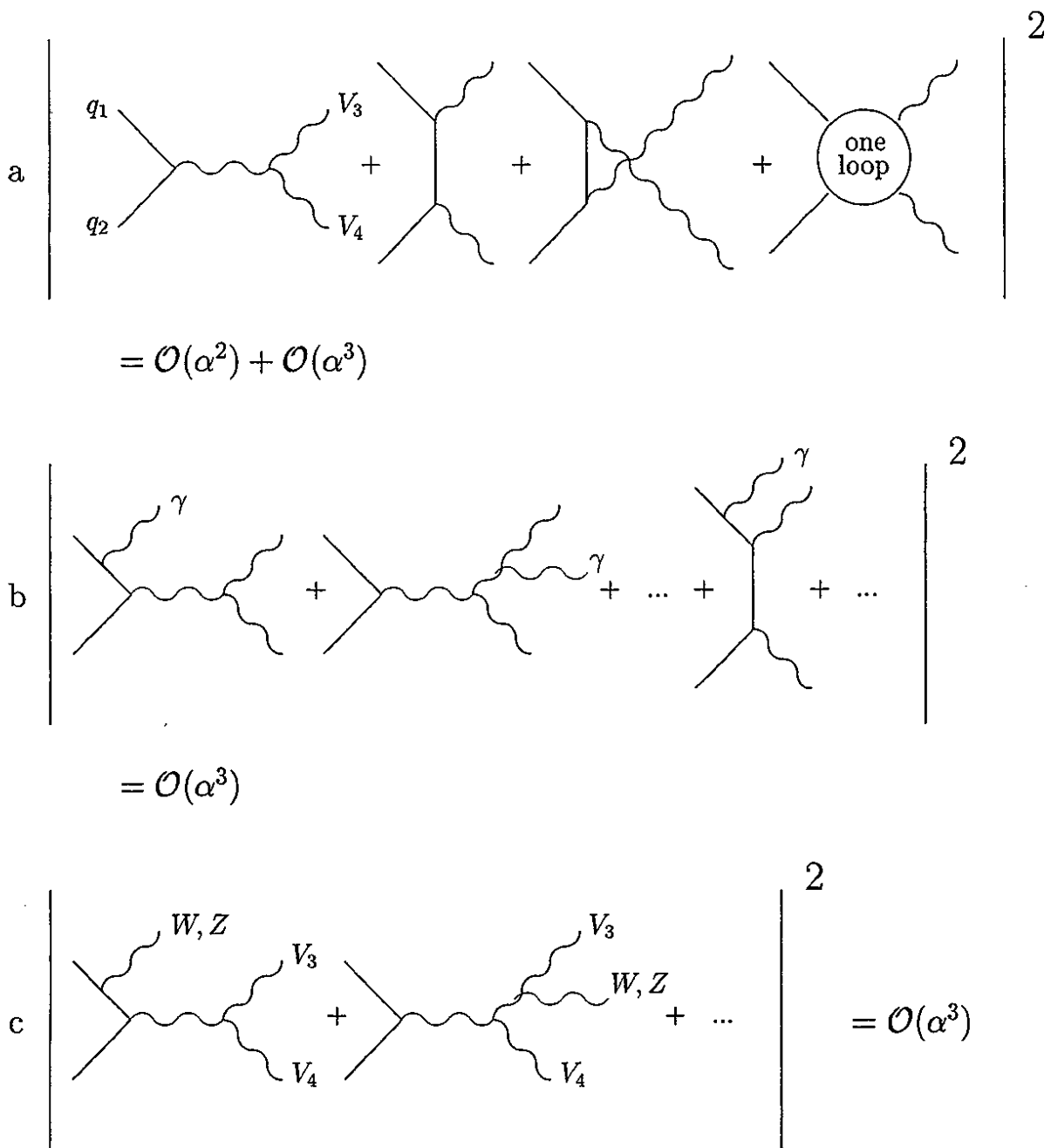
Figure 3.1: Feynman diagrams for the lowest order electroweak processes, in which a V_3V_4-pair is produced in the collision of a parton q_1 with a parton q_2. a: Drell-Yan process with virtual corrections, b: Photon-bremsstrahlung to the Drell-Yan process, $q_1q_2 \rightarrow V_3V_4\gamma$, c: The process $q_1q_2 \rightarrow V_3V_4V$, where $V = W$ or $V = Z$.

$\mu_0^2 = 5$ GeV^2. We do not attempt to calculate the contribution from $q_1 q_2 \to V_3 V_4 \gamma$ here. Its effects could be considered in a more refined calculation.

Concerning the numerical values of electroweak radiative corrections, the corrections for $q\bar{q}' \to WZ$ have not been calculated yet to my knowledge. To give an example of the order of magnitude which electroweak radiative corrections can have, I briefly discuss the corrections for the process $e^+ e^- \to W^+ W^-$. This process is an example of the generic process $q\bar{q}' \to V_3 V_4$. The radiative corrections have been presented and discussed in [58]. For LEP 2 energies, $\sqrt{s_{e^+ e^-}} \simeq 200$ GeV, the magnitude of the corrections is of the order of 10% of the lowest order cross-section. The value depends on the scattering angle. At $\sqrt{s_{e^+ e^-}} = 1$ TeV, the corrections amount to about -30% of the Born cross-section if the W-bosons are produced at right angle to the $e^+ e^-$ beam direction. The exact value of the corrections depends on a cut-off for the maximum energy of the photon (a soft-photon cut-off). For larger energies $\sqrt{s_{e^+ e^-}}$, simple approximate formulae for the radiative corrections have been given in [59]. These formulae were obtained by performing a high-energy expansion to the exact expressions. We will perform an approximation of the same kind to the lowest order cross-sections for the parton-processes to be considered here. This will be discussed in later chapters. Returning to the radiative corrections for $e^+ e^- \to W^+ W^-$, a maximum value for the soft-photon cut-off was chosen for a numerical evaluation in [59]. The cut-off was chosen to be equal to the energy of one of the incoming leptons[1]. With this choice, it was found that the radiative corrections amount to only 2.2% of the Born cross-section at $\sqrt{s_{e^+ e^-}} = 1$ TeV. An integration over the scattering angle was performed in deriving this result. Similarly, for $\sqrt{s_{e^+ e^-}} = 2$ TeV, it was found that the corrections amount to -11% of the Born cross-section. For $\sqrt{s_{e^+ e^-}} = 3$ TeV they amount to -21%.

At large scattering energies also the emission of a *massive* real vector-boson, W or Z, is possible. These are the processes $q_1 q_2 \to V_3 V_4 V$, $V = W, Z$, shown in Figure 3.1c. They also give, like the $q_1 q_2 \to V_3 V_4 \gamma$ processes, a $\sigma = \mathcal{O}(\alpha^3)$ contribution which can become large if the vector-boson V is emitted near the hadron-beam pipe, where it cannot be detected. However, the large logarithms which can appear will only contain the smaller ratio s_{qq}/M_V^2 instead of s_{qq}/μ_0^2. We do not include the contribution of these processes here, either.

Further, the QCD radiative corrections to the Drell-Yan process contribute. They are formally of the order $\mathcal{O}(\alpha^2 \alpha_s)$ but they are enhanced by logarithmic factors. The corrections contain contributions from virtual corrections, real corrections with the emission of a gluon, $q\bar{q}' \to V_3 V_4 g$, and from the gluon-quark scattering processes $qg \to V_3 V_4 q'$ and $\bar{q}' g \to V_3 V_4 \bar{q}$. For WZ-production these corrections have been calculated and discussed in [25, 27]. The contribution of these corrections to the total cross-section for $pp \to WZX$ at the LHC amounts to between 50% and 70% of the contribution from the lowest-order Drell-Yan processes (in the standard model). In spite of the magnitude of this contribution, we will not consider it here since it has already been discussed in detail in [25, 27]. The discussion has been given for the standard model and for anomalous couplings. In a more refined treatment, this contribution could be added to the cross-sections calculated here. The expected sensitivity of the experiment to anomalous couplings is slightly reduced if this contribution is taken into account. Quantitatively, the sensitivity limits for anomalous couplings grow by 30% or less in magnitude if the corrections are taken into

---

[1]For a correct treatment of high-energy photons, the contribution from hard photons has to be added and a smaller value for the cut-off has to be chosen.

account [27].

Finally, to order $\mathcal{O}(\alpha^4)$ there are the processes $q_1 q_2 \rightarrow V_3 V_4 V_5 V_6$ and $q_1 q_2 \rightarrow q'_1 q'_2 V_3 V_4$, where V_5, V_6 are also vector-bosons. The four–vector-boson production processes can only play a role for the $V_3 V_4$ production-rate if both additional vector-bosons are not experimentally detected. We will not consider it here. The $q_1 q_2 \rightarrow q'_1 q'_2 V_3 V_4$ processes will be the subject of following investigations. They obtain contributions from the vector-boson scattering processes, $V_1 V_2 \rightarrow V_3 V_4$. These processes appear as sub-processes. Due to the appearance of the vector-bosons $V_1 V_2$, the rate for the processes $q_1 q_2 \rightarrow q'_1 q'_2 V_3 V_4$ is enhanced by logarithmic factors of $\ln(\tilde{Q}^2 / M_V^2)$, where $\tilde{Q}^2$ is of the order of magnitude of s_{qq}.

We included the formal discussion of contributions, classified in terms of powers of coupling constants, only for completeness here. It is clear that the contribution from the processes $q_1 q_2 \rightarrow q'_1 q'_2 V_3 V_4$ is not the dominating one and that there are other contributions which might also contribute. Our interest here, however, is in the vector-boson self-couplings. It is through the vector-boson–vector-boson scattering processes, $V_1 V_2 \rightarrow V_3 V_4$, appearing as sub-processes to the processes $q_1 q_2 \rightarrow q'_1 q'_2 V_3 V_4$, that anomalous self-couplings might manifest themselves. It has been shown that for a resonant heavy Higgs boson, for example, the cross-section for $V_1 V_2$-scattering is dramatically increased so that the cross-section for the processes $q_1 q_2 \rightarrow q'_1 q'_2 V_3 V_4$ can exceed the one for the Drell-Yan processes [35]. The natural question which arises, and which will be addressed here, is whether a similar increase of the cross-section can also be caused by anomalous interactions of the vector-bosons. We know about these interactions that they lead to a dramatic increase of the cross-sections for vector-boson scattering. The increase in the cross-section for $q_1 q_2 \rightarrow q'_1 q'_2 V_3 V_4$ must be compared to an increase in the Drell-Yan rate caused by the anomalous interactions. The other processes might be added later in a more sophisticated analysis if this point has been clarified.

Thus, we will consider here the lowest order contribuition from the Drell-Yan processes and from the processes $q_1 q_2 \rightarrow q'_1 q'_2 V_3 V_4$. The cross-section for a parton-parton scattering process will be approximated by the sum of the cross-section for these two processes,

$$\sigma(q_1 q_2 \rightarrow V_3 V_4 X') = \sigma(q\bar{q}' \rightarrow V_3 V_4) + \sigma(q_1 q_2 \rightarrow q'_1 q'_2 V_3 V_4). \tag{3.3}$$

The cross-section for hadron-hadron scattering will also be calculated as a sum of the two contributions,

$$\sigma(p_1 p_2 \rightarrow V_3 V_4 X) = \sigma(p_1 p_2 \rightarrow q\bar{q}' \rightarrow V_3 V_4) + \sigma(p_1 p_2 \rightarrow q_1 q_2 \rightarrow q'_1 q'_2 V_3 V_4). \tag{3.4}$$

Chapter 4

Effective Vector-Boson Approximation for Fermion-Fermion Scattering Processes

4.1 Introduction

In this chapter an improved approximative method to calculate the cross-sections for the processes $q_1 q_2 \to q'_1 q'_2 W$, where W is an arbitrary final state, is derived. This method is applicable if the scattering energy $\sqrt{s}$ of the fermions $q_1 q_2$ is very large compared to the masses of the electroweak vector-bosons. Parts of this chapter have been published in [61].

4.1.1 Effective Photon Approximation

The method of the effective vector-boson approximation is similar to the Weizsäcker-Williams-approximation of QED (effective photon approximation, EPA) [34], in which the cross-section for a fermion-fermion scattering process is written as a product of the probability for the emission of a photon-pair from the fermion-pair and a cross-section for photon-photon scattering. With the help of Feynman diagrams the content of the EPA can be explained. For illustration, we choose the final state W as two massless particles $V_3 V_4$. The method is, however, applicable to arbitrary final states. We will also neglect the masses of the involved fermions in the following, i.e., we will assume that the scattering energy $\sqrt{s}$ is much larger than these masses. This is a necessary assumption for the EPA. Figure 4.1 shows some of the diagrams, which contribute to a process $q_1 q_2 \to q'_1 q'_2 V_3 V_4$ in lowest order of perturbation theory. The particles V_1, V_2, as well as V and V' are also photons (since we are dealing with a QED problem). The diagram in the top right corner is proportional to the product of the propagator for the photons V_1 and V_2. We will call this diagram the vector-boson scattering diagram. The mentioned propagators become singular if the squared four momenta, k_1^2 and k_2^2, of the photons V_1 and V_2 approach the value zero. This is the case if the photons go on their mass-shell. They are then produced in the foreward direction with respect to the fermions. The mentioned singularities are only removed if the finite masses of the fermions, which increase the lower limits for the integration variables $|k_1^2|$ and $|k_2^2|$, are taken into account. The magnitude of the vector-boson scattering diagram is therefore very large compared to the other diagrams. One
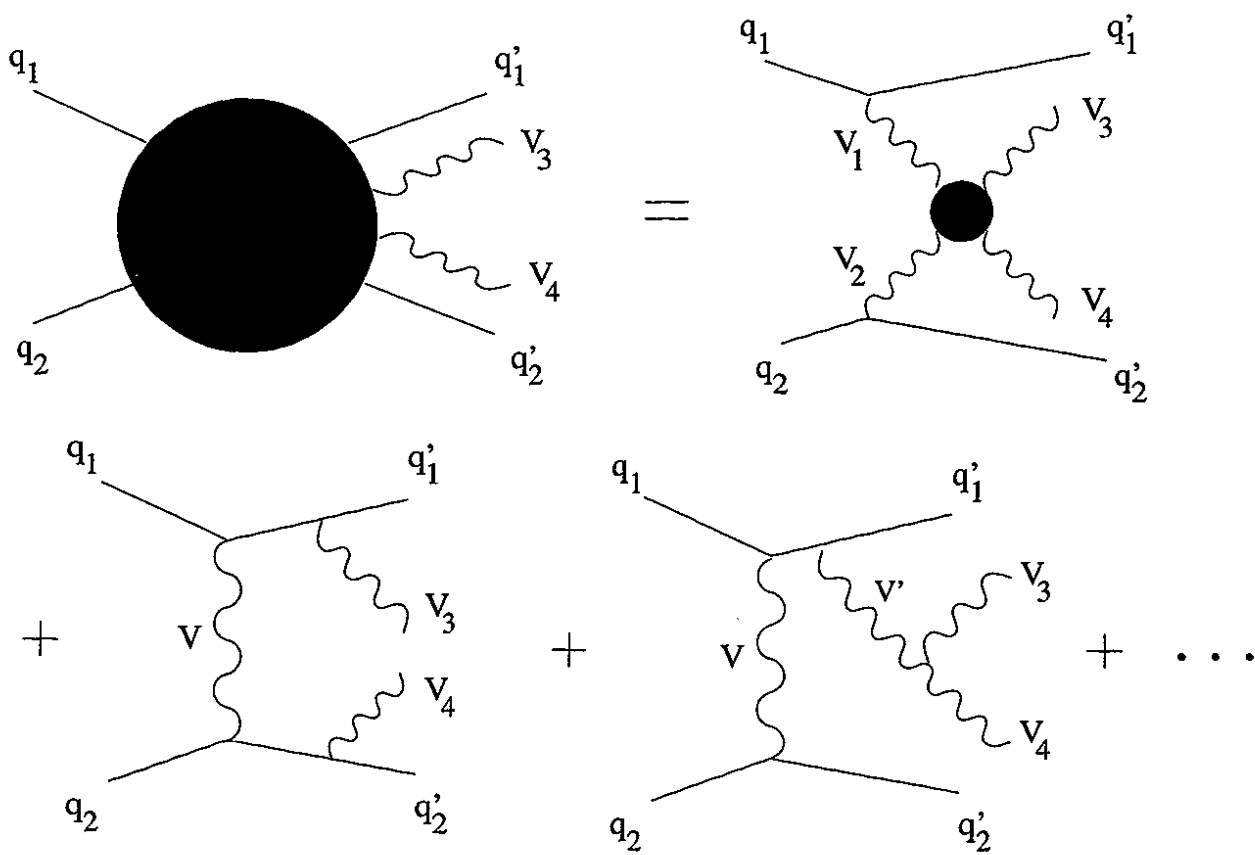
Figure 4.1: Feynman diagrams for a process $q_1 q_2 \rightarrow q'_1 q'_2 V_3 V_4$ in a complete perturbative calculation. To the top right is the diagram for vector-boson scattering, which is the only diagram which is considered in the effective vector-boson approximation. The lower row shows diagrams of bremsstrahlung-type.

should note that this is not anymore the case if the particles V_3 or V_4 are produced in the forward direction. In this case the contribution from the bremsstrahlung-type diagrams, shown in the lower row of Figure 4.1, can also be very large, because then the squared four-momentum of one or two of the virtual fermions also tends to zero. The propagator-function for such a fermion is then of the same order of magnitude as the propagators for the photons V_1, V_2. However, small angles of the directions of motion of the partilces V_3 and V_4 with respect to the directions of motion of the fermions can be avoided by applying suitable cuts. In fact, such cuts have to be employed anyway, because a particle near the beam pipe can not be detected.

Thus, in the effective photon approximation, a restriction to the vector-boson scattering diagrams is made. For the calculation of these diagrams, two basic ingredients are required: the known couplings of the photons V_1, V_2 to the quarks and an expression for the cross-section for photon-photon scattering, $V_1 V_2 \to W$. This cross-section must be evaluated for arbitrary values of the four-momenta squared k_1^2 and k_2^2. We must thus have an expression for a cross-section with incoming particles which can be off-shell. If the dependence of the cross-section on k_1^2, k_2^2 is not known, we can make a suitable assumption about this dependence. This assumption must be made in such a way that the cross-section is a smooth function of k_1^2, k_2^2 and that it becomes equal to the on-shell cross-section if $k_1^2 = k_2^2 = 0$ is chosen. We note that the magnitude of the vector-boson scattering diagram, however, will not depend very much on such an assumption, since the main contribution to the diagram comes from the region of the q_1', q_2'-phase space, where $k_1^2, k_2^2 \simeq 0$, because the propagators are very large there. In this region, the cross-section is very well approximated by the (known) on-shell cross-section.

It should be noted that only the squared amplitude, $|\mathcal{M}_{pol}|^2$ for photon-photon scattering enters into the expression for the cross-section of the fermion-fermion process. The squared amplitude is related to the cross-section $\hat{\sigma}_{pol}$ for photon-photon scattering by a flux-factor, κ,

$$|\mathcal{M}_{pol}(k_1^2, k_2^2)|^2 \sim \kappa(k_1^2, k_2^2)\hat{\sigma}(k_1^2, k_2^2)_{pol}, \qquad (4.1)$$

where we have explicitly written down the dependence of all quantities on the squared four-momenta of the photons. It is thus the product of the cross-section and the flux-factor, for which an assumption about the continuation to off-shell photons must be made.

Carrying out the integration over the phase-space of the fermions q_1' and q_2', the expression for the $q_1 q_2$ cross-section is written as a product of a function, which describes the emission of a photon-pair from the fermions $q_1 q_2$, and the cross-sections for on-shell $V_1 V_2 \to W$-scattering. The mentioned function is called a luminosity for photon-photon emission. It describes the probability that a photon-pair is emitted from the fermion-pair. We note that the exact form of this function will depend on the dependence of the photon-photon cross-sections on k_1^2, k_2^2, or, respectively, on the assumption which has been made about this dependence.

In summary, the EPA consists of evaluating only the vector-boson scattering diagrams and possibly of an assumption about the photon-photon cross-sections for off-shell photons, if this latter quantity is not known. Finally, we note that the number, the masses and the types of the particles in the final state can be arbitrary. This generalization does not affect the validity of the approximations we discussed above.
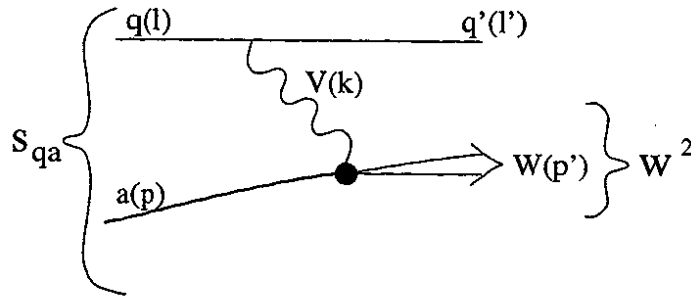
Figure 4.2: Feynman diagram in the effective vector-boson approximation for the reaction of a fermion q with a particle a at a scattering energy $\sqrt{s_{qa}}$ in which a final state W with the invariant mass squared $\mathcal{W}^2$ is produced. The particle V is the exchanged vector-boson. The quantities l, l', k, p and p' denote the four-momenta of the involved particles.

4.1.2 Effective Vector-Boson Approximation

We now turn to the effective vector-boson approximation. The generaliziation of the EPA to electroweak processes is straightforward. If the vector-bosons V_1 and V_2 are massive particles, the approximations of the EPA can still be made as long as the scattering energy is very large compared to the vector-boson masses, $s \gg M_1^2, M_2^2$. The assumptions leading to the effective vector-boson approximation (EVBA) are otherwise the same as the ones of the EPA. The possibility to extend the method of the EPA to the case of massive vector-bosons was first noted in [62] and explicitly formulated in [31, 32, 33].

The effective-vector boson approximation was first applied to processes, which proceed via the exchange of only one vector-boson, as shown in Figure 4.2. In the EVBA, the fermion is considered to be the source of a vector-boson V, the momentum of which is to be integrated over. The vector-boson in turn initiates a scattering process with the particle a, in which the final state W is produced, $Va \to W$. The cross-section σ_{qa} for the entire process can be calculated with the help of distribution-functions of vector-bosons in fermions, $f_V^q(x)$, and the cross-sections σ_{Va} for the scattering of vector-bosons V with the particle a. The expression for the cross-section σ_{qa} is given by

$$\sigma_{qa}(s_{qa}) = \int\limits_0^1 dx \sum_V \sum_{pol} f_{V,pol}^q\left(x, \frac{M_V^2}{s_{qa}}\right) \sigma_{Va,pol}(\mathcal{W}^2). \tag{4.2}$$

In (4.2), x is the scaling variable for the vector-boson distribution functions. By definition of the distribution functions, this variable connects, at least approximately, the invariant mass squared of the produced final state W, $\mathcal{W}^2$, to the invariant mass squared s_{qa},

$$\mathcal{W}^2 = x s_{qa}. \tag{4.3}$$

A summation over the helicity states $pol = \pm, 0$ of the vector-boson V is carried out in (4.2). The distribution function $f_{V,pol}^q(x)$ is the probability density that a vector-boson V with helicity pol is emitted from the fermion q. The distribution function f_V^q depends on a second quantity, which is the ratio of the vector-boson mass squared, M_V^2, and the scattering energy squared, s_{qa}. The quantity s_{qa} in this ratio might be expressed in terms of other quantities, like energies or transverse momenta of the involved particles defined in

certain reference frames. Some of the distribution functions $f^q_{V,pol}(x)$ which can be found in the literature have been expressed in terms of such quantities. Apart from this subtle point, equation (4.2) is the general EVBA expression for the cross-section of processes proceeding via the exchange of one vector-boson.

For the transverse helicity eigenstates, $pol = \pm$, the summation in (4.2) is usually re-expressed in terms of linear combinations of these helicites,

$$\sum_{pol=+,-} f^q_{V,pol} \sigma_{Va,pol} = \sum_{pol=T,\overline{T}} f^q_{V,pol} \sigma_{Va,pol}, \tag{4.4}$$

with

$$f^q_{V,T} \equiv f^q_{V,+} + f^q_{V,-} \qquad f^q_{V,\overline{T}} \equiv f^q_{V,+} - f^q_{V,-} \tag{4.5}$$

and

$$\sigma_{Va,T} \equiv \frac{1}{2}(\sigma_{Va,+} + \sigma_{Va,-}) \qquad \sigma_{Va,\overline{T}} \equiv \frac{1}{2}(\sigma_{Va,+} - \sigma_{Va,-}). \tag{4.6}$$

The distribution $f^q_{V,\overline{T}}$ only exists if the interaction between the fermion a and the vector-boson V is parity violating. Thus, this distribution is absent for photon interactions.

In the application of the EVBA to processes with *two* intermediate vector-bosons, V_1 and V_2, as shown in Figure 4.3, it was assumed that *convolutions* of the distributions of single vector-bosons can describe the luminosities for vector-boson pairs,

$$\mathcal{L}^{q_1 q_2}_{V_1,pol_1 V_2,pol_2} = \int_{z_{min}}^{1} \frac{dz}{z} f^{q_1}_{V_1,pol_1}(z) f^{q_2}_{V_2,pol_2}(x/z). \tag{4.7}$$

In (4.7) the symbols q_1 and q_2 denote the fermions in the initial state. With the help of the luminosities (4.7) the cross-section for the scattering of two fermions was expressed in the following way,

$$\sigma(q_1 q_2 \to W, s) = \int_{x_{min}}^{1} dx \sum_{V_1,V_2} \sum_{pol_1,pol_2} \mathcal{L}^{q_1 q_2}_{V_1,pol_1,V_2,pol_2} \sigma(V_{1,pol_1} V_{2,pol_2} \to W, xs). \tag{4.8}$$

In (4.8) xs is the invariant mass squared of the final state W. Non-diagonal terms in the helicity indices pol_1 and pol_2 were not considered. It has been noticed, however, for the specific example of Higgs boson procuction that such terms can be important [63].

4.1.3 Exposition

In this work an improved formulation of the EVBA is presented, which is applicable to the case of *two* intermediate massive vector-bosons. It will be shown that the simple formalism of convolutions does not treat the phase-space for the two vector-bosons correctly. In fact, in a correct treatment, the emission probability of one vector-boson depends on the kinematical variables of the other vector-boson. Among these variables is the squared four-momentum of this vector-boson. In the formalism of convolutions the dependence of the emission probability on this squared four-momentum has not been taken into account. Rather, a specific value, $k^2 = 0$, has been inserted for this squared four-momentum.

The present work combines the exact treatment of the two-boson kinematics, presented for photons in [64], with the exact definition of vector-boson distributions, presented for

single vector-bosons in [65]. In the derivation we will not use any kinematic approximations. We will give expressions for improved luminosities. It turns out that non-diagonal terms in the helicity combinations of the intermediate bosons are present. We will identify in detail the approximations which lead to the previously given formalism of convolutions.

In Section 4.2 we review the formulations and the use of the EVBA in the literature. In Section 4.3 we derive the improved luminosities. The Sections 4.4 and 4.5 contain approximative treatments.

4.2 Effective Vector-Boson Approximation: Formulations in the Literature

4.2.1 The Different Existing Versions of the EVBA

We will discuss in some detail the differences between the various versions of the effective vector-boson method which can be found in the literature.

The distribution-functions in the literature differ as a result of different approximations. They can be classified into three groups:

1. In the derivation of the distribution-function f_V^q in [32, 66], terms proportional to the transverse momentum squared, $k_\perp^2$, of the vector-boson with respect to the fermion q have been neglected. Only the leading terms for $k_\perp^2 \to 0$ have been retained. The scaling variable x of the distribution-function was defined as the ratio of the longitudinal component k^L of the vector-boson's momentum and the energy E_q of the fermion q, $x \equiv k^L/E_q$. The subprocess energy $\mathcal{W}^2$ is, in the approximation $k_\perp^2 \to 0$, proportional to the scaling variable x, $\mathcal{W}^2 = xs + \mathcal{O}(k_\perp^2)$. This is true if x and $k_\perp^2$ are evaluated in a frame in which q and a move in opposite directions and their masses can be neglected in this frame. Instead of s_{qa} in (4.2) the maximum transverse momentum squared of the emitted vector boson, $P_\perp^2$, was used. In the center-of-mass frame of the fermion q and the particle a the relation between s_{qa} and $P_\perp^2$ is given by

$$P_\perp^2 = (2E - M_0)^2 - E^2(1-x)^2. \tag{4.9}$$

In (4.9), x is the scaling variable for the f_V^q-distributions, E is related to s_{qa} via $E = \sqrt{s_{qa}}/2$, and M_0 is the sum of the masses of the particles in the final state W.

2. The distribution-functions [31, 67, 68] were derived without approximations in the integration over the vector-boson's momentum. The scaling variable x was defined as the ratio of the vector-boson's energy, k^0, and the energy E_q of the fermion q. The energies E_q and k^0 were defined in the rest-frame of the particle a.

I argue here that the definition of the energies in this frame is not viable and that the distributions [31, 67, 68] can only be used in a slightly modified form, which will be defined in the following. In the rest-frame of the particle a, the relation $x = \mathcal{W}^2/s_{qa}$ is violated by terms of the order

$$\mathcal{O}\left(\frac{s_{qa}}{M_a^2}\theta'^2\right),$$

where M_a is the mass of the particle a and θ' is the angle between the direction of motion of the particle q and the vector-boson V. Clearly, for $s_{qa} \gg M_a^2$, already for

very small values of θ' the relation $x = \mathcal{W}^2/s$ is completely disturbed. We conclude that E_q and k^0 must not be defined in the rest-frame of a.

One can convince oneself, however, that the expressions $f_V^q(x, E_q, M_V)$, i.e., the functional dependence of f_V^q on the variables x, E_q and M_V given in [31, 67, 68], is hardly affected by the choice of the reference-frame for the definition of x and E_q. This functional form is only affected via the ratio r_f of the on-shell flux-factor for the Va-process and the one for the qa-process,

$$r_f \equiv \sqrt{(k \cdot p)^2 - k^2 p^2}/\sqrt{(l \cdot p)^2 - l^2 p^2} = 2\sqrt{(k \cdot p)^2 - k^2 p^2}/s_{qa}. \qquad (4.10)$$

In (4.10), the four-momenta k, p and l are as specified in Figure 4.2 and must be evaluated on mass-shell. In the rest-frame of a, one finds $r_f = x\sqrt{1 - M_V^2/(x^2 E_q^2)}$. The ratio r_f appears only as a multiplicative constant to the distribution-functions. The distribution-functions $f_V^q(x, E_q, M_V)|_{\text{arb.}}$, in which x and E_q might be defined in an arbitrary reference frame, are therefore related to the distribution-functions $f_V^q(x, E_q, M_V)|_{\text{rest}}$ given in [31, 67, 68] by

$$f_V^q(x, E_q, M_V)|_{\text{arb.}} = \frac{r_f|_{\text{arb.}}}{r_f|_{\text{rest}}} f_V^q(x, E_q, M_V)|_{\text{rest}}. \qquad (4.11)$$

In the cms-frame of q and a, the relation $\mathcal{W}^2 = xs$ holds exactly. In this frame, $r_f = x(1 - M_V^2/(4x E_q^2))$ and $4E_q^2 = s_{qa}$. One might therefore define the variables x and E_q in this frame and use the distribution functions [31, 67, 68] in the form

$$f_V^q(x, E_q, M_V) \longrightarrow \frac{1 - \dfrac{M_V^2}{4x E_q^2}}{\sqrt{1 - \dfrac{M_V^2}{x^2 E_q^2}}} f_V^q(x, E_q, M_V), \qquad (4.12)$$

where $f_V^q(x, E_q, M_V)$ are the functions listed in the references and $4E_q^2 = s_{qa}$. We will use the form on the right hand side of (4.12) in our later numerical examples.

We note that an obvious error (or misprint) in [68] has to be corrected. To be specific, the correct expressions for the integrals I_1, I_2 and I_3 in the appendix of [68] are given by

$$
\begin{aligned}
I_1 &= \frac{z^2 E_l^4}{(z^2 E_l^2 - M^2)^2} \ln\left(\frac{Q_M^2 q_E^2}{q_M^2 Q_E^2}\right) + \frac{M^2 E_l^2}{z^2 E_l^2 - M^2}\left\{\frac{1}{Q_M^2} - \frac{1}{q_M^2}\right\}, \\
I_2 &= \frac{1}{(z^2 E_l^2 - M^2)^2}\left\{z^4 E_l^4 \ln\left(\frac{Q_E^2}{q_E^2}\right) - M^2(2z^2 E_l^2 - M^2)\ln\left(\frac{Q_M^2}{q_M^2}\right)\right\} \\
&\quad - \frac{M^4}{z^2 E_l^2 - M^2}\left\{\frac{1}{Q_M^2} - \frac{1}{q_M^2}\right\}, \\
I_3 &= \ln\left(\frac{Q_M^2}{q_M^2}\right) + \frac{M^2}{Q_M^2} - \frac{M^2}{q_M^2}. \qquad (4.13)
\end{aligned}
$$

In (4.13), the definition of all variables is as in [68]. We further remark that for the function f_L in [31], an approximation $M_V^2 \ll E_q^2$ has been made.

Concerning the continuation of the sub-process cross-sections to off-shell values of the vector-boson's four-momentum, $k^2 \neq M_V^2$, the most simple assumption, namely

that the product of the flux-factor and the cross-section does not depend on k^2 at all,

$$\kappa(k^2)\hat{\sigma}_{pol}(k^2) = \kappa(M_V^2)\hat{\sigma}_{pol}(M_V^2), \qquad (4.14)$$

has been made in [31, 32, 66, 67]. In [68], different assumptions have been made. These assumptions were made on the k^2-dependence of Lorentz-invariant structure functions $W_i(k^2)$ describing the interaction of the fermions with the vector-bosons. They amount to the same simple relation, (4.14), for the transverse polarization T, but, however, for different relations for the polarizations $\overline{T}$ and L. This is the reason why the $\overline{T}$- and L-distributions of [67] and [68] differ.

3. All distributions discussed so far are only approximative in the definition of the helicity of the vector-boson V. Terms of the order $k_\perp^2$ were not treated exactly. In contrast, the functions given in [33, 65] are exact in the definition of the vector-boson helicity.

As already mentioned, an integration over the momentum of the outgoing fermion, q', is carried out in the derivation of the distribution-functions. The subprocess cross-section $\sigma_{Va,pol}(xs)$, however, must be evaluated for definite values of the components of the momenta k and p, i.e. values, which do not depend on the integration variables. Of course, for a given set of integration variables, a Lorentz-transformation into a frame, in which k and p have given components, can be applied. However, this transformation in general changes the helicity of the vector-boson V since the helicity of a massive vector-boson is not a Lorentz-invariant quantity. Only in frames, which are related to each other by a boost in the direction of motion of the vector-boson, the helicity is the same. Therefore, in the frame in which the helicity is defined, the transverse components of p with respect to k must be the same for all values of the integration variables. For the distributions [31, 67, 68], the helicity was specified in the same frame in which x and E_q were defined. As we identified this frame with the qa-cms-frame, the transverse components of p with respect to k are equal to the transverse components of k with respect to l. The square of these components we denoted by $k_\perp^2$. The variable $k_\perp$, however, changes its value in the course of the integration. Therefore, for the distributions [31, 67, 68], mixing between the transverse and the longitudinal components of V appears at the order $\mathcal{O}(k_\perp^2)$.

In [33, 65], in contrast, the helicity (i.e. the polarization vector for V) was specified in a frame in which the three-momenta $\vec{k}$ and $\vec{p}$ are parallel independently of the values of the integration variables. In [65], e.g., the polarization-vectors for V were specified in a system, in which k has no time-like momentum and points in the positive z-direction (Breit-system), whereas p points in the negative z-direction,

$$k = (0; 0, 0, \sqrt{-k^2}), \quad p = \sqrt{-k^2}/2(1 - \mathcal{W}^2/k^2; 0, 0, \mathcal{W}^2/k^2 - 1),$$

and

$$p' = \sqrt{-k^2}/2(1 - \mathcal{W}^2/k^2; 0, 0, 1 + \mathcal{W}^2/k^2).$$

The helicity of V was thus well-defined for all values of the integration variables.

In addition, the scale variable x in [33, 65] was directly defined in terms of Lorentz-invariant quantities, $x \equiv \mathcal{W}^2/s$.

Thus, in [33, 65], exact expressions for vector-boson distributions in fermions were derived. The only remaining necessary assumption concerned the continuation of the cross-sections into the off-shell-region. In [33], the specific assumption that the final-state W couples like a fermion to the intermediate vector-boson has been made,

$$\kappa(k^2)\hat{\sigma}_{pol}(k^2) = \kappa(k^2)\hat{\sigma}_{pol}(k^2)|_{\text{ferm.}}.$$

In [65], the off-shell behavior was described in terms of the k^2-dependence of the vector-boson polarization-vectors. In addition, the flux-factor was evaluated at $k^2 = 0$. This leads to

$$
\begin{aligned}
\kappa(k^2)\hat{\sigma}_{pol}(k^2) &= \kappa(0)\hat{\sigma}_{pol}(M_V^2), \quad pol = T, \overline{T}, \\
\kappa(k^2)\hat{\sigma}_L(k^2) &= \frac{M_V^2}{|k^2|}\kappa(0)\hat{\sigma}_L(M_V^2).
\end{aligned}
\tag{4.15}
$$

Replacing the approximate choice $\kappa(0)$ in (4.15) by the precise choice $\kappa(M_V^2)$[1] is equivalent to multiplying the distributions of [65] with a factor

$$f_V^q(x, s_{qa}, M_V^2) \longrightarrow \frac{\kappa(M_V^2)}{\kappa(0)} f_V^q(x, s_{qa}, M_V^2) = \left(1 - \frac{M_V^2}{x s_{qa}}\right) f_V^q(x, s_{qa}, M_V^2). \tag{4.16}$$

We will use this form in our later numerical examples.

Concerning the allowed values for x, the distributions [32, 66] are defined for all values of x in the range $0 < x < 1$. For the distributions [31, 67, 68], the variable x is restricted to values of

$$x > M_V/E_q = 2M_V/\sqrt{s_{qa}}.$$

The distributions vanish for smaller values of x. The distributions [33, 65] are defined for all values of x in the range

$$M_V^2/s_{qa} < x < 1.$$

The lower limit arises because the real flux-factor for the subprocess $Va \to WX$, which has been included in the definition, vanishes if x is smaller than M_V^2/s_{qa}. Note that the definition of the variable x is different for the different distributions. It should also be noted that in any application, x will anyway be greater than the value $x = M_0^2/s_{qa}$, where M_0 is the sum of the particles in the final state W.

All distributions reduce to the same analytical forms if a crude approximation is made. This approximation is obtained by retaining only the leading terms in the limit of vanishing vector-boson masses, $M_V^2 \ll x s_{qa}$ and $M_V^2 \ll (1-x)x s_{qa}$. This approximation has been frequently used in the literature and is called the leading logarithmic approximation (LLA)[2]. We will give the expressions for the luminosities and distributions in the LLA in Chapter 4.5. They can also be found e.g. in [68, 69, 70].

Table 4.1 summarizes the differences between the existing sets of vector-boson distributions.

---

[1]The expressions (4.15) must reduce to the on-shell expressions for $k^2 = M_V^2$.

[2]It should be noted that not all leading terms are of logarithmic type.

Author(s) (only one named)	Definition of x	Kinematic Approximations			Definition of helicities
		T	T	L	
Kane [32]	$x \equiv k^L/E_q, \quad \mathcal{W}^2 = xs + \mathcal{O}(k_\perp^2)$	$M_V^2 \ll k_\perp^2 \ll E_q^2$			$k_\perp^2 \simeq 0$
Abbasabadi [66]		$k_\perp^2 \ll E_q^2$			
Dawson [31]		ex.	N/A	$M_V \ll E_q$	
Godbole [67]	$x \equiv k^0/E_q, \quad \mathcal{W}^2 = xs$	exact			$k_\perp^2 \simeq 0$
Capdequi [68]					
Lindfors [33]	$x \equiv \mathcal{W}^2/s$	exact			exact
Johnson [65]					

Author(s)	Assumptions about off-shell behavior, $\kappa(k^2)\hat{\sigma}_{pol}(k^2) =$
Kane [32]	$\kappa(M_V^2)\hat{\sigma}_{pol}(M_V^2)$
Abbasabadi [66]	
Dawson [31]	
Godbole [67]	
Capdequi [68]	structure funct. $\Rightarrow$ $\kappa(M_V^2)\hat{\sigma}_T(M_V^2),$ $\neq \kappa(M_V^2)\hat{\sigma}_{\overline{T},L}(M_V^2)$
Lindfors [33]	coupling like fermion: $\kappa(k^2)\hat{\sigma}_{pol}(k^2)\vert_{\text{ferm.}}$
Johnson [65]	from pol.-vectors: $\kappa(0)\hat{\sigma}_{T,\overline{T}}(M_V^2),$ $M_V^2/\vert k^2 \vert \kappa(0)\hat{\sigma}_L(M_V^2)$

Table 4.1: Differences of the various existing versions of vector-boson distribution-functions in the literature. The variables are defined in the text.

4.2.2 Applications of the EVBA and Comparisons with Exact Calculations

We review the use of the EVBA in the literature. The formulation of the EVBA in terms of convolutions of vector-boson distributions was applied to the production of Higgs bosons [36, 68, 71], of heavy fermions and for vector-boson scattering. The study of the latter processes was carried out in models in which $W^{\pm}$- and Z-bosons interact strongly with each other [35, 36, 72], in models with anomalous vector-boson self-couplings [40, 70], in models, which exhibit both of these features [39] and in the standard model [73].

Concerning the production of heavy fermions, comparisons with exact calculations with EVBA calculations showed that the EVBA is in good agreement with exact results [31, 65, 68, 74]. Comparisons were also carried out for the production of Higgs bosons, where the Higgs boson decays into two vector-bosons [31, 66, 67, 75, 76, 77]. On the Higgs boson resonance and for large values of the Higgs boson mass, $M_H > 600$ GeV, the EVBA could reproduce the exact results. In these cases, the contribution from longitudinally polarized intermediate vector-bosons dominates. The contribution from *transversely* polarized intermediate vector-bosons, which becomes important off the Higgs resonance and which is the dominant contribution if the Higgs boson mass is small against the vector-boson scattering energy, could not be predicted by the EVBA reliably. The EVBA overestimated the exact results and the discrepancy grew if the Higgs boson mass was decreased. In the region 300 GeV $< M_H < 600$ GeV the discrepancy could reach a factor of 2 or 3. This weakness of the EVBA could be reduced by the use of the exact vector-boson distributions [65, 78].

The EVBA in this form was still realized by convolutions of single vector-boson distributions. Also, it was not discussed whether off-diagonal terms in the helicities of the vector-bosons might play a role. From early works about the effective photon approximation it was known [64, 79] that non-diagonal terms exist. In an effort to improve the formalism of convolutions numerical results for luminosities were given [68]. Here, we will present an exact derivation of vector-boson–vector-boson luminosities which has not been given in the literature before. We will see that only approximately these luminosities can be cast into the form of convolutions of single vector-boson–distributions.

4.3 Formulation of an Improved Effective Vector Boson Approximation

4.3.1 Derivation of the Improved Luminosities

We derive expressions for improved luminosities for a vector-boson pair in a fermion-pair and present numerical results.

We consider the production of an arbitrary state W in the scattering process of two fermions q_1 and q_2, in which also the two fermions q_1' and q_2' are produced, see Figure 4.3,

$$q_1(l_1) + q_2(l_2) \rightarrow q_1'(l_1') + q_2'(l_2') + W(p_W). \tag{4.17}$$

The four-momenta of the incoming and outgoing fermions are denoted by l_1, l_2 and l_1', l_2', respectively, and the total center-of-mass energy squared is given by $s = (l_1 + l_2)^2$. The final state W, which may contain any number of particles, has four-momentum p_W and
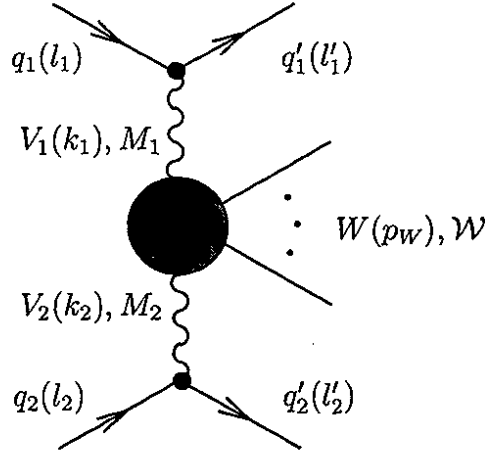
Figure 4.3: The contribution of vector-boson scattering to the scattering process $q_1 q_2 \rightarrow q_1' q_2' W$.

its invariant mass squared will be denoted by $\mathcal{W}^2 = p_W^2$. The cross-section for the process (4.17) is given by

$$\sigma_{qq} = \frac{1}{2s}\frac{1}{(2\pi)^2} \int \frac{d^3 l_1'}{2l_1'^0} \int \frac{d^3 l_2'}{2l_2'^0} \int d\rho_W \overline{|\mathcal{M}_{qq}|^2} \delta^{(4)}(l_1 + l_2 - l_1' - l_2' - p_W). \qquad (4.18)$$

In (4.18), $\overline{|\mathcal{M}_{qq}|^2}$ is the squared amplitude for the two-fermion initiated process, averaged and summed over helicities and $d\rho_W$ is the phase space element for the state W.

For high energies $\sqrt{s}$ one can neglect the masses of the fermions[3]. With the help of the momentum transfers $k_j = l_j - l_j'$, $j = 1, 2$ and using the dimensionless variables

$$x \equiv \frac{\mathcal{W}^2}{s}, \qquad z \equiv \frac{M_X^2}{s}, \qquad \text{with} \quad M_X^2 \equiv (p_W + l_2')^2, \qquad (4.19)$$

as well as

$$K_2^2 = \frac{1}{1 - \frac{k_1^2}{M_X^2}} k_2^2, \qquad (4.20)$$

one can parametrize the phase space by

$$\begin{aligned} \sigma_{qq} &= \frac{1}{32s} \int\limits_{x_0}^{1} dx \int\limits_{x}^{1} \frac{dz}{z} \int\limits_{-s(1-z)}^{0} dk_1^2 \int\limits_{-sz(1-x/z)}^{0} dK_2^2 \int\limits_{0}^{2\pi} \frac{d\varphi_1}{2\pi} \int\limits_{0}^{2\pi} \frac{d\varphi_2}{2\pi} \\ &\quad \cdot \int d\rho_W \overline{|\mathcal{M}_{qq}|^2} \delta^{(4)}(l_1 + l_2 - l_1' - l_2' - p_W) \end{aligned} \qquad (4.21)$$

Here, $x_0 = \mathcal{W}_0^2/s$ is the minimal value of the invariant mass squared of the final state W normalized to the total center-of-mass energy. In case of an n-particle final state, $\mathcal{W}_0$ is equal to the sum of the masses of these particles. φ_1 and φ_2 are azimuthal angles for the

---

[3]This is not possible in the case of photons as vector-bosons. Photons will be treated approximately below (see Chapters 5 and 7).

momenta l_1' and l_2', respectively, defined in the Breit systems B_1 and B_2 in which either the four-momentum k_1 or k_2 has only a non-vanishing z-component. The definition of the Breit systems is given in Appendix A.1.

The process is assumed to proceed via the vector-boson scattering mechanism, as shown in Figure 4.3. We write down the cross-section for the production of fermions q_1' and q_2' of unspecified type, i.e. a sum over all possible fermion types q_1' and q_2' is taken. This cross-section can be expressed alternatively as a sum over V_1 and V_2,

$$\sum_{q_1',q_2'} \sigma(q_1 q_2 \rightarrow q_1' q_2' W) = \sum_{V_1,V_2} \sigma(q_1 q_2 \rightarrow q_1' q_2' (V_1 V_2 \rightarrow W)), \qquad (4.22)$$

where the sum runs over all vector-bosons V_j, which can couple to the fermions q_j. On the right hand side of Eq. (4.22) the type of the fermions q_j' is determined by the type of q_j and V_j. Our treatment neglects interference-terms which appear if the fermion-pair q_1', q_2' is the same one for different types of the vector-boson–pair V_1, V_2. There are two types of those interference terms,

1. The fermion-pair is identical in the same order, i.e. $q_1' \rightarrow q_1'$ and $q_2' \rightarrow q_2'$ if $V_1 \rightarrow V_1'$ and $V_2 \rightarrow V_2'$. In this case, interference-terms between exchanged γ- and Z-bosons appear. These terms are small, although not always very small (see e.g. [68] for a discussion). We will not treat these terms here.

2. The particles are identical if their order is exchanged, i.e. $q_1' \leftrightarrow q_2'$. These terms are very small, because the two interfering diagrams have sharp maxima in different regions of the q_1', q_2'-phase-space. This has been discussed in [77].

We note that our formalism can be easily extended to include the interference terms.

If the process proceeds via a particular vector-boson pair V_1, V_2 according to Figure 4.3, the expression for the amplitude $\mathcal{M}_{qq}$ in (4.21) is given by

$$\mathcal{M}_{qq} = e^2 \sum_{m,n=-1}^{1} (-1)^{m+n} \frac{j_1(l_1, l_1') \cdot \epsilon_1^*(m)}{k_1^2 - M_1^2} \frac{j_2(l_2, l_2') \cdot \epsilon_2^*(n)}{k_2^2 - M_2^2} \mathcal{M}(m, n), \qquad (4.23)$$

where the $\epsilon_j(m)$ are polarization vectors for the vector-boson V_j with mass M_j and helicity $m = 0, \pm 1$ in the center-of-mass system C of the vector-bosons. The $j_j(l_j, l_j')$ are fermionic current four-vectors and $\mathcal{M}(m, n)$ is the amplitude for the production of the final state W in the scattering process of the vector-bosons V_1 and V_2 with helicities m and n, respectively. The amplitudes $\mathcal{M}(m, n)$ must be evaluated at off-shell values of k_1^2 and k_2^2. The polarization vectors are normalized according to

$$\epsilon_j(m) \cdot \epsilon_j^*(m') = \delta_{m,m'}(-1)^m, \qquad j = 1, 2, \qquad (4.24)$$

and they satisfy the completeness relation

$$\sum_{m=-1}^{1} \epsilon_j^\mu(m) \epsilon_j^{*\nu}(m) = -g^{\mu\nu} + \frac{k_j^\mu k_j^\nu}{M_j^2}, \qquad \text{(no sum on } j\text{)}. \qquad (4.25)$$

The right hand side of this equation is identical with the numerator of the propagator for a vector-boson in the unitary gauge.

The expression for the squared amplitude, averaged over the spin states of the initial state fermions and summed over the spins of the final state fermions is

$$\overline{|\mathcal{M}_{qq}|^2} = 4\,e^4 \sum_{m,m',n,n'=-1}^{1} (-1)^{m+m'+n+n'} \frac{\tilde{T}_1(m,m')}{(k_1^2 - M_1^2)^2} \frac{\tilde{T}_2(n,n')}{(k_2^2 - M_2^2)^2}$$

$$\cdot \mathcal{M}(m,n)\mathcal{M}^*(m',n'), \tag{4.26}$$

with the fermionic tensors,

$$\tilde{T}_j(m,m') = \frac{1}{4}\sum_{pol} j_j(l_j,l_j') \cdot \epsilon_j^*(m) j_j^*(l_j,l_j') \cdot \epsilon_j(m'). \tag{4.27}$$

The tensor $\tilde{T}_j(m,m')$ can be decomposed into two parts with different combinations of the vector and axial-vector coupling constants v_j and a_j of the vector bosons V_j by the relation

$$\tilde{T}_j(m,m') = (v_j^2 + a_j^2)\tilde{C}_j(m,m') + 2v_j a_j \tilde{S}_j(m,m'). \tag{4.28}$$

The tensors $\tilde{C}_j(m,m')$ and $\tilde{S}_j(m,m')$ are given by

$$\tilde{C}_j(m,m') = l_j' \cdot \epsilon_j^*(m) l_j \cdot \epsilon_j(m') + l_j' \cdot \epsilon_j(m') l_j \cdot \epsilon_j^*(m) - l_j' \cdot l_j \epsilon_j^*(m) \cdot \epsilon_j(m') \tag{4.29}$$

and

$$\tilde{S}_j(m,m') = i\epsilon_{\alpha\beta\gamma\delta} l_j'^{\,\alpha} \epsilon_j^{\beta*}(m) l_j^\gamma \epsilon_j^\delta(m'), \tag{4.30}$$

with $\epsilon_{0123} = 1$. They are tensors in helicity space.

The φ_2-dependence of the tensor components of $\tilde{C}_j(m,m')$ and $\tilde{S}_j(m,m')$ appears in terms of simple exponential functions. Factorizing these functions, we define φ_2-independent tensors $C_j(m,m')$ and $S_j(m,m')$:

$$\begin{aligned}
\tilde{C}_1(m,m') &= C_1(m,m')e^{i(m-m')\varphi_2}, \\
\tilde{S}_1(m,m') &= S_1(m,m')e^{i(m-m')\varphi_2}, \\
\tilde{C}_2(n,n') &= C_2(n,n')e^{-i(n-n')\varphi_2}, \\
\tilde{S}_2(n,n') &= S_2(n,n')e^{-i(n-n')\varphi_2},
\end{aligned} \tag{4.31}$$

for which the following relations hold:

$$\begin{aligned}
C_j(m',m) &= C_j^*(m,m'), \\
S_j(m',m) &= S_j^*(m,m'), \\
C_j(-m',-m) &= (-1)^{m+m'}C_j(m,m'), \\
S_j(-m',-m) &= -(-1)^{m+m'}S_j(m,m').
\end{aligned} \tag{4.32}$$

The last relation in (4.32) implies

$$\begin{aligned}
S_j(+-) &= 0 \quad \text{and} \\
S_j(00) &= 0.
\end{aligned} \tag{4.33}$$

Consequently, $C_j(++)$, $C_j(00)$, $C_j(+-)$ and $C_j(+0)$ can be chosen as the 2×4 independent components of $C_j(m,m')$ and the $S_j(m,m')$ have the 2×2 independent components $S_j(++)$

and $\mathcal{S}_j(+0)$. We illustrate this situation by writing down $\tilde{\mathcal{C}}_1(m, m')$ and $\tilde{\mathcal{S}}_1(m, m')$ in matrix form:

$$\tilde{\mathcal{C}}_1(m, m') = \begin{pmatrix} \mathcal{C}_1(++) & \mathcal{C}_1^*(+0)e^{-i\varphi_2} & \mathcal{C}_1^*(+-)e^{-2i\varphi_2} \\ \mathcal{C}_1(+0)e^{i\varphi_2} & \mathcal{C}_1(00) & -\mathcal{C}_1^*(+0)e^{-i\varphi_2} \\ \mathcal{C}_1(+-)e^{2i\varphi_2} & -\mathcal{C}_1(+0)e^{i\varphi_2} & \mathcal{C}_1(++) \end{pmatrix} \tag{4.34}$$

and

$$\tilde{\mathcal{S}}_1(m, m') = \begin{pmatrix} \mathcal{S}_1(++) & \mathcal{S}_1^*(+0)e^{-i\varphi_2} & 0 \\ \mathcal{S}_1(+0)e^{i\varphi_2} & 0 & \mathcal{S}_1^*(+0)e^{-i\varphi_2} \\ 0 & \mathcal{S}_1(+0)e^{i\varphi_2} & -\mathcal{S}_1(++) \end{pmatrix}, \tag{4.35}$$

where the columns from left to right correspond to $m = +, 0, -$ and the rows from top to bottom to $m' = +, 0, -$. Expressions for the independent components in terms of the integration variables in (4.21) are given in Appendix A. Similar decompositions can be obtained for $\tilde{\mathcal{C}}_2(m, m')$ and $\tilde{\mathcal{S}}_2(m, m')$. The corresponding expressions are also given in Appendix A. The quantities $\mathcal{C}_2(m, m')$ and $\mathcal{S}_2(m, m')$ turn out to be real.

Carrying out the integration over φ_2, altogether 19 terms in the m, m', n, n' helicity space remain, out of which nine have $h = m - m' = n - n' = 0$ (they are diagonal in the helicities of V_1 and V_2), four have $h = 1$, four have $h = -1$ and the other two have $h = 2$ and $h = -2$, resp. For the case of two-photon interactions this classification has been given in [64]. Using this decomposition, one can write the expression in Eq. (4.26) in the following way:

$$\frac{1}{2\pi} \int_0^{2\pi} d\varphi_2 \sum_{m,m',n,n'=-1}^{1} (-1)^{m+m'+n+n'} \tilde{T}_1(m, m')\tilde{T}_2(n, n')\mathcal{M}(m, n)\mathcal{M}^*(m', n')$$

$$\begin{aligned} = \; & (v_1^2 + a_1^2)(v_2^2 + a_2^2)\left(K_{TT}M_{TT} + K_{TL}M_{TL} + K_{LT}M_{LT} + K_{LL}M_{LL} \right. \\ & \left. + K_{TLTL}M_{TLTL} + K_{TTTT}M_{TTTT} - K_{TTTT}^{Im}M_{TTTT}^{Im} - K_{TLTL}^{Im}M_{TLTL}^{Im}\right) \\ & + (2v_1a_1)(2v_2a_2)\left(K_{\overline{TT}}M_{\overline{TT}} + K_{\overline{TL}\overline{TL}}M_{\overline{TL}\overline{TL}} - K_{\overline{TL}\overline{TL}}^{Im}M_{\overline{TL}\overline{TL}}^{Im}\right) \\ & + (v_1^2 + a_1^2)(2v_2a_2)\left(K_{T\overline{T}}M_{T\overline{T}} + K_{L\overline{T}}M_{L\overline{T}} + K_{TL\overline{TL}}M_{TL\overline{TL}} - K_{TL\overline{TL}}^{Im}M_{TL\overline{TL}}^{Im}\right) \\ & + (2v_1a_1)(v_2^2 + a_2^2)\left(K_{\overline{T}T}M_{\overline{T}T} + K_{\overline{T}L}M_{\overline{T}L} + K_{\overline{TL}TL}M_{\overline{TL}TL} - K_{\overline{TL}TL}^{Im}M_{\overline{TL}TL}^{Im}\right) \end{aligned} \tag{4.36}$$

$$= \sum_{pol} c_{q_1(V_1)}^{pol} c_{q_2(V_2)}^{pol} K_{pol} M_{pol}, \tag{4.37}$$

where the last line defines the notation to be used below, with *pol* being labels for the polarizations, $pol = TT, \overline{TT}$, etc. The quantities $c_{q_i(V_i)}^{pol}$ contain the fermionic coupling constants and can take on the values $c_{q_i(V_i)}^{pol} = (v_i^2 + a_i^2)$ or $c_{q_i(V_i)}^{pol} = (2v_ia_i)$, depending on the index *pol*. The quantities K_{pol}, which are five-fold differential luminosities—they depend on $\mathcal{W}^2, k_1^2, k_2^2, M_X^2$ and φ_1—are defined by

$$\begin{aligned} K_{TT} &= 4\mathcal{C}_1(++)\mathcal{C}_2(++), \\ K_{\overline{TT}} &= 4\mathcal{S}_1(++)\mathcal{S}_2(++), \\ K_{TL} &= 2\mathcal{C}_1(++)\mathcal{C}_2(00), \\ K_{LT} &= 2\mathcal{C}_1(00)\mathcal{C}_2(++), \\ K_{LL} &= \mathcal{C}_1(00)\mathcal{C}_2(00), \end{aligned}$$

$$
\begin{aligned}
K_{TLTL} &= 8Re[\mathcal{C}_1(+0)]\mathcal{C}_2(+0), \\
K_{\overline{T}L\overline{T}L} &= 8Re[\mathcal{S}_1(+0)]\mathcal{S}_2(+0), \\
K_{TTTT} &= 2Re[\mathcal{C}_1(+-)]\mathcal{C}_2(+-), \\
K_{T\overline{T}} &= 4\mathcal{C}_1(++)\mathcal{S}_2(++), \\
K_{\overline{T}T} &= 4\mathcal{S}_1(++)\mathcal{C}_2(++), \\
K_{\overline{T}L} &= 2\mathcal{S}_1(++)\mathcal{C}_2(00), \\
K_{L\overline{T}} &= 2\mathcal{C}_1(00)\mathcal{S}_2(++), \\
K_{TL\overline{T}L} &= 8Re[\mathcal{C}_1(+0)]\mathcal{S}_2(+0), \\
K_{\overline{T}LTL} &= 8Re[\mathcal{S}_1(+0)]\mathcal{C}_2(+0), \\
K_{TL\overline{T}L}^{Im} &= 8Im[\mathcal{C}_1(+0)]\mathcal{S}_2(+0), \\
K_{\overline{T}LTL}^{Im} &= 8Im[\mathcal{S}_1(+0)]\mathcal{C}_2(+0), \\
K_{TLTL}^{Im} &= 8Im[\mathcal{C}_1(+0)]\mathcal{C}_2(+0), \\
K_{\overline{T}L\overline{T}L}^{Im} &= 8Im[\mathcal{S}_1(+0)]\mathcal{S}_2(+0), \\
K_{TTTT}^{Im} &= 2Im[\mathcal{C}_1(+-)]\mathcal{C}_2(+-),
\end{aligned}
\tag{4.38}
$$

with $\mathcal{C}_j(m, m')$ and $\mathcal{S}_j(m, m')$ from (4.31). The averaged sums of products of amplitudes for the vector-boson scattering processes, M_{pol}, to be simply called squared amplitudes in the following, are defined through

$$
\begin{aligned}
M_{TT} &= \frac{1}{4}(|\mathcal{M}(++)|^2 + |\mathcal{M}(--)|^2 + |\mathcal{M}(+-)|^2 + |\mathcal{M}(-+)|^2), \\
M_{\overline{TT}} &= \frac{1}{4}(|\mathcal{M}(++)|^2 + |\mathcal{M}(--)|^2 - |\mathcal{M}(+-)|^2 - |\mathcal{M}(-+)|^2), \\
M_{TL} &= \frac{1}{2}(|\mathcal{M}(+0)|^2 + |\mathcal{M}(-0)|^2), \\
M_{LT} &= \frac{1}{2}(|\mathcal{M}(0+)|^2 + |\mathcal{M}(0-)|^2), \\
M_{LL} &= |\mathcal{M}(00)|^2, \\
M_{TLTL} &= \frac{1}{4}Re[\mathcal{M}(++)\mathcal{M}^*(00) + \mathcal{M}(--)\mathcal{M}^*(00) \\
&\quad -\mathcal{M}(+0)\mathcal{M}^*(0-) - \mathcal{M}(-0)\mathcal{M}^*(0+)], \\
M_{\overline{T}L\overline{T}L} &= \frac{1}{4}Re[\mathcal{M}(++)\mathcal{M}^*(00) + \mathcal{M}(--)\mathcal{M}^*(00) \\
&\quad +\mathcal{M}(+0)\mathcal{M}^*(0-) + \mathcal{M}(-0)\mathcal{M}^*(0+)], \\
M_{TTTT} &= Re[\mathcal{M}(++)\mathcal{M}^*(--)], \\
M_{T\overline{T}} &= \frac{1}{4}(|\mathcal{M}(++)|^2 - |\mathcal{M}(--)|^2 - |\mathcal{M}(+-)|^2 + |\mathcal{M}(-+)|^2), \\
M_{\overline{T}T} &= \frac{1}{4}(|\mathcal{M}(++)|^2 - |\mathcal{M}(--)|^2 + |\mathcal{M}(+-)|^2 - |\mathcal{M}(-+)|^2), \\
M_{\overline{T}L} &= \frac{1}{2}(|\mathcal{M}(+0)|^2 - |\mathcal{M}(-0)|^2), \\
M_{L\overline{T}} &= \frac{1}{2}(|\mathcal{M}(0+)|^2 - |\mathcal{M}(0-)|^2), \\
M_{TL\overline{T}L} &= \frac{1}{4}Re[\mathcal{M}(++)\mathcal{M}^*(00) - \mathcal{M}(--)\mathcal{M}^*(00) \\
&\quad +\mathcal{M}(+0)\mathcal{M}^*(0-) - \mathcal{M}(-0)\mathcal{M}^*(0+)], \\
M_{\overline{T}LTL} &= \frac{1}{4}Re[\mathcal{M}(++)\mathcal{M}^*(00) - \mathcal{M}(--)\mathcal{M}^*(00) \\
&\quad -\mathcal{M}(+0)\mathcal{M}^*(0-) + \mathcal{M}(-0)\mathcal{M}^*(0+)], \\
M_{TL\overline{T}L}^{Im} &= \frac{1}{4}Im[\mathcal{M}(++)\mathcal{M}^*(00) + \mathcal{M}(--)\mathcal{M}^*(00) \\
&\quad +\mathcal{M}(+0)\mathcal{M}^*(0-) + \mathcal{M}(-0)\mathcal{M}^*(0+)],
\end{aligned}
$$

$$
\begin{aligned}
M_{\overline{T}LTL}^{Im} &= \frac{1}{4}Im[\mathcal{M}(++)\mathcal{M}^*(00) + \mathcal{M}(--)\mathcal{M}^*(00) \\
&\quad -\mathcal{M}(+0)\mathcal{M}^*(0-) - \mathcal{M}(-0)\mathcal{M}^*(0+)], \\
M_{TLTL}^{Im} &= \frac{1}{4}Im[\mathcal{M}(++)\mathcal{M}^*(00) - \mathcal{M}(--)\mathcal{M}^*(00) \\
&\quad -\mathcal{M}(+0)\mathcal{M}^*(0-) + \mathcal{M}(-0)\mathcal{M}^*(0+)], \\
M_{\overline{T}L\overline{T}L}^{Im} &= \frac{1}{4}Im[\mathcal{M}(++)\mathcal{M}^*(00) - \mathcal{M}(--)\mathcal{M}^*(00) \\
&\quad +\mathcal{M}(+0)\mathcal{M}^*(0-) - \mathcal{M}(-0)\mathcal{M}^*(0+)], \\
M_{T\overline{T}T\overline{T}}^{Im} &= Im[\mathcal{M}(++)\mathcal{M}^*(--)].
\end{aligned} \tag{4.39}
$$

The squared amplitudes

$$
M_{T\overline{T}}, M_{\overline{T}T}, M_{\overline{T}L}, M_{L\overline{T}}, M_{TL\overline{T}L}, M_{\overline{T}LTL}, M_{\overline{T}L\overline{T}L}^{Im}, M_{TLTL}^{Im} \tag{4.40}
$$

vanish if both the interaction responsible for the transition $V_1 V_2 \to W$ is parity conserving and a summation over the polarization states of the final state W is performed. Thus they vanish if $\mathcal{M}(m,n) = \mathcal{M}(-m,-n)$. The luminosities K_{pol}^{Im} vanish after integrating over the azimuthal angle φ_1. We also note that the squared amplitudes M_{pol}^{Im} are zero if all amplitudes $\mathcal{M}(m,n)$ can be chosen as real numbers. Therefore we restrict the following discussion to the remaining eight luminosities

$$
K_{TT}, K_{\overline{T}T}, K_{TL}, K_{LT}, K_{LL}, K_{TLTL}, K_{\overline{T}L\overline{T}L}, K_{T\overline{T}T\overline{T}}. \tag{4.41}
$$

The expression Eq. (4.37) shows explicitly the trivial factorization of the cross-section into parts describing the vector-boson emission from the incoming fermions and parts pertaining to the vector-boson vector-boson scattering. These latter pieces, combined with the phase space integral for the final state W, can be interpreted as cross-sections and correlations for virtual vector-boson scattering processes:

$$
\sigma_{pol}(\mathcal{W}^2; k_1^2, k_2^2) = (2\pi)^4 \frac{1}{2\kappa} \int d\rho_W M_{pol}\delta^{(4)}(k_1 + k_2 - p_W). \tag{4.42}
$$

In Eq. (4.42) we included a 'flux-factor' κ. Its presence ensures that for on-shell vector-boson scattering, σ_{pol} in Eq. (4.42) is indeed a cross-section. In this case one has $\kappa \to \kappa_0$ with

$$
\kappa_0 = \sqrt{\mathcal{W}^4 + M_1^4 + M_2^4 - 2\mathcal{W}^2 M_1^2 - 2\mathcal{W}^2 M_2^2 - 2M_1^2 M_2^2}, \tag{4.43}
$$

where $\mathcal{W}^4 \equiv (\mathcal{W}^2)^2$. The specific form of κ for off-shell bosons in (4.42) is irrelevant since only the combination $\kappa\,\sigma_{pol}$ appears in the expression for the fermion-fermion cross-section.

In terms of the cross-sections (4.42) for virtual vector-boson scattering, the cross-section (4.21) for the two-fermion initiated process is given by

$$
\begin{aligned}
\sigma_{qq} &= \left(\frac{\alpha}{2\pi}\right)^2 \int_{x_0}^1 dx \int_x^1 \frac{dz}{z} \int_{-s(1-z)}^0 dk_1^2 \int_{-zs(1-\frac{x}{z})}^0 dK_2^2 \frac{1}{(k_1^2 - M_1^2)^2} \frac{1}{(k_2^2 - M_2^2)^2} \\
&\quad \cdot \int_0^{2\pi} \frac{d\varphi_1}{2\pi} \kappa \sum_{pol} c_{q_1(V_1)}^{pol} c_{q_2(V_2)}^{pol} K_{pol}\,\sigma_{pol}(\mathcal{W}^2; k_1^2, k_2^2),
\end{aligned} \tag{4.44}
$$

where α is the fine structure constant.

Up to this point, the calculation has been an exact evaluation of a given Feynman diagram. The basic assumption of the equivalent vector boson method concerns the dependence of the off-shell cross-sections $\sigma_{pol}(\mathcal{W}^2; k_1^2, k_2^2)$ on the off-shell masses k_i^2. For transverse polarization it is certainly a good approximation to identify $\sigma_{TT}(\mathcal{W}^2; k_1^2, k_2^2)$ with its on-shell value $\sigma_{TT}(\mathcal{W}^2; M_1^2, M_2^2)$. However, for longitudinal polarizations, $\sigma_{pol}(\mathcal{W}^2; k_1^2, k_2^2)$ contains kinematic singularities at $k_1^2 = 0$ and $k_2^2 = 0$, as can be seen from the explicit form of the polarization vectors given in Appendix A.2. Therefore, for longitudinal polarization, the resulting factors M_i^2/k_i^2 should be taken into account explicitly.

For the extrapolation to virtual masses we introduce simple proportionality factors,

$$P_{pol}(\mathcal{W}^2; k_1^2, k_2^2) \quad \text{with} \quad P_{pol}(\mathcal{W}^2; M_1^2, M_2^2) = 1, \tag{4.45}$$

and write

$$\kappa\, \sigma_{pol}(\mathcal{W}^2; k_1^2, k_2^2) = \kappa_0\, P_{pol}(\mathcal{W}^2; k_1^2, k_2^2)\, \sigma_{pol}(\mathcal{W}^2; M_1^2, M_2^2), \tag{4.46}$$

where $\sigma_{pol}(\mathcal{W}^2; M_1^2, M_2^2)$ are the cross-sections for on-shell vector-boson scattering evaluated at the rescaled energy squared $\mathcal{W}^2 = (k_1+k_2)^2 = xs$ of the vector-boson vector-boson scattering process.

To describe the k_j^2-dependence of the off-shell cross-sections, we will consider the following specific forms of the proportionality factors P_{pol} which take into account the k_j^2-dependence of the longitudinal polarization vectors $\epsilon_j(0)$:

$$P_{TT} = P_{\overline{T}\overline{T}} = P_{TTTT} = 1,$$
$$P_{TL} = \frac{M_2^2}{-k_2^2},$$
$$P_{LT} = \frac{M_1^2}{-k_1^2},$$
$$P_{LL} = \frac{M_1^2}{-k_1^2}\frac{M_2^2}{-k_2^2},$$
$$P_{TLTL} = P_{\overline{T}L\overline{T}L} = \frac{M_1}{\sqrt{-k_1^2}}\frac{M_2}{\sqrt{-k_2^2}}. \tag{4.47}$$

We now introduce luminosities $\mathcal{L}_{pol}(x)$ which are differential in the variable x, writing the differential cross-section in the form

$$\frac{d\sigma_{qq}}{dx} = \sum_{pol} \mathcal{L}_{V_1,V_2,pol}^{q_1 q_2}(x)\, \sigma_{pol}(xs; M_1^2, M_2^2), \tag{4.48}$$

with the luminosities,

$$\mathcal{L}_{V_1,V_2,pol}^{q_1 q_2}(x) = \left(\frac{\alpha}{2\pi}\right)^2 \frac{\kappa_0}{s} c_{q_1(V_1)}^{pol} c_{q_2(V_2)}^{pol} \int_x^1 \frac{dz}{z} \mathcal{L}_{pol}\left(x, z, \frac{M_1^2}{s}, \frac{M_2^2}{s}\right). \tag{4.49}$$

In (4.49) the quantities

$$\mathcal{L}_{pol}\left(x, z, \frac{M_1^2}{s}, \frac{M_2^2}{s}\right) = \int\limits_{-s(1-z)}^{0} dk_1^2 \int\limits_{-sz(1-\frac{x}{z})}^{0} dK_2^2 \frac{1}{(k_1^2 - M_1^2)^2} \frac{1}{(k_2^2 - M_1^2)^2} \int\limits_0^{2\pi} \frac{d\varphi_1}{2\pi} P_{pol}\, K_{pol} \tag{4.50}$$

are "amputated" differential luminosities, which do not anymore contain the fermionic coupling constants. They depend on the variables x and z, and, since they are dimensionless, on the masses of the vector-bosons via the ratios M_1^2/s und M_2^2/s. The quantity

$\mathcal{L}_{V_1,V_2,pol}^{q_1 q_2}(x)\,dx$ is the probability that a vector-boson–pair V_1, V_2 with specified polarization and with center-of-mass energy in the interval $[xs, (x + dx)s]$ is emitted from the fermion pair q_1 and q_2, where V_1 is emitted from q_1 and V_2 from q_2.

We evaluate the expressions (4.49) adopting the forms (4.47) for the behavior of the virtual cross-sections. No other assumptions are made. We rewrite the phase space integral in (4.49) in the following way,

$$\int\limits_x^1 \frac{dz}{z} \int\limits_{-s(1-z)}^0 dk_1^2 \int\limits_{-sz(1-x/z)}^0 dK_2^2 \int\limits_0^{2\pi} \frac{d\varphi_1}{2\pi} = \int\limits_{-s+\mathcal{W}_1^2}^0 dk_1^2 \int\limits_{-s+\mathcal{W}_2^2}^0 dk_2^2 \int\limits_{\hat{x}s}^s \frac{d\mu_X}{\mu_X} \int\limits_0^{2\pi} \frac{d\varphi_1}{2\pi}, \qquad (4.51)$$

where we have introduced the variables

$$\begin{aligned}
\mathcal{W}_1^2 &\equiv \mathcal{W}^2, \\
\mathcal{W}_2^2 &\equiv \mathcal{W}^2 \frac{s}{s + k_1^2}, \\
\hat{x} &\equiv (\nu + K\mathcal{W})/s, \\
\mu_X &\equiv M_X^2 - k_1^2.
\end{aligned} \qquad (4.52)$$

In the definition of $\hat{x}$ in (4.52), we introduced the variables

$$\begin{aligned}
\nu &\equiv k_1 \cdot k_2 = \frac{1}{2}(\mathcal{W}^2 - k_1^2 - k_2^2), \\
K &\equiv \kappa/(2\mathcal{W}),
\end{aligned} \qquad (4.53)$$

and we used the variable $\mathcal{W} = \sqrt{\mathcal{W}^2}$. The variable K in (4.53) is the magnitude of the three-momentum of the vector-bosons V_1, V_2 in their center-of-mass frame and κ is defined by

$$\kappa \equiv \sqrt{\mathcal{W}^4 + k_1^4 + k_2^4 - 2\mathcal{W}^2 k_1^2 - 2\mathcal{W}^2 k_2^2 - 2k_1^2 k_2^2}. \qquad (4.54)$$

The integration limits for k_1^2 and k_2^2 in (4.51) follow from the requirement $(k_1^2+s)(k_2^2+s) > \mathcal{W}^2 s$ with $k_1^2 < 0$ and $k_2^2 < 0$. The luminosities vanish for $x < (M_1 + M_2)^2/s$.

Using Eq. (4.51), the expressions (4.49) for the luminosities become

$$\mathcal{L}_{V_1,V_2,pol}^{q_1 q_2}(x) = \left(\frac{\alpha}{2\pi}\right)^2 \frac{\kappa_0}{s} c_{q_1(V_1)}^{pol} c_{q_2(V_2)}^{pol} \int\limits_{-s+\mathcal{W}_1^2}^0 dk_1^2 \int\limits_{-s+\mathcal{W}_2^2}^0 dk_2^2 \frac{k_1^2}{(k_1^2 - M_1^2)^2} \frac{k_2^2}{(k_2^2 - M_2^2)^2} P_{pol} J_{pol}, \qquad (4.55)$$

with the triple-differential luminosities—they are functions of x, k_1^2 and k_2^2—

$$J_{pol} = \frac{1}{k_1^2 k_2^2} \int\limits_{\hat{x}s}^s \frac{d\mu_X}{\mu_X} \int\limits_0^{2\pi} \frac{d\varphi_1}{2\pi} K_{pol}, \qquad (4.56)$$

and K_{pol} were defined in (4.38). The integrations over z and φ_1 in (4.56) can be performed analytically and the results are given in (4.59). We will discuss later which limiting cases will lead to results already obtained in the literature.

The singularities of the integrands in Eq. (4.55) at $k_j^2 = M_j^2$ lead, after integration, to mass singular terms. In the high-energy limit $s \gg M_j^2$ they appear either as familiar logarithms $\ln(s/M_j^2)$, or as a pole singularity $1/M_j^2$. The latter happens, e.g., for both masses for the LL-term, or in one of the masses for the TL and LT-luminosities. Since we will evaluate the two-dimensional integration over k_1^2 and k_2^2 in (4.55) numerically,

specific care has to be taken of these singularities. This is done by introducing new integration variables x_j, y_j, and z_j $(j = 1, 2)$ depending on the type of the singularity. The new variables are chosen such that the integration region becomes the unit cube in two dimensions. The relations of the new variables to the k_j^2 are given by:

$$
\begin{aligned}
k_j^2 &= M_j^2 \left[1 - \left(\frac{M_j^2 + s - \mathcal{W}_j^2}{M_j^2} \right)^{x_j} \right] \\
&= M_j^2 \left[1 - \frac{M_j^2 + s - \mathcal{W}_j^2}{(s - \mathcal{W}_j^2)(1 - y_j) + M_j^2} \right] \\
&= (-s + \mathcal{W}_j^2) z_j, \qquad j = 1, 2 \, ,
\end{aligned}
\tag{4.57}
$$

and the luminosities (4.55) take on the final form

$$
\begin{aligned}
\mathcal{L}_{V_1 V_2, TT}^{q_1 q_2}(x) &= \left(\frac{\alpha}{2\pi} \right)^2 (v_1^2 + a_1^2)(v_2^2 + a_2^2) \frac{\kappa_0}{s} \ln \left(\frac{M_1^2 + s - \mathcal{W}_1^2}{M_1^2} \right) \int\limits_0^1 dx_1 \int\limits_0^1 dx_2 \\
&\quad \ln \left(\frac{M_2^2 + s - \mathcal{W}_2^2}{M_2^2} \right) \frac{k_1^2}{k_1^2 - M_1^2} \frac{k_2^2}{k_2^2 - M_2^2} J_{TT},
\end{aligned}
$$

$$
\begin{aligned}
\mathcal{L}_{V_1 V_2, \overline{TT}}^{q_1 q_2}(x) &= \left(\frac{\alpha}{2\pi} \right)^2 (2v_1 a_1)(2v_2 a_2) \frac{\kappa_0}{s} \ln \left(\frac{M_1^2 + s - \mathcal{W}_1^2}{M_1^2} \right) \int\limits_0^1 dx_1 \int\limits_0^1 dx_2 \\
&\quad \ln \left(\frac{M_2^2 + s - \mathcal{W}_2^2}{M_2^2} \right) \frac{k_1^2}{k_1^2 - M_1^2} \frac{k_2^2}{k_2^2 - M_2^2} J_{\overline{TT}},
\end{aligned}
$$

$$
\begin{aligned}
\mathcal{L}_{V_1 V_2, TL}^{q_1 q_2}(x) &= \left(\frac{\alpha}{2\pi} \right)^2 (v_1^2 + a_1^2)(v_2^2 + a_2^2) \frac{\kappa_0}{s} \ln \left(\frac{M_1^2 + s - \mathcal{W}_1^2}{M_1^2} \right) \int\limits_0^1 dx_1 \int\limits_0^1 dy_2 \\
&\quad \left(1 - \frac{M_2^2}{M_2^2 + s - \mathcal{W}_2^2} \right) \frac{k_1^2}{k_1^2 - M_1^2} J_{TL},
\end{aligned}
$$

$$
\begin{aligned}
\mathcal{L}_{V_1 V_2, LT}^{q_1 q_2}(x) &= \left(\frac{\alpha}{2\pi} \right)^2 (v_1^2 + a_1^2)(v_2^2 + a_2^2) \frac{\kappa_0}{s} \left(1 - \frac{M_1^2}{M_1^2 + s - \mathcal{W}_1^2} \right) \int\limits_0^1 dy_1 \int\limits_0^1 dx_2 \\
&\quad \ln \left(\frac{M_2^2 + s - \mathcal{W}_2^2}{M_2^2} \right) \frac{k_2^2}{k_2^2 - M_2^2} J_{LT},
\end{aligned}
$$

$$
\begin{aligned}
\mathcal{L}_{V_1 V_2, LL}^{q_1 q_2}(x) &= \left(\frac{\alpha}{2\pi} \right)^2 (v_1^2 + a_1^2)(v_2^2 + a_2^2) \frac{\kappa_0}{s} \left(1 - \frac{M_1^2}{M_1^2 + s - \mathcal{W}_1^2} \right) \int\limits_0^1 dy_1 \int\limits_0^1 dy_2 \\
&\quad \left(1 - \frac{M_2^2}{M_2^2 + s - \mathcal{W}_2^2} \right) J_{LL},
\end{aligned}
$$

$$
\begin{aligned}
\mathcal{L}_{V_1 V_2, TLTL}^{q_1 q_2}(x) &= \left(\frac{\alpha}{2\pi} \right)^2 (v_1^2 + a_1^2)(v_2^2 + a_2^2) \frac{\kappa_0}{s} M_1 M_2 \ln \left(\frac{M_1^2 + s - \mathcal{W}_1^2}{M_1^2} \right) \int\limits_0^1 dx_1 \int\limits_0^1 dx_2 \\
&\quad \ln \left(\frac{M_2^2 + s - \mathcal{W}_2^2}{M_2^2} \right) \frac{k_1^2}{k_1^2 - M_1^2} \frac{k_2^2}{k_2^2 - M_2^2} \frac{J_{TLTL}}{\sqrt{-k_1^2} \sqrt{-k_2^2}},
\end{aligned}
$$

$$
\begin{aligned}
\mathcal{L}_{V_1 V_2, \overline{TL}\,\overline{TL}}^{q_1 q_2}(x) &= \left(\frac{\alpha}{2\pi} \right)^2 (2v_1 a_1)(2v_2 a_2) \frac{\kappa_0}{s} M_1 M_2 \ln \left(\frac{M_1^2 + s - \mathcal{W}_1^2}{M_1^2} \right) \int\limits_0^1 dx_1 \int\limits_0^1 dx_2
\end{aligned}
$$

$$\ln\left(\frac{M_2^2 + s - \mathcal{W}_2^2}{M_2^2}\right) \frac{k_1^2}{k_1^2 - M_1^2} \frac{k_2^2}{k_2^2 - M_2^2} \frac{J_{\overline{T}L\overline{T}L}}{\sqrt{-k_1^2}\sqrt{-k_2^2}},$$

$$\mathcal{L}_{V_1V_2,TTTT}^{q_1q_2}(x) = \left(\frac{\alpha}{2\pi}\right)^2 (v_1^2 + a_1^2)(v_2^2 + a_2^2)\frac{\kappa_0}{s}(s - \mathcal{W}_1^2)\int_0^1 dz_1 \int_0^1 dz_2$$

$$(s - \mathcal{W}_2^2)\frac{k_1^4}{(k_1^2 - M_1^2)^2}\frac{k_2^4}{(k_2^2 - M_2^2)^2}\frac{J_{TTTT}}{k_1^2 k_2^2}, \tag{4.58}$$

and the J_{pol} are given by

$$\begin{aligned}
J_{TT} &= \frac{8}{\kappa^4}\left[(2\nu^2(s+\nu)^2 + k_1^2 k_2^2(s^2 + 8s\nu + k_1^2 k_2^2))\ln\left(\frac{1}{\hat{x}}\right) - 6s^2\nu^2 - 4s\nu^3 + 2\nu^4\right.\\
&\quad + k_1^2 k_2^2(-3s^2 + 4s\nu + 6\nu^2 + k_1^2 k_2^2)\\
&\quad \left. + K\mathcal{W}(3s^2\nu + 8s\nu^2 + 2\nu^3 + k_1^2 k_2^2(4s+\nu))\right],\\
J_{\overline{TT}} &= \frac{4}{\kappa^2}\left[(2s\nu + \nu^2 + k_1^2 k_2^2)\ln\left(\frac{1}{\hat{x}}\right) - 4s\nu + 2\nu^2 + 2k_1^2 k_2^2 + 2K\mathcal{W}(s+\nu)\right],\\
J_{TL} &= \frac{4}{\kappa^4}\left[(4s^2\nu^2 + 8s\nu^3 + 2k_1^2 k_2^2(s^2 + 8s\nu + 3\nu^2))\ln\left(\frac{1}{\hat{x}}\right) - 13s^2\nu^2 - 4s\nu^3\right.\\
&\quad + 2\nu^4 + k_1^2 k_2^2(-5s^2 + 4s\nu + 13\nu^2 + 3k_1^2 k_2^2)\\
&\quad \left. + 2K\mathcal{W}(3\nu^2 + 8s\nu^2 + \nu^3 + 2k_1^2 k_2^2(2s+\nu))\right],\\
J_{LT} &= J_{TL},\\
J_{LL} &= \frac{8}{\kappa^4}\left[(2s^2\nu^2 + 4s\nu^3 + k_1^2 k_2^2(s^2 + 8s\nu + 2\nu^2 + k_1^2 k_2^2))\ln\left(\frac{1}{\hat{x}}\right) - 7s^2\nu^2\right.\\
&\quad \left. + k_1^2 k_2^2(-2s^2 + 7\nu^2 + 2k_1^2 k_2^2) + K\mathcal{W}(3s^2\nu + 8s\nu^2 + k_1^2 k_2^2(4s + 3\nu))\right],\\
J_{TLTL} &= \frac{32}{\kappa^4}\sqrt{-k_1^2}\sqrt{-k_2^2}\left[(3s^2\nu + 9s\nu^2 + \nu^3 + k_1^2 k_2^2(3s + 2\nu))\ln\left(\frac{1}{\hat{x}}\right) - \frac{\nu^2(s+\nu)}{\hat{x}}\right.\\
&\quad \left. - 8s^2\nu + 3\nu^3 + k_1^2 k_2^2(s + 6\nu) + K\mathcal{W}(2s^2 + 11s\nu + 2\nu^2 + k_1^2 k_2^2)\right],\\
J_{\overline{T}L\overline{T}L} &= \frac{8}{\kappa^2}\sqrt{-k_1^2}\sqrt{-k_2^2}\left[(s+\nu)\ln\left(\frac{1}{\hat{x}}\right) - \frac{\nu}{\hat{x}} + 2\nu - s + K\mathcal{W}\right],\\
J_{TTTT} &= \frac{4}{\kappa^4}k_1^2 k_2^2\left[(3s^2 + 12s\nu + 2\nu^2 + k_1^2 k_2^2)\ln\left(\frac{1}{\hat{x}}\right) + \frac{\nu^2}{\hat{x}^2} - \frac{5s\nu + 4\nu^2}{\hat{x}}\right.\\
&\quad \left. - 5s^2 + 4s\nu + 6\nu^2 + 3k_1^2 k_2^2 + K\mathcal{W}(8s + 3\nu)\right]. \tag{4.59}
\end{aligned}$$

For the case of two-photon processes initiated by electron-electron scattering, analogous expressions have been derived in [64]. Our results are related to the corresponding $\hat{J}_{pol}$ from [64] by $J_{pol} = \hat{J}_{pol}/x^2$ for $pol = TT$, TL and LL, $J_{TTTT} = \hat{J}_{TT}^{ex}/x^2$ and $J_{TLTL} = 2\hat{J}_{LT}^{ex}/x^2$ (note that we have neglected the fermion masses). We finally remark that, for $M_1 = M_2$, we have $\mathcal{L}_{LT}(x) = \mathcal{L}_{TL}(x)$.

The integrals in Eq. (4.58) are well-suited for numerical evaluation. Their integrands contain no singularities; instead, the poles of order one show up as logarithms of the form $\ln\left((M_j^2 + s - \mathcal{W}_j^2)/M_j^2\right)$, while the poles of order two (which would by themselves lead to a factor M_j^{-2}) have been canceled by corresponding factors M_j^2. These factors were included in our assumptions for the behaviour of the $P_{pol}(\mathcal{W}^2; k_1^2, k_2^2)$, Eq. (4.47).

Since the expressions Eq. (4.58) involve two-dimensional numerical integrations of the momentum transfers k_1^2 and k_2^2, it would be straightforward to replace the model assumptions of Eq. (4.47) by better ones if required. The contribution from the leading singularities would not change then; however, subleading terms (non-logarithmic contributions for transverse polarization, logarithmic contributions for longitudinal polarization)

are model-dependent. For the cases of Higgs production and heavy quark production, modifications of single vector-boson boson distributions following from the exact off-shell behaviour of the corresponding hard cross-sections have been studied in [80].

4.3.2   Discussion of Numerical Results

In presenting numerical results for luminosities of vector-boson pairs, we restrict ourselves to the representative case of e^+e^- annihilation. In our numerical examples we use $\alpha = 1/137$, $M_W = 80.17$ GeV and $M_Z = 91.19$ GeV. The fermion vector-boson couplings are determined using the weak mixing angle as given by $\cos\theta_W = M_W/M_Z$. We will always use these electroweak parameters also in later numerical examples of this work if not explicitly stated otherwise.

In Figs. 4.4 and 4.5 we show the exact luminosities (4.58) for finding a W^+W^- pair in an e^+e^- pair of $\sqrt{s} = 2$ TeV. The luminosity $\mathcal{L}_{TT}$ for transversely polarized $W^\pm$ is the largest one, followed by $\mathcal{L}_{TL}$ and $\mathcal{L}_{LL}$. From Fig. 3 one concludes that the non-diagonal luminosities $\mathcal{L}_{TLTL}$ and $\mathcal{L}_{TTTT}$ are smaller than the diagonal ones, however they are of the same order of magnitude. The parity violating luminosity $\mathcal{L}_{\overline{TT}}$ varies comparatively little with x at not too high x, and at higher x it becomes equal to the TT luminosity.
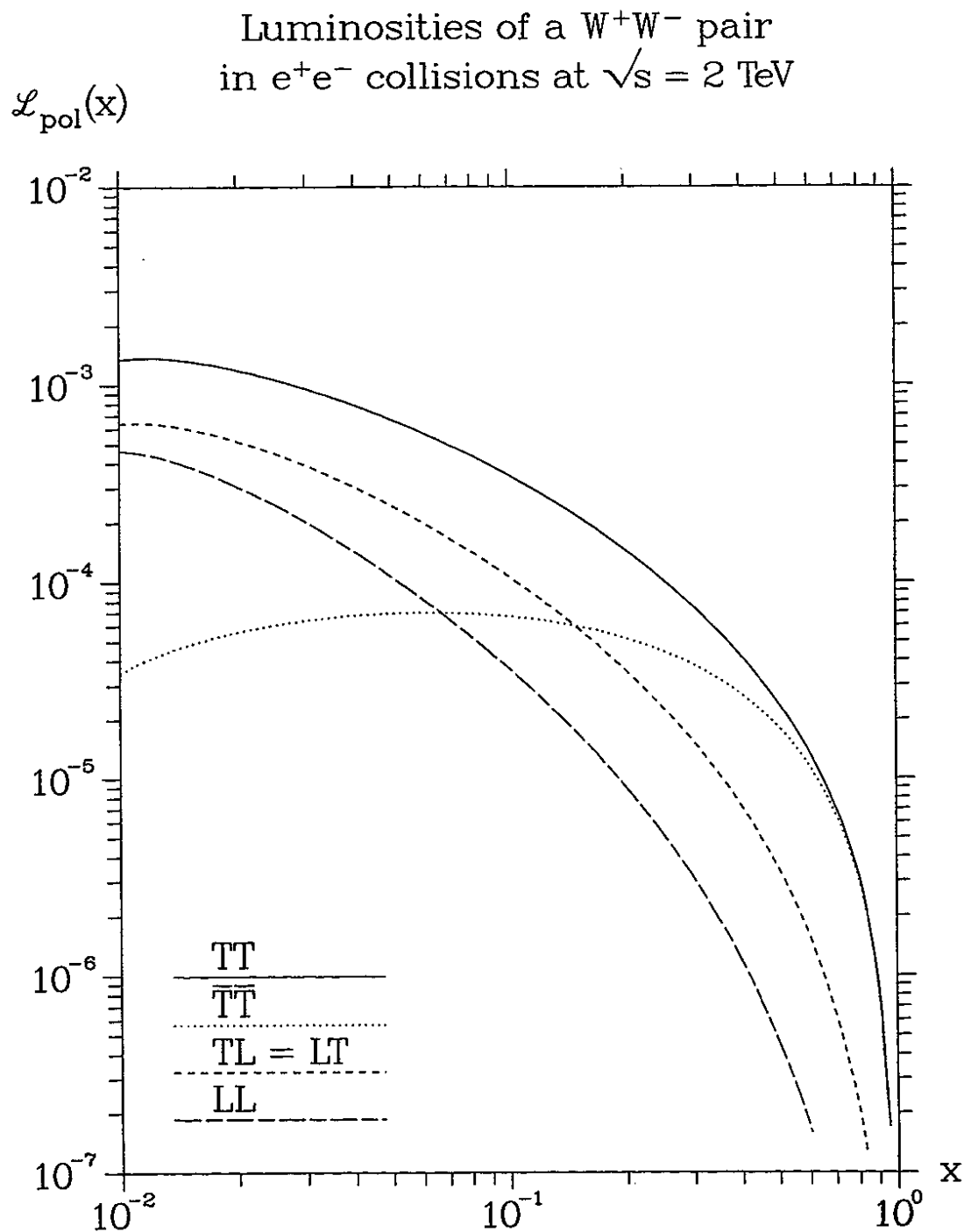
Figure 4.4: The luminosities $\mathcal{L}^{e^+e^-}_{W^+W^-,pol}(x)$, (4.58), for the diagonal helicity combinations at $\sqrt{s} = 2$ TeV.
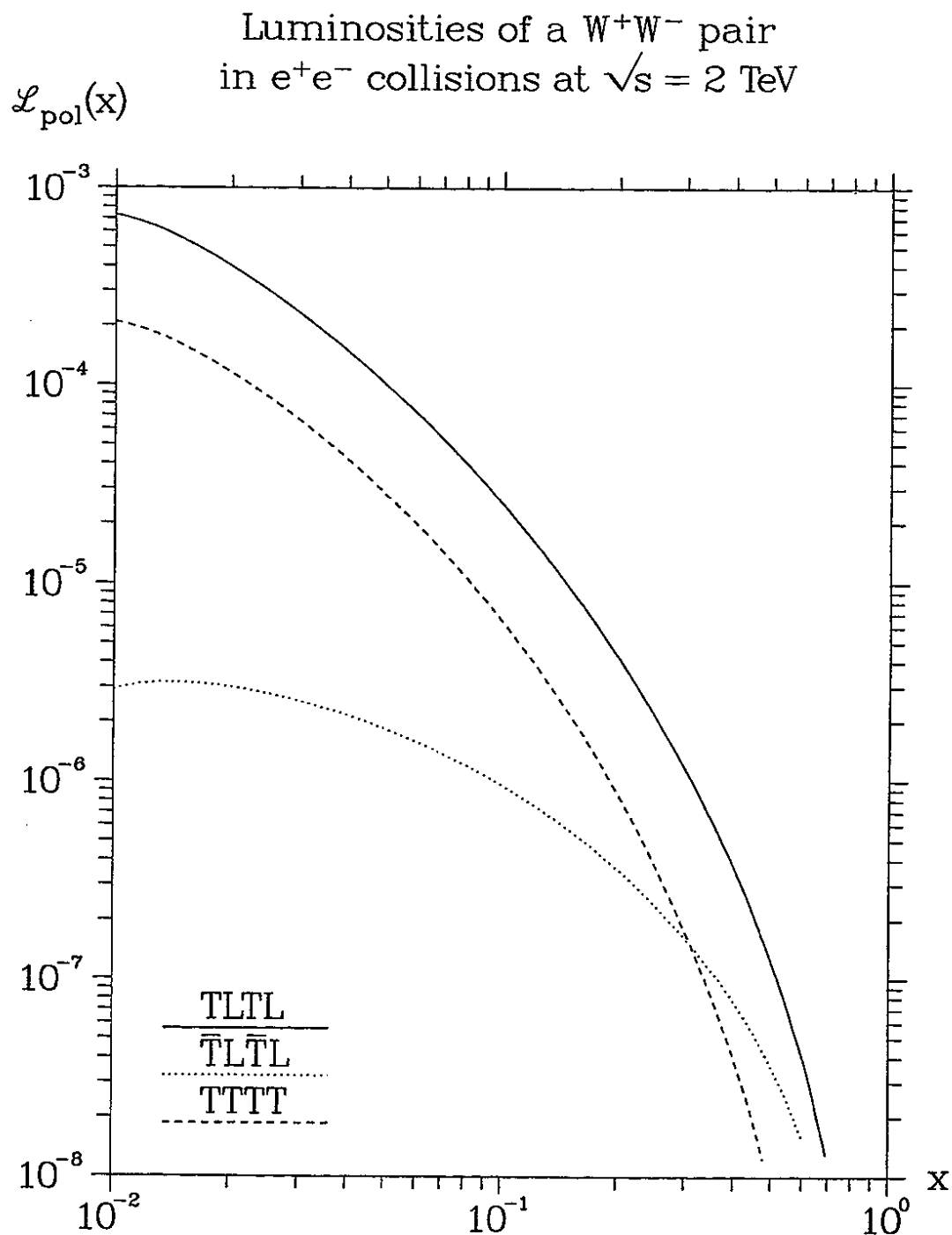
Figure 4.5: The luminosities $\mathcal{L}_{W^+W^-,pol}^{e^+e^-}(x)$, (4.58), for the non-diagonal helicity combinations at $\sqrt{s} = 2$ TeV.

4.4 Convolutions of Vector-Boson Distributions as an Approxmation to the Improved Luminosities

4.4.1 Factorization into Vector-Boson Distributions

The luminosities (4.58) can be approximately written as a convolution of single vector-boson distributions. The approximations which lead to this formulation are identified in the following.

Since helicities of massive particles are no Lorentz-invariant quantities, the polarization vectors have to be defined in a definite reference frame, which we chose to be the center-of-mass system of the two vector bosons. Therefore, the C_i and S_i depend on both momentum transfers k_1^2 and k_2^2 at the same time. This means that the emission of a vector boson V_1 with definite helicity from the fermion q_1 is not independent from the off-shell mass of the second vector boson V_2, and the two-boson luminosities do not factorize into single-boson densities. However, since at high energies the process is dominated by small momentum transfers, one can neglect this mutual dependence on k_i^2 as an approximation. Then the expressions (4.49) for the two-vector-boson luminosities reduce to convolutions of single-vector-boson densities. These single-vector-boson distributions have been reported in [65].

To be specific, we consider the following simplifications:

1. Set $k_2^2 = 0$ in $C_1(m, m')$ and $S_1(m, m')$;

2. Set $k_1^2 = 0$ in $C_2(n, n')$ and $S_2(n, n')$;

3. Set $K_2^2 = k_2^2$ in Eq. (4.50), i.e. omit the factor $(1 - k_1^2/M_X^2)^{-1}$ in the definition Eq. (4.20) of K_2^2.

Note that with the simplifications 1 and 2, the luminosities for the non-diagonal squared amplitudes, $\mathcal{L}_{TLTL}(x), \mathcal{L}_{\overline{T}L\overline{T}L}(x)$ and $\mathcal{L}_{TTTT}(x)$ vanish.

With the above simplifications the integrals over k_1^2 and K_2^2 in (4.49) can be carried out independently and the luminosities (4.49) take on the factorized form

$$\mathcal{L}^{q_1 q_2}_{V_{1,\lambda_1} V_{2,\lambda_2}}(x) = \frac{\kappa_0}{\mathcal{W}^2} \int_x^1 \frac{dz}{z} \tilde{f}^{q_1}_{V_1,\lambda_1}\left(z, \frac{M_1^2}{s}\right) \tilde{f}^{q_2}_{V_2,\lambda_2}\left(\frac{x}{z}, \frac{M_2^2}{z s}\right). \tag{4.60}$$

For the amputated differential luminosities, (4.50), one obtains the forms

$$\mathcal{L}_{\lambda_1 \lambda_2}\left(x, z, \frac{M_1^2}{s}, \frac{M_2^2}{s}\right) = h_{\lambda_1}\left(z, \frac{M_1^2}{s}\right) h_{\lambda_2}\left(\frac{x}{z}, \frac{M_2^2}{z s}\right), \tag{4.61}$$

where $\lambda_i = T, \overline{T}, L$. The functions $\tilde{f}^{q_i}_{V_i,T}, \tilde{f}^{q_i}_{V_i,\overline{T}}$ and $\tilde{f}^{q_i}_{V_i,L}$ in (4.60),

$$\tilde{f}^{q_i}_{V_i,\lambda_i}(z, \mu) = \frac{\alpha}{2\pi} z \, c^{\lambda_i}_{q_i(V_i)} h_{\lambda_i}(z, \mu), \tag{4.62}$$

are the distribution-functions of single vector-bosons in fermions from [65] and the functions $h_T, h_{\overline{T}}$ and h_L in (4.61) and (4.62) are the amputated distributions of single vector-bosons. They are of the explicit form

$$h_T(z, \mu) = \frac{1}{2} \int\limits_{-1+z}^{0} \frac{d(k^2)(-k^2)(c_0^2 + 1)}{(k^2 - \mu)^2},$$

$$h_{\overline{T}}(z,\mu) = \int\limits_{-1+z}^{0} \frac{d(k^2)\,(-k^2)\,c_0}{(k^2-\mu)^2},$$

$$h_L(z,\mu) = \frac{\mu}{2} \int\limits_{-1+z}^{0} \frac{d(k^2)\,s_0^2}{(k^2-\mu)^2}, \tag{4.63}$$

with

$$c_0 \equiv \frac{2-z+\frac{k^2}{s}}{z-\frac{k^2}{s}} \qquad \text{and} \qquad s_0 \equiv 2\frac{\sqrt{1-z+\frac{k^2}{s}}}{z-\frac{k^2}{s}}. \tag{4.64}$$

The integrals in (4.63) can be carried out analytically [65] with the result

$$\begin{aligned} h_T(z,\mu) &= h_1(z,\mu) + h_2(z,\mu), \\ h_{\overline{T}}(z,\mu) &= h_2(z,\mu) - h_1(z,\mu), \end{aligned} \tag{4.65}$$

with

$$\begin{aligned}
h_1(z,\mu) &= -\frac{(1-z)(2-\omega)}{\omega^2} + \frac{(1-\omega)(\xi-\omega^2)}{\omega^3}\ln\left(\frac{1}{\mu'}\right) \\
&\quad -\frac{\xi-2z\omega}{\omega^3}\ln\left(\frac{1}{z}\right), \\
h_2(z,\mu) &= -\frac{(1-z)(2-\omega)}{\omega^2(1-\omega)} + \frac{\xi}{\omega^3}\ln\left(\frac{z}{\mu'}\right), \\
h_L(z,\mu) &= \frac{2(1-z)\xi}{\omega^2 z} - \frac{2\mu(2-\omega)}{\omega^3}\ln\left(\frac{z}{\mu'}\right).
\end{aligned} \tag{4.66}$$

In (4.66), $\omega \equiv z-\mu$, $\xi \equiv z+\mu$ and $\mu' \equiv \mu/(1-\omega)$.

We note that a flux-factor $\kappa_0/\mathcal{W}^2$ appears in (4.60). This factor makes the luminosities vanish at $x < (M_1^2 + M_2^2)/s$. This is similar to the vanishing of the distribution-functions of single vector-bosons, [33, 65] with the correction (4.16), which vanish at at $x < M_i^2/s$.

Concerning the meaning of the variables in (4.60) and (4.61), z is the ratio of the energy of the vector-boson V_1 and the energy of the fermion q_1 if $k_1^2 = 0$. For $k_1^2 = 0$ and $k_2^2 = 0$, x/z is the ratio of the energy of the vector-boson V_2 and the one of the fermion q_2. This holds in any reference frame.

4.4.2   Symmetrization of the Convolutions

The form of the luminosities (4.61) is not invariant under the simultaneous exchange of the vector-bosons V_1 and V_2 (i.e. their masses, fermionic couplings and helicities λ_1 and λ_2) and the fermions q_1 and q_2, but it should be. The exact luminosities obey this symmetry, as can be seen from their form (4.55). The symmetry is thus broken by the simplifications introduced in 4.4.1.

The breaking of the symmetry is connected to keeping z as an integration variable in (4.61). This variable describes not only, in the case $k_1^2 = 0$, the ratio of the energy of the vector-boson V_1 and of the fermion q_1, but also, through the relation $M_X^2 = zs$, the reduced energy M_X^2 available for the scattering process, in which the fermion q_2 is involved, after V_1 has been already emitted. It thus describes a reduction of the available scattering energy for the fermions due to the emission of a vector-boson from the other

fermion. This reduction has not been taken into account in previous calculations of the luminosities as convolutions. Instead, at both vertices the full energy, $\sqrt{s}$, was admitted. This led to the expression [65]

$$\mathcal{L}_{\lambda_1\lambda_2}\left(x, z, \frac{M_1^2}{s}, \frac{M_2^2}{s}\right) = h_{\lambda_1}\left(z, \frac{M_1^2}{s}\right) h_{\lambda_2}\left(\frac{x}{z}, \frac{M_2^2}{s}\right) \tag{4.67}$$

instead of (4.61). The expression (4.67) does not violate the above symmetry. A numerical comparison of the convolutions (4.67), however, with the exact amputated luminosities (4.50), and, compared to this, a comparison of the convolutions (4.61) with (4.50) shows that the deviation of the convolutions (4.67) from the exact luminosities is much larger than for the convolutions (4.61). This is not surprising and shows the non-negligible effect of the reduction of the available energy.

We would like to obtain a symmetrized form of convolutions, derived as an approximation to the forms (4.61), which takes into account the reduction of the scattering energy. We introduce such a symmetrization by the form

$$\mathcal{L}_{\lambda_1\lambda_2}\left(x, z, \frac{M_1^2}{s}, \frac{M_2^2}{s}\right) = h_{\lambda_1}\left(z, \frac{M_1^2}{\sqrt{z}s}\right) h_{\lambda_2}\left(\frac{x}{z}, \frac{M_2^2\sqrt{z}}{\sqrt{x}s}\right). \tag{4.68}$$

The available energies for the fermion q_1 and the fermion q_2 in the form (4.68) are $\sqrt{z}s$ and $\sqrt{x}/\sqrt{z}s$, respectively. The product of these energies is $\sqrt{x}s^2$. This product must be compared to the corresponding product in (4.61), which is zs^2. It should be noted in this connection that $z = \sqrt{x}$ is a mean value for the integration variable z in (4.60).

The luminosities, using (4.68), are of the form

$$\mathcal{L}_{V_1,\lambda_1 V_2,\lambda_2}^{q_1 q_2}(x) = \frac{\kappa_0}{\mathcal{W}^2} \int_x^1 \frac{dz}{z} f_{V_1,\lambda_1}^{q_1}\left(z, \frac{M_1^2}{s}\right) f_{V_2,\lambda_2}^{q_2}\left(\frac{x}{z}, \frac{M_2^2}{s}\right), \tag{4.69}$$

instead of (4.60), with the vector-boson distributions

$$f_{V_i,\lambda_i}^{q_i}\left(z, \frac{M_V^2}{s}\right) = \frac{\alpha}{2\pi} z\, c_{q_i(V_i)}^{\lambda_i} h_{\lambda_i}\left(z, \frac{M_V^2}{\sqrt{z}s}\right). \tag{4.70}$$

We will use the expression (4.70) in the following as the distribution-function of vector-bosons in a fermion. The quantity $f_{V_i,\lambda_i}^{q_i}(z, M^2/s)$ is the probability density for the emission of a vector-boson V_i with the mass M_i and helicity λ_i from a fermion f_i with the couplings v_i and a_i. The scale variable z describes the square of the invariant mass, which remains after the emission of the vector-boson and s is the square of the invariant mass of the fermion (before the emission) and another particle (e.g. another fermion), which interacts with the fermion via the exchange of the vector-boson.

It should be noted that the distribution (4.70) is to be used only to describe processes which proceed via two intermediate vector-bosons. Processes proceeding via one intermediate vector-boson are described by the forms (4.62) with $\mu = M_V^2/s$.

We have chosen the value $\sqrt{z}s$ for the scattering energy to be inserted for a single vector-boson distribution function, where z is the energy of the vector-boson relative to the fermion from which it was emitted. A numerical comparison shows that the deviation of the convolutions (4.61) from the exact luminosities is even improved by the choice of (4.68) instead of (4.61)[4].

---

[4]The deviation for the TL and LT distributions does not decrease for all values of s and x.

We make a remark on the reference frame in which the helicities of the vector-bosons have been defined. Since k_2^2 has been neglected in describing the emission of V_1, the center-of-mass system of the two vector-bosons and the center-of-mass system of the vector-boson V_1 and the fermion q_2 are connected by a Lorentz-boost along the direction of motion of the fermion q_2. The helicities of the vector-boson V_1, originally defined in the center-of-mass system C, are therefore identical in both reference frames. The same line of thought can be applied to the emission of V_2 from q_2 and the center-of-mass system of V_2 and q_1.

Numerical Results

Figure 4.6 shows the ratio of the convolutions in the conventional formalism, (4.49) with (4.67), and the improved luminosities for a W^+W^--pair in an e^+e^--pair of $\sqrt{s} = 2$ TeV. The ratios grow with decreasing x. At $x = 10^{-1}$ the ratio amounts to approximately a factor of two for the $TT, \overline{TT}$ and $TL = LT$ luminosities. At $x = 10^{-2}$, the deviation for the TT-luminosity amounts to a factor of four. For the LL-luminosity, the ratio is closer to the value one than for any other luminosity. Figure 4.7 shows the same ratios for a scattering energy of $\sqrt{s} = 4$ TeV. This is a typical scattering energy for q_1q_2-collisions in pp collisions at 14 TeV. The ratios are smaller in this case.

Figure 4.8 shows the ratios of the improved convolutions (4.69) and the improved luminosities for a W^+W^--pair in an e^+e^--pair of $\sqrt{s} = 2$ TeV. Compared to the convolutions (4.67), the ratios are closer to the value one. This is especially true for the luminosities TT and $\overline{TT}$. The ratio is largest for the $TL(LT)$ helicities, for which it reaches a factor of 1.75 at $x = 0.01$. The same ratios are shown in Figure 4.9 for a scattering energy of $\sqrt{s} = 4$ TeV. The deviation of the TT luminosity is never greater than 36% in this case.

Concluding this section, the luminosities (4.58) can be approximated by convolutions (4.69) of distributions of single vector-bosons (4.70) if certain kinematical approximations are made. The luminosities for the non-diagonal helicity combinations vanish in this case. The numerical agreement of the convolutions (4.69) with the improved luminosities (4.58) is better than for the conventional convolutions, (4.49) with (4.67).
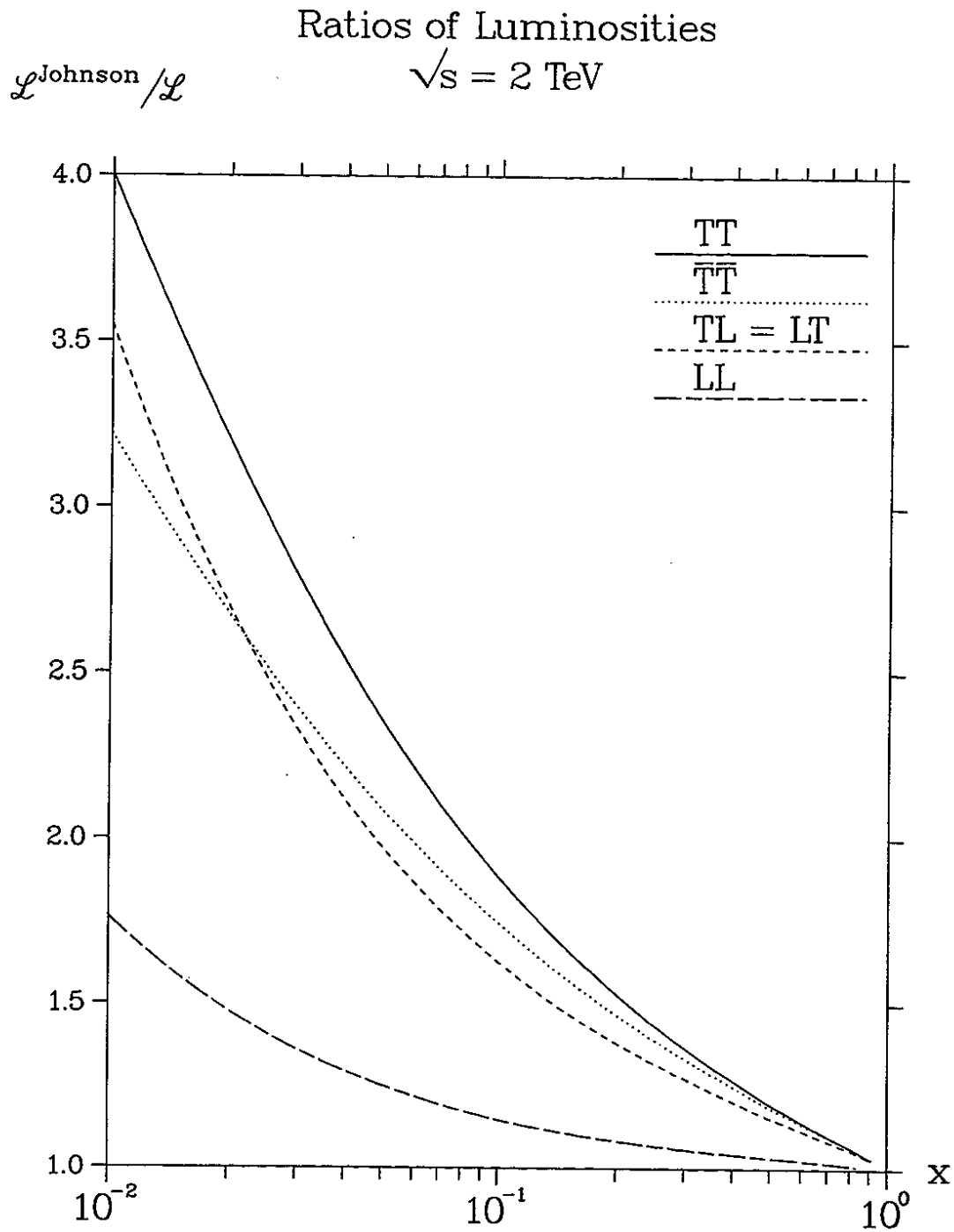
Figure 4.6: Ratios of the conventional convolutions [65] of single vector-bosons, (4.49) with (4.67), and the improved luminosities for helicities $pol = TT$, $\overline{TT}$, LT and LL for a W^+W^--pair in e^+e^- collisions at $\sqrt{s} = 2$ TeV.
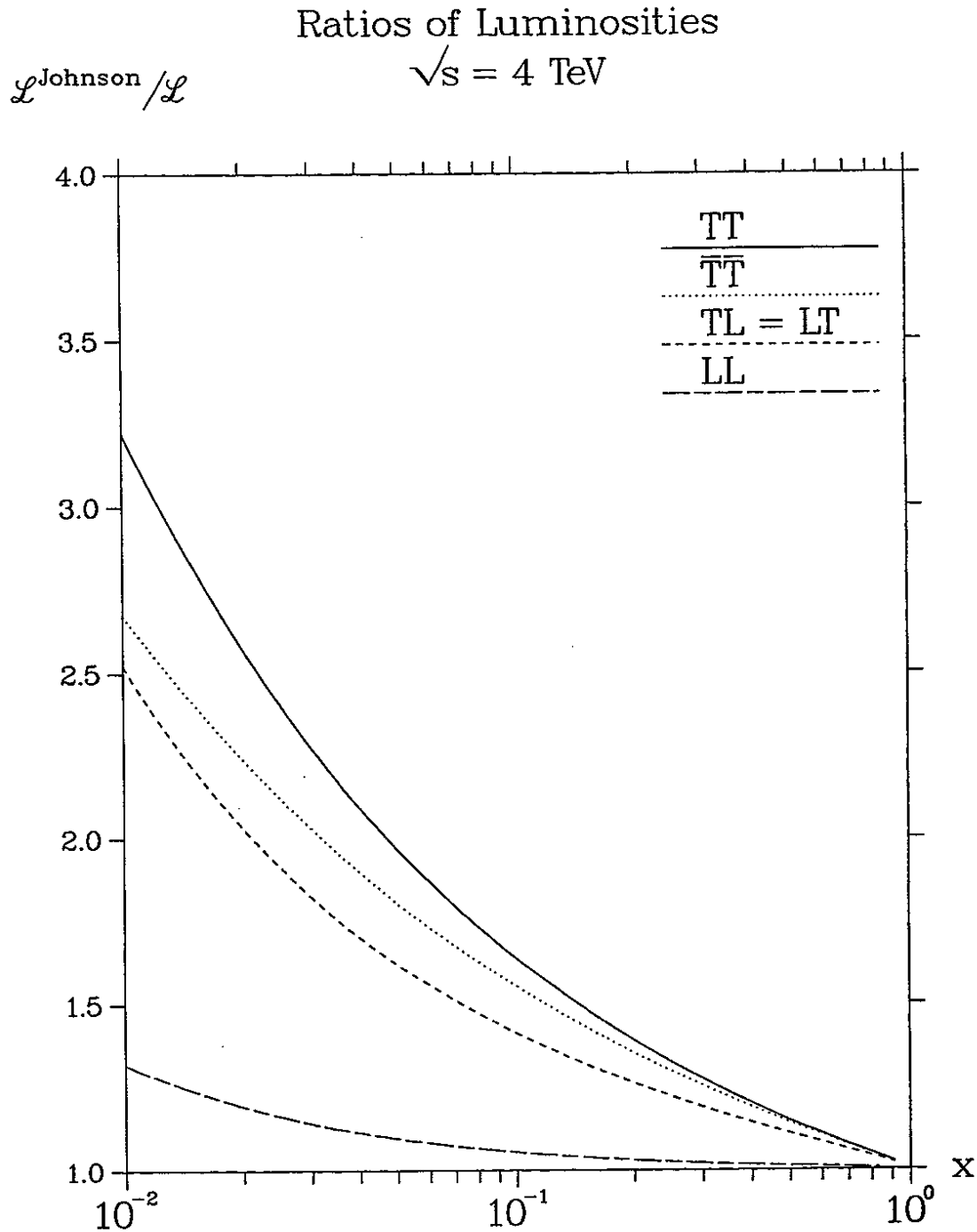
Figure 4.7: Ratios of the conventional convolutions [65] of single vector-bosons, (4.49) with (4.67), and the improved luminosities for helicities $pol = TT$, $\overline{TT}$, LT and LL for a W^+W^--pair in e^+e^- collisions at $\sqrt{s} = 4$ TeV.
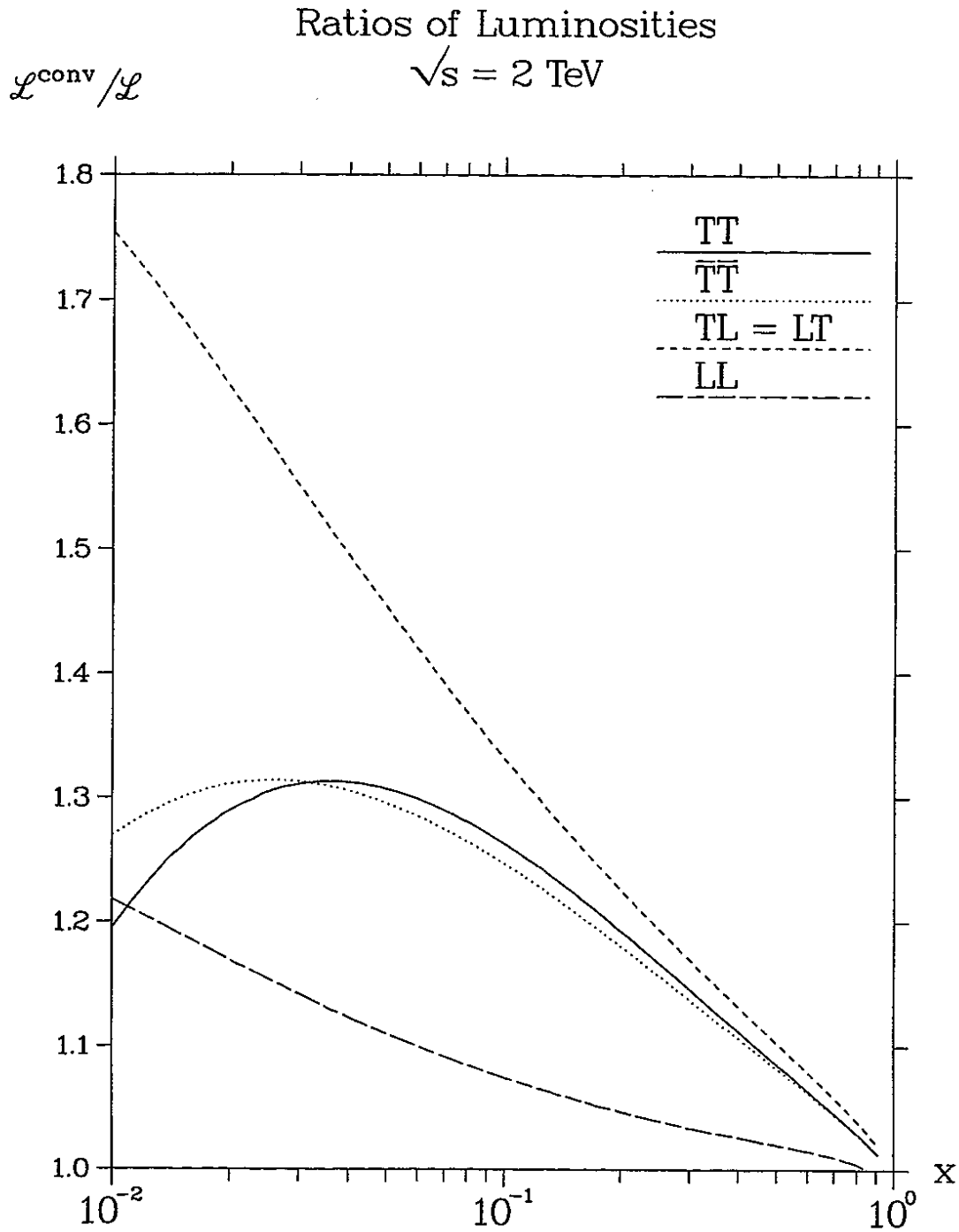
Figure 4.8: Ratios of the improved convolutions of single vector-bosons, (4.49) with (4.68), and the improved luminosities for helicities $pol = TT, \overline{TT}, LT$ and LL for a W^+W^--pair in e^+e^- collisions at $\sqrt{s} = 2$ TeV.
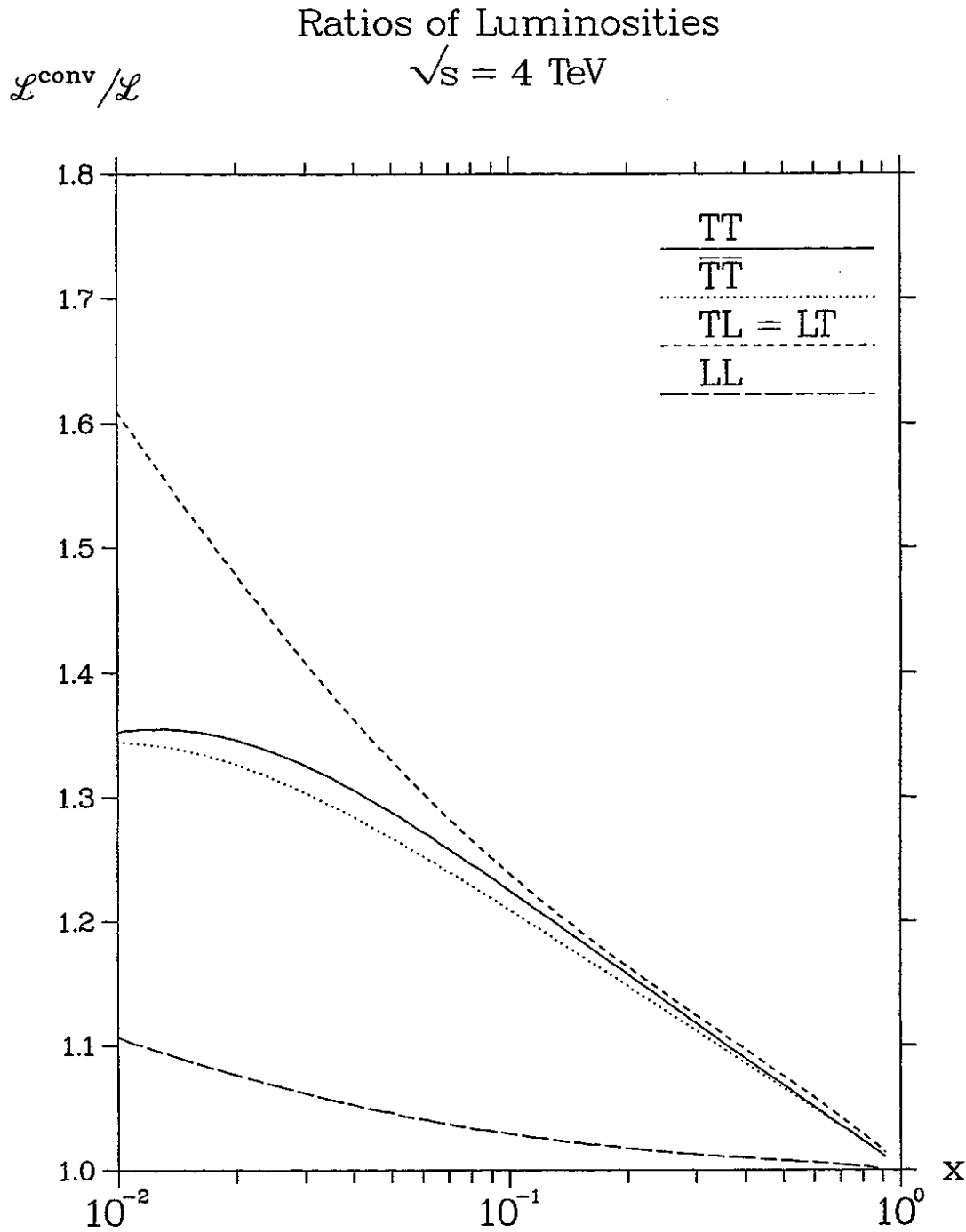
Figure 4.9: Ratios of the improved convolutions of single vector-bosons, (4.49) with (4.68), and the improved luminosities for helicities $pol = TT, \overline{TT}, LT$ and LL for a W^+W^--pair in e^+e^- collisions at $\sqrt{s} = 4$ TeV.

4.5 Leading Logarithmic Approximation

Further approximations in Eqs. (4.58) allow one to derive simplified expressions which have often been used in the literature and are referred to as the leading logarithmic approximation (LLA). The approximation consists of neglecting the off-shell masses k_i^2 in the J_{pol} and performing a high-energy limit, $s \gg M_j^2$. To be precise, with the following substitutions in (4.58),

$$
\begin{aligned}
\ln\left(\frac{M_j^2 + s - \mathcal{W}_j^2}{M_j^2}\right) &\rightarrow \ln\left(\frac{s}{M_j^2}\right), \\
\left(1 - \frac{M_j^2}{M_j^2 + s - \mathcal{W}_j^2}\right) &\rightarrow 1, \\
\frac{k_j^2}{k_j^2 - M_j^2} &\rightarrow 1, \\
\kappa_0 &\rightarrow \mathcal{W}^2,
\end{aligned}
\tag{4.71}
$$

one obtains

$$
\begin{aligned}
\mathcal{L}_{V_1 V_2, TT}^{q_1 q_2}(x) &\rightarrow \left(\frac{\alpha}{2\pi}\right)^2 (v_1^2 + a_1^2)(v_2^2 + a_2^2)\frac{1}{x}\left[(2+x)^2 \ln\left(\frac{1}{x}\right) - 2(1-x)(3+x)\right] \cdot \\
&\qquad \ln\left(\frac{s}{M_1^2}\right) \ln\left(\frac{s}{M_2^2}\right), \\
\mathcal{L}_{V_1 V_2, \overline{TT}}^{q_1 q_2}(x) &\rightarrow \left(\frac{\alpha}{2\pi}\right)^2 (2v_1 a_1)(2v_2 a_2)\left[(4+x)\ln\left(\frac{1}{x}\right) - 4(1-x)\right]\ln\left(\frac{s}{M_1^2}\right) \ln\left(\frac{s}{M_2^2}\right), \\
\mathcal{L}_{V_1 V_2, TL}^{q_1 q_2}(x) &\rightarrow \left(\frac{\alpha}{2\pi}\right)^2 (v_1^2 + a_1^2)(v_2^2 + a_2^2)\frac{1}{x}\left[4(1+x)\ln\left(\frac{1}{x}\right) - (1-x)(7+x)\right]\ln\left(\frac{s}{M_1^2}\right), \\
\mathcal{L}_{V_1 V_2, LT}^{q_1 q_2}(x) &\rightarrow \left(\frac{\alpha}{2\pi}\right)^2 (v_1^2 + a_1^2)(v_2^2 + a_2^2)\frac{1}{x}\left[4(1+x)\ln\left(\frac{1}{x}\right) - (1-x)(7+x)\right]\ln\left(\frac{s}{M_2^2}\right), \\
\mathcal{L}_{V_1 V_2, LL}^{q_1 q_2}(x) &\rightarrow \left(\frac{\alpha}{2\pi}\right)^2 (v_1^2 + a_1^2)(v_2^2 + a_2^2)\frac{4}{x}\left[(1+x)\ln\left(\frac{1}{x}\right) - 2(1-x)\right].
\end{aligned}
\tag{4.72}
$$

The expressions for $\mathcal{L}_{TT}$, $\mathcal{L}_{TL}$ and $\mathcal{L}_{LL}$ have been given already in [69] and the complete set of luminosities including $\mathcal{L}_{\overline{TT}}$, $\mathcal{L}_{\overline{TL}}$ and $\mathcal{L}_{L\overline{T}}$ can be found in [40].

In a similar way, LLA expressions for single-vector-boson distributions can be obtained from the exact ones. These distributions are obtained by taking the limits $M_V^2 \ll xs$ and $M_V^2 \ll (1-x)s$ in Eq. (4.62). One obtains

$$
\begin{aligned}
f_{V_T}^q\left(z, \frac{M_V^2}{s}\right) &= \frac{\alpha}{2\pi}(v^2 + a^2)\frac{1 + (1-z)^2}{z}\ln\left(\frac{s}{M_V^2}\right), \\
f_{V_{\overline{T}}}^q\left(z, \frac{M_V^2}{s}\right) &= \frac{\alpha}{2\pi}(2va)(2-z)\ln\left(\frac{s}{M_V^2}\right), \\
f_{V_L}^q\left(z, \frac{M_V^2}{s}\right) &= \frac{\alpha}{\pi}(v^2 + a^2)\frac{1-z}{z}.
\end{aligned}
\tag{4.73}
$$

The same distributions are obtained from the distributions [31, 32, 33, 66, 67, 68] by taking the same limits. Before taking the limit, one has to connect $P_\perp^2$ of [32, 66] and $4E_q^2$ of [31, 67, 68] to the variable s, as discussed in 4.2.

We conclude that a simple approximation exists in which all versions of the distribution-functions f_V^q reduce to the same expressions, (4.73). The convolutions of the LLA-distributions (4.73) again lead to the luminosities (4.72). The LLA formulae are obtained

from the exact ones by taking into account only the contributions from the singularities at $k_j^2 \to 0$ to the k_j^2-integrals and neglecting the contribution from other regions in the k_1^2, k_2^2 integration.

We discuss modifications of the LLA. Instead of s/M_i^2 as the argument of the logarithms in (4.72) one can also take xs/M_i^2, because in the limit $M_i^2 \ll xs \Leftrightarrow s/M_i^2 \gg 1/x$, one has $\ln(s/M_i^2) \simeq \ln(s/M_i^2) - \ln(1/x) = \ln(xs/M_i^2)$. This choice is further motivated by considering the first line of (4.71), which tells us that the argument of one of the logarithms is really $(s - \mathcal{W}_2^2)/M_i^2$ (in the limit $M_i^2 \to 0$), which varies within the whole interval $[0, s]$ as k_1^2 varies within its limits. Equivalently, one might use zs/M_V^2 instead of s/M_V^2 in the argument of the logarithms in (4.73). This choice was indeed used in [33, 69]. A numerical comparison shows that the LLA with this choice of the logarithms deviates less from the improved luminosities than if the choice s/M_i^2 is made. Similarly, since we assumed $s/M_i^2 \gg 1/(1 - x)$, we may also choose $x(1 - x)s/M_i^2$ as arguments of the logarithms in (4.72) and analogously $z(1 - z)s/M_V^2$ in (4.73). This choice is further motivated by considering again the first line of (4.71), which tells us that the argument of the other one of the logarithms is $s - \mathcal{W}^2 = (1 - x)s$. The inclusion of the factors $(1 - x)$ and $(1 - z)$ only modifies the luminosities and distributions in the regions $x \to 1$ and $z \to 1$, respectively, where they are very small anyway. A numerical comparison shows that the inclusion of these factors greatly reduces the deviations of the LLA from the improved luminosities in the region $x \to 1$. We will use this latter form, $x(1 - x)s$, in the following numerical example.

Numerical Results

Fig. 4.10 shows the ratio of the LLA version of the luminosities, Eq. (4.72), and the improved luminosities for a W^+W^--pair in e^+e^--collisions at 2 TeV. The LLA always overestimates the exact result by far and only for the LL luminosity at not too small values of x the LLA might be useful. For the dominating TT-luminosity the disagreement amounts to a factor of 3 to 4.5. Figure 4.11 shows the same ratios for a scattering energy of $\sqrt{s} = 4$ TeV. The deviation for the TT-luminosity amounts to a factor of between 2 and 3.5.
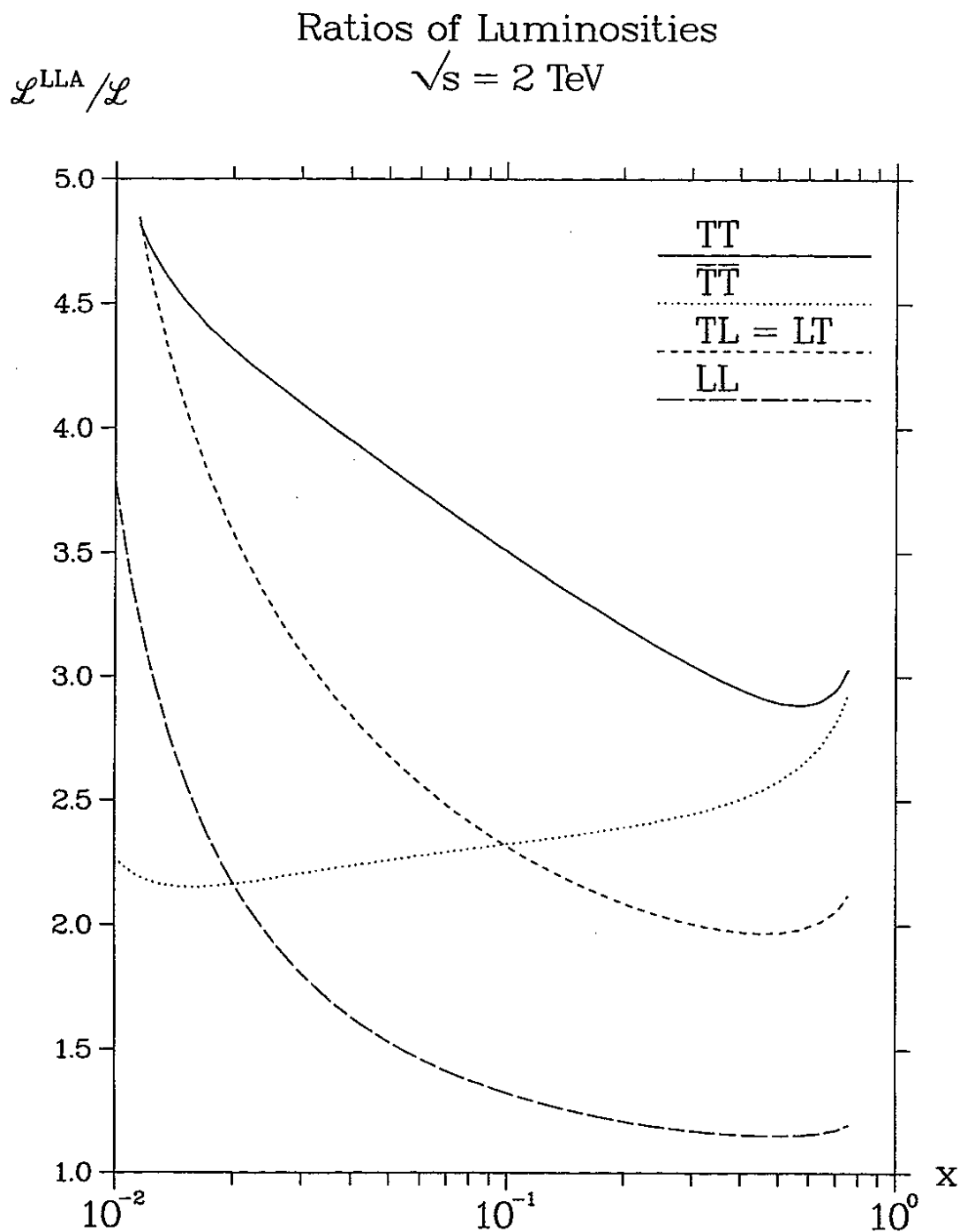
Figure 4.10: Ratios of the luminosities in the leading logarithmic approximation and the improved luminosities for $pol = TT$, $\overline{TT}$, $TL = LT$ and LL for a W^+W^- pair in e^+e^- collisions at $\sqrt{s} = 2$ TeV.
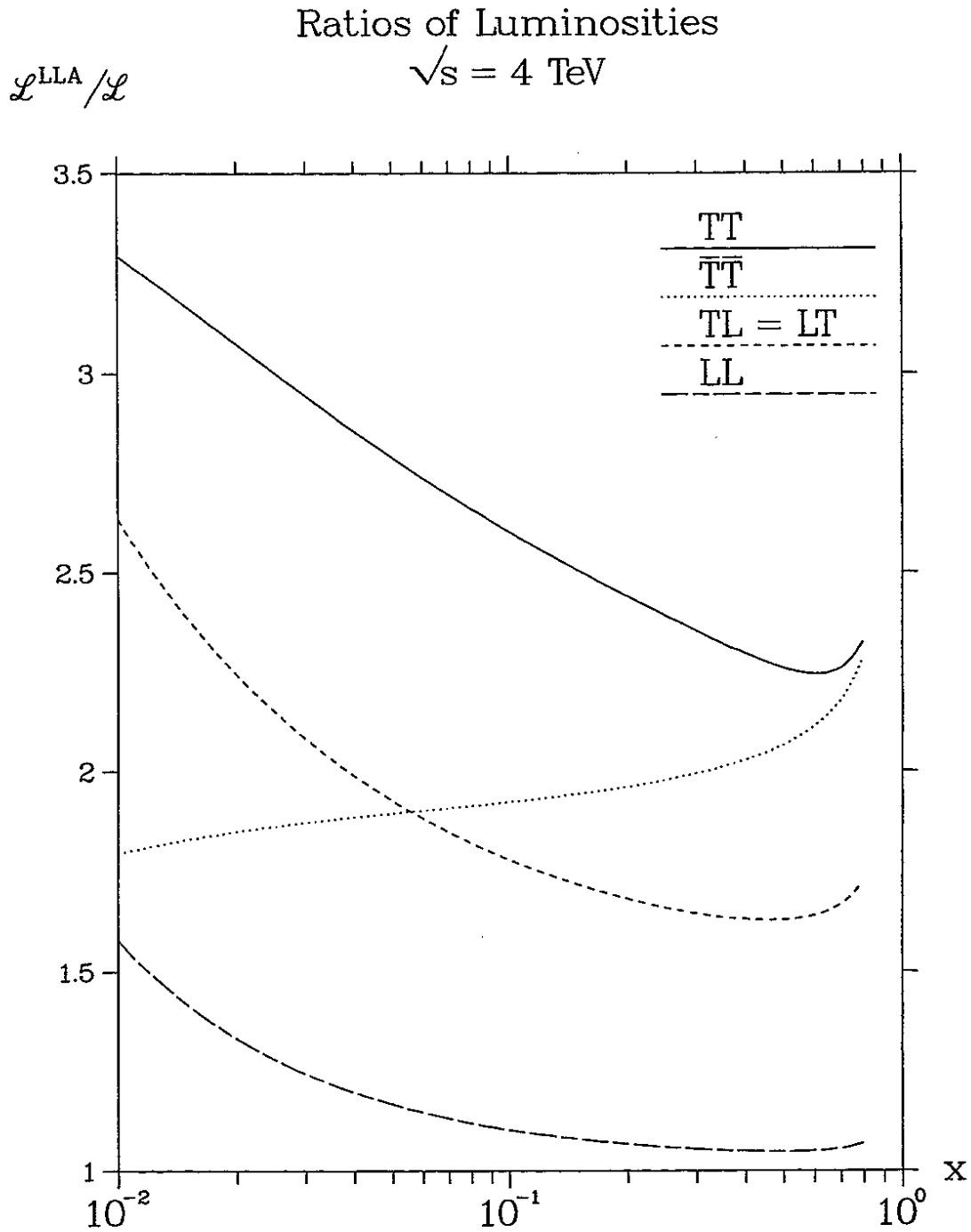
Figure 4.11: Ratios of the luminosities in the leading logarithmic approximation and the improved luminosities for $pol = TT$, $\overline{TT}$, $TL = LT$ and LL for a W^+W^- pair in e^+e^- collisions at $\sqrt{s} = 4$ TeV.

4.6 Conclusion

We have derived improved luminosities for a pair of vector-bosons inside a pair of fermions. In contrast to previously used approximations, our luminosities take into account the full phase space of one vector-boson in the calculation of the emission probability of the other vector-boson.

The commonly used leading logarithmic approximation and a convolution of exact distribution functions for single vector-bosons inside fermions are obtained as an approximation to the improved luminosities if one neglects regions in phase space in which the virtual vector-bosons have four-momenta squared much larger than their squared masses.

A numerical comparison of the improved luminosities and the luminosities in the leading logarithmic approximation shows that the latter approximation can not reproduce the exact calculation for transverse helicities. Only the luminosities for longitudinally polarized vector-bosons in the region of large $\sqrt{s}$ and not too small x can be described by the LLA. We derived convolutions of vector-boson distributions, which deviate by at most 36% from the improved luminosities for the dominant TT helicity if $\sqrt{s} < 4$ TeV.

One should keep in mind that the question, whether the vector-boson scattering diagrams are indeed the very dominant ones, is not touched by the improved formulation of the EVBA. Further, it was argued that the extrapolation to off-shell masses might not always be guaranteed [81]. However, for the example of heavy Higgs-boson production it was shown in that same reference that the extrapolation to off-shell masses is indeed a smooth one.

Our final explicit expressions for the two-vector-boson luminosities were obtained with specific simple assumptions for the off-shell behavior of the vector-boson scattering cross-sections. However, we keep a clean separation of exactly calculable parts and model dependent assumptions. Our expressions are written in a form which allows for an easy accomodation of an improved off-shell dependence, as soon as the corresponding information will be available. Apart from these caveats, our luminosities are exact results of a calculation of a subset of Feynman diagrams.

We did not attempt to take into account any kind of experimental cuts on kinematical variables for final state particles, like transverse momenta or rapidities. As long as those cuts only imply restrictions on the momentum transfers k_j^2 and the scale variable x, taking into account those cuts in the improved luminosities (4.58) is a straightforward task. For the approximative formula, the convolution (4.68), a kinematic situation of the kind $k_1^2 = k_2^2 = 0$, thus massless intermediate vector-bosons V_1, V_2 moving in the direction of the fermions, might be assumed as an approximation. Cuts of all kind can then be applied. We will discuss such cuts in Chapter 5.3.

Chapter 5

Luminosities for Vector-Boson Pairs in a Hadron-Pair

The method described in Chapter 4 to calculate the cross-sections for the parton-parton processes $q_1 q_2 \to q_1' q_2' V_3 V_4$ is now applied to the corresponding hadron-hadron processes. Improved luminosities for vector-boson–pairs in a hadron-pair are derived. With the help of these luminosities, cross-sections for hadron-hadron collision processes proceeding via intermediate vector-bosons can be calculated. We discuss an approximation which again leads to the formalism of vector-boson distributions. We will also give various comparisons with results which have been obtained in the literature.

5.1 Derivation of Improved Luminosities

We derive improved luminosities for finding a vector-boson pair in a hadron-pair. The luminosities describe the process shown in Figure 5.1.

The cross-section for the process $q_1 q_2 \to q_1' q_2' V_3 V_4$ in (3.3) is given in the framework of the EVBA, (4.22) und (4.48), by the expression

$$
\sigma(q_1 q_2 \to q'_1 q'_2 (V_1 V_2 \to V_3 V_4), s_{qq})
$$
$$
= \sum_{V_1, V_2} \sum_{pol} \int_0^1 d\hat{x}\, \mathcal{L}^{q_1 q_2}_{V_1, V_2, pol}(\hat{x}) \sigma(V_1 V_2 \to V_3 V_4, \mathcal{W}^2 = \hat{x} s_{qq}). \tag{5.1}
$$

In (5.1), $\hat{x}$ is the ratio of the invariant mass squared of the vector-boson pair and the one of the parton-pair [1]. According to (4.49), the luminosities for vector-boson pairs in a parton-pair appearing in (5.1) can be written as

$$
\mathcal{L}^{q_1 q_2}_{V_1, V_2, pol} = \left(\frac{\alpha}{2\pi}\right)^2 \frac{\kappa_0}{s_{qq}} c^{pol}_{q_1(V_1)} c^{pol}_{q_2(V_2)} \int_{\hat{x}}^1 \frac{d\hat{z}}{\hat{z}} \mathcal{L}_{pol}\left(\hat{x}, \hat{z}, \frac{M_1^2}{s_{qq}}, \frac{M_2^2}{s_{qq}}\right), \tag{5.2}
$$

where $\hat{z}$ is identical to the variable z defined in (4.19). It is the ratio of the squared invariant mass of a system consisting of V_1 and the parton q_2 and the squared invariant mass of the parton-pair, s_{qq}. If the momentum of V_1 is light-like, $k_1^2 = 0$, the directions

---

[1]The variable x of Chapter 4 is replaced in this Chapter by the variable $\hat{x}$. The same is true for the variables $\hat{z}$ and z. The variables x and z used in this Chapter will obtain a new meaning in the context of hadron-collisions.
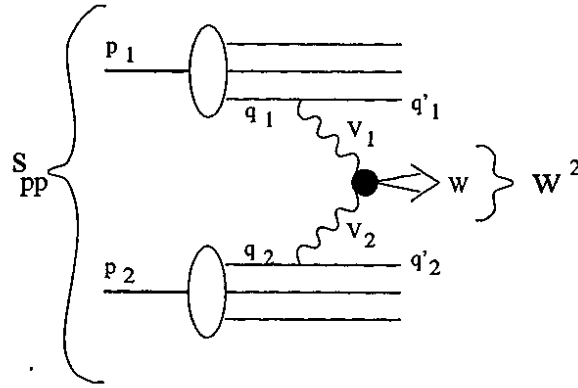
Figure 5.1: Diagram for the hadron-hadron scattering process proceeding via two intermediate vector-bosons, $p_1p_2 \to q_1q_2 \to q'_1q'_2V_1V_2$, $V_1V_2 \to W$.

of motion of V_1 and q_1 are parallel. In this case, $\hat{z}$ is the ratio of the energy of V_1 and the energy of q_1. Inserting (5.1) into (3.2) yields an expression for the hadron-hadron cross-section for vector-boson pair-production, $\sigma(p_1p_2 \to q_1q_2 \to q'_1q'_2V_3V_4)$, derived within the EVBA,

$$\sigma(p_1p_2 \to q_1q_2 \to q'_1q'_2(V_1V_2 \to V_3V_4))$$
$$\equiv \sigma(p_1p_2 \to V_1V_2 \to V_3V_4, s_{pp})$$
$$= \sum_{q_1,q_2} \sum_{V_1,V_2} \sum_{pol} \int_0^1 d\tau \int_{\frac{1}{2}\ln(\tau)}^{-\frac{1}{2}\ln(\tau)} dy\, f_{q_1}^{p_1}(\sqrt{\tau}e^y, Q_1^2) f_{q_2}^{p_2}(\sqrt{\tau}e^{-y}, Q_2^2)$$
$$\cdot \int_0^1 d\hat{x}\, \mathcal{L}_{V_1,V_2,pol}^{q_1q_2}(\hat{x})\sigma(V_1V_2 \to V_3V_4, \mathcal{W}^2 = \tau\hat{x}s_{pp}). \tag{5.3}$$

In (5.3), y is the rapidity of the quark-quark pair in the p_1p_2 center-of-mass system, taken along the direction of motion of the hadron which emits V_1.

The expression (5.3) allows one to define luminosities $\mathcal{L}_{V_1,V_2,pol}^{p_1p_2}$ of ordered vector-boson pairs in a hadron-pair,

$$\sigma(p_1p_2 \to V_1V_2 \to V_3V_4, s_{pp})$$
$$= \sum_{V_1,V_2,pol} \int_0^1 dx\, \mathcal{L}_{V_1,V_2,pol}^{p_1p_2}(x)\sigma(V_1V_2 \to V_3V_4, \mathcal{W}^2 = xs_{pp}), \tag{5.4}$$

where

$$x \equiv \mathcal{W}^2/s_{pp} \tag{5.5}$$

is the ratio of the squares of the invariant masses of the vector-boson pair and of the hadron-pair. The summations in (5.4) are extended over all vector-bosons V_1 and V_2, which can produce the pair V_3V_4, and the luminosities are given by the expression

$$\mathcal{L}_{V_1,V_2,pol}^{p_1p_2}(x) = \sum_{q_1(V_1)} \sum_{q_2(V_2)} \int_x^1 \frac{d\tau}{\tau} \int_{\frac{1}{2}\ln(\tau)}^{-\frac{1}{2}\ln(\tau)} dy\, f_{q_1}^{p_1}(\sqrt{\tau}e^y, Q_1^2) f_{q_2}^{p_2}(\sqrt{\tau}e^{-y}, Q_2^2)$$

$$\cdot \mathcal{L}^{q_1 q_2}_{V_1,V_2,pol}\left(\frac{x}{\tau}\right). \tag{5.6}$$

The summations in (5.6) are extended over all quarks q_1 and q_2, which can couple to the vector-bosons V_1 and V_2, respectively. In (5.4), V_1 is emitted from p_1 and V_2 from p_2.

A notation as a sum over all different, un-ordered vector-boson pairs $(V_1 V_2)$ instead of the two independent summations over single vector-bosons is convenient,

$$\sigma(p_1 p_2 \to V_1 V_2 \to V_3 V_4, s_{pp})$$

$$= \sum_{(V_1 V_2)_{pol}} \cdot \int_0^1 dx\, \mathcal{L}^{p_1 p_2}_{(V_1 V_2)_{pol}}(x)\sigma_{pol}(V_1 V_2 \to V_3 V_4, \mathcal{W}^2 = x s_{pp}), \tag{5.7}$$

where the luminosities for unordered pairs are defined by the expression

$$\mathcal{L}^{p_1 p_2}_{(V_1 V_2)_{pol}}(x) \equiv N_c \left(\mathcal{L}^{p_1 p_2}_{V_1,V_2,pol}(x) + \mathcal{L}^{p_1 p_2}_{V_2,V_1,\overline{pol}}(x) \right). \tag{5.8}$$

In (5.8), $\overline{pol}$ is the index of helicity, which is obtained from pol by the exchange of V_1 and V_2 (e.g. $TT \to TT$, $TL \to LT$), and

$$N_c \equiv \begin{cases} 1 & ; \quad \text{if} \quad V_1 \neq V_2 \\ 1/2 & ; \quad \text{if} \quad V_1 = V_2 \end{cases} \tag{5.9}$$

ist a combinatorial factor.

The expression for the luminosities, (5.8) with (5.6) and (5.2), can be brought into a more comprehensible form, if the integral over the rapidity y is parametrized as a function $I^{p_1 p_2}_{y,pol}(\tau)$ of the remaining integration variable τ,

$$\mathcal{L}^{p_1 p_2}_{(V_1 V_2)_{pol}}(x) = N_c \left(\frac{\alpha}{2\pi}\right)^2 \tilde{x} \int_0^{-\ln(x)} \frac{d\left[\ln(\frac{1}{\tau})\right]}{\tau} \left\{ I^{p_1 p_2}_{y,pol}(\tau) + I^{p_2 p_1}_{y,pol}(\tau) \right\}$$

$$\cdot \int_{\frac{1}{2}\ln(\hat{x})}^{-\frac{1}{2}\ln(\hat{x})} d\hat{y} \mathcal{L}_{pol}\left(\hat{x}, \sqrt{\hat{x}}e^{\hat{y}}, \frac{M_1^2}{s_{qq}}, \frac{M_2^2}{s_{qq}} \right), \tag{5.10}$$

with

$$I^{p_1 p_2}_{y,pol}(\tau) = \int_{\frac{1}{2}\ln(\tau)}^{-\frac{1}{2}\ln(\tau)} dy \left(\sum_{q_1(V_1)} c^{pol}_{q_1(V_1)} f^{p_1}_{q_1}(\sqrt{\tau}e^y, Q_1^2) \right) \left(\sum_{q_2(V_2)} c^{pol}_{q_2(V_2)} f^{p_2}_{q_2}(\sqrt{\tau}e^{-y}, Q_2^2) \right). \tag{5.11}$$

In (5.10), the variable

$$\tilde{x} \equiv x\sqrt{1 + \left(\frac{M_1^2}{\mathcal{W}^2}\right)^2 + \left(\frac{M_2^2}{\mathcal{W}^2}\right)^2 - 2\frac{M_1^2}{\mathcal{W}^2} - 2\frac{M_2^2}{\mathcal{W}^2} - 2\frac{M_1^2}{\mathcal{W}^2}\frac{M_2^2}{\mathcal{W}^2}}, \tag{5.12}$$

contains the flux-factor and the variable

$$\hat{y} \equiv \frac{1}{2}\ln\left(\hat{z}^2 \hat{x}\right) \tag{5.13}$$

has been introduced. In the case of light-like momenta of the vector-bosons V_1 and V_2, the variable $\hat{y}$ is the rapidity of the $(V_1 V_2)$ center-of-mass motion in the quark-quark center-of-mass sytem, taken along the direction of motion of the quark from which V_1 was emitted. Further, in the derivation of (5.10), (5.11) we made use of the symmetry property of luminosities for vector-boson pairs in quark-pairs,

$$\int d\hat{y}\, \mathcal{L}_{pol}\left(\hat{x}, \sqrt{\hat{x}}e^{\hat{y}}, \frac{M_1^2}{s_{qq}}, \frac{M_2^2}{s_{qq}}\right) = \int d\hat{y}\, \mathcal{L}_{\overline{pol}}\left(\hat{x}, \sqrt{\hat{x}}e^{\hat{y}}, \frac{M_2^2}{s_{qq}}, \frac{M_1^2}{s_{qq}}\right). \tag{5.14}$$

The functions $I_{y,pol}^{p_1 p_2}(\tau)$ contain all dependence on the type of the partons $q_i(V_i)$, i.e., on the distribution-functions of the partons in the hadrons and on their couplings to the vector-bosons. The remaining part of the τ-integral in (5.10) does only depend on kinematical variables.

An equivalent expression for (5.10) is

$$\begin{aligned}
\mathcal{L}_{(V_1 V_2)_{pol}}^{p_1 p_2}(x) &= N_c \left(\frac{\alpha}{2\pi}\right)^2 \tilde{x} \int\limits_x^1 \frac{dz}{z} \int\limits_z^1 \frac{dx_1}{x_1} \int\limits_{\frac{x}{z}}^1 \frac{dx_2}{x_2} \frac{1}{x_1 x_2} \\
&\quad \times \left[\left(\sum_{q_1(V_1)} c_{q_1(V_1)}^{pol} f_{q_1}^{p_1}(x_1, Q_1^2)\right) \cdot \left(\sum_{q_2(V_2)} c_{q_2(V_2)}^{pol} f_{q_2}^{p_2}(x_2, Q_2^2)\right) + p_1 \leftrightarrow p_2\right] \\
&\quad \cdot \mathcal{L}_{pol}\left(\hat{x} = \frac{x}{x_1 x_2}, \hat{z} = \frac{z}{x_1}, \frac{M_1^2}{s_{qq}}, \frac{M_2^2}{s_{qq}}\right).
\end{aligned} \tag{5.15}$$

We will use this expression later to derive vector-boson distribution functions in hadrons. In (5.15), x_1 and x_2 are the variables from (3.1); $x_1 \equiv \sqrt{\tau}e^y$ is the ratio of the energy of the quark, from which V_1 was emitted, and the energy of the hadron, from which this quark was emitted. Similarly, $x_2 \equiv \sqrt{\tau}e^{-y}$ is the ratio of the energy of the quark, from which V_2 was emitted, and the other hadron. The variable

$$z \equiv x_1 \hat{z} \tag{5.16}$$

introduced in (5.15) is the fraction of the energy of the vector-boson V_1 and the one of the hadron, from which it was emitted, if V_1 has a light-like momentum. We further note the relation $s_{qq} = x_1 x_2 s_{pp}$.

We will write the luminosity to find a WZ-pair in a proton-pair, where the W can be either a W^+ or a W^-, as

$$\mathcal{L}_{((W^+ + W^-)Z)_{pol}}^{pp} \equiv \mathcal{L}_{(W^+ Z)_{pol}}^{pp} + \mathcal{L}_{(W^- Z)_{pol}}^{pp}. \tag{5.17}$$

5.1.1 Discussion of Numerical Results

The Figures 5.2 and 5.3 show the improved luminosities (5.10) of a WZ-pair in a proton-pair of $\sqrt{s_{pp}} = 14$ TeV as a function of the invariant mass of the WZ pair. The MRSA(A) parametrization [82] in the DIS-scheme was used for the parton-distributions $f_{q_i}^p(x_i, Q_i^2)$ in a proton. For Q_i^2, the invariant mass of the quark q_i and the other proton, thus $Q_i^2 = x_i s_{pp}$, was used. We will always use these distributions and this choice of Q_i^2 in the following if not explicitly stated otherwise. A contribution from top-quarks was not taken into account. This contribution is small.
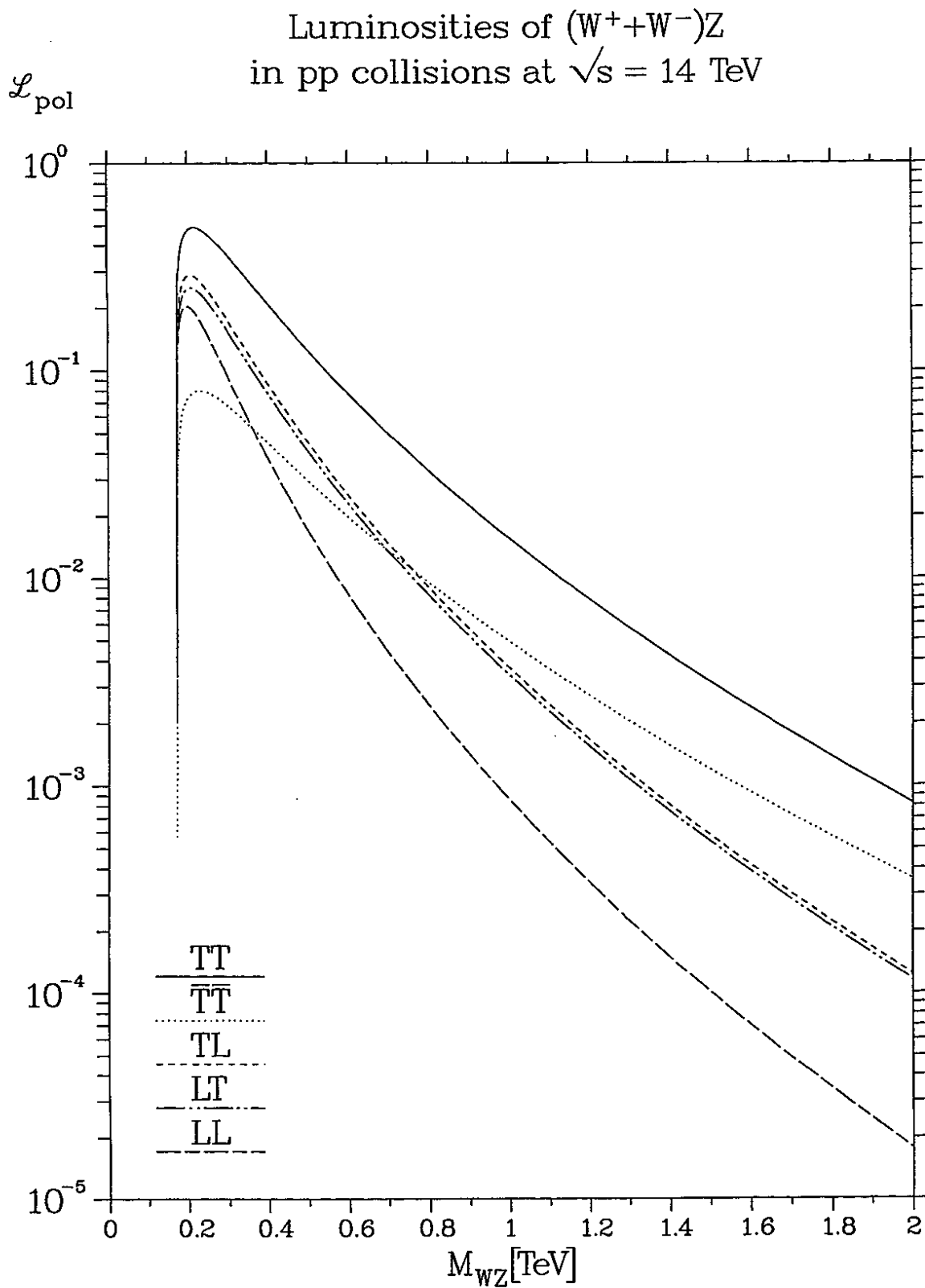
Figure 5.2: The improved luminosities for the diagonal helicity combinations of a $(W^+ + W^-)Z$-pair in a proton-pair at an invariant mass of 14 TeV as a function of the invariant mass of the WZ-pair.
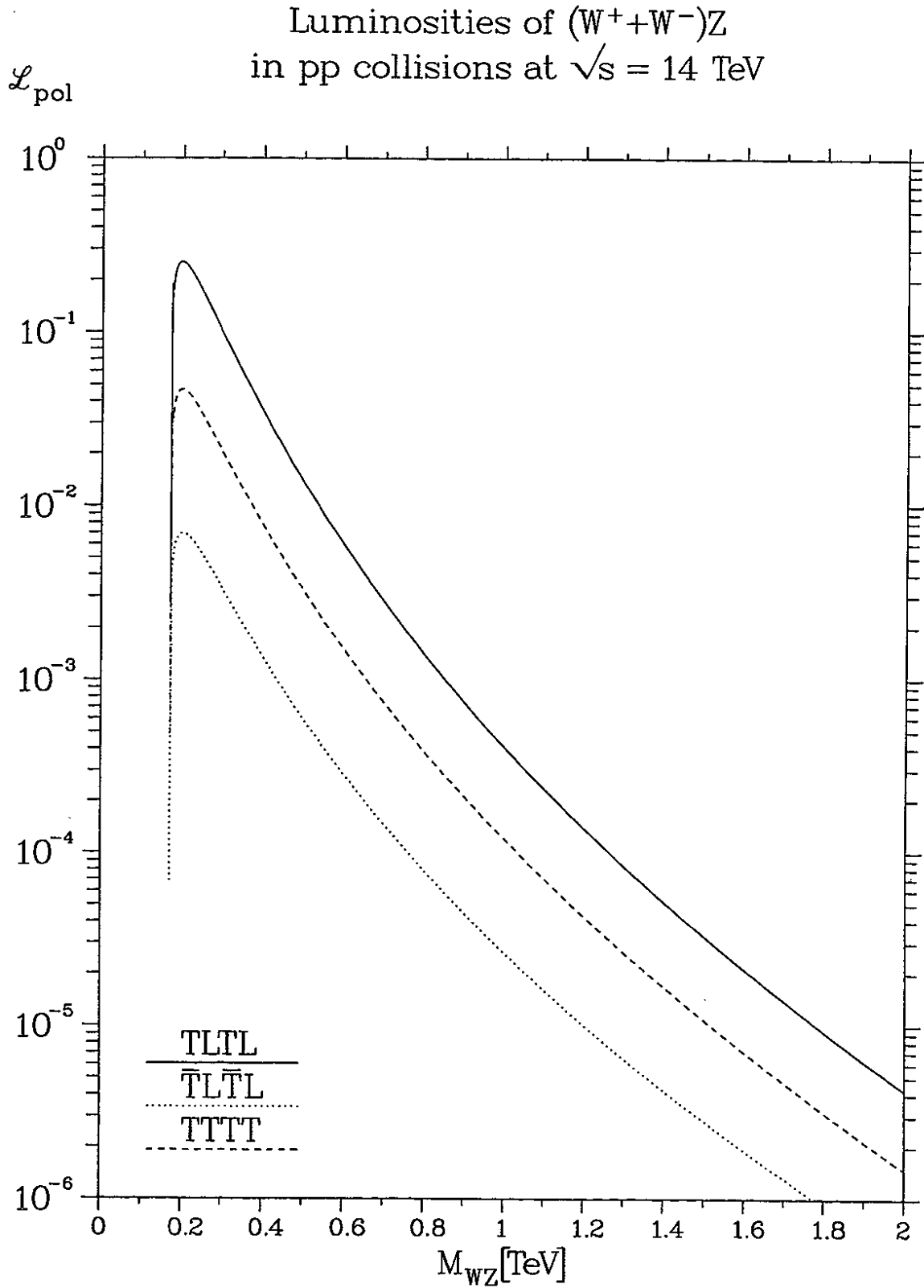
Figure 5.3: The improved luminosities for the non-diagonal helicity combinations of a $(W^+ + W^-)Z$-pair in a proton-pair at an invariant mass of 14 TeV as a function of the invariant mass of the WZ-pair.

5.2 Convolutions of Vector-Boson Distributions in a Hadron as an Approximation to the Improved Luminosities

We derive convolutions of single vector-boson distributions in a hadron as an approximation to the improved luminosities (5.10). The approximations which lead to the convolutions are discussed.

5.2.1 Derivation of Convolutions and Distribution Functions

The improved lumiosities for a vector-boson pair in a proton pair, (5.10) can be written approximately as convolutions of single vector-boson distributions f_V^p in a proton. To see this, one uses the luminosities for a vector-boson pair in a quark-pair, $\mathcal{L}_{V_1,V_2,pol}^{q_1 q_2}$, in the approximative form of convolutions of vector-boson distributions f_V^q. In addition, a further approximation, leading to a factorization into a product of distribution-functions, has to be applied.

We start from Eq. (5.2) and use for the quantities $\mathcal{L}_{pol}$ the symmetrical products of amputated vector-boson distributions in quarks, (4.68),

$$\mathcal{L}_{\lambda_1 \lambda_2}\left(\hat{x}, \hat{z}, \frac{M_1^2}{s_{qq}}, \frac{M_2^2}{s_{qq}}\right) = h_{\lambda_1}\left(\hat{z}, \frac{M_1^2}{\sqrt{\hat{z}}\, s_{qq}}\right) h_{\lambda_2}\left(\frac{\hat{x}}{\hat{z}}, \frac{M_2^2 \sqrt{\hat{z}}}{\sqrt{\hat{x}}\, s_{qq}}\right). \tag{5.18}$$

Inserting (5.18) into (5.10) gives an expression for luminosities for vector-boson pairs in a hadron-pair,

$$
\begin{aligned}
\mathcal{L}_{(V_1 V_2)_{kl}}^{p_1 p_2}(x) &= N_c\left(\frac{\alpha}{2\pi}\right)^2 \tilde{x} \int\limits_0^{-\ln(x)} \frac{d\left[\ln\left(\frac{1}{\tau}\right)\right]}{\tau} \int\limits_{\hat{x}=\frac{x}{\tau}}^1 \frac{d\hat{z}}{\hat{z}} h_{\lambda_1}\left(\hat{z}, \frac{M_1^2}{\sqrt{\hat{z}}\, s_{qq}}\right) h_{\lambda_2}\left(\frac{\hat{x}}{\hat{z}}, \frac{M_2^2 \sqrt{\hat{z}}}{\sqrt{\hat{x}}\, s_{qq}}\right) \\
&\quad \cdot \left\{ I_{y,pol}^{p_1 p_2}(\tau) + I_{y,pol}^{p_2 p_1}(\tau) \right\},
\end{aligned}
\tag{5.19}
$$

with the functions $I_{y,pol}^{p_1 p_2}(\tau)$ from (5.11). The transition to the variables x_1, x_2 and z from (5.15) brings (5.19) into the form

$$
\begin{aligned}
\mathcal{L}_{(V_1 V_2)_{kl}}^{p_1 p_2}(x) &= N_c\left(\frac{\alpha}{2\pi}\right)^2 \tilde{x} \int\limits_x^1 \frac{dz}{z} \int\limits_z^1 \frac{dx_1}{x_1} \int\limits_{\frac{x}{z}}^1 \frac{dx_2}{x_2} \frac{1}{x_1 x_2} \\
&\quad \cdot \left[h_{\lambda_1}\left(\frac{z}{x_1}, \frac{M_1^2 \sqrt{x_1}}{\sqrt{z}\, s_{qq}}\right) \sum_{q_1(V_1)} c_{q_1(V_1)}^{\lambda_1} f_{q_1}^{p_1}(x_1, Q_1^2) \right. \\
&\qquad \left. \cdot h_{\lambda_2}\left(\frac{x}{z\, x_2}, \frac{M_2^2 \sqrt{z\, x_2}}{\sqrt{x}\, s_{qq}}\right) \sum_{q_2(V_2)} c_{q_2(V_2)}^{\lambda_2} f_{q_2}^{p_2}(x_2, Q_2^2) + p_1 \leftrightarrow p_2 \right] \\
&= N_c \frac{\tilde{x}}{x} \int\limits_x^1 \frac{dz}{z} \int\limits_z^1 \frac{dx_1}{x_1} \int\limits_{\frac{x}{z}}^1 \frac{dx_2}{x_2} \\
&\quad \cdot \left[x_1 \frac{df_{V_1,\lambda_1}^{p_1}}{dx_1}(z, Q_1^2) x_2 \frac{df_{V_2,\lambda_2}^{p_2}}{dx_2}\left(\frac{x}{z}, Q_2^2\right) + p_1 \leftrightarrow p_2 \right]
\end{aligned}
\tag{5.20}
$$

with $s_{qq} = x_1 x_2 s_{pp}$. The differential distribution-functions of a vector-boson V_i in a hadron $p = p_1$ or $p = p_2$ appearing in (5.20) are given by

$$x_i \frac{df^p_{V_i, \lambda_i}}{dx_i}(\xi_i, Q_i^2) = \frac{\alpha}{2\pi} \frac{\xi_i}{x_i} \sum_{q_i(V_i)} c^{\lambda_i}_{q_i(V_i)} f^p_{q_i}(x_i, Q_i^2) h_{\lambda_i} \left(\frac{\xi_i}{x_i}, \frac{M_i^2}{\sqrt{\xi_i\, x_i\, x_j\, s_{pp}}} \right),$$
$$i, j = 1, 2 \quad i \neq j. \tag{5.21}$$

In (5.21), $\xi_1 \equiv z$ and $\xi_2 \equiv x/z$ is, for light-like vector-bosons V_i, the ratio of the energy of the vector-boson and the energy of the hadron, from which it is emitted.

The integrations over x_1 and x_2 in (5.20) cannot be carried out independently because of the x_j-dependence, $i \neq j$, of the differential distributions (5.21). As an approximation, however, we may replace x_j in Eq. (5.21) by the variable x_i. The approximation $x_j \to x_i$ is to be briefly explained. Without the approximation one obtains the quantity x_j, thus the momentum of the other vector-boson, V_j, in units of the momentum of the hadron, from which V_j is emitted. Then, the x_1- and x_2-integrals in (5.21) can not be carried out independently. An approximative value for x_j, $x_{j,max}$ is the one which maximizes the integrand of the x_j-integral. This integrand is one of the differential vector-boson distributions in (5.20). We assume that the differential distributions (5.21) for the different vector-bosons V_i have essentially the same dependence on x_i. In this case the value of $x_{j,max}$ is essentially identical to the value of a corresponding variable $x_{i,max}$, which is defined as the value of x_i, at which the distribution (5.21) gives the largest contribution to the x_i-integral. Keeping now, as an approximation, the relation $x_i = x_j$ for all x_i (it is then valid in particular at $x_{i,max} = x_{j,max}$), one obtains the replacement $x_j \to x_i$ in (5.21). One has thus chosen an extrapolated value for x_j. A numerical investigation of the error induced by this approximation will be given below. For the dominant TT-luminosity the error is less than 7% for not too small values of x at $\sqrt{s_{pp}} = 14$ TeV.

With the replacement $x_i \to x_j$, the x_1- and x_2-integrals in (5.20) can be carried out independently from each other and the integrand in the z-integral in (5.20) becomes a product of vector-boson distribution-functions in hadrons,

$$\mathcal{L}^{p_1 p_2}_{(V_1 V_2)_{\lambda_1 \lambda_2}}(x)$$
$$= N_c \frac{\tilde{x}}{x} \int_{\frac{1}{2}\ln(x)}^{-\frac{1}{2}\ln(x)} dy' \left[f^{p_1}_{V_1, \lambda_1} \left(\sqrt{x} e^{y'}, s_{pp}, Q_1^2 \right) f^{p_2}_{V_2, \lambda_2} \left(\sqrt{x} e^{-y'}, s_{pp}, Q_2^2 \right) + p_1 \leftrightarrow p_2 \right] \tag{5.22}$$

In (5.22), the variable

$$y' \equiv \frac{1}{2} \ln \left(z^2/x \right) \tag{5.23}$$

is the rapidity of the $V_1 V_2$ center-of-mass motion, taken along the direction of motion of the hadron which emitted V_1, if the vector-bosons V_1, V_2 are light-like. The functions

$$f^p_{V_\lambda}(\xi, s_{pp}, Q^2) = \int_\xi^1 \frac{dx'}{x'} \sum_{q(V)} f^p_q(x', Q^2) f^q_{V_\lambda} \left(\frac{\xi}{x'}, \frac{M_V^2}{s_{qq}} \right), \tag{5.24}$$

in (5.22) with $\xi = \xi_1$ or $\xi = \xi_2$ and $s_{qq} = x'^2 s_{pp}$, are distribution-functions of a vector-boson V with the helicity λ and the mass M_V in a hadron p of energy $E_p = \sqrt{s_{pp}}/2$. The variable x' in (5.24) is the ratio of the momenta of the quark q and the hadron p. The

variable ξ is the ratio of the energy of the vector-boson and the energy of the hadron, if the vector-boson is light-like. The distribution function (5.24) is only to be used for the processes proceeding via two vector-bosons as shown in Figure 5.1. The functions $f_{V_\lambda}^q$ in (5.24) are given by

$$f_{V_\lambda}^q\left(\hat{z}, \frac{M_V^2}{s_{qq}}\right) = \frac{\alpha}{2\pi}\hat{z}\, c_{q(V)}^\lambda h_\lambda\left(\hat{z}, \frac{M_V^2}{\sqrt{\hat{z}}\, s_{qq}}\right).$$ (5.25)

They are the distributions of vector-bosons V with the helicity λ and the mass M_V in the quark q, given already in (4.70). The quantity s_{qq} is the invariant mass squared of a parton-pair from which a vector-boson pair is emitted. The functions $h_\lambda(z, \mu)$ were given in (4.66).

The approximation we carried out here means that an estimated (mean) value is taken for the quark-quark scattering energy s_{qq}, which has to be inserted into the differential vector-boson distributions (5.21)[2]. This estimated value does only depend on the energy $x_i\sqrt{s_{pp}}/2$ of one of the quarks[3], namely that one, which emits the vector-boson, while the same energy is taken for the (unknown) energy of the other quark. Thus, $s_{qq} = x_i^2 s_{pp}$ has been chosen for the quark-quark scattering energy. Without an approximation of this kind the formalism of vector-boson distributions in a hadron can not be obtained.

Concerning again the meaning of the variables in (5.24), we note that the variable ξ represents the momentum fraction of the vector-boson and the hadron only in certain regions of the k_1^2, k_2^2 phase-space in (4.49), namely for $k_1^2 = 0$ in the case $\xi = \xi_1$ and for $k_1^2 = k_2^2 = 0$ in the case $\xi = \xi_2$. In particular, for on-shell massive vector-bosons V, ξ_i is never exactly this quantity. However, the interpretation of the ξ_i as momentum fractions is in analogy to the corresponding quantities x_i in (3.1) for the (massless) quarks and gluons. We finally note that the relation $\xi_1\xi_2 = x$ holds without any approximation.

In summary, the formulae (5.22) and (5.24) have been derived with only the mentioned approximations (using the factorized forms (4.68) and choosing an estimated value for s_{qq}) from the improved luminosities for a vector-boson pair in a proton-pair, (5.10) with (5.11). The formulation of vector-boson distributions is recovered if these approximations are made.

5.2.2 Discussion of Numerical Results

Figure 5.4 shows the luminosities (5.22) for $W\gamma$-pairs in a $\sqrt{s_{pp}} = 14$ TeV proton pair as a function of the invariant mass of the $W\gamma$-pair. The luminosities were calculated as a convolution of the vector-boson distributions (5.24) and the photon distribution $f_\gamma^p(x)$ in a proton of M. Glück et.al. [83]. For the scale Q^2 of the quark-distributions in (5.24) again the invariant mass of the quark and the particle, which reacts with the quark, was chosen. For pp-collisions in the pp-cms, this particle is a proton of energy $E_p = 7$ TeV and direction of motion opposite to the quark. From this, one obtains $Q^2 = x' s_{pp}$ where x' is

---

[2]The dependence of the distributions (5.21) on s_{qq} becomes explicit, if one rewrites the distributions in the form

$$x_i\frac{d}{dx_i}f_{V_i,\lambda_i}^p(\xi_i, Q_i^2) = \frac{\alpha}{2\pi}\frac{\xi_i}{x_i}\sum_{q_i(V_i)}c_{q_i(V_i)}^{\lambda_i}f_{q_i}^p(x_i, Q_i^2)h_{\lambda_i}\left(\frac{\xi_i}{x_i}, \frac{\sqrt{x_i}M_i^2}{\sqrt{\xi_i}s_{qq}}\right),\ i,j = 1,2,\ i \neq j.$$

[3]The energy has been evaluated in the hadron-hadron center-of-mass system.

variable in (5.24). For the scale Q^2 of the distribution-function f_γ^p the choice $Q^2 = x\, s_{pp}$ was made, where x is the scale variable of $f_\gamma^p(x)$.

Figures 5.5, 5.6 and 5.7 show the distribution-functions (5.24) of W^+, W^- and Z-bosons, respectively, in a proton of energy $E_p = \sqrt{s_{pp}}/2 = 7$ TeV. We will give a comparison of these distribution functions with distribution functions from the literature in the next section. We note that the dependence on the precise choice of Q^2 is small. One finds that the distributions change by 13% or less, for $x \geq 10^{-4}$, if $Q^2 = \max(x'^2 s_{pp}, M_W^2)$ is chosen instead of $Q^2 = x's_{pp}$.

Figure 5.8 shows the photon distribution $f_\gamma^p(x)$ of [83] in a proton of $E_p = 7$ TeV, where $Q^2 = xs_{pp}$ has been chosen. This distribution takes into account higher-order corrections of QCD. The figure also shows a photon distribution which has been calculated according to Eq. (5.24). Instead of a vector-boson mass, masses for the quarks have been inserted. By this prescription one obtains the photon distribution in the leading logarithmic approximation. The values $m_u = 5$ MeV, $m_d = 10$ MeV, $m_s = 200$ MeV (current masses for the light quarks) and $m_c = 1.3$ GeV, $m_b = 4.3$ GeV were used. The approximate distribution is greater than the distribution [83] at small values of x, $x \lesssim 10^{-1}$, and smaller at greater values of x. This observation has also been made in [83]. The deviations amount to +21% at $x = 10^{-3}$, +28% at $x = 10^{-2}$, −2% at $x = 10^{-1}$ and −33% at $x = 0.3$.

We discuss the quality of the approximations we made in deriving the convolutions. Figure 5.9 shows the ratios of the approximate luminosities for WZ-pairs, (5.22), and the improved luminosities, (5.10). The deviation of the approximation is for none of the helicity combinations greater than 25% of the improved luminosity, if the invariant mass $\mathcal{W}$ of the produced vector-boson pair is greater than 0.5 TeV. For the dominant luminosity, TT, the deviation is less than 7%. At $\mathcal{W} > 0.8$ TeV we have the following deviations: $TT < 7\%, \overline{TT} < 6\%, TL < 19\%, LT < 21\%, LL < 2\%$.

We discuss the quality of the approximations in terms of the cross-section for $pp \to ZZX$. This cross-section will be discussed in Section 5.4. Figure 5.10 shows the ratio of an approximation to the cross-section $d\sigma/dM_{ZZ}$ and the cross-section in the improved EVBA (the sum over all helicities was taken). Different approximations, finally leading to the convolution of vector-boson distributions, are shown. As the first of the approximations, the asymmetrical products, (4.61), instead of the exact expressions, (4.50), were used in Eq. (5.10)[4]. This leads to a deviation of 12% at $M_{ZZ} = 2$ TeV, which grows to 28% at $M_{ZZ} = 0.5$ TeV (we do not consider the effect of the Higgs-resonance in this discussion). If one uses the symmetrical products, (4.68), instead of the asymmetrical ones, the deviation does not change much. It grows by only a further 2% in the region 0.5 TeV $< M_{ZZ} < 2$ TeV. If one now uses the extrapolated value $s_{qq} = x_i^2 s_{pp}$ instead of the exact value $s_{qq} = x_1 x_2 s_{pp}$ of s_{qq} in the differential distributions in (5.21), the deviation is diminished to 10% at $M_{ZZ} = 2$ TeV and it is always less than 18% for smaller values of M_{ZZ}. So far, $Q^2 = s_{qq}/4$ was used in the quark-distributions. If we choose $Q^2 = x's_{pp}$ instead, where x' is the variable used in Eq. (5.24), the cross-section is virtually unchanged. The calculation is now equivalent to a calculation with vector-boson distributions in protons from (5.24).

In summary, the formalism of convolutions leads to a (positive) deviation of 10% at $\mathcal{W} = M_{ZZ} = 2$ TeV compared to the improved EVBA. The deviation grows to 18% at $M_{ZZ} \simeq 0.5$ TeV. This result was obtained for $pp \to ZZX$ at $\sqrt{s_{pp}} = 16$ TeV. For the pro-

---

[4]We used a rapidity-cut. This will be discussed in Section 5.3.

duction of other vector-boson pairs we expect a similar result because the approximations we made did not refer to any particular type of vector-boson.

Concluding this section, we described a formalism to calculate luminosities for vector-boson pairs in a hadron-pair approximately as convolutions of vector-boson distributions. We discussed the errors induced by this approximation.
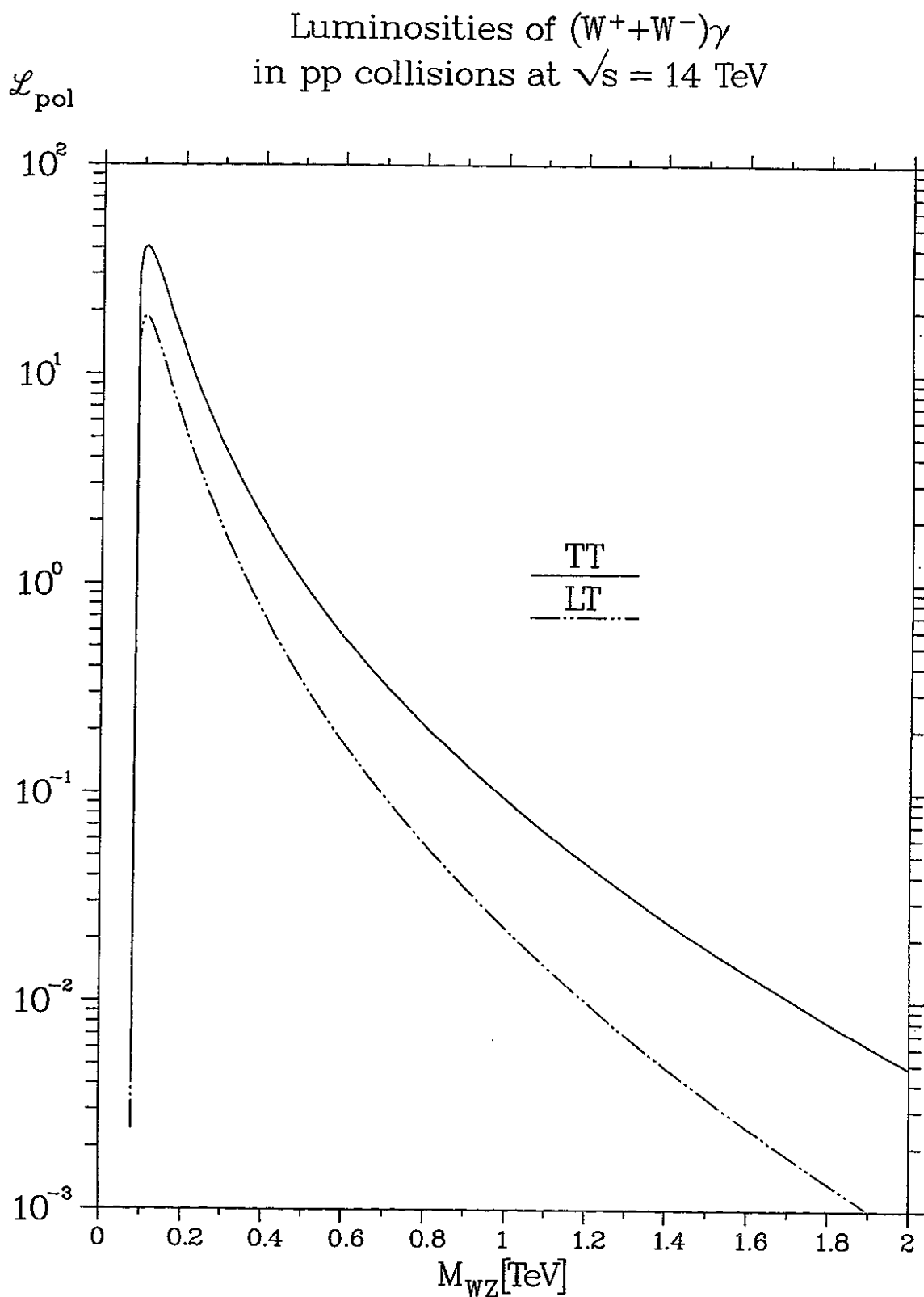
Figure 5.4: The luminosities of a $(W^+ + W^-)\gamma$-pair in a proton pair of invariant mass 14 TeV as a function of the invariant mass of the $W\gamma$-pair.

Figure 5.5: The distribution-functions (5.24) of a W^+-boson in a proton of the energy $E_p = 7$ TeV as a function of the scale variable x.

W^- distribution functions
in a proton of $E_p = 7$ TeV
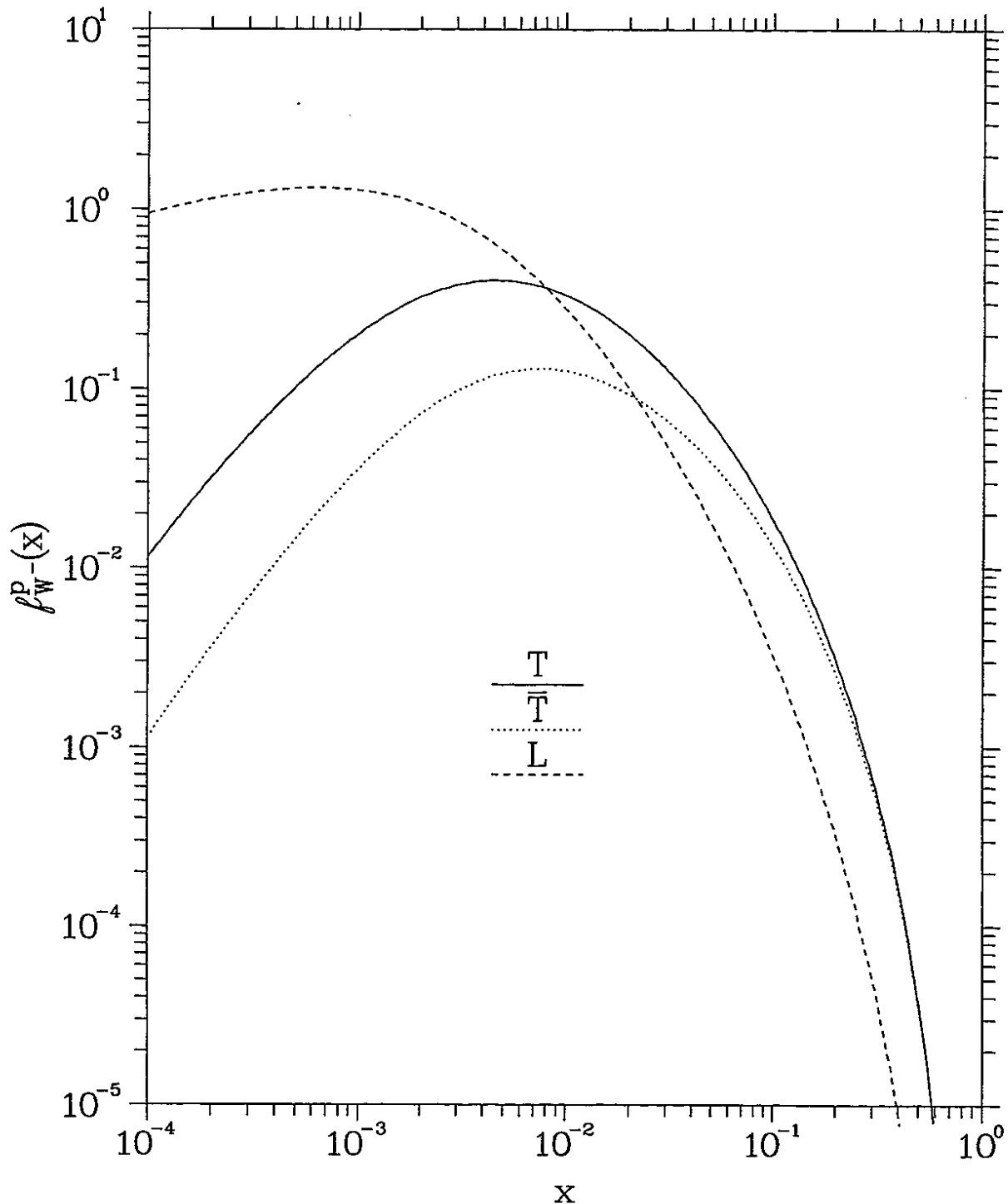
Figure 5.6: The distribution-functions (5.24) of a W^--boson in a proton of the energy $E_p = 7$ TeV as a function of the scale variable x.
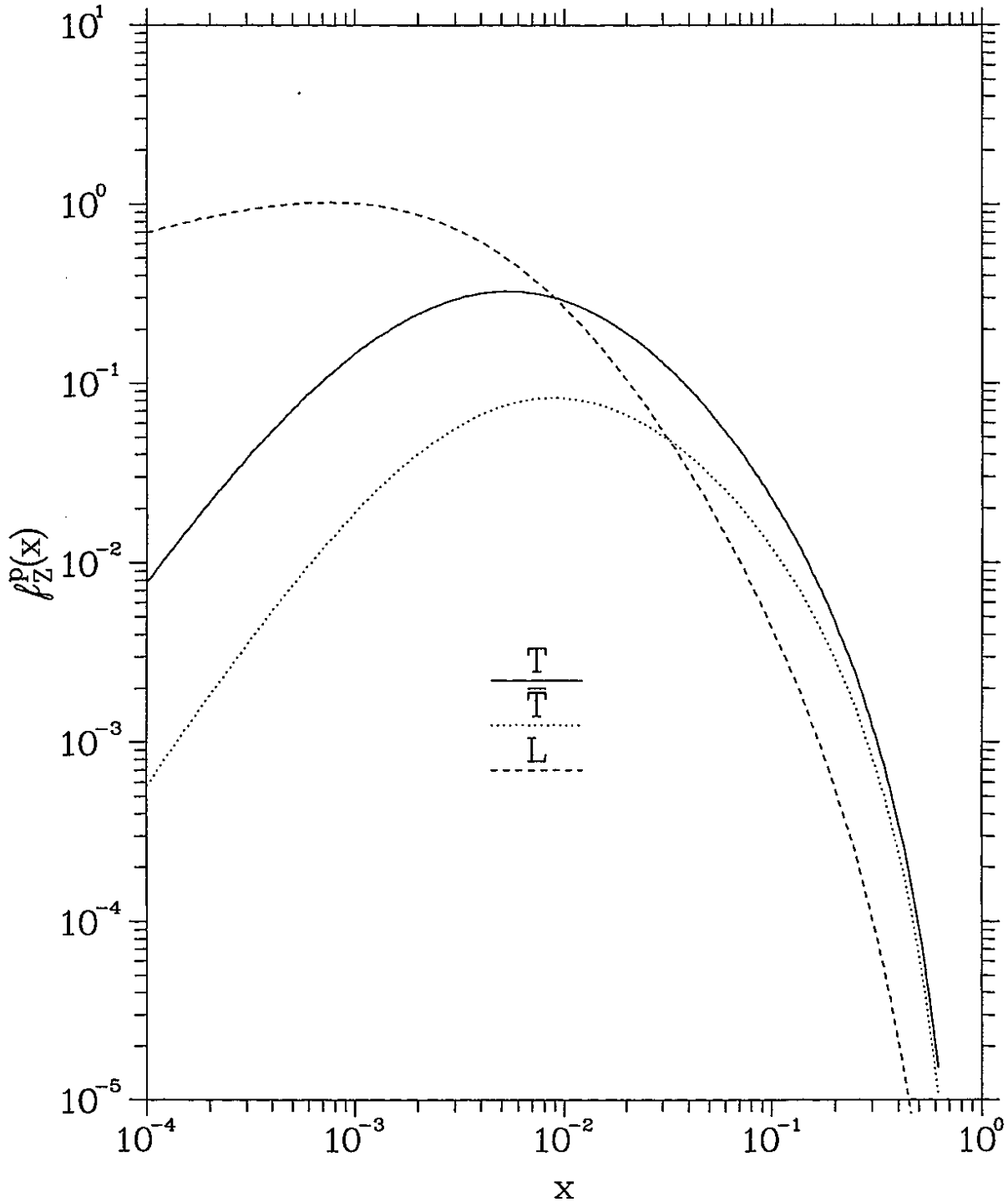
Figure 5.7: The distribution-functions (5.24) of a Z-boson in a proton of the energy $E_p = 7$ TeV as a function of the scale variable x.
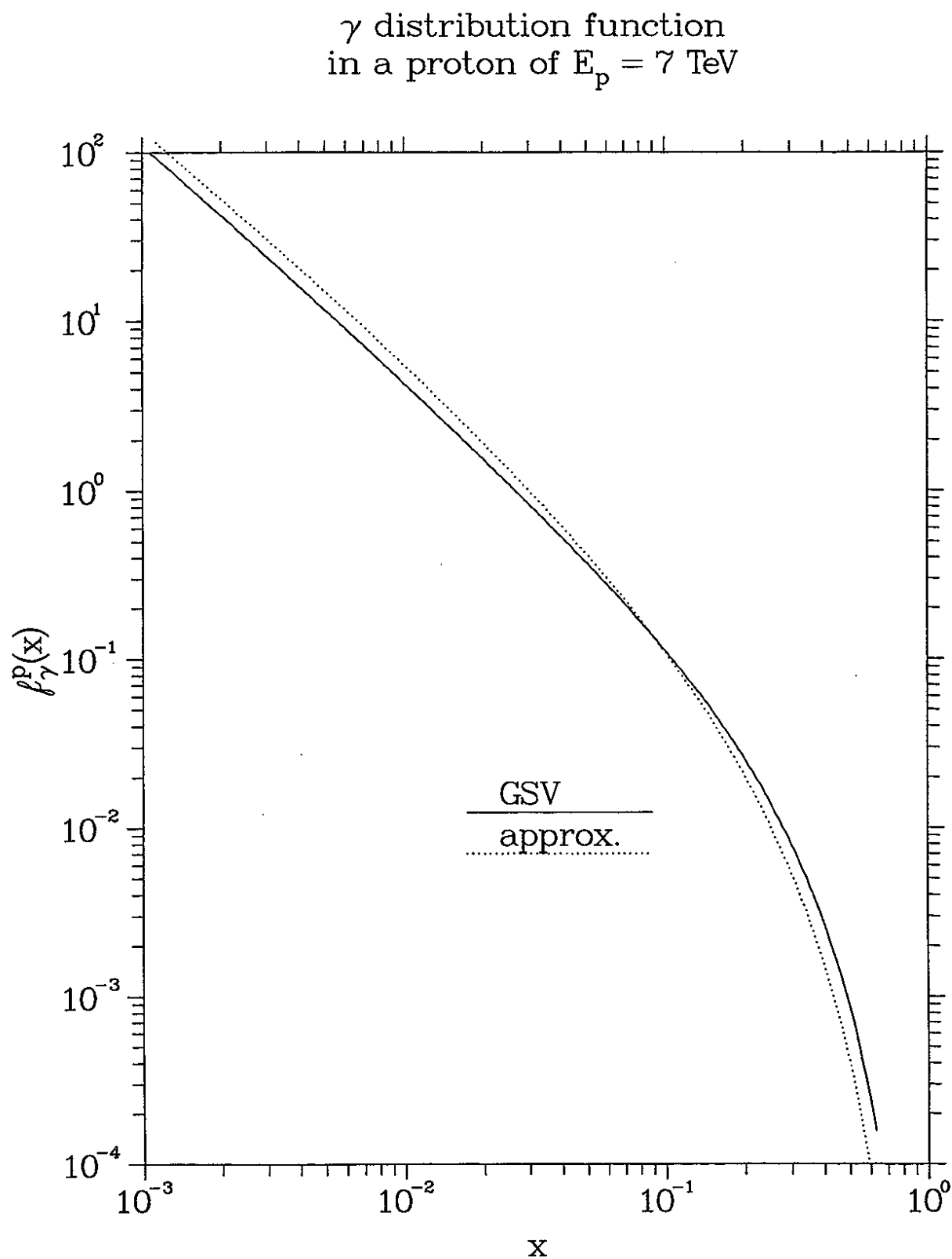
Figure 5.8: The distribution-function of a photon in a proton of the energy $E_p = 7$ TeV as a function of the scale variable x. Shown is the distribution of [83] and an approximate distribution calculated from Eq. (5.24).
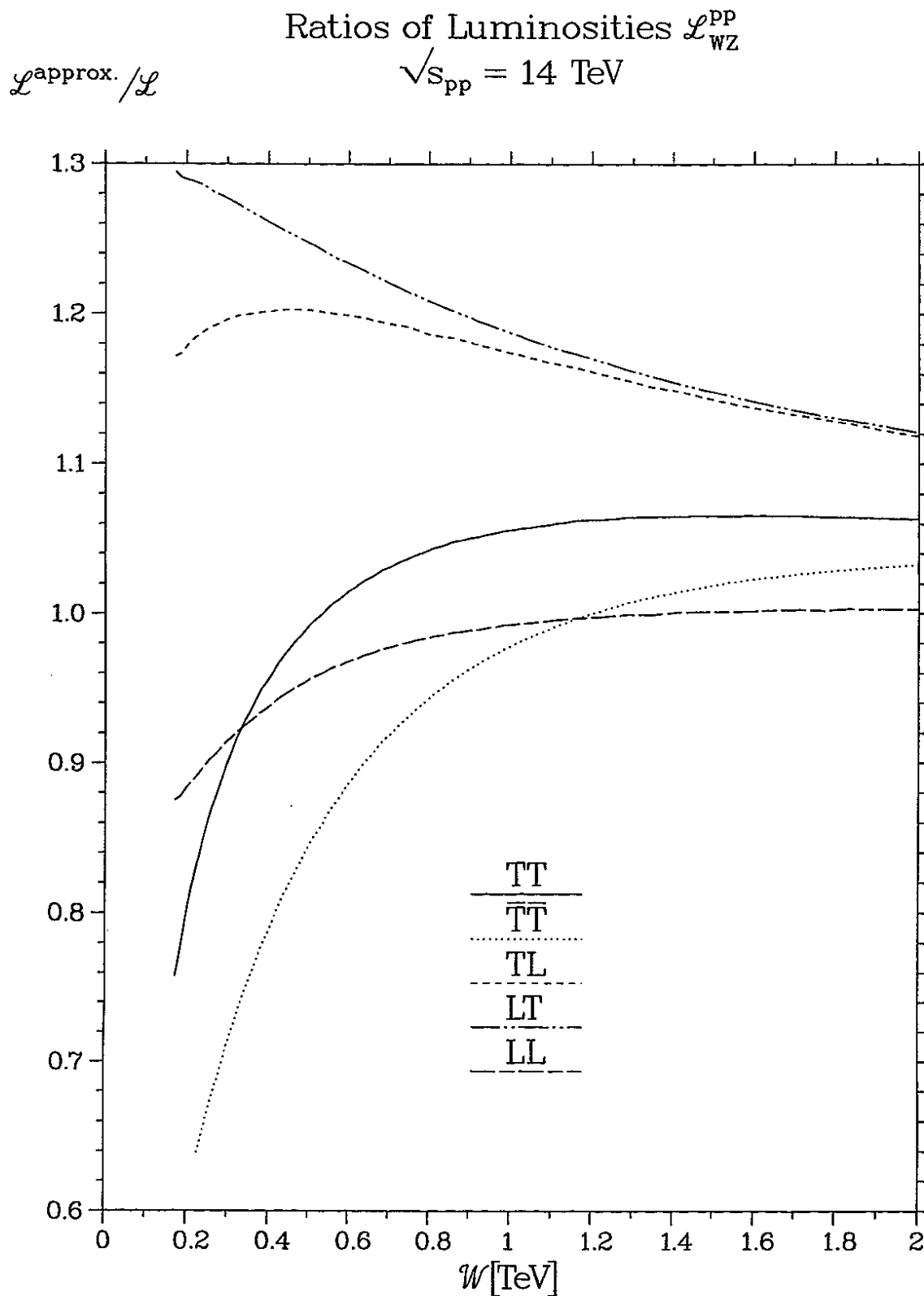
Figure 5.9: The ratio of the luminosities $\mathcal{L}^{pp}_{WZ}$ as convolutions of vector-boson distributions and the improved luminosities as a function of the invariant mass of the WZ-pair.

Approximations to improved EVBA
Ratios of cross-sections
$pp \to ZZ$ X at $\sqrt{s} = 16$ TeV, Y=2.5, $M_H = 0.5$ TeV

asymmetrical convolutions, $Q^2 = \tau s_{pp}/4$
symmetrical convolutions, $Q^2 = \tau s_{pp}/4$
sym. conv., s_{qq} in $f_V^q(x)$ approx., $Q^2 = \tau s_{pp}/4$
sym. conv, s_{qq} in $f_V^q(x)$ approx., $Q^2 = x's_{pp}$
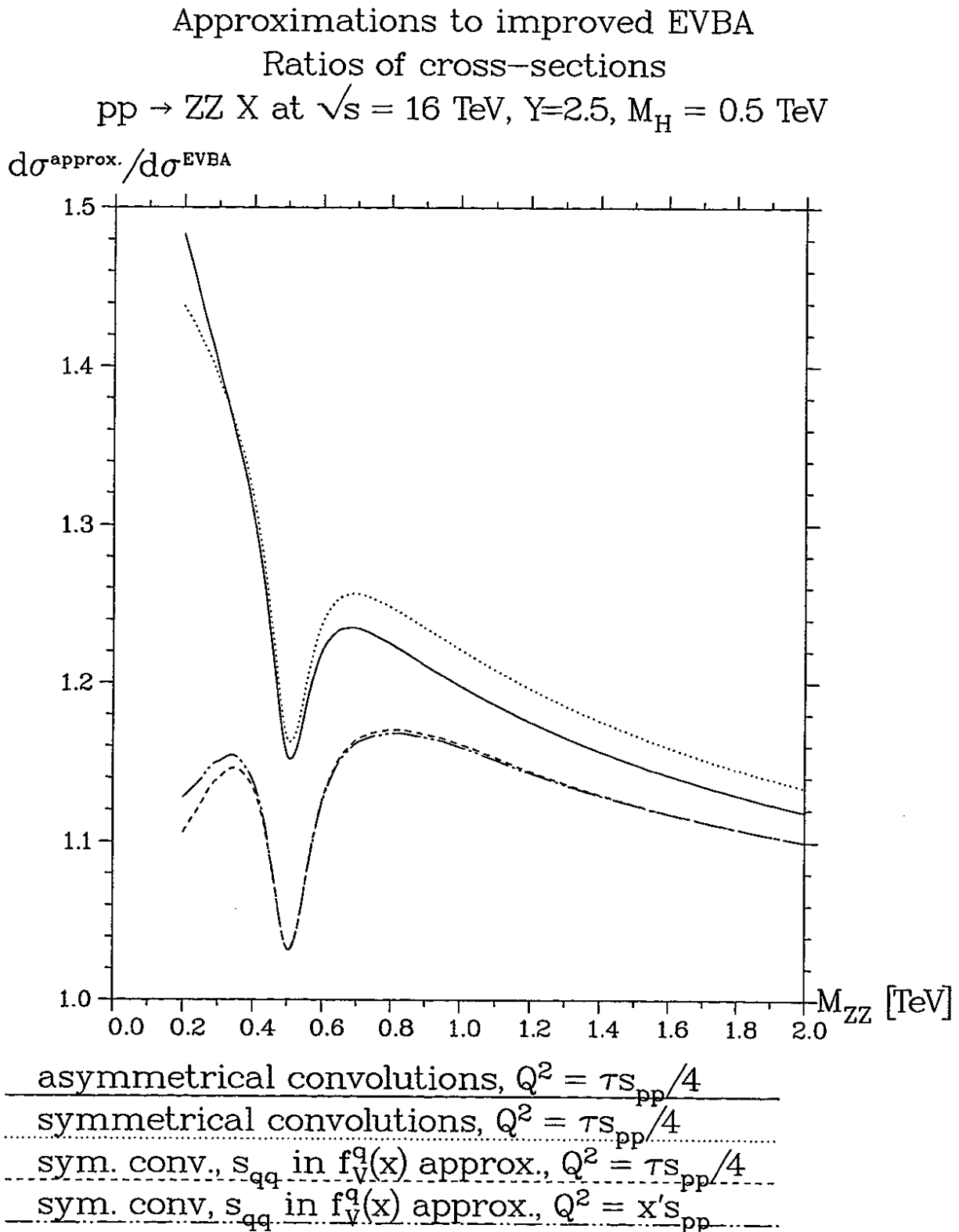
Figure 5.10: Ratios of cross-sections for $pp \to ZZX$ via vector-boson scattering as a function of M_{ZZ}. The ratios are for different approximations on the improved EVBA (see the text) and a calculation with the improved luminosities. A rapidity-cut of $Y = 2.5$ was chosen.
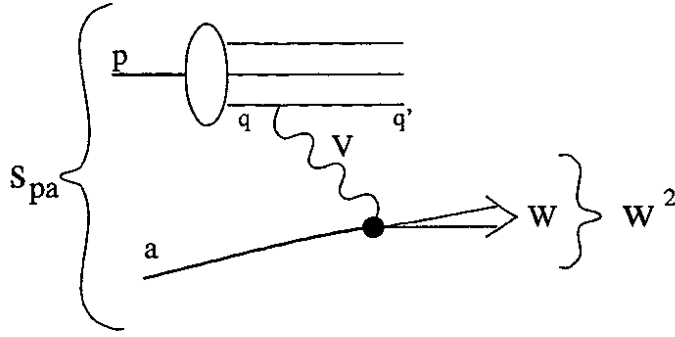
Figure 5.11: Schematical diagram for the scattering of a proton p with a particle a proceeding via the exchange of a vector-boson V. A final state W is produced.

5.2.3   Comparison with Vector-boson Distributions in a Proton from the Literature

We give a comparison of the distribution functions (5.24) with (5.25) and (4.63), with existing versions of distribution functions in the literature.

The distribution functions (5.24) were derived for the process shown in Figure 5.1. We now consider the process shown in Figure 5.11 in which a proton p reacts with a particle a. The reaction proceeds via the exchange of a single vector-boson. In this process, a final state W is produced and in addition one is left with the remnants of the proton, X, $pa \rightarrow WX$. The particle a can be of arbitrary type. The invariant mass squared of the pa initial state will be denoted by s_{pa}.

In the EVBA, the reaction happens as a two-step process. First, in the quark-parton model, the proton interacts via a quark q. We assume again that the quark has no transverse momentum with respect to the proton. The fraction of the quark momentum and the proton momentum will be called z. The cross-section for the reaction is described with the help of the quark-distributions in the proton, $f_q^p(z)$,

$$\sigma_{pa}(s_{pa}) = \int\limits_0^1 dz \sum_q f_q^p(z, Q^2)\sigma_{qa}(s_{qa}). \tag{5.26}$$

In (5.26), $\sigma_{qa}(s_{qa})$ is the cross-section for the reaction of the quark q with the particle a which happens at a reduced center-of-mass energy squared s_{qa}. We need an expression for s_{qa}. If we treat the proton and the quark as massless particles, the fraction of their momenta, z, is the same in any reference frame. We can thus choose any reference frame in which the proton- and quark-energies are large as compared to their respective masses, in order to evaluate s_{qa}. In the pa cms-frame one finds

$$s_{qa} = z s_{pa}. \tag{5.27}$$

Inserting the expression for the quark cross-section, (4.2), into (5.26) one obtains the cross-section $pa \rightarrow WX$ in the effective vector-boson approximation,

$$\sigma_{pa}(s_{pa}) = \int\limits_0^1 dz \int\limits_0^1 dy \sum_{q,V} f_q^p(z, Q^2) f_V^q\left(y, \frac{M_V^2}{s_{qa}}\right) \sigma_{Va}(yzs_{pa}). \tag{5.28}$$

Introducing the variable $x \equiv yz$, which connects the squared invariant masses $\mathcal{W}^2$ and s_{pa} by the relation

$$\mathcal{W}^2 = x s_{pa}, \tag{5.29}$$

we write the cross-section (5.28) differential in the variable x and obtain the expression

$$\frac{d\sigma_{pa}}{dx}(s_{pa}) = \sum_V \underbrace{\int_x^1 \frac{dz}{z} \sum_{q(V)} f_q^p(z, Q^2) f_V^q\left(\frac{x}{z}, \frac{M_V^2}{s_{qa}}\right)}_{\equiv f_V^p(x, s_{pa})} \sigma_{Va}(x s_{pa}). \tag{5.30}$$

In (5.30) we defined the vector-boson distribution function $f_V^p(x, s_{pa})$ describing the emission of a vector-boson V from the proton p.

The expression (5.30) is of the same form as is Eq. (5.24), with the formal difference that the type of the particle a is unspecified in (5.30).

It should be noted, however, that the two expressions describe different quantities. The distribution (5.24) with (5.25) is to be used in the luminosities (5.22) to describe the pp-processes proceeding via two virtual vector-bosons, shown in Figure 5.1. In contrast, the distribution-functions (5.30) describe the process shown in Fig. 5.11, which proceeds via only one vector-boson, and are to be used in Eq. (5.30). We note that the distributions (5.24) with (5.25) contain the variable $s_{qq} = x'^2 s_{pp}$, while the distributions (5.30) contain the variable $s_{qa} = z s_{pa}$ instead. It is instructive to numerically compare the two distributions.

We numerically compare f_V^p from (5.24), (5.25) with f_V^p from (5.30), using the various distributions f_V^q discussed in Section 4.2 as well as the LLA distributions (4.73). For the distributions [32, 66], we use $M_0 = M_W + M_Z$ as the sum of the masses in the final state. We also compare with the LLA distributions using $z s_{qa}(1-z)$ instead of s_{qa} as argument of the logarithms. These are the LLA distributions of [33], apart from the factor $1-z$, which is only of marginal relevance.

Our numerical example is for pp-reactions at $\sqrt{s_{pp}} = 14$ TeV. We will only plot the W^+-distributions as an example. The qualitative behavior of the W^-- and Z-distributions is the same. Figures 5.12, 5.13 and 5.14 show the T-, $\overline{T}$- and L-distribution-functions[5]. We see that the distribution function (5.24) is smaller than the other functions[6]. This smallness of the distribution function clearly reflects the effects of the mutual boson-boson phase-space which was taken into account. Expressed in another way, if one would use one of the other distribution-functions to calculate the luminosity (5.22), one would get a too large result. This is true for any calculation with transverse bosons. The deviation to smaller values appears only at very small values of x in the longitudinal case. Thus, only for the LL-polarization, the use of the distributions (5.30) in (5.22) can lead to a reliable result.

---

[5]I note that the deviation to positive values at small x observed for the distribution-function W_L^+ of [68] in Figure 5.14 is due to a specific model assumption.

[6]The $\overline{T}$-distribution of [33] is an exception. It becomes negative for small values of x.
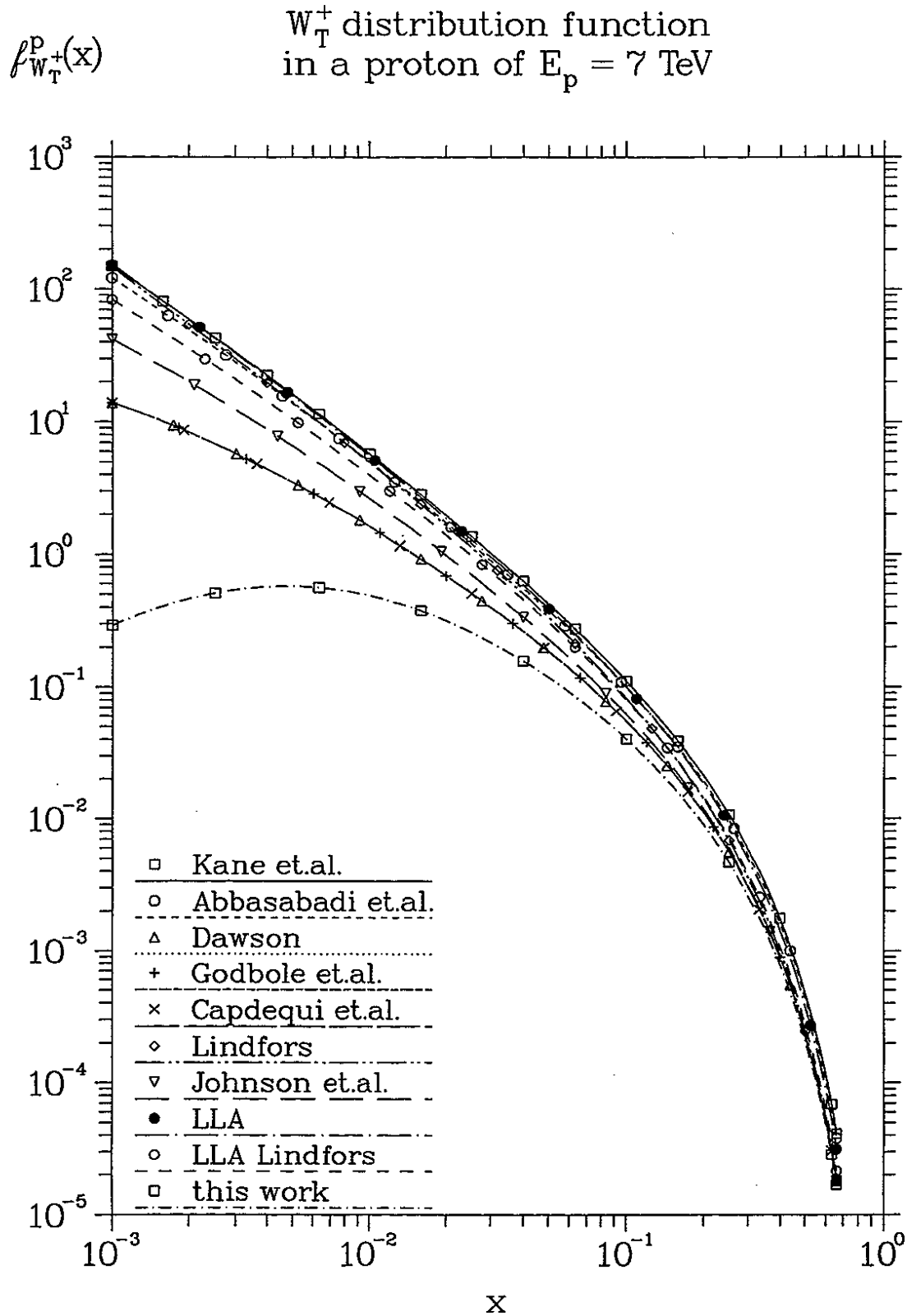
Figure 5.12: The distribution function of W^+-bosons with polarization T in a proton of energy $E_p = 7$ TeV. Calculated from (5.30), with different choices for f_V^q from the literature. Also shown is the distribution function (5.24) derived in this work, applicable to processes proceeding via two intermediate vector-bosons.
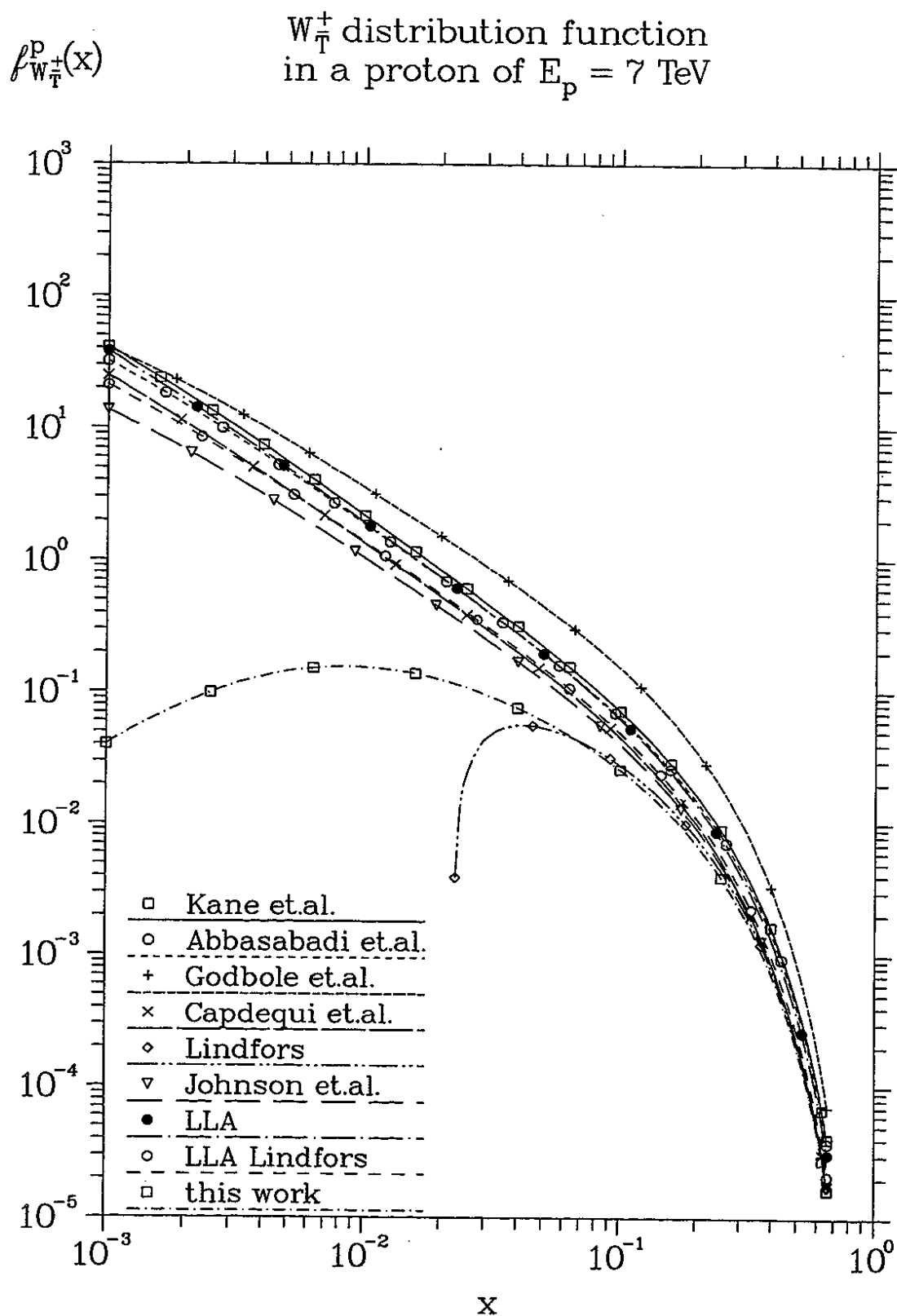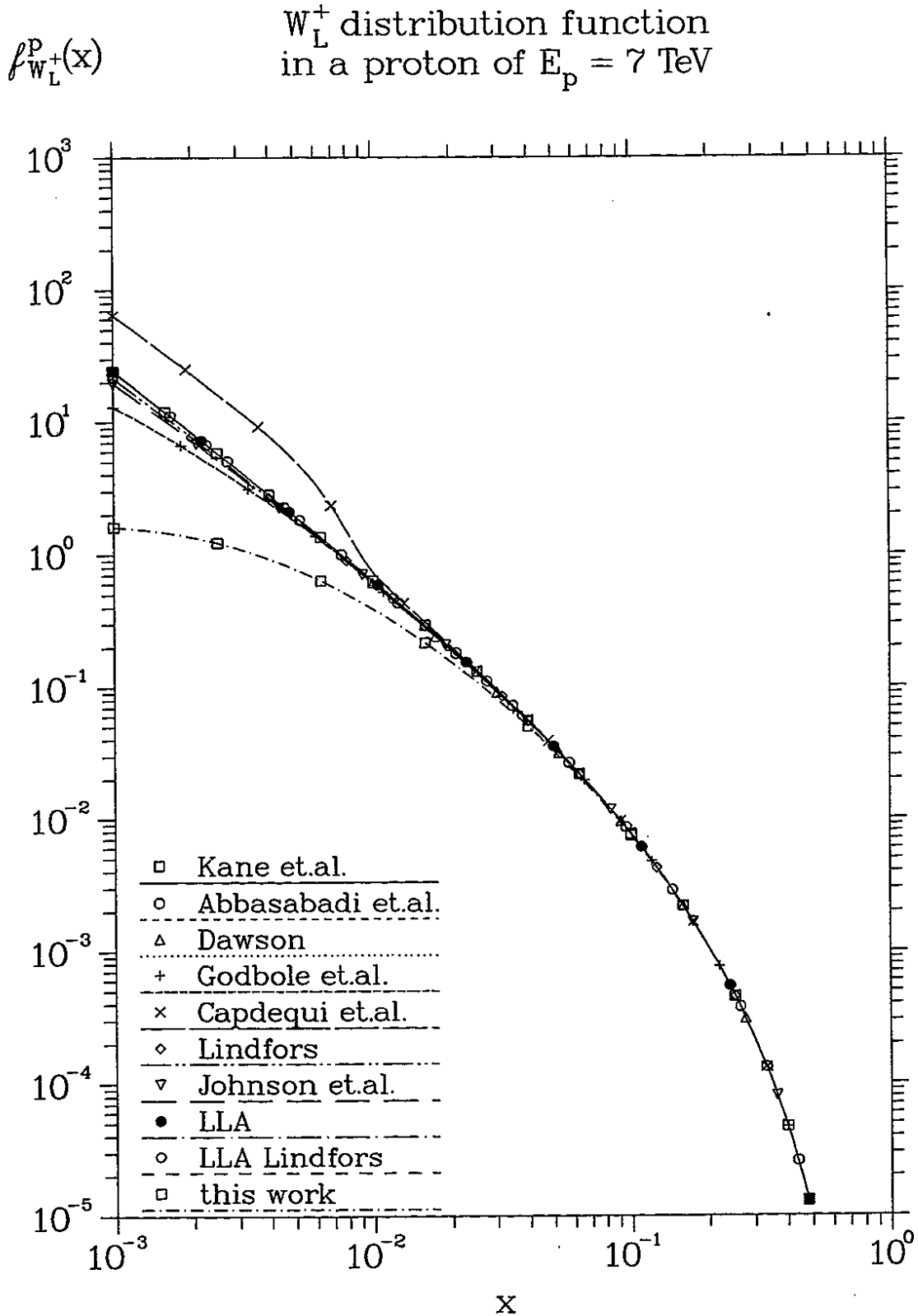
Figure 5.13: The distribution function of W^+-bosons with polarization $\overline{T}$ in a proton of energy $E_p = 7$ TeV. Calculated from (5.30), with different choices for f_V^q from the literature. Also shown is the distribution function (5.24) derived in this work, applicable to processes proceeding via two intermediate vector-bosons.

Figure 5.14: The distribution function of W^+-bosons with polarization L in a proton of energy $E_p = 7$ TeV. Calculated from (5.30), with different choices for f_V^q from the literature. Also shown is the distribution function (5.24) derived in this work, applicable to processes proceeding via two intermediate vector-bosons.

5.3 Application of Kinematical Cuts

In the following sections, we will have to apply kinematical cuts on the produced vector-bosons. This is already required considering that the detection of a particle with its direction of flight near the (hadron-) beam-pipe is not possible. In addition, the application of kinematical cuts allows to filter out the signal from anomalous couplings. If the energies of the produced vector-bosons are large compared to their masses, a rapidity-cut can be applied. Otherwise, a pseudorapidity-cut can be used. We will discuss both types of cuts in the following.

5.3.1 Application of a Rapidity Cut

We discuss the application of a rapidity-cut on the produced vector-bosons V_3 and V_4. The cut will be applied in the hadron-hadron center-of-mass system.

The rapidity y of a particle with four-momentum $p = (E; \vec{p})$ along a certain direction in space, in which a unity vector $\hat{x}_i$ may point, is given by $y \equiv \tanh^{-1}(\beta)$, where $\beta = \hat{x}_i \cdot \vec{p}/E$.

In order to apply rapidity-cuts to the produced vector-bosons V_3 and V_4, strictly the knowledge of all kinematical variables, which describe the intermdiate vector-bosons V_1 and V_2 in the parton-parton system, thus the variables $x, z, k_1^2, k_2^2, \varphi_1$ and φ_2 in (4.21), as well as a scattering angle θ for the process $V_1 V_2 \to V_3 V_4$, is required. The rapidities y_3 and y_4 of the vector-bosons V_3 and V_4 in the hadron-hadron system are then functions of all these variables and of the rapidity y of the parton-parton system. The application of a rapidity cut then implies restrictions on the integration regions of all these eight variables.

A principal simplification can be achieved if one treats the intermediate vector-bosons V_1 and V_2 as moving parallel to the hadron beam direction, as is the case for $k_j^2 = 0$. In this way, approximate expressions for the rapidities y_3 and y_4 are obtained. This approximation does not mean, that the k_1^2- and k_2^2-integrals are not anymore carried out over the entire phase-space. It means that one neglects the dependece of the rapidities on k_1^2 and k_2^2.

With this approximation one can obtain an expression for the rapidity y' of the motion of the $(V_1 V_2)$-center-of-mass in the $p_1 p_2$ center-of-mass system, taken along the direction of motion of the hadron, from which V_1 was emitted, by adding the rapidities y and $\hat{y}$ which appear in (5.3) and (5.10), respectively,

$$y' = y + \hat{y}. \tag{5.31}$$

The rapidity of the vector-boson V_3 in the $(V_1 V_2)$ center-of-mass system, taken along the direction of motion of the hadron, from which V_1 was emitted, is given by the expression

$$y_3^* = \tanh^{-1} \left(\frac{q \cos\theta}{\sqrt{q^2 + M_3^2}} \right). \tag{5.32}$$

In (5.32), θ is the angle between the directions of motion of V_1 and V_3, evaluated in the $(V_1 V_2)$ center-of-mass system. The variable q is the magnitude of the space-like momentum of the vector-boson V_3 in this system,

$$q = \frac{\mathcal{W}}{2} \sqrt{1 - \frac{2}{\mathcal{W}^2}(M_3^2 + M_4^2) + \frac{1}{\mathcal{W}^4}(M_3^2 - M_4^2)^2}. \tag{5.33}$$

The rapidity of the vector-boson V_4 in the (V_1V_2) center-of-mass system, taken along the direction of motion of the same hadron, is given by the expression

$$y_4^* = \tanh^{-1}\left(\frac{-q\cos\theta}{\sqrt{q^2 + M_4^2}}\right). \tag{5.34}$$

The rapidities y_3, y_4 of the vector-bosons V_3, V_4 in the (p_1p_2) center-of-mass system, taken along the direction of motion of the hadron, from which V_1 was emitted, are obtained by addition: $y_3 = y' + y_3^*$ and $y_4 = y' + y_4^*$.

We now demand that the rapidities of both produced vetor-bosons in the (p_1p_2)-cms do not exceed an upper limit Y,

$$|y_3| < Y \quad \text{and, in the same event,} \quad |y_4| < Y. \tag{5.35}$$

Events, which do not satisfy the above restriction, are to be cut away. The quantity Y is a rapidity-cut.

The cross-section for $p_1p_2 \to V_1V_2 \to V_3V_4$, (5.7) with (5.10) and (5.11), with the rapidity-cut (5.35), is given by the expression,

$$
\begin{aligned}
&\frac{d\sigma}{dx}(p_1p_2 \to V_1V_2 \to V_3V_4, s_{pp})|_{\text{Cut}} \\
&= \left(\frac{\alpha}{2\pi}\right)^2 \int_{-y'_{\max}}^{y'_{\max}} dy' \int_0^{\ln\left(\frac{1}{x}\right)} \frac{d\ln\left(\frac{1}{\tau}\right)}{\tau} \int_{\max[-\frac{1}{2}\ln\left(\frac{1}{\tau}\right),-\frac{1}{2}\ln\left(\frac{\tau}{x}\right)+y']}^{\min[\frac{1}{2}\ln\left(\frac{1}{\tau}\right),\frac{1}{2}\ln\left(\frac{\tau}{x}\right)+y']} dy \sum_{(V_1V_2)} N_c \tilde{x} \sum_{pol} \\
&\quad \cdot \left[\left(\sum_{q_1(V_1)} f_{q_1}^{p_1}(\sqrt{\tau}e^y, Q_1^2) c_{q_1(V_1)}^{pol} \right) \cdot \left(\sum_{q_2(V_2)} f_{q_2}^{p_2}(\sqrt{\tau}e^{-y}, Q_2^2) c_{q_2(V_2)}^{pol} \right) \right. \\
&\qquad \left. \cdot \mathcal{L}_{pol}(\hat{x}, \sqrt{\frac{x}{\tau}}e^{y'-y}, \frac{M_1^2}{s_{qq}}, \frac{M_2^2}{s_{qq}}) \quad + \quad p_1 \leftrightarrow p_2 \right] \\
&\quad \cdot \int_{z_{\min}(y')}^{z_{\max}(y')} d\cos\theta \frac{d\sigma}{d\cos\theta}((V_1V_2)_{pol} \to V_3V_4, \mathcal{W}^2),
\end{aligned}
\tag{5.36}
$$

where the integration limits are determined by the rapidity-cut,

$$
\begin{aligned}
y'_{\max} &= \min\left[Y, \frac{1}{2}\left(\frac{1}{x}\right)\right], \\
z_{\min}(y') &= \max\left[\frac{-\tanh(Y+y')}{\beta(M_3^2, M_4^2)}, \frac{-\tanh(Y-y')}{\beta(M_4^2, M_3^2)}, -\cos\theta_{\min}\right], \\
z_{\max}(y') &= \min\left[\frac{\tanh(Y-y')}{\beta(M_3^2, M_4^2)}, \frac{\tanh(Y+y')}{\beta(M_4^2, M_3^2)}, \cos\theta_{\min}\right],
\end{aligned}
\tag{5.37}
$$

with

$$
\begin{aligned}
\beta(M^2, M'^2) &\equiv \frac{\sqrt{1 - \frac{2}{\mathcal{W}^2}(M^2 + M'^2) + \frac{1}{\mathcal{W}^4}(M^2 - M'^2)^2}}{1 + \frac{M^2 - M'^2}{\mathcal{W}^2}} \\
&= \frac{q}{\sqrt{q^2 + M^2}},
\end{aligned}
\tag{5.38}
$$

and $\cos\theta_{\min} = 1$. In the vicinity of the threshold for the production of the pair V_3V_4, the rapidity-cut has no effect anymore, i.e. $z_{\max}(y')$ and $z_{\min}(y')$ are determined by $\cos\theta_{\min} =$

1. In order to have a cut also at small energies, one can insert an absolute upper limit on $|\cos\theta|$, $\cos\theta_{\min} \leq 1$, instead of the value $\cos\theta_{\min} = 1$. Here, $\theta_{\min}$ must be an angle, which is greater than or equal to the minimal angle with respect to the beam-direction, under which an event can still be detected. A reasonable choice is $\cos\theta_{\min} = \tanh(Y)$. This approximative treatment for small energies can be avoided if one uses a pseudorapidity-cut instead of a rapidity-cut (see 5.3.2).

If the masses of the vector-bosons V_3 and V_4 are equal or only slightly different, $M_3^2 \simeq M_4^2$, or if the momenta of the bosons are large against their masses, $q^2 \gg \max(M_3^2, M_4^2)$, the expressions (5.37) for $z_{\min}$ and $z_{\max}$ simplify to give $z_{\max} = -z_{\min} = z_0$, where

$$z_0 = \min\left[\frac{\tanh(Y - |y'|)}{\beta_{\max}}, \cos\theta_{\min}\right], \tag{5.39}$$

with $\beta_{\max} = \frac{q}{\sqrt{q^2 + \min(M_3^2, M_4^2)}}$. $\beta_{\max}$ is the greater one of the two values $\beta(M_3^2, M_4^2)$ and $\beta(M_4^2, M_3^2)$. One could have also chosen the smaller one of the two values. By choosing the greater value, slightly more, by choosing the smaller value, slightly less events are cut away as in the exact treatment of the cut given by (5.37).

5.3.2 Application of a Pseudorapidity-Cut

Near the threshold for the production of massive particles it is not anymore possible to use a rapidity-cut in order to cut away events near the beam-pipe. Particles whose magnitude of the space-like momentum is small against their energy are not cut away near the beam-direction by a rapidity-cut, as we saw above. A pseudorapidity-cut always excludes these events.

The pseudorapdtity η along a certain direction in space for some particle is defined in terms of the angle ϑ between the direction of motion of the particle and that direction in space, $\eta \equiv \tanh^{-1}(\cos\vartheta)$. For massless particles, the rapidity and the pseudorapidity are identical quantities, while for massive particles $y < \eta$. If a cut on the pseudorapidity is applied, there are therefore more events of massive particles being cut away than for a rapidity-cut of the same magnitude.

The application of a pseudorapidity-cut, $|\eta_3| < \eta$ and, for the same event, $|\eta_4| < \eta$, leads to the same formula, (5.36), as for a rapidity-cut, if the collinear approximation for the motion of V_1 and V_2 relative to the hadron-hadron beam-direction is made. However, the limits of integration $y'_{\max}$, $z_{\min}(y')$ and $z_{\max}(y')$ in (5.36) are given by the expressions

$$
\begin{aligned}
y'_{\max} &= \min\left[\frac{1}{2}\ln\left(\frac{1}{x}\right), \tanh^{-1}\left(\sqrt{\frac{1}{1 + \frac{\max(M_3^2, M_4^2)}{q^2}\sin^2\vartheta_{\min}}}\right)\right], \\
z_{\min}(y') &= \max\left[\frac{-t^2\gamma^2\beta^2 E_3 - \sqrt{q^2(1 + t^2\gamma^2) - t^2\gamma^2\beta^2 E_3^2}}{q(1 + t^2\gamma^2)},\right. \\
&\qquad\left.\frac{t^2\gamma^2\beta^2 E_4 - \sqrt{q^2(1 + t^2\gamma^2) - t^2\gamma^2\beta^2 E_4^2}}{q(1 + t^2\gamma^2)}\right] \\
z_{\max}(y') &= \min\left[\frac{-t^2\gamma^2\beta^2 E_3 + \sqrt{q^2(1 + t^2\gamma^2) - t^2\gamma^2\beta^2 E_3^2}}{q(1 + t^2\gamma^2)},\right.
\end{aligned}
$$

$$\left. \frac{t^2\gamma^2\beta^2 E_4 + \sqrt{q^2(1+t^2\gamma^2) - t^2\gamma^2\beta^2 E_4^2}}{q(1+t^2\gamma^2)} \right], \qquad (5.40)$$

instead of (5.37). Before using (5.40) on has to make sure that $z_{\min} < z_{\max}$; if this is not the case the contribution from the given y' is zero. In (5.40), $t^2 \equiv \tan^2\vartheta_{\min}$ and the quantity $\beta \equiv \tanh(y')$ is the boost-parameter for a transformation from the $(p_1 p_2)$ cms-system into the $(V_1 V_2)$ cms-system. Further, $\gamma^2 \equiv 1/(1-\beta^2)$. The quantities $E_3 \equiv \sqrt{q^2 + M_3^2}$ and $E_4 \equiv \sqrt{q^2 + M_4^2}$ are the energies of V_3 and V_4. The quantity $\vartheta_{\min}$ is the smallest allowed angle in the $(p_1 p_2)$ cms-system between the direction of motion of a produced vector-boson and the hadron-beam direction. It is related to the cut η by $\tanh(\eta) = \cot\vartheta_{\min}$.

For equal or nearly equal masses of the produced vector-bosons, $M_3^2 \simeq M_4^2$, or, equivalently, for large energies of the produced vector-bosons, $q^2 \gg \max(M_3^2, M_4^2)$, the limits of integration in (5.40) take on the simplified forms

$$y'_{max} = \min\left[\tanh^{-1}\left(\sqrt{\frac{1}{1 + \tan^2\vartheta_{\min}\frac{E^2}{q^2}}} \right), \frac{1}{2}\ln\left(\frac{1}{x}\right) \right],$$

$$z_0(y') = \frac{\frac{1}{\cos\vartheta_{\min}}\sqrt{q^2 - \min(M_3^2, M_4^2)\sin^2\vartheta_{\min}\beta^2\gamma^2} - \tan^2\vartheta_{\min}\gamma^2|\beta|E}{q(1 + \tan^2\vartheta_{\min}\gamma^2)}, \qquad (5.41)$$

where $E = \sqrt{q^2 + \min(M_3^2, M_4^2)}$ is the energy of the lighter one of the produced vector-bosons.

5.3.3 Application of Cuts to Convolutions

If one applies a rapidity- or pseudorapidity-cut to the expression for convolutions of vector-boson distributions, (5.7) with (5.22), one obtains the expression

$$\frac{d\sigma}{dx}(p_1 p_2 \to V_1 V_2 \to V_3 V_4)|_{\text{Cut}}$$

$$= \sum_{(V_1 V_2)} N_c \frac{\tilde{x}}{x} \sum_{pol=\lambda_1\lambda_2} \int_{-y'_{max}}^{y'_{max}} dy' \left[f_{V_1,\lambda_1}^{p_1}(\sqrt{x}e^{y'}, Q_1^2) f_{V_2,\lambda_2}^{p_2}(\sqrt{x}e^{-y'}, Q_2^2) + p_1 \leftrightarrow p_2 \right]$$
$$\cdot \sigma(z_0(y'), V_{1,\lambda_1}V_{2,\lambda_2} \to V_3 V_4), \qquad (5.42)$$

with y'_{max} and $z_0(y')$ from (5.37) or (5.40), respectively. If the V_3, V_4-particles are produced via $q\bar{q}'$-annihilation, instead, one obtains a formula similar to (5.42),

$$\frac{d\sigma}{dx}(p_1 p_2 \to q\bar{q}' \to V_3 V_4)|_{\text{Cut}}$$

$$= \int_{-y'_{max}}^{y'_{max}} dy' \sum_{(q\bar{q}')} \left[f_q^{p_1}(\sqrt{x}e^{y'}, Q_1^2) f_{\bar{q}'}^{p_2}(\sqrt{x}e^{-y'}, Q_2^2) + p_1 \leftrightarrow p_2 \right]$$
$$\cdot \sigma(z_0(y'), q\bar{q}' \to V_3 V_4), \qquad (5.43)$$

with y'_{max} and $z_0(y')$ also from (5.37) or (5.40), respectively. The formula (5.43) follows from (3.2). In deriving (5.43), the masses of the quarks q and $\bar{q}'$ were neglected.
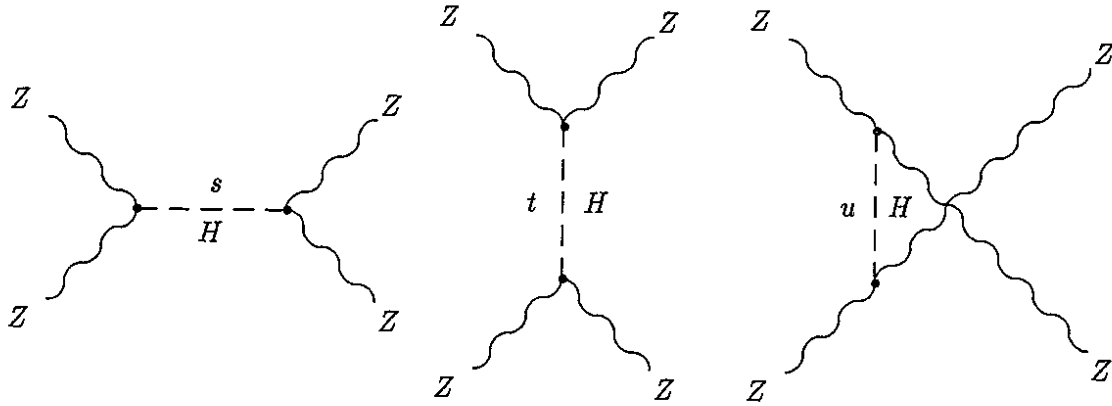
Figure 5.15: The Feynman diagrams for $ZZ \to ZZ$ in the Born approximation.

5.4 Comparison with a Complete Perturbative Calculation for the example $pp \to ZZX$

We are now going to present numerical comparisons of improved EVBA results with results of complete perturbative calculations. The complete perturbative calculation includes the contribution from bremsstrahlung diagrams. As an example, we choose the process $pp \to ZZX$, for which complete results are available. To my knowledge, a calculation for $pp \to WZX$ has never been performed. We will also compare with conventional formulations of the EVBA.

A complete perturbative treatment (to lowest order in the coupling α) of the process on the quark-level, $q_1 q_2 \to q_1' q_2' ZZ$, can be found in [76] and [77]. In [84], also the $\mathcal{O}(\alpha_s)$ radiative corrections for this process have been considered.

In the EVBA, the process proceeds via the vector-boson scattering-processes $W^+ W^- \to ZZ$ and $ZZ \to ZZ$. The amplitudes for $W^+ W^- \to ZZ$ are obtained from those for $W^+ Z \to W^+ Z$ by exchanging the kinematical variables s and t as well as the helicities λ_i of the particles according to

$$\mathcal{M}\left(W^+_{\lambda_1} W^-_{\lambda_2} \to Z_{\lambda_3} Z_{\lambda_4}\right)(s, t, u) = \mathcal{M}\left(W^+_{\lambda_1} Z_{-\lambda_3} \to W^+_{-\lambda_2} Z_{\lambda_4}\right)(t, s, u). \quad (5.44)$$

The process $W^+ Z \to W^+ Z$ will be discussed in Chapter 7.

For the process $ZZ \to ZZ$ there are three Feynman diagrams in the Born approximation, each of which describes the exchange of a Higgs particle, see Figure 5.15. The amplitude for the process is given in the SM by

$$\mathcal{M}(ZZ \to ZZ) = \frac{g^2 M_W^2}{c_W^2} \left(\frac{(\epsilon_1 \cdot \epsilon_2)(\epsilon_3^* \epsilon_4^*)}{s - M_H^2} + \frac{(\epsilon_1 \cdot \epsilon_3^*)(\epsilon_2 \cdot \epsilon_4^*)}{t - M_H^2} + \frac{(\epsilon_1 \cdot \epsilon_4^*)(\epsilon_2 \cdot \epsilon_4^*)}{u - M_H^2} \right), \quad (5.45)$$

where $\epsilon_i, i = 1, 2, 3, 4$ are polarization vectors and s, t, u are the Mandelstam variables.

Following the calculation in [84], we calculate the differential cross-section

$$d\sigma/dM_{ZZ}(pp \to (W^+ W^- + ZZ) \to ZZ, s_{pp})|_{\text{Cut}}$$

at $\sqrt{s_{pp}} = 16$ TeV for a rapidity cut of $Y = 2.5$. We use Eq. (5.36) and choose all parameters and the parametrizations for vector-boson- and quark-distributions as in [84]. Thus, for the differential vector-boson luminosities in a quark-pair the product of vector-boson distributions $f_{V,\lambda}^q(x)$ from [66] is inserted. However, in an attempt to obtain an improvement for the use of the distributions in processes proceeding via two vector-bosons the distributions [66] have been modified in [84]. This modification was obtained by the replacement $P_\perp^2 \to Q^2$. Different choices for Q^2 were made. We will specify them below. For definiteness, we first give the expressions for the amputated luminosities used in [84],

$$\mathcal{L}_{kl}\left(\hat{x},\hat{z},\frac{M_1^2}{s_{qq}},\frac{M_2^2}{s_{qq}}\right) = \hat{h}_k\left(\hat{z},\frac{M_1^2}{Q^2}\right)\hat{h}_l\left(\frac{\hat{x}}{\hat{z}},\frac{M_2^2}{Q^2}\right), \qquad (5.46)$$

where the functions $\hat{h}_{pol}$ are the amputated distributions,

$$\begin{aligned}
\hat{h}_T\left(x,\frac{M^2}{Q^2}\right) &= \frac{1+(1-x)^2}{x^2}\left[\ln\left(\frac{Q^2+M^2(1-x)}{M^2(1-x)}\right) - \frac{Q^2}{Q^2+M^2(1-x)}\right] \\
\hat{h}_{\overline{T}}\left(x,\frac{M^2}{Q^2}\right) &= \frac{2-x}{x}\left[\ln\left(\frac{Q^2+M^2(1-x)}{M^2(1-x)}\right) - \frac{Q^2}{Q^2+M^2(1-x)}\right] \\
\hat{h}_L\left(x,\frac{M^2}{Q^2}\right) &= 2\frac{1-x}{x^2}\frac{Q^2}{Q^2-M^2(1-x)}.
\end{aligned} \qquad (5.47)$$

In [84], $Q^2 = M_{ZZ}^2$ was chosen and the calculation was repeated for $Q^2 = M_{ZZ}^2/4$. For the quark-distributions $f_q^p(x,Q^2)$ the parametrisations of Duke and Owens [85], set 1, with $Q^2 = s_{qq}/4$ were used. The remaining parameters were $\alpha = 1/128$, $M_Z = 91.1$ GeV, $s_W^2 = 0.23$, $M_H = 500$ GeV and $\Gamma_H = 62$ GeV for the width of the Higgs particle.

We repeat the calculation of [84] in order to later discuss the improvement obtained by using the improved EVBA instead. For the same purpose, we will also show a result obtained by using the convolutions of the vector-boson distributions of [65]. This result is thus obtained by using (4.67) instead of (5.46). We will then compare all three calculations with the complete calculation.

The cross-sections obatined by using (4.67) and (5.46) are shown in Figure 5.16. The contributions from two longitudinally polarized intermediate vector-bosons, LL, and the one from the remaining helicity combinations are shown separately. The contribution from the longitudinal degrees of freedom is almost identical in all calculations and only shows a very weak dependence on the choice of Q^2 in (5.47). It is the dominating contribution in the vicinity of the Higgs resonance but becomes negligibly small if one is far away from the Higgs resonance, especially at $M_{ZZ}^2 \gg M_H^2$. The contribution from the transverse degrees of freedom, in contrast, depends principally on the exact choice of the distribution functions. It is very different for the two choices of Q^2. This contribution determines the cross-section at large M_{ZZ}, $M_{ZZ}^2 \gg M_H^2$.

The same calculation is now conducted with the improved differential luminosities, (4.50), instead of (4.67) or (5.46). The result is shown in Figure 5.17, where again the contributions from different helicity combinations are shown separately. The figure also shows the sum of the non-diagonal helicity combinations, $TLTL$, $\overline{T}L\overline{T}L$ and $TTTT$, which is negative and only plays a subordinate role here.

Figure 5.18, finally, shows again the results of the above calculations (only the result for $Q^2 = M_{ZZ}^2/4$ is shown) together with the complete (or exact) result from [84]. The sum of all intermediate helicities has been taken. The improved EVBA lies nearest to

the exact result. The deviation to the exact curve is, however, as large as a factor of two at $M_{ZZ} = 1$ TeV. We will give a possible explanation for this deviation further down. Also shown in Figure 5.18 is once again the contribution from longitudinally polarized intermediate vector-bosons. This contribution reproduces the cross-section on the Higgs-resonance very well. It was because of this observation that the EVBA could be used to calculate the cross-section for vector-boson pair production in strongly-interacting models of longitudinal vector-bosons. In these models, as on the Higgs-resonance, the longitudinal helicities give the dominant contribution.

We make another comparison of the EVBA with an exact calculation. This time also the result for a lower value of the cut, $Y = 1.5$, will be considered. Numerical results of the exact calculation are only available for $\sqrt{s} = 40$ TeV and can be found in [77] and [66, 86]. Only the production via W^+W^--pairs, $pp \to W^+W^- \to ZZ$, was considered[7]. We again calculate the differential cross-section $d\sigma/dM_{ZZ}$ from Eq. (5.36) with the luminosities of the improved EVBA. As in [66], the quark-distributions of EHLQ, [17], set 2, are used and the electroweak parameters are $\alpha = 1/128$, $s_W^2 = 0.22$, $M_W = 80$ GeV, $M_H = 0.5$ TeV and $\Gamma_H = 51.5$ GeV. For the scale Q^2 in the quark-distributions, $Q^2 = s_{qq}/4$ is chosen. We also carry out a calculation with the convolutions of vector-boson distributions from Eq. (5.42) [8]. Figure 5.19 shows the result of these calculations together with the exact result from [66]. A rapidity cut of $Y = 2.5$ was applied. The cross-section of the improved EVBA again deviates by a factor of two from the exact result at $M_{ZZ} = 1$ TeV. The result obtained with the convolutions deviates by 10% ($M_{ZZ} = 2$ TeV) and 18% ($M_{ZZ} = 0.8$ TeV) from the improved EVBA result.

Figure 5.20, finally, shows the same comparison for $Y = 1.5$. For this value of the rapidity-cut, a good agreement between the improved EVBA and the exact calculation is found. The EVBA deviates by less than 10% from the exact result for $M_{WZ} > 0.4$ TeV.

A possible explanation for the different results for $Y = 2.5$ and $Y = 1.5$ is that the bremsstrahlung-type diagrams in Fig. 4.1 begin to play a role if the angle between the produced vector-boson and the hadron beam-direction is small. This would be the case for $Y = 2.5$. In contrast, the bremsstrahlung-diagrams can be neglected if only large angles are involved. For a cut of $Y = 2.5$ angles down to $\theta_{min} = 9.4°$ are allowed, while the smallest angle for $Y = 1.5$ is $\theta_{min} = 25.2°$.

Summarizing this section, we have seen that the improved EVBA deviates by only 10% from the result of a complete perturbative calculation for a cut of $Y = 1.5$. This result was found for $pp \to ZZX$ at $\sqrt{s_{pp}} = 14$ TeV and invariant masses of $\mathcal{W} > 0.4$ TeV. The use of convolutions instead of the improved EVBA leads to an additional error of 10% at $\mathcal{W} = 2$ TeV. The error grows as $\mathcal{W}$ becomes smaller, but is stays below 18% if $\mathcal{W} \geq 0.5$ TeV. We have made an attempt to understand the observed failure of the EVBA for larger values of the cut in terms of the contribution from bremsstrahlung diagrams.

There is no reason that a similar conclusion could not also be drawn for the general process $pp \to V_3V_4X$. We expect this because the EVBA only pertains to the process-

---

[7]A separation into a contribution from intermediate W^+W^--pairs and a contribution from intermediate ZZ-pairs is also possible in the exact calculation (in a very good approximation) [77]. The diagrams of the exact calculation can be grouped into two classes. One class contains the W^+W^--diagrams of the EVBA and additional bremsstrahlung-type diagrams, the other class contains the ZZ-diagrams and also additional bremsstrahlung-diagrams. Both classes are a gauge-invariant subset. The interference term between the two classes, which arises when the amplitude is squared, is very small. The reason for this is the same one as for the neglect of the interference terms in the EVBA, see 4.3.1.

[8]The value of Q^2 in $f_q^p(x, Q^2)$ was $Q^2 = xs_{pp}$.

independent vector-boson luminosities.

pp→ZZ X at √s = 16 TeV, Y = 2.5

$M_H = 0.5$ TeV

$f_V^q(x)$ of Johnson and Baur

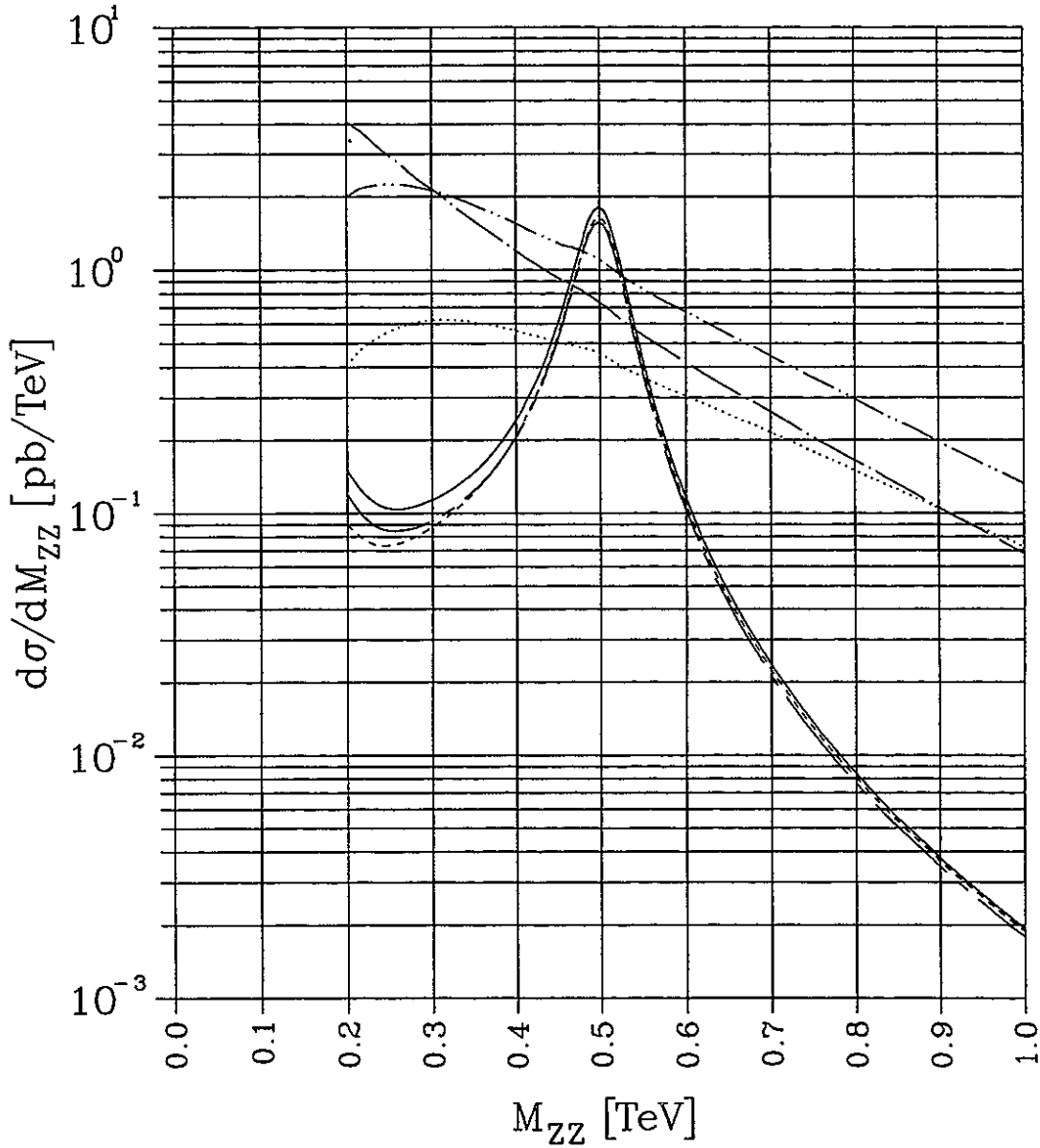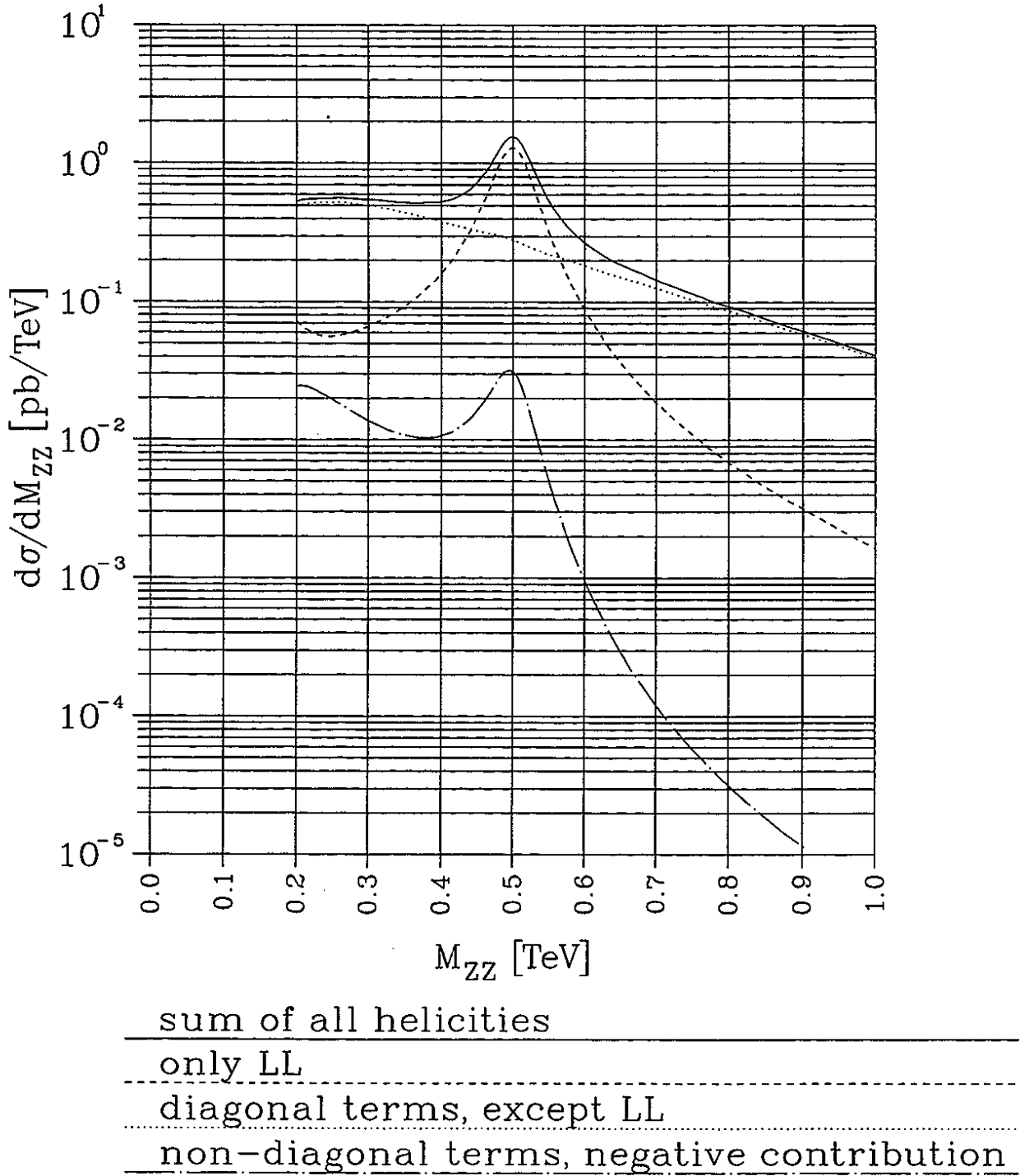| Baur	Johnson
only LL, $Q^2 = M_{ZZ}^2$	only LL
other helicities, $Q^2 = M_{ZZ}^2$	other helicities
only LL, $4Q^2 = M_{ZZ}^2$	
other helicities, $4Q^2 = M_{ZZ}^2$	

Figure 5.16: Contributions of different helicity combinations to the cross-section $pp \rightarrow$ ZZX via W^+W^-- and ZZ-scattering as a function of M_{ZZ}, calculated according to [84] with the convolutions (5.46) and according to [65] with the convolutions (4.67).

Figure 5.17: Contributions of different helicity combinations to the cross-section $pp \rightarrow ZZX$ via W^+W^-- and ZZ-scattering as a function of M_{ZZ}, calculated with the improved EVBA.

pp→ZZ X at √s = 16 TeV, Y = 2.5

$M_H = 0.5$ TeV

EVBAs versus exact calculation

EVBA Johnson

EVBA Baur, $4Q^2 = M_{ZZ}^2$

improved EVBA

exact

only LL,EVBA Baur, $4Q^2 = M_{ZZ}^2$

Figure 5.18: The cross-section for $pp \rightarrow ZZX$ via W^+W^-- and ZZ-scattering as a function of M_{ZZ}. Shown is the result of an exact calculation and different formulations of the EVBA (see text).

Figure 5.19: The cross-section for $pp \rightarrow ZZX$ via W^+W^--scattering as a function of M_{ZZ} at $\sqrt{s} = 40$ TeV and $Y = 2.5$. Shown is the result of a complete perturbative (exact) calculation, of the improved EVBA and of the convolutions of vector-boson distributions.

pp → WW → ZZ X at √s = 40 TeV, Y = 1.5
M_H = 0.5 TeV
EVBA versus exact calculation
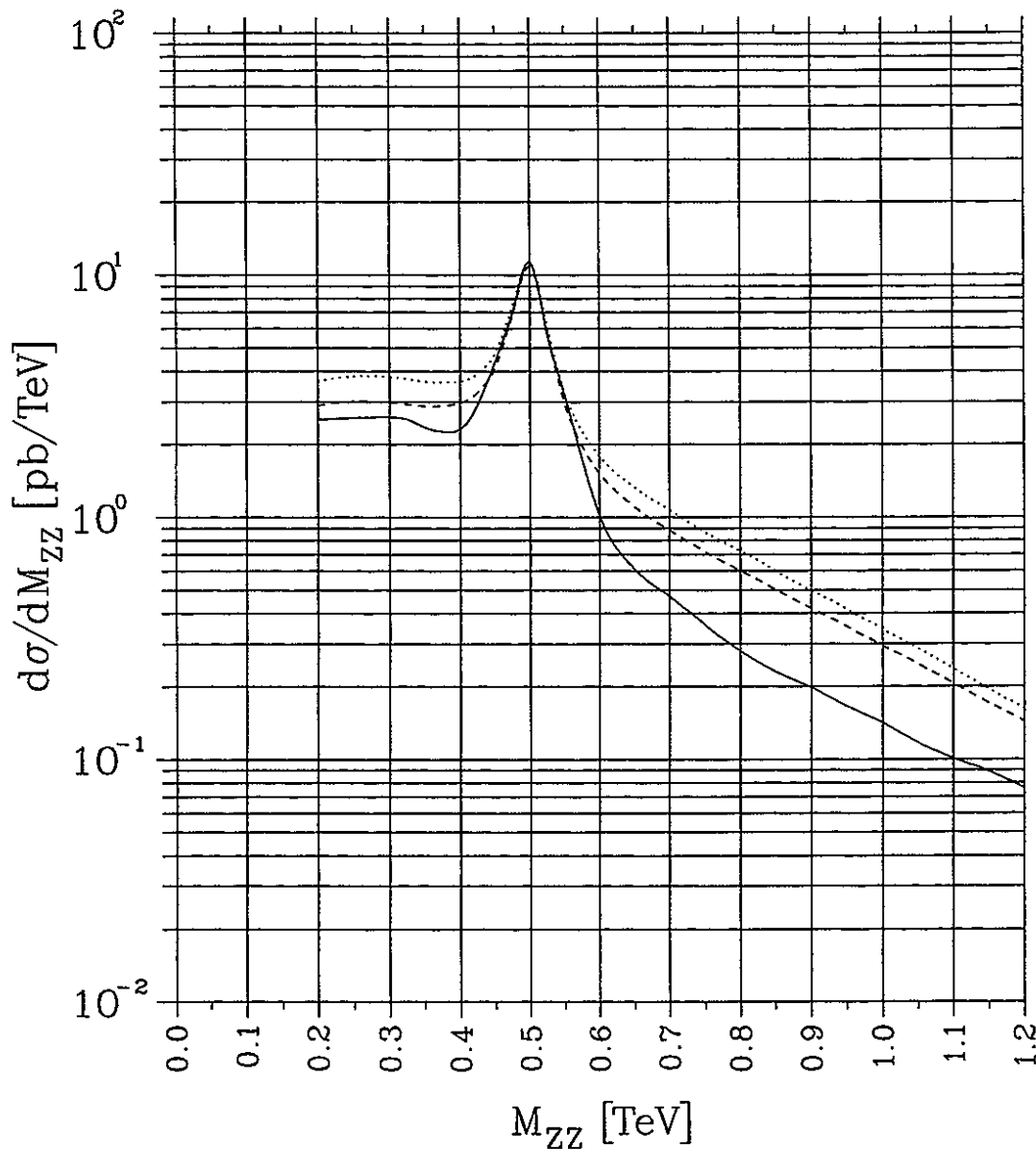
exact calculation

improved EVBA

convolutions of vector−boson distributions
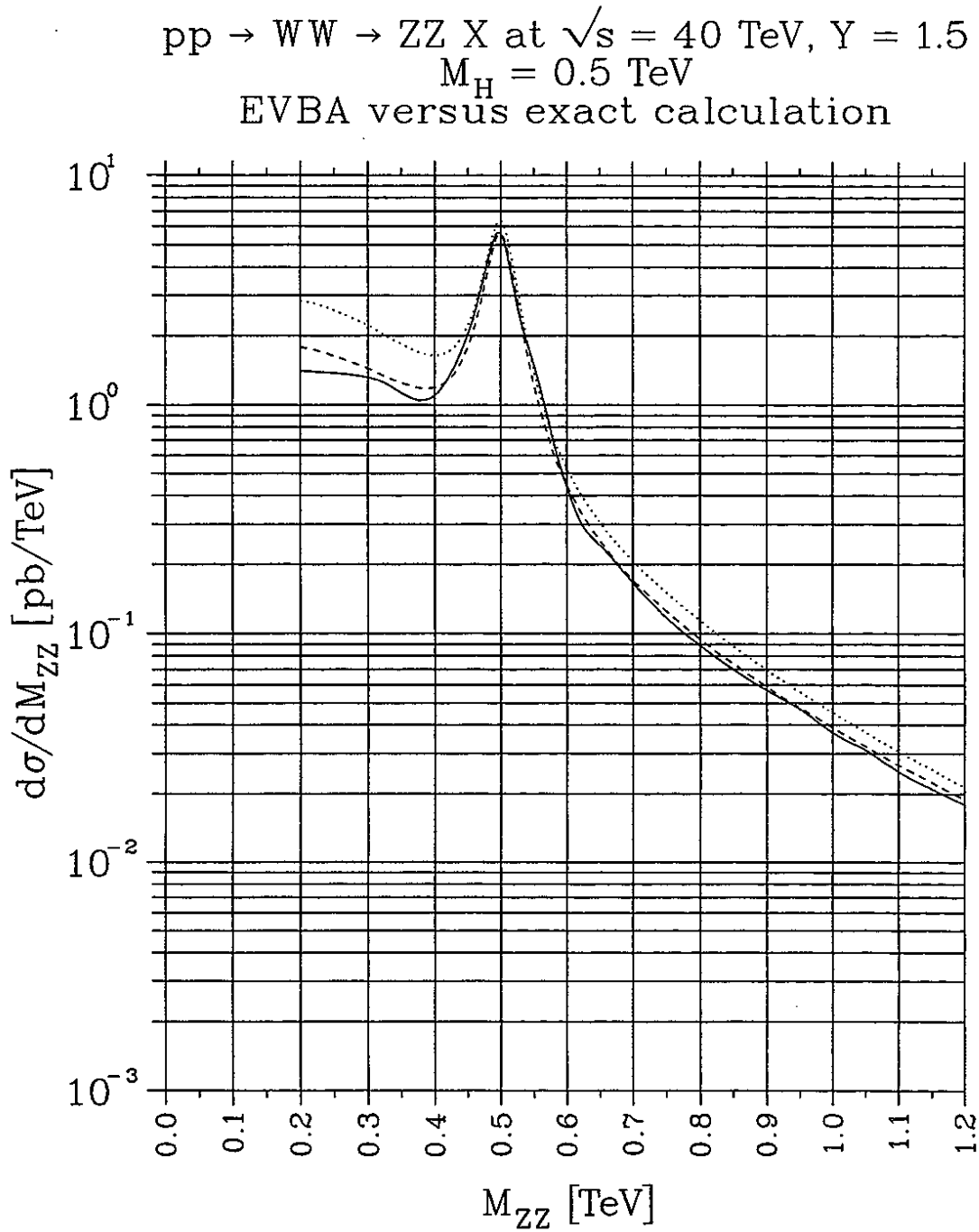
Figure 5.20: The cross-section for $pp \rightarrow ZZX$ via W^+W^--scattering as a function of M_{ZZ} at $\sqrt{s}$ = 40 TeV and Y = 1.5. Shown is the result of a complete perturbative (exact) calculation, of the improved EVBA and of the convolutions of vector-boson distributions.

Chapter 6

Cross-Sections for WZ-Production Processes

This chapter contains a discussion of the cross-sections for the production of WZ-pairs. We apply the treatments given in Chapters 3 and 5 to the production of WZ-pairs. We will first discuss the cross-sections for the parton-processes $q\bar{q}' \to WZ$ and $WV \to WZ$, $V = \gamma, Z$. A discussion of the effects of anomalous couplings and of the variation of the Higgs boson mass will be included. The cross-section for $pp \to WZX$ is then calculated according to Eq. (3.4) with (5.43) and (5.36) or (5.42). The contributions from the different parton-processes to the proton-proton cross-section will be compared. We will consider the differential cross-section $d\sigma/dM_{WZ}$ for the proton-proton process.

6.1 Cross-Sections for the Parton Processes

We discuss the cross-sections for $q\bar{q}' \to WZ$ and $WV \to WZ$ including the effects of anomalous couplings.

6.1.1 Cross-Section for $q\bar{q}' \to WZ$

For quark-antiquark annihilation into a WZ-pair, $W = W^+$ or W^-, there are the processes $u\bar{d} \to W^+Z$ and $\bar{u}d \to W^-Z$, where u is a quark of the up-type (up, charm or top) and d is a quark of the down-type (down, strange or bottom). We denote both processes generically by $q\bar{q}' \to WZ$. In the Born approximation there are three diagrams, as shown in Figure 6.1. The cross-section in the standard model for such a process has been first given in [16]. In [40] one finds an expression for the cross-section for arbitrary values of ϵ_W. I calculated the cross-section for arbitrary anomalous couplings $\epsilon_W, \epsilon_{W\Phi}$ and $\epsilon_{B\Phi}$. The cross-section, averaged over the helicities and colors of the incoming particles and summed over the helicities of the outgoing particles, is given by the expression

$$
\frac{d\sigma}{d\cos\theta}(q\bar{q}' \to WZ) = \frac{1}{32\pi s}\frac{\beta}{12}g^4\,|V_{q\bar{q}'}|\Bigg\{
$$
$$
\frac{1}{2}\left(\frac{s_W}{s - M_W^2}\right)^2\left[g_Z^2 s^2 A_0 + g_Z x_Z A_x + g_Z \frac{yz}{M_W^2}A_y \right.
$$
$$
\left. + x_Z \frac{yz}{M_W^2}A_{xy} + x_Z^2 A_{x^2} + \left(\frac{yz}{M_W^2}\right)^2 A_{y^2}\right]
$$
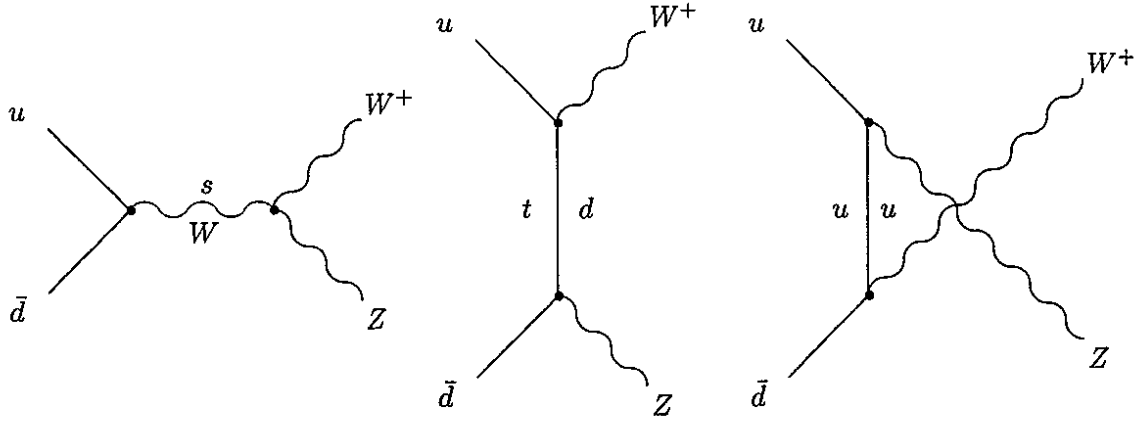
Figure 6.1: Feynman diagrams for $u\bar{d} \to W^+Z$ in the Born approximation.

$$+\frac{s_W}{s - M_W^2}\left[c_d\left(g_Z s I_0(s,t,u) + x_Z I_x(s,t,u) + \frac{y_Z}{M_W^2}I_y(s,t,u)\right)\right.$$
$$\left.-c_u\left(g_Z s I_0(s,u,t) + x_Z I_x(s,u,t) + \frac{y_Z}{M_W^2}I_y(s,u,t)\right)\right]$$
$$+(c_u - c_d)^2 E_0 + 2c_u^2\frac{tu - M_W^2 M_Z^2}{u^2} + 2c_d^2\frac{tu - M_W^2 M_Z^2}{t^2}$$
$$+4c_u c_d\frac{s(M_W^2 + M_Z^2)}{tu}\Bigg\}. \tag{6.1}$$

The relation between the parameters g_Z, x_Z and y_Z in (6.1) and the parameters $\epsilon_W, \epsilon_{W\Phi}, \epsilon_{B\Phi}$ has been given in (2.53). In (6.1), θ is the angle between the direction of motion of the W-particle and the u- or $\bar{u}$-quark, the quantity β is given by

$$\beta \equiv \sqrt{1 - 2\frac{M_W^2 + M_Z^2}{s} + \frac{(M_W^2 - M_Z^2)^2}{s^2}}, \tag{6.2}$$

and $g = e/s_W$ is the weak coupling constant. The quantity $V_{q\bar{q}'}$ is the corresponding element of the CKM matrix. The quantities s, t and u are the Mandelstam variables, given by

$$\begin{aligned} s &\equiv (p_q + p_{\bar{q}'})^2 \\ t &\equiv (p_u - p_{W^+})^2 = (p_{\bar{u}} - p_{W^-})^2 \\ &= -\frac{1}{2}\left(s(1 - \beta\cos\theta) - M_W^2 - M_Z^2\right), \\ u &\equiv (p_u - p_Z)^2 = (p_{\bar{u}} - p_Z)^2 \\ &= -\frac{1}{2}\left(s(1 + \beta\cos\theta) - M_W^2 - M_Z^2\right). \end{aligned} \tag{6.3}$$

The quantities c_d and c_u are the sums of the vector- and axial-vector-coupling (thus the lefthanded couplings), $c_i \equiv v_i + a_i$, $i = u, d$, for the coupling $-ig\gamma^\mu(v_i - a_i\gamma_5)$ of the Z^μ-boson to the d- and u-quark, respectively. They are given by

$$c_d = \frac{1}{2c_W}\left(1 - \frac{4}{3}s_W^2\right)$$

$$c_u = \frac{1}{2c_W}\left(-1 + \frac{2}{3}s_W^2\right).$$ (6.4)

The functions of the Mandelstam variables in (6.1) are given by,

$$A_0 = \left(\frac{tu}{M_W^2 M_Z^2} - 1\right)\left(\beta^2 + 12\frac{M_W^2 M_Z^2}{s^2}\right) + 2s\frac{M_W^2 + M_Z^2}{M_W^2 M_Z^2}\beta^2$$

$$A_x = \frac{2}{M_W^2}\left(s - 5M_W^2 - M_Z^2\right)\left(M_W^2 M_Z^2 - tu\right) + 2\frac{s^3}{M_W^2}\beta^2$$

$$A_y = 4s^3\beta^2 \quad , \quad A_{xy} = 2s\left(tu - M_W^2 M_Z^2\right) + s^3\beta^2$$

$$A_{x^2} = \frac{M_W^2 M_Z^2 - tu}{M_W^2}\left(s - 2M_W^2 - M_Z^2\right) + \frac{s^3}{2M_W^2}\beta^2$$

$$A_{y^2} = s\left(tu - M_W^2 M_Z^2\right)\left(2s - M_W^2 - M_Z^2\right) + \frac{s^3}{2}\left(M_W^2 + M_Z^2\right)\beta^2$$

$$I_0(s,t,u) = \left(\frac{tu}{M_W^2 M_Z^2} - 1\right)\left(1 - \frac{M_W^2 + M_Z^2}{s} - 4\frac{M_W^2 M_Z^2}{st}\right)$$
$$+ 2\frac{M_W^2 + M_Z^2}{M_W^2 M_Z^2}\left(s - M_W^2 - M_Z^2 + 2\frac{M_W^2 M_Z^2}{t}\right)$$

$$I_x(s,t,u) = \frac{1}{M_W^2}\left[st + s^2 + t^2 - M_Z^2(s+t)\right] - u - M_W^2 + 2\frac{M_Z^2}{t}(s + M_W^2)$$

$$I_y(s,t,u) = 2s\left(s - M_W^2 - M_Z^2\right) + 4M_W^2 M_Z^2\frac{s}{t}$$

$$E_0 = \frac{1}{2}\left(\frac{tu}{M_W^2 M_Z^2} - 1\right) + s\frac{M_W^2 + M_Z^2}{M_W^2 M_Z^2}.$$ (6.5)

The connection to the functions $A(s,t,u), I(s,t,u)$ and $E(s,t,u)$ in [16] is given by

$$A_0 = 4A(s,t,u), \quad I_0(s,t,u) = 4I(s,t,u), \quad E_0 = 2E(s,t,u).$$

High-Energy Approximation

For large scattering-energies, $s \gg M_W^2$, simple approximative formulae for the cross-section can be obtained. We assume that the couplings ϵ_i are small, $\epsilon_i = \mathcal{O}\left(M_W^2/s\right)$. Equivalently, we define the parameters

$$a_i \equiv \frac{s}{4M_W^2}\epsilon_i,$$ (6.6)

and assume that they are of the order $a_i = \mathcal{O}(1)$ or smaller. The leading terms in an asymptotic expansion of (6.1) in powers of M_W^2/s are given by

$$\frac{d\sigma}{d\cos\theta} = \frac{g^4}{32\pi s}\frac{\beta}{12}\left(\frac{1}{2c_W^2}\left(\frac{1 + \cos\theta}{1 - \cos\theta} + \frac{1 - \cos\theta}{1 + \cos\theta}\right)\left(c_W^2\cos\theta + \frac{s_W^2}{3}\right)\right.$$
$$\left. + 4\sin^2\theta c_W^2 a_W^2 + \frac{\sin^2\theta}{8}\left(1 - 4a_{W\Phi}\right)^2\right).$$ (6.7)

The expansion has been carried out at a fixed scattering-angle θ. Concerning the validity of the high-energy approximation, it should be noted that not only M_W^2/s, but also M_W^2/t and M_W^2/u play the role of an expansion parameter. These variables are smaller than a parameter δ,

$$\left|\frac{M_W^2}{t}\right|, \left|\frac{M_W^2}{u}\right| < \delta, \quad \text{with} \quad \delta = \frac{2M_W^2}{s(1 - z_0)},$$ (6.8)

where z_0 is the largest possible value of $|\cos\theta|$. An upper limit for z_0 is given in terms of the rapidity-cut η in the pp-system, $z_0 \leq \tanh(\eta)$. The equality in this last relation holds if the pp- and the WZ-cms-systems coincide. The parameter δ must not exceed a certain small value ϵ. The parameter ϵ is a measure for the relative error which is introduced by the high-energy approximation. For a given ϵ one obtains, via the requirement $\delta < \epsilon$, an upper limit on the rapidity cut, above which the high-energy approximation should not be used, namely

$$\eta < \eta_{max} = \tanh^{-1}\left(1 - \frac{2M_W^2}{s\epsilon}\right). \tag{6.9}$$

At $\sqrt{s} = 1$ TeV one obtains: $\epsilon = 0.1 \Rightarrow \eta_{max} = 1.34$, $\epsilon = 0.2 \Rightarrow \eta_{max} = 1.70$.

The expression (6.7) does not depend on $a_{B\Phi}$, i.e. there are no effects enhanced by powers of s/M_W^2 concerning this parameter. There are linear and quadratic effects of the parameter $a_{W\Phi}$ and quadratic effects of a_W.

One obtains the same expression, (6.7), by squaring and summing the high-energy expressions for the helicity amplitudes $u(\sigma = -\frac{1}{2})\bar{d}(\sigma = \frac{1}{2}) \to W^+(\lambda_W)Z(\lambda_Z)$, $\lambda_W, \lambda_Z = \pm 1, 0$, where σ are the helicities of the fermions and λ_W and λ_Z the helicities of the vector-bosons. These expressions for the helicity amplitudes are given by

$$\begin{aligned}
\mathcal{M}(\pm\pm) &= -2g^2\frac{\sin\theta}{\sqrt{2}}c_W a_W \\
\mathcal{M}(\pm\mp) &= \mp\frac{g^2}{\sqrt{2}}\frac{\sin\theta}{1\pm\cos\theta}\frac{1}{c_W}\left(c_W^2\cos\theta + \frac{s_W^2}{3}\right) \\
\mathcal{M}(00) &= -\frac{g^2}{2\sqrt{2}}\sin\theta\left(1 - 4a_{W\Phi}\right).
\end{aligned} \tag{6.10}$$

The cross-section is obtained in terms of the amplitudes by the relation

$$\frac{d\sigma}{d\cos\theta} = \frac{1}{32\pi s}\frac{\beta}{12}\sum_{\lambda_W,\lambda_Z}|\mathcal{M}(\lambda_W,\lambda_Z)|^2. \tag{6.11}$$

The expressions for $\mathcal{M}(\pm\pm)$ and $\mathcal{M}(\pm\mp)$ can be found in [20, 41]. The expression for $\mathcal{M}(00)$ has been calculated by myself. An approximate expression can be found in [20].

In the high-energy approximation, a simple expression also exists for the integrated cross-section,

$$\begin{aligned}
\sigma(z_0) &\equiv \int_{-z_0}^{z_0} d\cos\theta \frac{d\sigma}{d\cos\theta} \\
&= \frac{g^4}{32\pi s}\frac{\beta}{12}\left[2\ln\left(\frac{1+z_0}{1-z_0}\right)c_W^2\left(1 + \frac{t_W^4}{9}\right) - 2c_W^2\left(z_0\left(2 + \frac{t_W^4}{9}\right) + \frac{z_0^3}{3}\right) \right. \\
&\quad \left. + \left(z_0 - \frac{z_0^3}{3}\right)\left(8a_W^2 c_W^2 + \frac{(1 - 4a_{W\Phi})^2}{4}\right)\right].
\end{aligned} \tag{6.12}$$

Discussion of Numerical Results

Figure 6.2 shows the differential cross-section (6.1) as a function of $\cos\theta$ at a scattering-energy of $\sqrt{s} = 1.5$ TeV in the standard model and for various values of the anomalous couplings. The energy $\sqrt{s} = 1.5$ TeV has been chosen as an example. The standard cross-section is very small at $\cos\theta \simeq (c_u + c_d)/(c_u - c_d) = -\frac{1}{3}t_W^2 \simeq -0.1$. This smallness

has been called an approximate amplitude zero [87]. For $\cos\theta \to \pm 1$ the cross-section becomes very large. This is due to the exchange of two very light particles in the t- and u-channel and it is reflected by the logarithm in (6.12). If the anomalous couplings are different from zero, the cross-section becomes larger especially at large scattering-angles θ. The parameter $\epsilon_{B\Phi}$ has to be much greater than the parameters $\epsilon_W, \epsilon_{W\Phi}$ in order to lead to comparable effects. For the cases $\epsilon_{B\Phi} = 0$, Figure 6.2 also shows the high-energy approximation (6.7). This approximation is very good at $\sqrt{s} = 1.5$ TeV.

Figure 6.3 shows the integrated cross-section as a function of the scattering energy $\sqrt{s}$ for various values of the anomalous couplings. A pseudorapidity-cut of $\eta = 1.5$ has been applied, which correspnds to an integration region for the scattering-angle of $25° < \theta < 155°$. Also shown is the high-energy approximation, (6.12), if $\epsilon_{B\Phi} = 0$. A positive value of $\epsilon_{W\Phi}$ leads to a decrease of the cross-section at small scattering-energies and to an increase at large energies. A negative value of $\epsilon_{W\Phi}$ always leads to an increase. At large energies the increase due to a negative value of $\epsilon_{W\Phi}$ is similarly large as the increase due to a comparable value of $|\epsilon_W|$, while for small energies the increase due to a negative $\epsilon_{W\Phi}$ is larger. This latter feature can be understood from the fact that a linear coefficient of a_W is absent in (6.12). The deviation of the high-energy approximation (6.12) from the integrated cross-section (6.1) is -16% in the SM at $\sqrt{s} = 0.5$ TeV, -7% at 0.8 TeV, -5% at 1 TeV and -1.3% at 2 TeV.

Figure 6.4 shows the dependence of the standard cross-section on the choice of the cut η. A scattering energy of $\sqrt{s} = 0.5$ TeV has been chosen as an example. Due to the mentioned singularities at extreme values of the scattering angle there is a steep increase of the cross-section with increasing η. The high-energy approximation does not become worse as η increases.
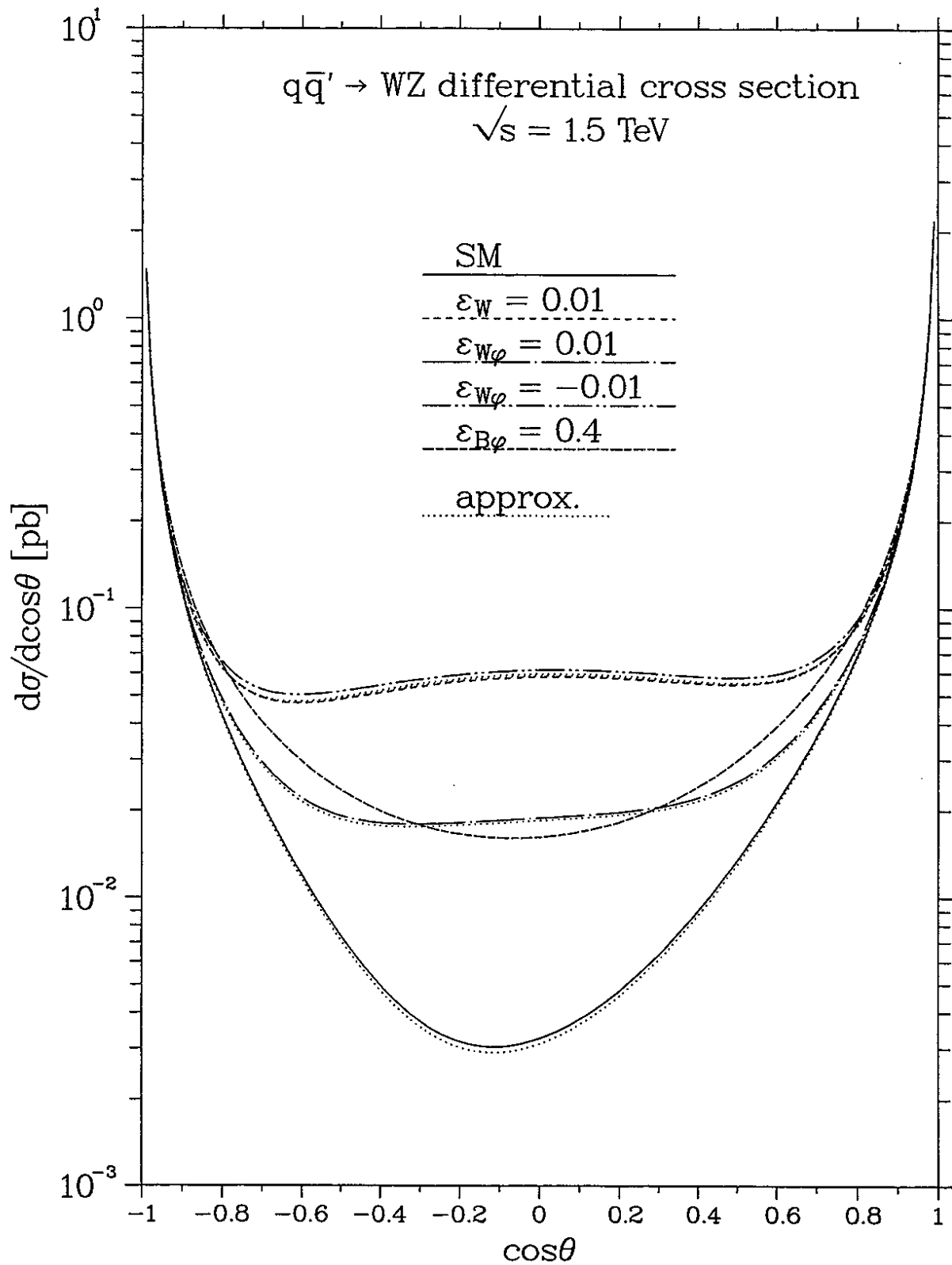
Figure 6.2: The differential cross-section for $q\bar{q}' \to WZ$ as a function of $\cos\theta$ at $\sqrt{s} = 1.5$ TeV for various values of the anomalous couplings. Also shown is the high-energy approximation.
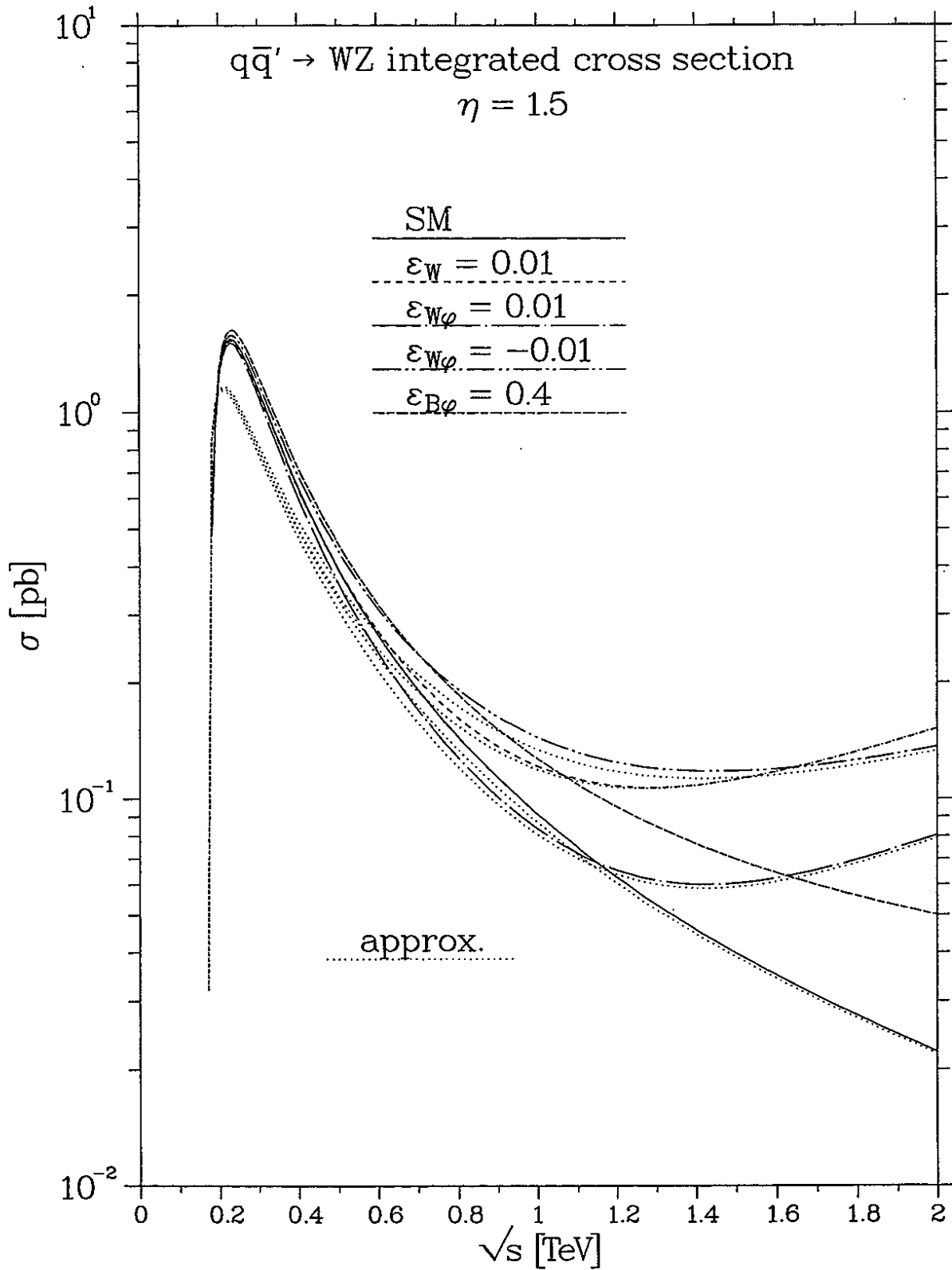
Figure 6.3: The integrated cross-section for $q\bar{q}' \to WZ$ as a function of the scattering-energy $\sqrt{s}$ for $\eta = 1.5$ and various values of the anomalous couplings. Also shown is the high-energy approximation.
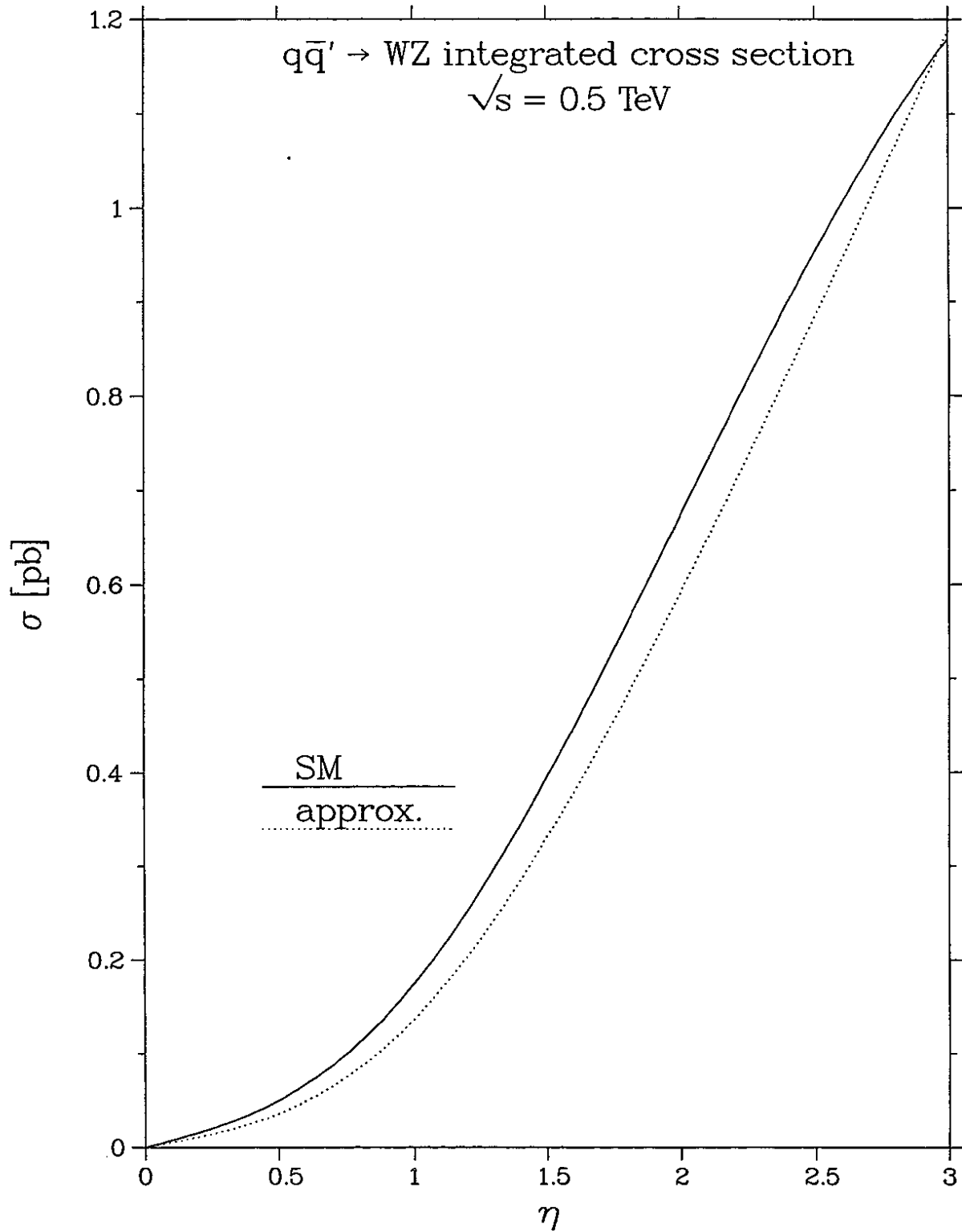
Figure 6.4: The integrated cross-section for $q\bar{q}' \to WZ$ as a function of the cut η at $\sqrt{s} = 0.5$ TeV. Also shown is the high-energy approximation.
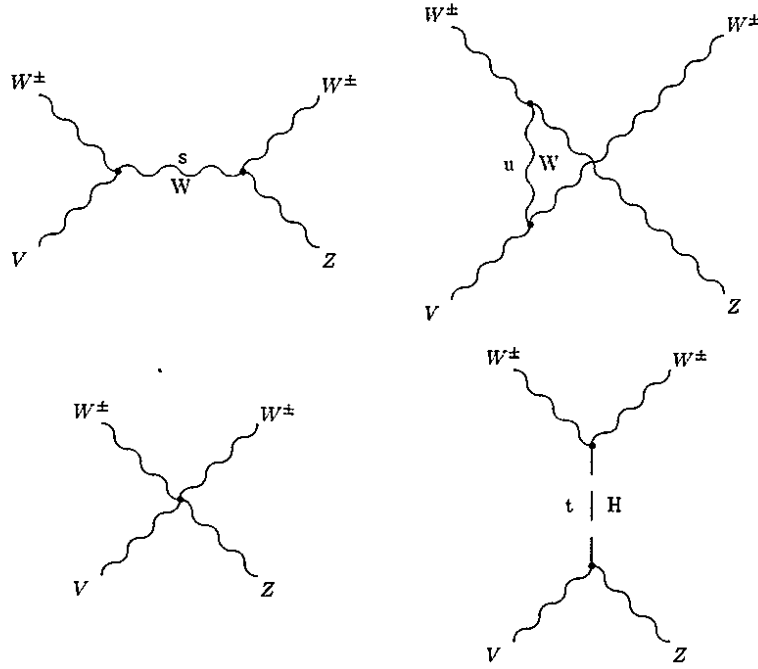
Figure 6.5: Feynman diagrams for $W^{\pm}V \to W^{\pm}Z$, $V = \gamma, Z$, in the Born approximation.

6.1.2   Cross-Sections for $W\gamma \to WZ$ and $WZ \to WZ$

We are going to discuss the cross-sections for the processes $WV \to WZ$, $W = W^+$ or W^- and $V = \gamma$ or Z. In the Born approximation there are four diagrams which contribute to each of the processes, as shown in Figure 6.5. The diagrams with vector-boson- or Higgs-boson–exchange in general contain contributions from the anomalos couplings which are quadratic and linear in the couplings, while the diagram with the four-particle interaction contains only linear terms. The Higgs-particle appears non-resonant in the t-channel. For the process $W\gamma \to WZ$ the Higgs-diagram is completely non-standard. An analytical expression for the helicity amplitudes $\mathcal{M}_{pol}$ in terms of polarization vectors has been given for $WZ \to WZ$ in [56]. The corresponding expression for $W\gamma \to WZ$ can be obtained by a straightforward modification of this expression. The vertices needed for this modification have also been given in [56].

The cross-section for a given helicity combination of the WV-pair is defined in terms of a sum of squared helicity amplitudes, M_{pol}, as defined in (4.39). We consider the integrated cross-sections with a pseudorapidity-cut η on both particles in the final state and sum over the helicities of the final state particles. The expression for the cross-sections is given by

$$\sigma_{pol} = \frac{1}{32\pi s}\frac{q}{p} \int\limits_{-\tanh(\eta)}^{\tanh(\eta)} d\cos\theta \, M_{pol}, \qquad (6.13)$$

In (6.13), p and q are the magnitudes of the space-like momenta of the particles in the initial state and in the final state, respectively, evaluated in the WZ cms-system, and θ is the angle between the directions of motion of the two W-particles evaluated in the same system. The quantity s is the square of the scattering energy. For the process $WZ \to WZ$ one has $q/p = 1$. The expressions for p and q for the process $W\gamma \to WZ$ are given in

Appendix B.

The quantities σ_{pol} of (6.13) are the same for $W^+V \to W^+Z$ and $W^-V \to W^-Z$, since also the amplitudes are the same. A further analytical manipulation of the expressions for the amplitudes given in [56] does not lead to useful results. I have evaluated the cross-sections numerically. I obtained, however, analytical results in a high-energy approximation.

High-Energy Approximation

For large scattering-energies, $s \equiv M_{WZ}^2 \gg M_W^2$, simple approximative forms for the cross-sections can be found. They are obtained by an asymptotic expansion of the scattering amplitudes in powers of M_W^2/s [41, 56, 88]. In this way, cancellations between different diagrams are explicitly carried out. The cancellations appear in the standard term and also in the anomalous terms [56]. For terms which remain after the cancellations have been performed simple analytical expressions can be given. The asymptotic amplitudes are then squared and the integration over the scattering-angle $\cos\theta$ is carried out analytically. Formulae for the resulting cross-sections are given in Appendix B.

We elaborate on the nature of the high-energy approximation. In the standard model, the leading terms of an amplitude is of the order of magnitude $\mathcal{O}(s/M_W^2)^0$, i.e. they approach a constant value for large scattering-energies. To obtain this result, one has to assume that the mass of the Higgs-particle is small against the scattering-energy, $M_H^2 \ll s$. This assumption has been made in deriving the expressions in Appendix B. I have also derived approximative forms applicable for arbitrary masses of the Higgs particle, but refrain from giving them here since they are very lenghty. Numeical results obtained with these forms will be given below.

Of the non-standard terms we are going to take into account those which are enhanced by powers of the scattering-energy, as we did previously for the process $q\bar{q}' \to WZ$. For this purpose, we use the parameters a_i defined in (6.6) instead of the ϵ_i. We take into account all powers of the a_i, which are not suppressed by negative powers of the the scattering-energy. The latter restriction is equivalent to the assumption, that the couplings are small, $\epsilon_i = \mathcal{O}(4M_W^2/s)$, or, expressed in another way, that the parameters a_i are not much greater than $a_i = \mathcal{O}(1)$.

If certain powers of the anomalous couplings do not appear, non-leading terms can become important. This is the case for the cross-sections $\sigma_{TT} = \frac{1}{2}(\sigma_{++} + \sigma_{+-})$ and $\sigma_{\overline{TT}} = \frac{1}{2}(\sigma_{++} - \sigma_{+-})$, which are multiplied by the dominating (at large M_{WZ}) luminosities $\mathcal{L}_{TT}$ and $\mathcal{L}_{\overline{TT}}$. The reason that the non-leading terms are important is that the cross-sections σ_{++} and σ_{+-} in the standard model are virtually determined by a single amplitude, $\mathcal{M}_{++++}$ and $\mathcal{M}_{+--+}$, respectively[1], which receives non-standard contributions from only a single anomalous coupling, namely ϵ_W in quadratic form, and no contribution from the other couplings nor contributions linear in ϵ_W. We therefore calculate the non-leading anomalous terms, $\mathcal{O}\left(M_W^2/s(a_i, a_i^2)\right)$, of the amplitudes $\mathcal{M}_{++++}$ and $\mathcal{M}_{+--+}$ and take into account the terms $2\mathcal{M}_{\text{standard}}\mathcal{M}_{\text{non-leading}}$, which arise when the amplitudes are squared. It is mainly these terms, which describe the effects linear in the ϵ_i, since such effects are not present in leading order in any of the amplitudes contributing to σ_{++} and σ_{--}.

---

[1]In the high-energy approximation of the standard model, σ_{++} is completely determined by the amplitude $\mathcal{M}_{++++}$, while the contribution of the amplitude $\mathcal{M}_{+--+}$ to σ_{+-} amounts to 97%. This is true for both processes $WZ \to WZ$ and $W\gamma \to WZ$. An angular cut $z_0 = \tanh(1.5)$, equivalent to a rapidity-cut of $y = 1.5$ on the produced vector-bosons in the WZ center-of-mass system, was assumed.

The approximation was so far confined to small anomalous couplings, $a_i = \mathcal{O}(1)$ or smaller. By taking into account certain further, non-leading terms the applicability of the approximation can be extended into the region of larger anomalous couplings, $a_i > \mathcal{O}(1)$ [2]. The effects of larger but not too large a_i manifest themselves most strongly in terms which are quartic in the couplings. These terms, to the first non-leading order, are proportional to $M_W^2/s \cdot a_i a_j a_k a_l$, $i,j,k,l = W, W\Phi, B\Phi$. Therefore, we also calculate those terms. They only appear in amplitudes which receive no leading order contribution at all, neither in the standard model nor for anomalous couplings[3]. These terms become important for the cross-sections σ_{TL} and σ_{LT} (only for large a_i). For these cross-sections amplitudes with the corresponding leading terms are missing.

All terms we have discussed are listed in Appendix B.

Discussion of Numerical Results

The Figures 6.6 to 6.14 show numerical results for the cross-sections for $WV \to WZ$.

Figure 6.6 shows the cross-sections for the process $WZ \to WZ$ in the standard model for the diagonal helicity combinations as a function of the scattering energy $\sqrt{s}$. A pseudorapidity-cut $\eta = 1.5$ has been chosen, further $M_H = 100$ GeV. The largest cross-section is for $W_T Z_T$, which is also to be multplied with the largest luminosity, $\mathcal{L}_{W_T Z_T}^{pp}$. The other $WZ \to WZ$ cross-sections are, in the order of decreasing magnitude, $TL \simeq LT$, $\overline{TT}$ and LL. Figure 6.7 shows the same cross-sections for the process $W\gamma \to WZ$. These cross-sections vanish at the production threshold for a WZ-pair. They show the same order in their magnitudes as do the cross-sections for $WZ \to WZ$. The cross-section for $W\gamma \to WZ$ for a given helicity combination is smaller by a factor of 3 to 4 than the corresponding cross-section for the process $WZ \to WZ$.

The cross-section for the non-diagonal terms in the helicity combinations for $WZ \to WZ$ and $W\gamma \to WZ$ are shown in Figure 6.8. At large scattering-energies these cross-sections are negligibly small against all cross-sections for the diagonal terms. I note that the terms with contributions from longitudinal polarization states give a negative contribution.

Figure 6.9 shows the dependence of the cross-sections on the cut η. Only the cross-sections for $W_T Z_T \to WZ$ and $W_L Z_L \to WZ$ are shown as an example. A scattering-energy of $\sqrt{s} = 1$ TeV was chosen as well as $M_H = 100$ GeV. The dependence on the cut is very strong. The reason for this is the exchange of a W-particle in the u-channel, which causes a significant rise of the cross-section at large scattering-angles, $\cos\theta \to -1$ (similar to the Coulomb pole for the exchange of a photon). This is reflected by the terms $\sim 1/(1 - z_0^2)$, which appear in the high-energy approximation in Appendix B. The rise is only halted by the finite values of the boson masses, an effect which is, however, not reproduced by the high-energy approximation. This approximation is also shown in the figure. It becomes worse with increasing η. The high-energy approximation deviates by 10% to 15% from the exact calculation at $\eta = 1.5$, depending on the considered process.

The effects of the variation of the Higgs boson mass, M_H, on the $W_L Z_L \to WZ$ cross-section are shown in Figure 6.10 for a cut of $\eta = 1.5$. For large Higgs boson masses the cross-section becomes very large. For $M_H = 800$ GeV and at large energies it is even much

---

[2] Again the extension is only necessary, because certain terms do not appear in the leading order. If leading-order terms were present for all powers of the couplings, the high energy approximation would be a good approximation for arbitrary values of the a_i.

[3] These are the amplitudes with an odd number of longitudinally polarized external vector-bosons.

larger than the otherwise dominating cross-section for $W_T Z_T$. Above a value of $M_H \simeq 800$ GeV a perturbative treatment (at least to lowest order) is not anymore possible. I note that the increase of the cross-section for $W_L Z_L \to WZ$ at large values of M_H is almost entirely due to the amplitude $W_L Z_L \to W_L Z_L$. Further, the variation of the Higgs boson mass has almost no effect on the cross-sections with one or more transversely polarized bosons. Figure 6.10 also shows the high-energy approximation for arbitrary values of M_H.

The Figures 6.11 to 6.14 show the effects of anomalous couplings on the cross-sections. Figure 6.11 shows cross-sections for $W_T Z_T \to WZ$ and $W_T \gamma \to WZ$ as a function of the scattering energy for various values of the coupling parameters ($M_H = 100$ GeV was chosen). The parameter ϵ_W has the greatest influence. The effect of $\epsilon_{W\Phi}$ is clearly smaller, still smaller is the effect of $\epsilon_{B\Phi}$. For the $W_T Z_T$ cross-section the effect of $\epsilon_{B\Phi}$ is even negligible. For the cross-sections with anomalous couplings also the high-energy approximation is shown in Figure 6.11.

The terms non-diagonal in the helicity combinations and for purely transverse helicities, $TTTT$, show a drastic dependence on the coupling parameters, as can be seen in Figure 6.12. The effect is so large, that already for moderate choices of the anomalous couplings the terms are of the same order of magnitude as the cross-sections for the diagional helicity combinations. The terms, however, do not exceed the cross-section for $W_T Z_T \to WZ$. The contributions of some of the helicity combinations can be negative, depending on the values of the anomalous couplings.

Figures 6.13 and 6.14 show the effects of anomalous couplings on the cross-sections with contributions from longitudinal helicities. A non-zero parameter $\epsilon_{W\Phi}$ leads to a strong increase of the cross-section for $W_L Z_L \to WZ$ at high energies (Figure 6.13, $M_H = 100$ GeV was chosen). The cross-section for $W_L Z_L$ is in this case even significantly larger than the cross-section for $W_T Z_T$. The effect of the couplings $\epsilon_{B\Phi}$ and ϵ_W on the cross-section for $W_L Z_L \to WZ$ is small. Also shown in Figure 6.13 are the cross-sections in the high-energy approximation. Figure 6.14 shows the effect of anomalous couplings on the cross-section for $W_L \gamma \to WZ$. The effect of $\epsilon_{W\Phi}$ is small compared to the effect of this parameter on the cross-section for $W_L Z_L \to WZ$. The effect of ϵ_W is of comparable magnitude as the effect of $\epsilon_{W\Phi}$. The effect of $\epsilon_{B\Phi}$ is very small.

Finally, Figures 6.15 and 6.16 show investigations about the validity of the high-energy approximation. Figure 6.15 shows the ratio of the approximation and the exact cross-section as a function of the scattering-energy for all helicities ($\eta = 1.5$ was chosen.). At $\sqrt{s} = 1$ TeV the deviations amount to between 12% and 18% of the exact cross-section; for the TT cross-sections the deviation is 14%. At $\sqrt{s} = 1.5$ TeV the deviations are between 5% and 8%, depending on the helicity combination (TT : 6%).

Figure 6.16 shows an investigation about the validity of the high-energy approximation for the non-standard terms. Plotted is the error $(\Delta\sigma^{\text{approx.}} - \Delta\sigma)/\sigma$, expressed in percent, as a function of one of the anomalous couplings, ϵ_i. For the other couplings the value zero was chosen. The quantity $\Delta\sigma \equiv \sigma - \sigma_{\text{SM}}$ is the deviation of the cross-section from its standard model value. The plotted error is thus induced in the cross-sections, if one uses the high-energy approximation to calculate the deviations from the standard model. It does not include the error induced to the standard cross-sections. This error has been discussed in Figure 6.15. One sees that the ϵ_W-dependence of the $W_T Z_T$ and $W_T \gamma$ cross-sections is correctly reproduced by the approximation because the curves take on a horizontal shape for increasing couplings, with a small error, 2% to 3%. The same is true for the $\epsilon_{W\Phi}$-dependence of the $W_L Z_L$ cross-section. The large, negative error in this

cross-section with an extreme value at $\epsilon_{W\Phi} \simeq -0.03$ appears in a region, in which the cross-section is very small ($\sigma \simeq 1$ pb). The dependence of the TT and $\overline{TT}$ cross-sections on $\epsilon_{W\Phi}$ and $\epsilon_{B\Phi}$ is not reproduced exactly, as can be seen from the shape of the curves at large values of the couplings. For values of $|\epsilon_i| < 0.05$, however, the error does not exceed 10%. The shape of the curve describing the $\epsilon_{W\Phi}$-dependence of the error in the $W_T\gamma$ cross-section hints to the existence of a non-leading cubic term. Such terms have not been calculated, since they only become relevant for large anomalous couplings. The dependence of the error induced to the W_TZ_L cross-section on the parameter ϵ_W also leads one to the conclusion that non-leading terms have an influence at larger values of ϵ_W.

In summary, the leading effects (ϵ_W in $TT,\overline{TT}$, $\epsilon_{B\Phi}$ in LL) are reproduced by the high-energy approximation with an accuarcy of 3%; for the relevant non-leading effects ($\epsilon_{W\Phi},\epsilon_{B\Phi}$ in TT, $\overline{TT}$) the error is also below 3% if the couplings are not too large, $|\epsilon_i| <$ 0.03. One expects that the errors become smaller for larger scattering-energies. For smaller scattering-energies the magnitude of the non-standard terms becomes smaller on the whole.

Summarizing our discussion of the $(WZ)_{pol} \to WZ$ and $(W\gamma)_{pol} \to WZ$ cross-sections, we have investigated the impact of anomalous couplings on these cross-sections. The largest cross-section for each process is the one with the helicity combination TT in the initial state, $W_TZ_T \to WZ$ and $W_T\gamma \to WZ$. Of the anomalous coupling parameters, the parameter ϵ_W has the largest impact on these cross-sections. The parameters $\epsilon_{W\Phi}$ and $\epsilon_{B\Phi}$ manifest themselves only through sub-leading terms in a high-energy approximation, as far as the TT (and $\overline{TT}$) cross-sections are concerned. The parameter $\epsilon_{W\Phi}$ has a large impact on the cross-section for $W_LZ_L \to WZ$. Varying the mass of the Higgs boson between $M_H = 80$ GeV and $M_H = 800$ GeV also has a large impact on the cross-section $W_LZ_L \to WZ$. This cross-section is, however, much smaller in magnitude than the $W_TZ_T \to WZ$ cross-section if we consider the standard model.
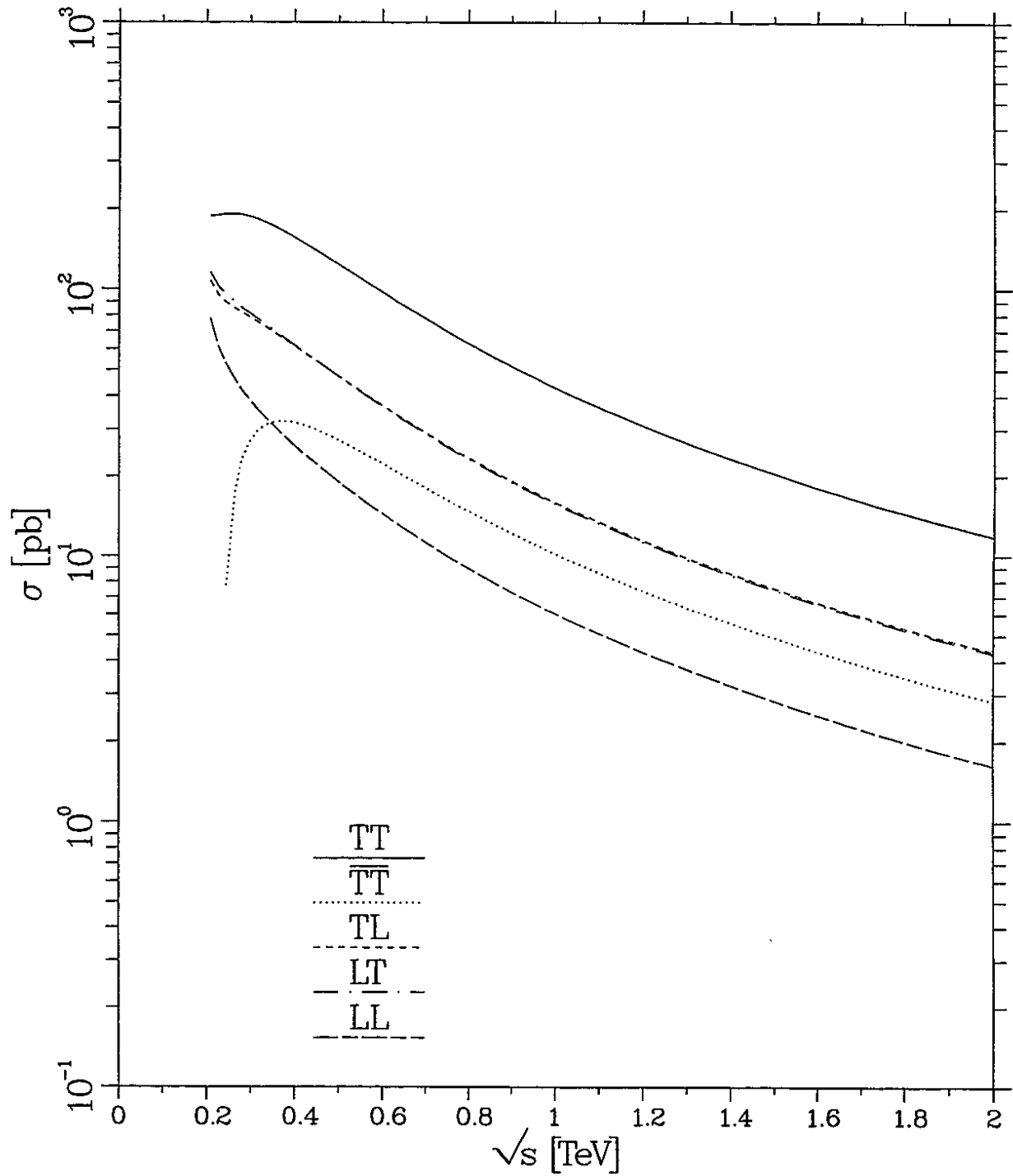
Figure 6.6: The cross-sections for the diagonal helicity combinations for $WZ \to WZ$ in the standard model as a function of the scattering energy.
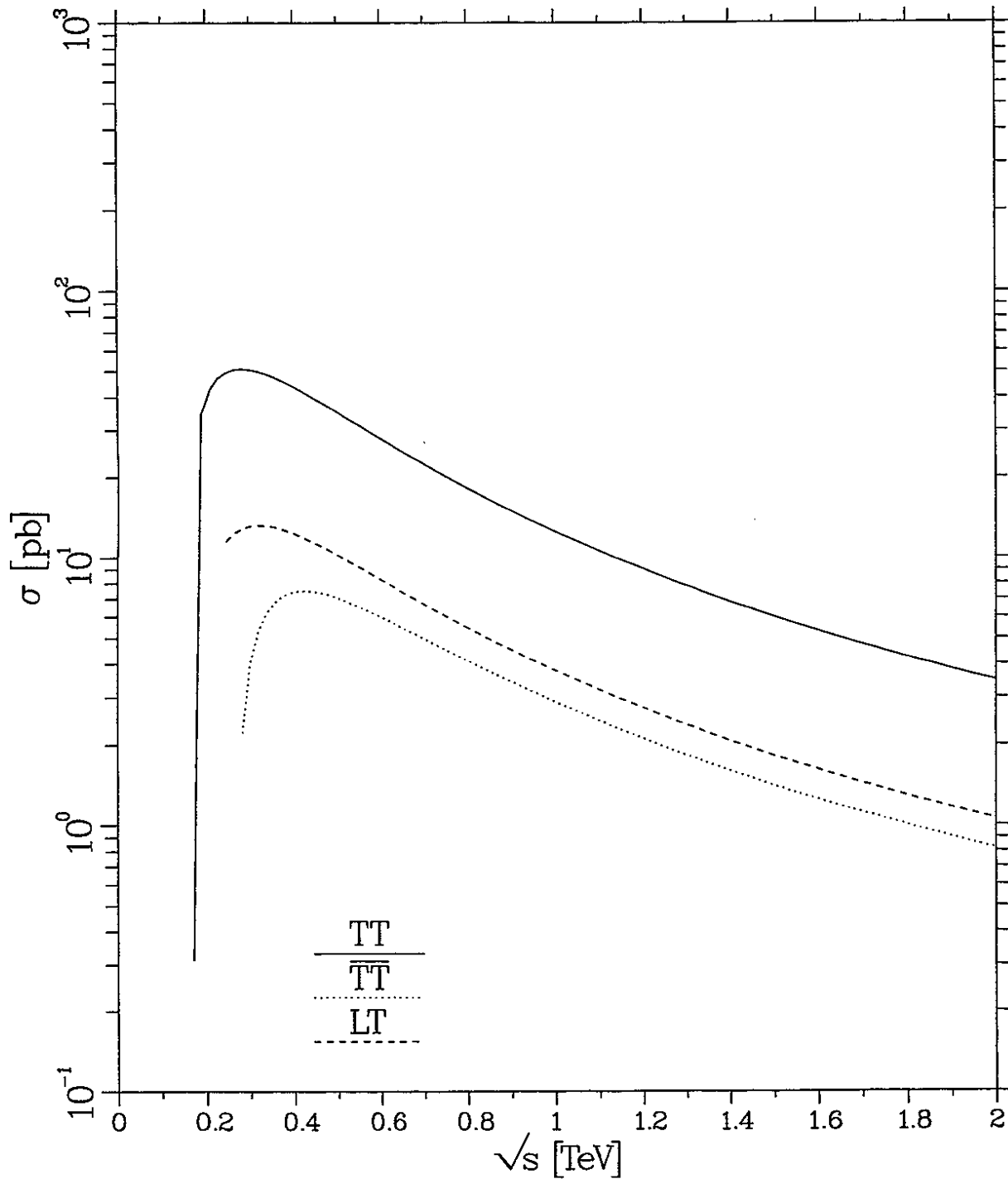
Figure 6.7: The cross-sections for the diagonal helicity combinations for $W\gamma \to WZ$ in the standard model as a function of the scattering energy.
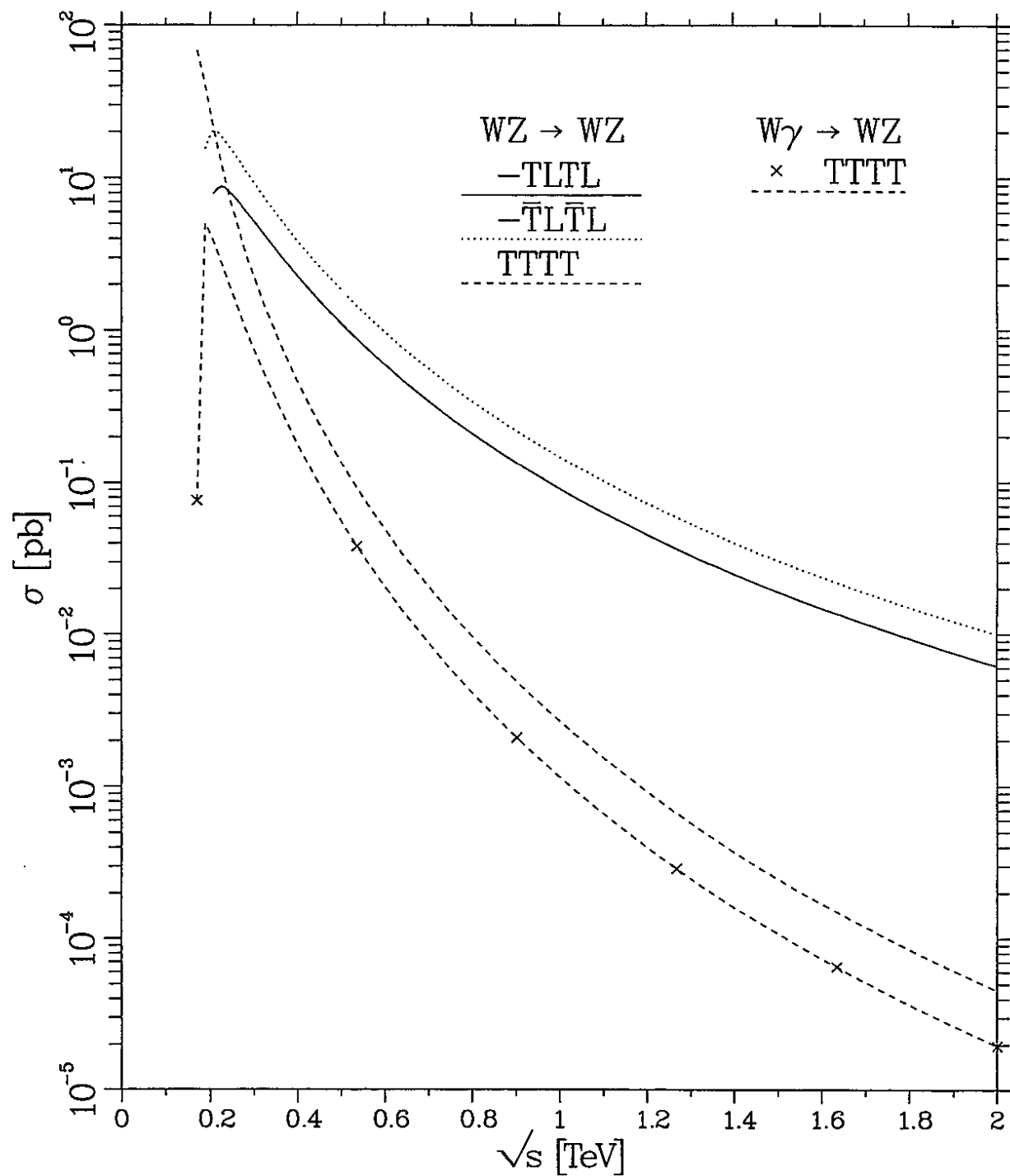
Figure 6.8: The cross-sections for the non-diagonal helicity combinations for $WZ \to WZ$ and $W\gamma \to WZ$ in the standard model as a function of the scattering energy.

Dependence of cross sections on the cut
SM, $M_H = 0.1$ TeV, $\sqrt{s} = 1$ TeV
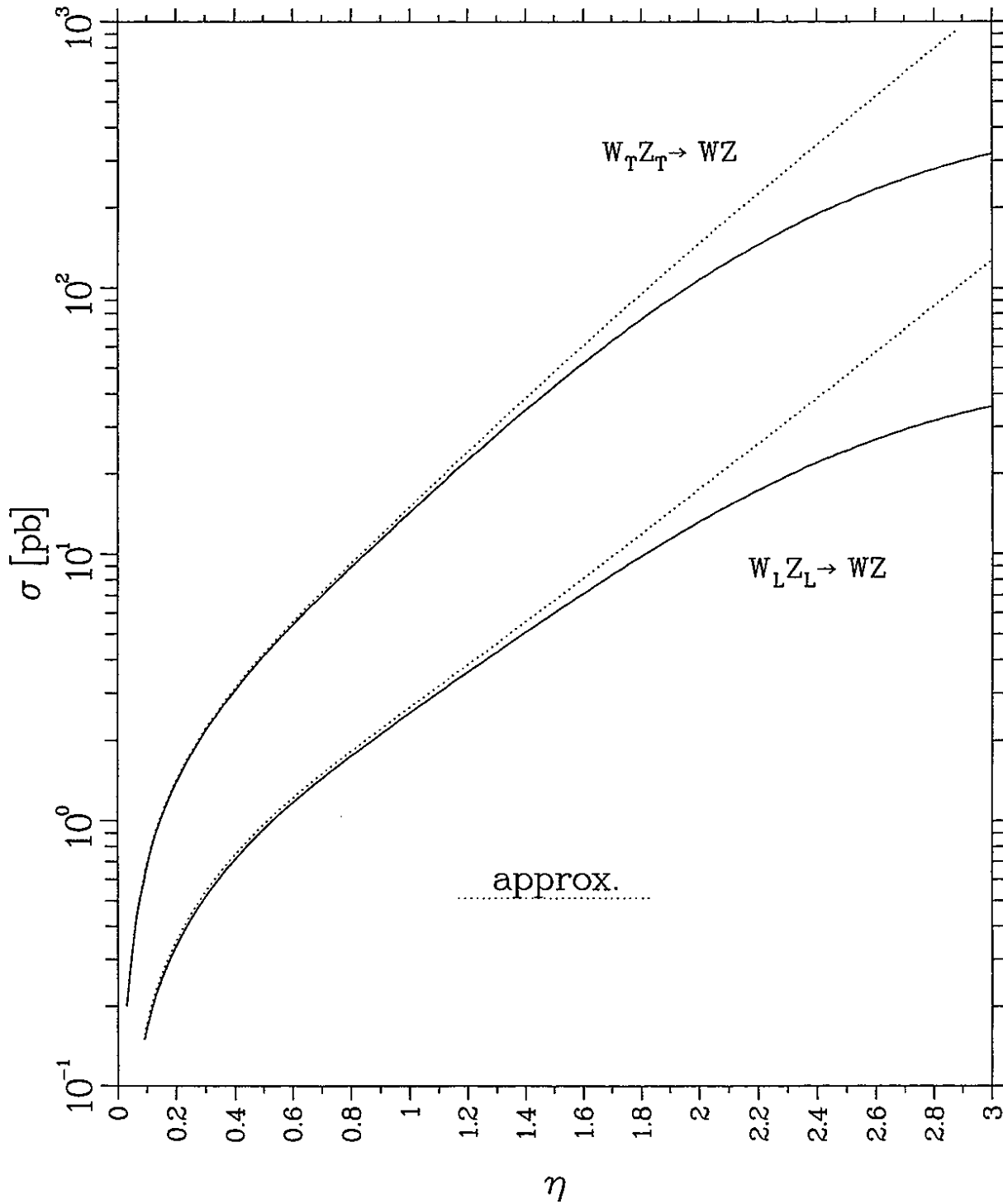
Figure 6.9: The cross-sections for $W_T Z_T \to WZ$ and $W_L Z_L \to WZ$ as a function of the pseudorapidity-cut η. Also shown is the high-energy approximation.
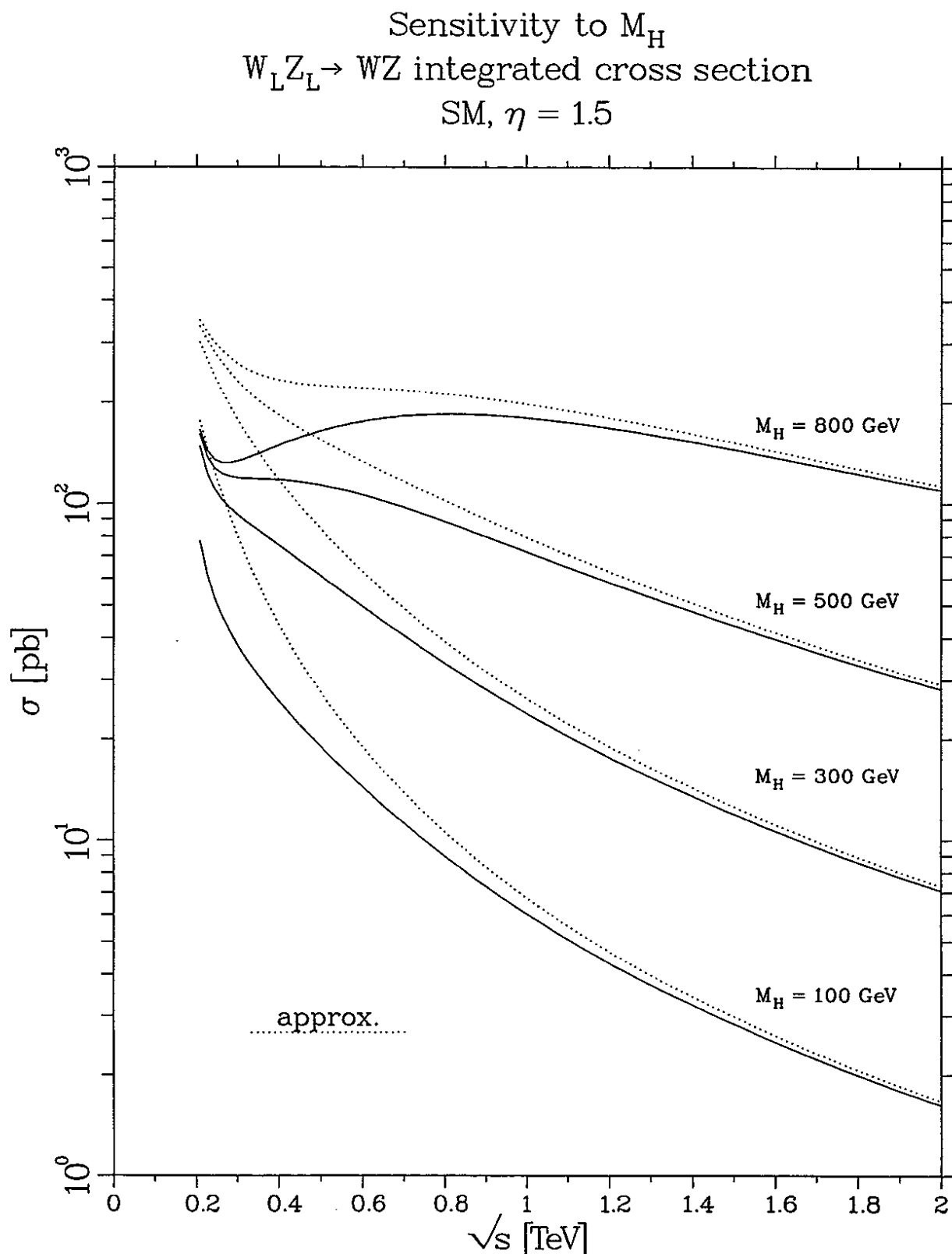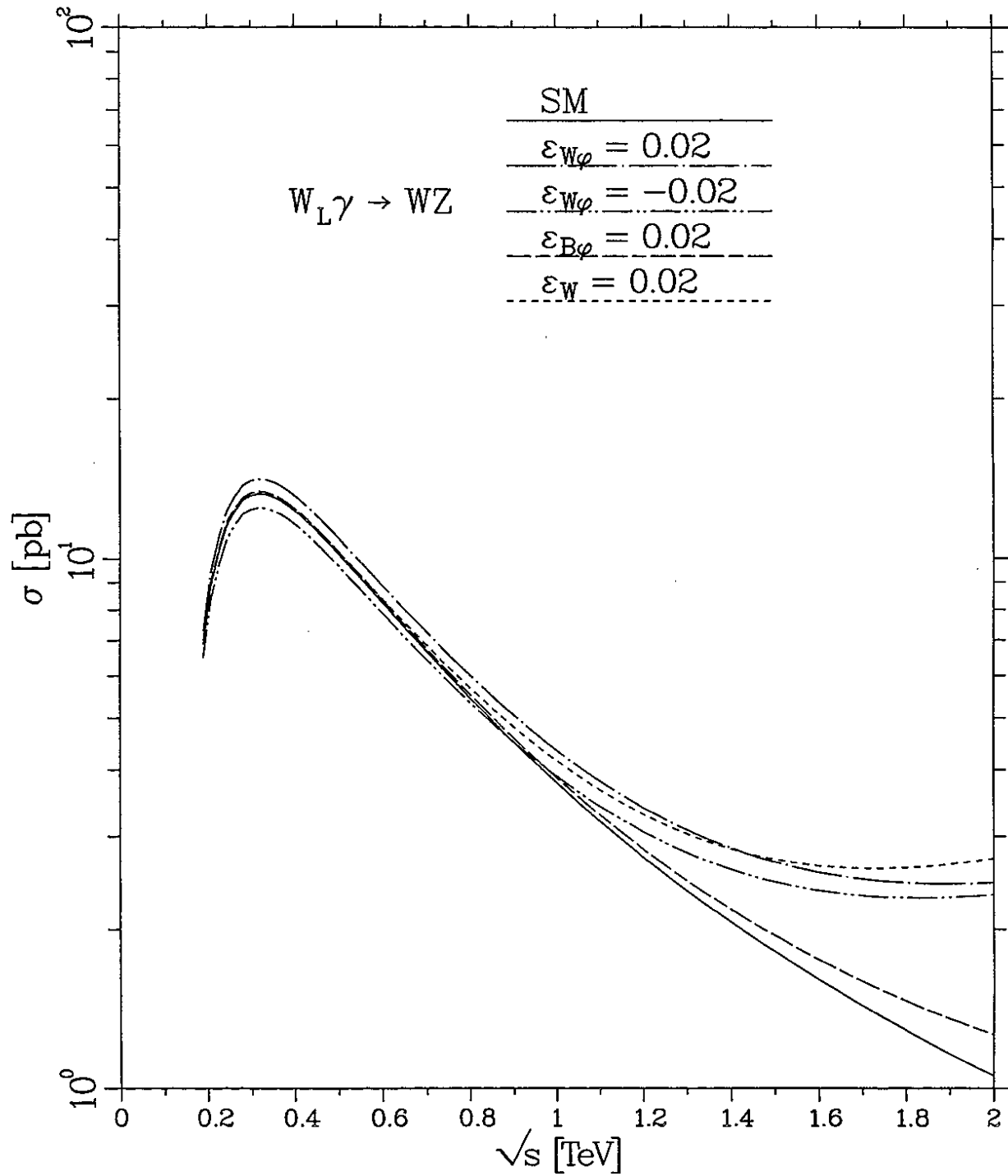
Figure 6.10: The cross-section for $W_L Z_L \rightarrow WZ$ as a function of the scattering-energy for various values of the mass of the Higgs boson. Also shown is the high-energy approximation.

cross sections with anomalous couplings
$$\eta = 1.5$$
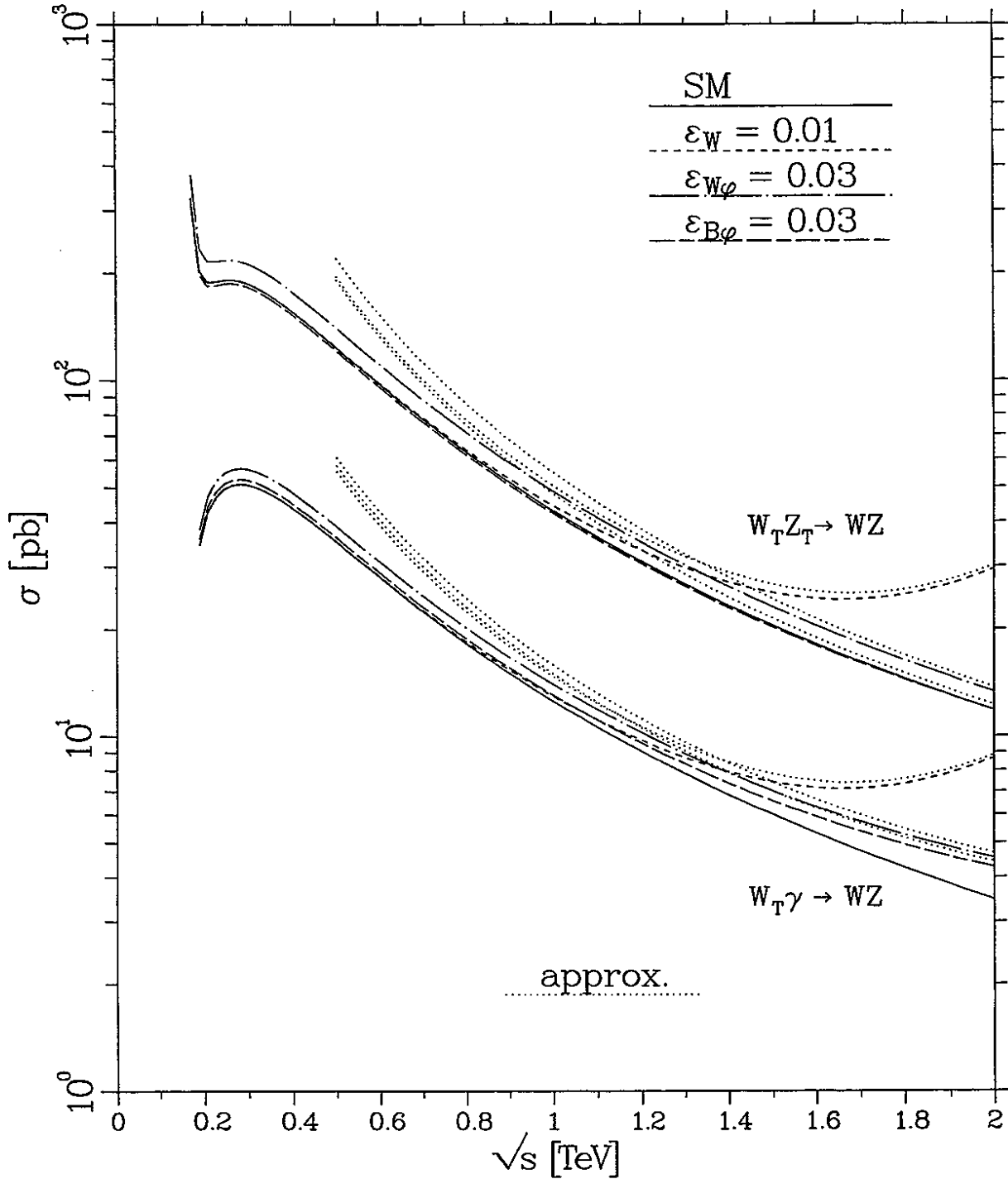
Figure 6.11: The cross-sections for $W_T Z_T \to WZ$ and for $W_T \gamma \to WZ$ as a function of the scattering energy for various values of the anomalous couplings. Also shown is the high-energy approximation.
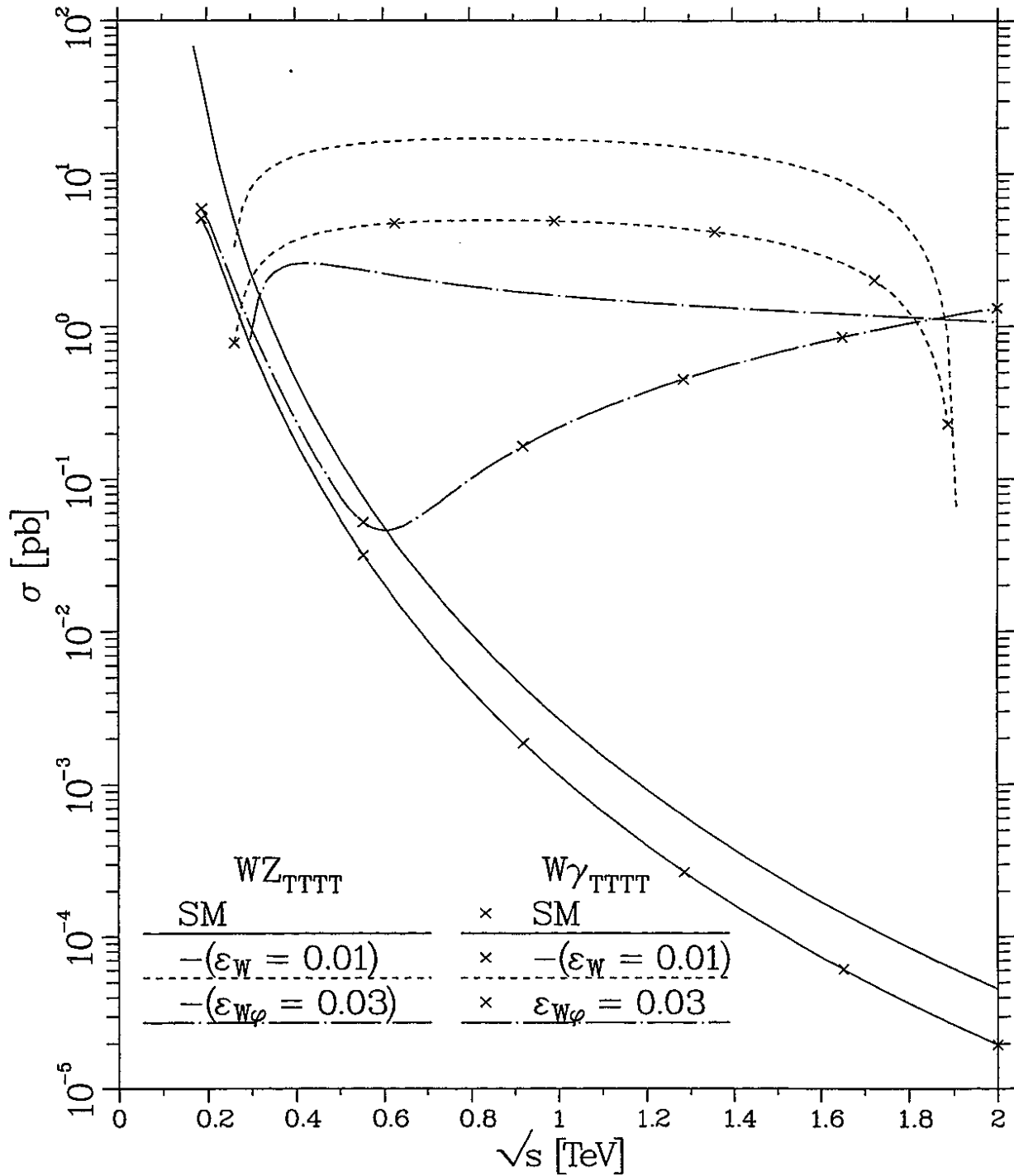
Figure 6.12: The cross-sections for the non-diagonal helicity combinations $WZ_{TTTT} \rightarrow WZ$ and $W\gamma_{TTTT} \rightarrow WZ$ as a function of the scattering-energy for various values of the anomalous couplings.
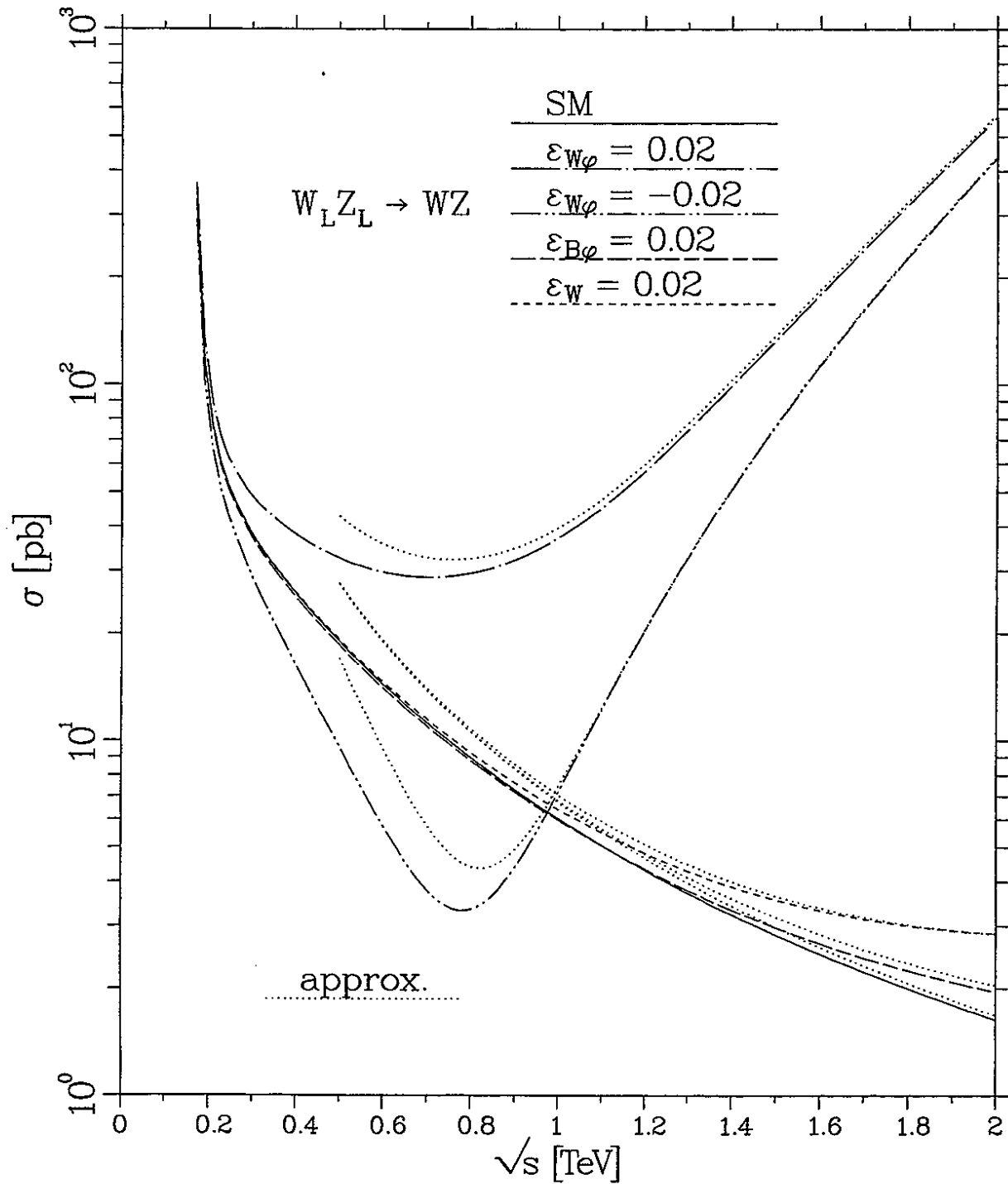
Figure 6.13: The cross-section for $W_L Z_L \to WZ$ as a function of the scattering-energy for various values of the anomalous couplings. Also shown is the high-energy approximation.

cross sections with anomalous couplings
$$\eta = 1.5$$

Figure 6.14: The cross-section for $W_L\gamma \to WZ$ as a function of the scattering-energy for various values of the anomalous couplings.

Validity of high energy approximation
Ratios of cross sections in SM
$\eta = 1.5$, $M_H = 0.1$ TeV
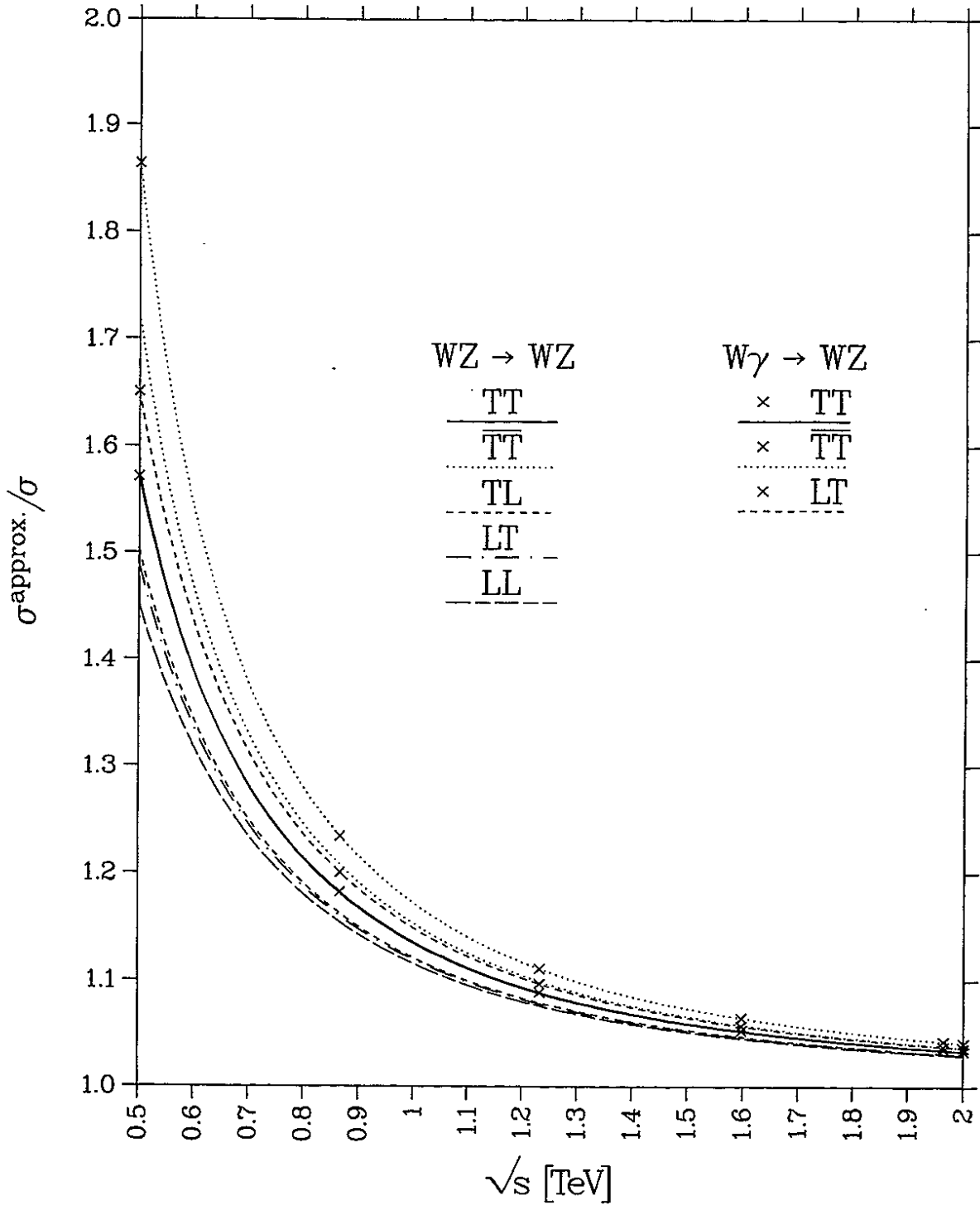
Figure 6.15: The ratio of the cross-sections for $WZ \to WZ$ and for $W\gamma \to WZ$ in the high-energy approximation and without an approximation as a function of the scattering-energy.
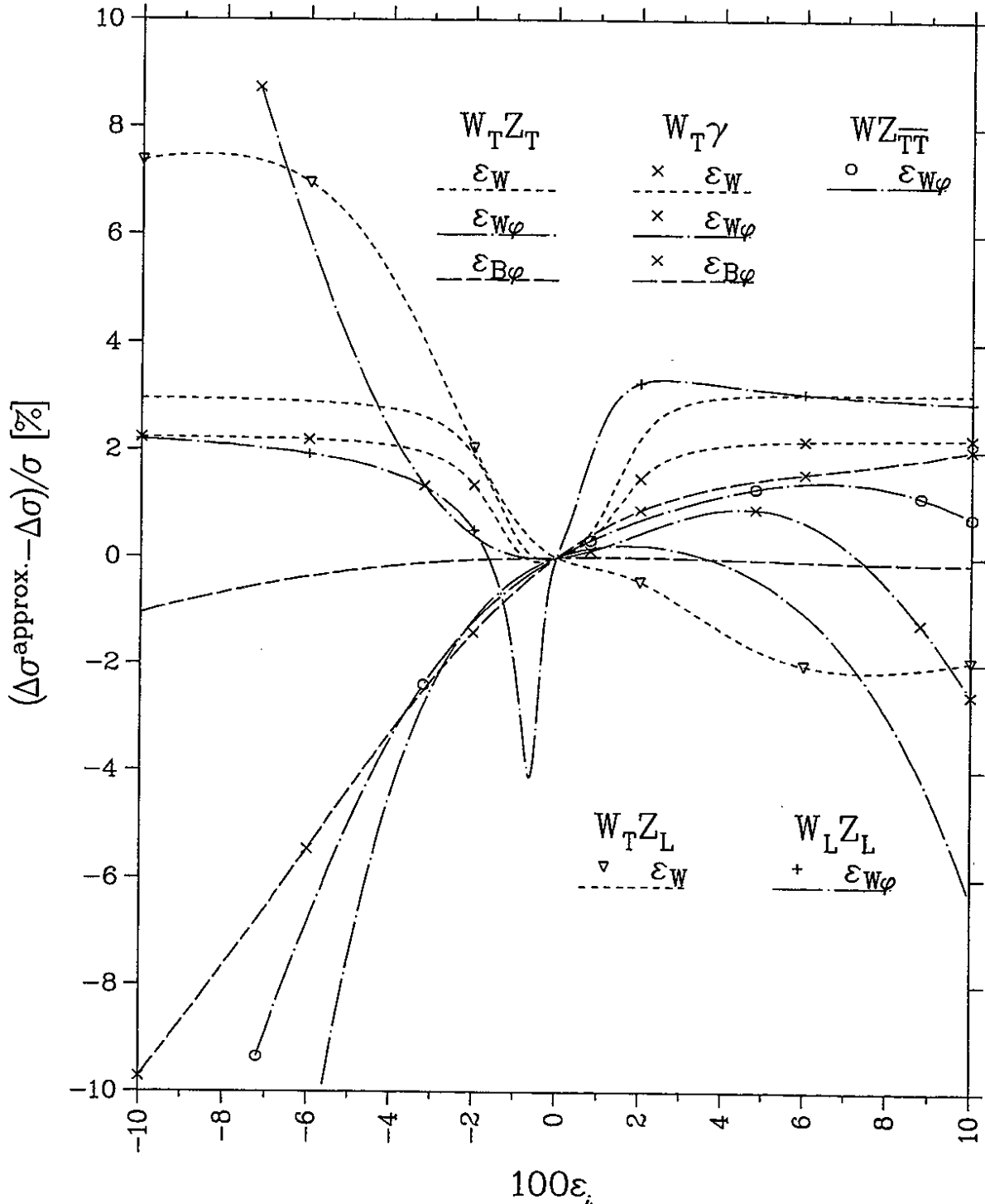
Figure 6.16: The error induced to the cross-sections by using the high-energy approximation to calculate the anomalous terms as a function of the anomalous couplings for various cross-sections and couplings.

6.2   Cross-Sections for $pp \to WZX$

We are now going to combine our treatments of parton-parton luminosities and parton-parton cross-sections to obtain predictions for the cross-section for $pp \to WZX$. According to (3.4), the cross-section will be approximated by the sum of the lowest order contributions from $q\bar{q}'$-annihilation and vector-boson scattering. This will be sufficient for our subsequent analysis of anomalous couplings.

In recent treatments, a dependence of the magnitudes of the couplings on the scattering-energy of the parton-process, M_{WZ}, has been assumed [11, 20, 21, 27, 29]. This dependence has been parametrized by a form-factor which depends on two unknown parameters. It was argued that such a dependence must necessarily be present in order not to violate the unitarity bounds for the parton cross-sections. In fact, however, the introduction of a form-factor is not necessary for small values of the anomalous couplings, $\epsilon_i \leq \mathcal{O}(10^{-2})$, as we consider them here.

6.2.1   Remark about Unitarity Limits and the Use of a Form-Factor

In order not to violate the unitarity of the S-matrix, it was proposed [20] that the anomalous couplings would depend via form-factors on the scattering-energy of the sub-process, $\hat{s} \equiv M_{WZ}$,

$$\epsilon_i = \frac{\epsilon_i^0}{\left(1 + \frac{\hat{s}}{\Lambda_{FF}^2}\right)^n}. \tag{6.14}$$

In (6.14), the ϵ_i are the couplings which enter the expressions for the cross-sections $q\bar{q}' \to WZ$ and $WV \to WZ$, while the parameters ϵ_i^0 are constant parameters which appear in the Lagrangian (2.46) instead of the ϵ_i. Λ_{FF} is the scale of new physics (cf. Chapter 2.3) and n is a positive number. The effect of the form-factor is a reduction of the effective anomalous coupling, ϵ_i, with growing $\hat{s}$. Lacking a better knowledge, the parameters Λ_{FF} and n must be chosen by hand.

I will argue here, that the introduction of a form-factor is not necessary for small anomalous couplings, $\epsilon_i \leq 10^{-2}$, since the unitarity limits are not even reached at large scattering energies, $\hat{s} \simeq 2$ TeV, for these small values of the couplings. The unitarity limits derived from $q\bar{q}' \to WZ$ are [20]

$$\left|\frac{\hat{s}\epsilon_W}{M_W^2}\right| \leq \frac{2\sqrt{3}s_W^2}{\alpha c_W} \simeq 124,$$
$$\left|\frac{\hat{s}\epsilon_{W\Phi}}{M_W^2}\right| \leq \frac{2\sqrt{3}s_W^2}{\alpha} \simeq 109, \tag{6.15}$$

so that unitarity at $\hat{s} = 2$ TeV is not violated by couplings strengths of the magnitude $|\epsilon_W| \leq 0.20$ and $|\epsilon_{W\Phi}| \leq 0.17$. The restriction on $\epsilon_{B\Phi}$ is even lower.

Stronger restrictions are obtained from the unitarity principle applied to the amplitudes for $WZ \to WZ$ and $W\gamma \to WZ$ [88, 89],

$$\left|\frac{\hat{s}\epsilon_W}{M_W^2}\right| \leq 19,$$

$$\left| \frac{\hat{s} \epsilon_{W\Phi}}{M_W^2} \right| \leq 15.5,$$

$$\left| \frac{\hat{s} \epsilon_{B\Phi}}{M_W^2} \right| \leq 49. \tag{6.16}$$

The restrictions from $WV \to WZ$ are stronger than those from $q\bar{q}' \to WZ$, because the amplitudes grow quadratically with the couplings. For $\hat{s} = 2$ TeV one obtains the unitarity bounds,

$$|\epsilon_W| \leq 0.031, \qquad |\epsilon_{W\Phi}| \leq 0.025, \qquad |\epsilon_{B\Phi}| \leq 0.079. \tag{6.17}$$

In the search for small deviations from the standard model, $\epsilon_i = \mathcal{O}\left(M_W^2/\Lambda^2\right), \Lambda > 1$ TeV, is it therefore not necessary to use a form-factor. Further, we will see that already fairly smaller values than the unitarity bounds for ϵ_W and $\epsilon_{W\Phi}$ will lead to observable effects in $pp \to WZX$. An exception is the parameter $\epsilon_{B\Phi}$ which only has marginal effects in this process and can not be further constrained below its unitarity limits.

6.2.2 Discussion of Numerical Results

We are first going to numerically compare the contributions from WZ and $W\gamma$ vector-boson scattering and from $q\bar{q}'$-annihilation to the differential cross-section for $d\sigma(pp \to WZX)/dM_{WZ}$. The calculation of the $q\bar{q}'$-contributions was carried out according to Eq. (5.43) with the MRS(A) parton-distributions in the DIS-scheme and $Q_1^2 = Q_2^2 = M_{WZ}^2$.

Figure 6.17 shows the cross-section as a function of M_{WZ} at $\sqrt{s_{pp}} = 14$ TeV in the standard model. A pseudorapidity-cut of $\eta = 1.5$ was applied. The contribution from $pp \to WZ \to WZ$ was calculated in two different ways. First, it was calculated without approximations according to Eq. (5.36). $M_H = 80$ GeV was chosen, as well as $Q_1^2 = x's_{pp}$ and $Q_2^2 = x's_{pp}$, where x' is the argument of $f_q^p(x')$. Secondly, it was calculated with the convolutions of vector-boson distributions, Eq. (5.42). The approximative calculation yields a value which is 22% greater than the exact one at $M_{WZ} = 0.5$ TeV, and 7.2% greater at $M_{WZ} = 2$ TeV. The contribution from $W\gamma$-scattering was calculated according to Eq. (5.42) with the photon distribution [83] and the choice $Q^2 = xs_{pp}$ for $f_\gamma^p(x, Q^2)$.

The contributions from $W\gamma$ and WZ scattering are of the same order of magnitude. Integrated over the region 0.5 TeV $< M_{WZ} < 2$ TeV, the cross-section amounts to $\sigma = 0.157$ pb for $q\bar{q}'$-annihilation and $\sigma = 0.019$ pb for WV-scattering. Thus, the contribution from WV-scattering amounts to **12%** of the one from $q\bar{q}'$-annihilation. In the low energy region, $M_{WZ} < 0.5$ TeV, the integrated $q\bar{q}'$ cross-section amounts to $\sigma = 2.24$ pb.

Figure 6.18 shows the influence of a variation of the Higgs boson mass. The contributions from $W\gamma$-scattering and WZ-scattering have been added. The convolutions (5.42) were used. For $M_H = 800$ GeV, the WV cross-section lies between 9% ($M_{WZ} = 0.5$ TeV) and 13% ($M_{WZ} = 2$ TeV) above its value for $M_H = 80$ GeV. The dependence on the value of the Higgs mass is thus small. We will always use $M_H = 80$ GeV in the following if not explicitly stated otherwise.

Figure 6.19 shows the $q\bar{q}'$ and WV cross-sections for a cut of $\eta = 2.5$. Integrated over the region 0.5 TeV $< M_{WZ} < 2$ TeV, the $q\bar{q}'$ cross-section amounts to $\sigma = 0.68$ pb, the WV cross-section to $\sigma = 0.099$ pb. The ratio of the cross-sections is thus 15%. This value is close to the value of 17% found in [37] which was obtained for a similar choice of cuts in an exact calculation.

Before we proceed, we will compare our results with results obtained in the literature. Numerical results for the cross-section $pp \to W^{\pm}ZX$ can be found e.g. in [20, 25, 27, 40, 41]. As examples, we compare with results in [41] and [27]. In [41] a plot of the cross-section $d\sigma/dM_{WZ}(pp \to W^+ZX)$ as a function of M_{WZ} at $\sqrt{s_{pp}} = 14$ TeV and $Y = 2$ can be found. The contributions from WV-scattering and $q\bar{q}'$-annihilation are shown separately. We calculate these contributions according to the formulae (5.42) and (5.43) with y'_{max} from (5.37) and $z_0(y')$ from (5.39), where we choose $\cos\theta_{min} = \tanh(Y)$. We choose all parameters and the quark- and vector-boson–distributions as in [41]: for the quark-distributions $f^p_q(x, Q^2)$ we use the parametrization [90] with $N_f = 5$ as the number of quark flavors and $Q^2 = M^2_{WZ}$. For the vector-boson distributions in a proton, $f^p_V(x, E_p)$, we choose the parametrizations from [68], LEWA forms, with $E_p = \sqrt{s_{pp}}/2$. These are distributions in the leading logarithmic approximation. The electroweak parameters are chosen as $M_Z = 91$ GeV, $s^2_W = 0.23$, $\alpha = 1/128$ and $M_H = M_W$. We use the high-energy approximations for the cross-sections for $q\bar{q}' \to WZ$ and $WV \to WZ$, where we omit the non-leading terms in Appendix B. As in [41], we do not use a form-factor. Figure 6.20 shows the result of our calculation. The agreement with the figure in [41] is given. We repeat the calculation for a pseudorapidity cut of $\eta = 1.5$ and include the production of W^-Z-pairs. In addition, we calculate the cross-sections exactly instead of using the high-energy approximation. The result is shown in Figure 6.21. It can be compared to our result of Figure 6.18. The difference in the $q\bar{q}'$-contributions is due to the use of the different quark-distributions and the different parameters. The difference in the contributions from WV-scattering is mainly due to the use of the LLA version of the EVBA instead of the improved vector-boson distributions. The ratio of the $q\bar{q}'$ and WV contributions as shown in Figure 6.21, integrated over the region 0.5 TeV $< M_{WZ} < 2$ TeV, amounts to 52%. This value can be compared to the value of 57% obtained in [36]. It is larger by more than a factor of four than the value of 12% which we obtained by using the improved vector-boson distributions.

We compare our calculations with a result in [27]. Like in that reference, we only calculate the contribution from $q\bar{q}'$-annihilation. Instead of the various cuts applied in [27] on the decay products of the W- and Z-particles, we only apply a rapidity-cut directly on the vector-bosons and multiply the $pp \to WZX$ cross-section with the decay rate for WZ-decays. This procedure should yield approximately the same results as for the more sophisticated cuts in [27] if $M^2_{WZ} \gg M^2_W$. The reason why we expect this is that the decay products of a vector-boson have approximately the same direction of motion as the decaying vector-boson if the energy of the vector-boson is large compared to its mass. In this case a cut on the rapidities of the decay products can be approximated by a rapidity-cut on the decaying particle. In addition to these cuts, also cuts on the absolute value of the transverse momentum of the decay products, $p_T > p_{T,min}$, were applied in [27]. These cuts can only play a role if the vector-bosons are produced under a small angle with respect to the beam-direction. In addition, these cuts become more and more unimportant if the energy of the vector-boson becomes larger. This is because in this case events with a small transverse momentum are excluded by the rapidity cut, anyway. In summary, the cuts in [27] can be approximated by a rapidity-cut on the vector-bosons if $M^2_{WZ} \gg M^2_W$ and if the vector-bosons are not produced under small angles with respect to the beam-direction. The larger M_{WZ} is, the less important the latter restriction becomes. We will discuss the differences of the two treatments further down by comparing numerical results.

We take into account decays into fermions of the first and second generation, $W^{\pm}Z \to \nu_l l^+ l^-$, $l = e, \mu$. For the decay rate we take $B_l = 0.014$ (see Chapter 7.3.1). We use Eq. (5.43) with y'_{max} from (5.37) with $Y = 3$ and $z_0(y')$ from (5.39) with $\cos\theta_{\min} = \tanh(Y)$. The cross-section for $q\bar{q}' \to WZ$ is calculated according to Eq. (6.1). As in [27], we use $Q^2 = M^2_{WZ}$ for the factorization scale, the quark-distributions [91], S0'-distributions in the DIS-scheme, and the parameters $M_Z = 91.17$ GeV, $M_W = 80.22$ GeV and $\alpha = 1/128$. As in [27], we use a form-factor according to Eq. (6.14) with $\hat{s} = M^2_{WZ}$, $\Lambda_{FF} = 1$ TeV and $n = 2$. Similarly to $\epsilon^0_W, \epsilon^0_{W\Phi}, \epsilon^0_{B\Phi}$ in (6.14), one defines the quantities $\Delta g_1^{Z,0}, \Delta\kappa^{Z,0}, \lambda^{Z,0}, \Delta\kappa^{\gamma,0}$ and $\lambda^{\gamma,0}$ instead of the parameters (2.27). As in [27], we will express the cross-section in terms of these parameters.

The result of our calculation for $pp \to W^+ZX$ at $\sqrt{s} = 14$ TeV is shown in Figure 6.22. Shown is the result in the standard model and for various values of the anomalous couplings as a function of the invariant mass M_{WZ}, where only one of the parameters $\Delta\kappa^{Z,0}, \Delta g_1^{Z,0}$ and $\lambda^{Z,0}$ at a time has been chosen unequal to zero. A comparison with the corresponding figure in [27] shows that the results of the two calculations do indeed agree at large M_{WZ} if the couplings are different from zero. For $M_{WZ} > 0.8$ TeV our results deviate by less than 30% from the results in [27]. At $M_{WZ} = 2$ TeV, the deviations are less than 15%. This is true for all three curves with anomalous couplings which are shown in the figure. The deviation for the standard model prediction, however, is larger and amounts to a factor of two at $M_{WZ} = 0.8$ TeV. At $M_{WZ} = 2$ TeV or result is larger by 30% than the result in [27]. Our calculation thus yields a higher value for the cross-section. An explanation is that the anomalous effects occur mainly at large transverse momenta of the produced W- and Z-particles so that the simplified treatment with a rapidity-cut is possible for them. The standard events, however, also take place at small transverse momenta with a large rate, so that the transverse momenta cuts are important for them. Since these cuts have not been applied in our calculation, our calculation can only give an upper bound on the result in [27]. In summary, our calculation has been confirmed by the comparison with [27].

We discuss the effects of anomalous couplings on the cross-sections. The cross-sections have been calculated as in Figure 6.18 using $M_H = 80$ GeV.

Figures 6.23 and 6.24 show the $q\bar{q}'$ cross-section as a function of M_{WZ} for various values of the anomalous couplings. The values have been chosen in such a way that they are of the order of magnitude of the 2σ observability limits at the LHC, to be derived in 7.4. The effect of ϵ_W is largest and virtually independent of the sign of this parameter. Positive values of $\epsilon_{W\Phi}$ lead to a reduction of the cross-section at small energies, and only at energies greater than $M_{WZ} \simeq 1$ TeV (for $\epsilon_{W\Phi} \simeq 0.01$) they lead to an increase of the cross-section. Negative values of $\epsilon_{W\Phi}$ lead to similarly large deviations than comparable values of ϵ_W. The influence of $\epsilon_{B\Phi}$ is very small.

Figures 6.25 and 6.26 show the cross-section proceeding via WV-scattering, Eq. (5.41), for various values of the anomalous couplings. The effects of ϵ_W are largest, the effects of $\epsilon_{W\Phi}$ and $\epsilon_{B\Phi}$ are of comparable magnitude and altogether smaller than the effects of ϵ_W.

The change in percent of the cross-section, caused by anomalous couplings, is for ϵ_W slightly and for $\epsilon_{W\Phi}$ a lot smaller as is the case for $q\bar{q}'$-annihilation.

Conclusion

We conclude that the rate of vector-boson scattering events in $pp \to WZX$ amounts to 12% of the one for $q\bar{q}'$-annihilation processes for a cut of $\eta = 1.5$. This is in contrast

to some results obtained in the literature, in which an unimproved version of the EVBA was used. The result is, however, in agreement with a complete perturbative calculation. Varying the Higgs mass in the region 80 GeV $< M_H <$ 800 GeV has only a negligible effect on the cross-section. It amounts to an increase of the contribution from vector-boson scattering by less than 13%

Concerning the effects of anomalous couplings, already small values of the anomalous couplings, $\epsilon_W, \epsilon_{W\Phi} = \mathcal{O}(10^{-2})$, lead to a pronounced increase of the cross section for $pp \rightarrow WZX$ at $M_{WZ} \gtrsim 1$ TeV. The rate of vector-boson scattering events, however, is less affected by anomalous couplings as is the rate of $q\bar{q}'$-annihilation events. This last statement is with the exception of the parameter $\epsilon_{B\Phi}$, which, however, has only a very small effect on the cross-section.
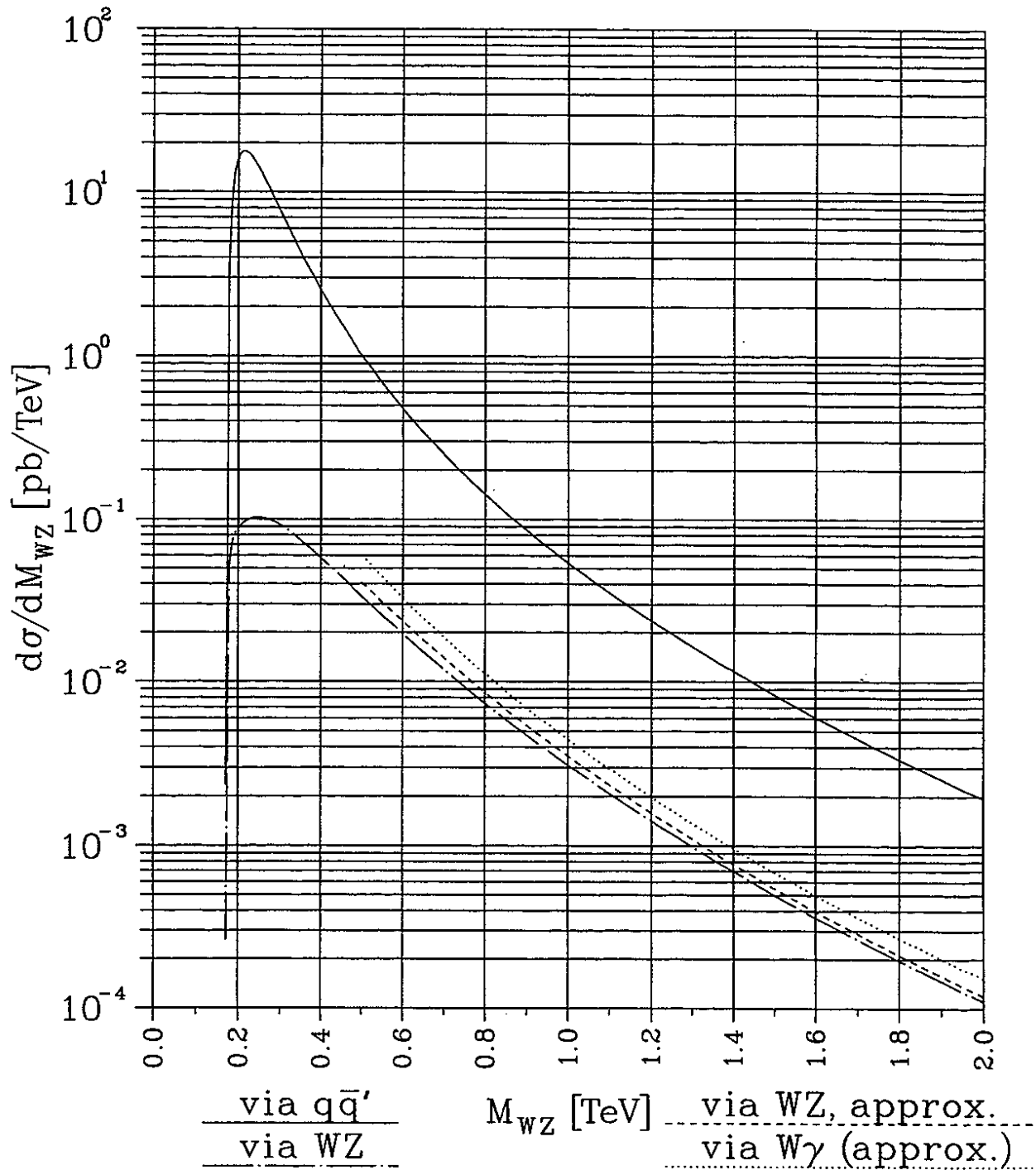
Figure 6.17: Contributions from $q\bar{q}'$-annihilation, WZ- and $W\gamma$-fusion to the cross-section for $pp \rightarrow WZX$ in the standard model as a function of M_{WZ}.

pp→WZ X at $\sqrt{s}$ = 14 TeV, η = 1.5
Standard Model

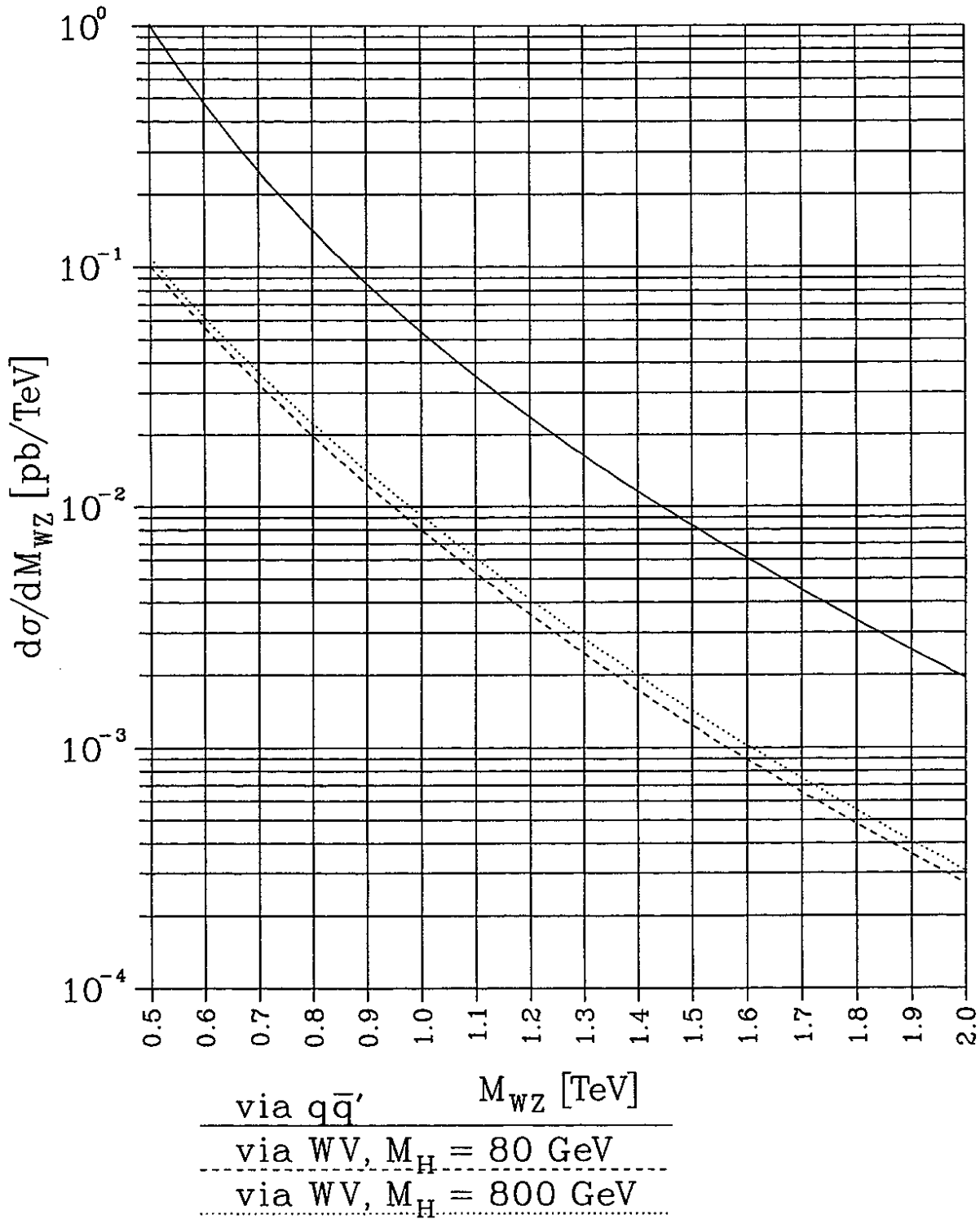via q$\bar{\text{q}}'$ M_{WZ} [TeV]

via WV, M_H = 80 GeV

via WV, M_H = 800 GeV

Figure 6.18: The contribution from WV-scattering to the cross-section for $pp \to WZX$ in the standard model for various values of M_H. Also shown is the contribution from $q\bar{q}'$-annihilation. A pseudorapidity-cut of $\eta = 1.5$ has been chosen.
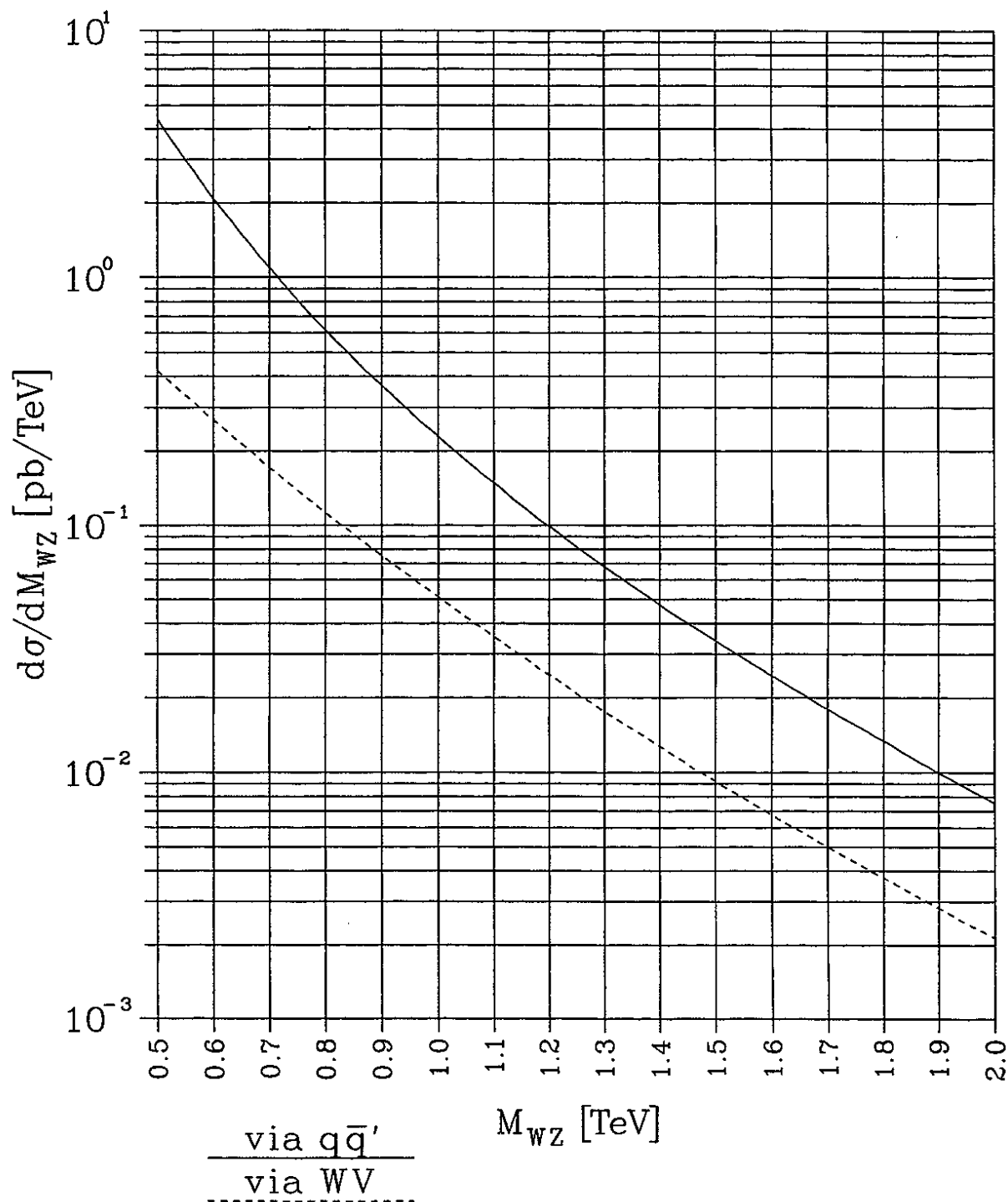
pp→WZ X at $\sqrt{s} = 14$ TeV, $\eta = 2.5$
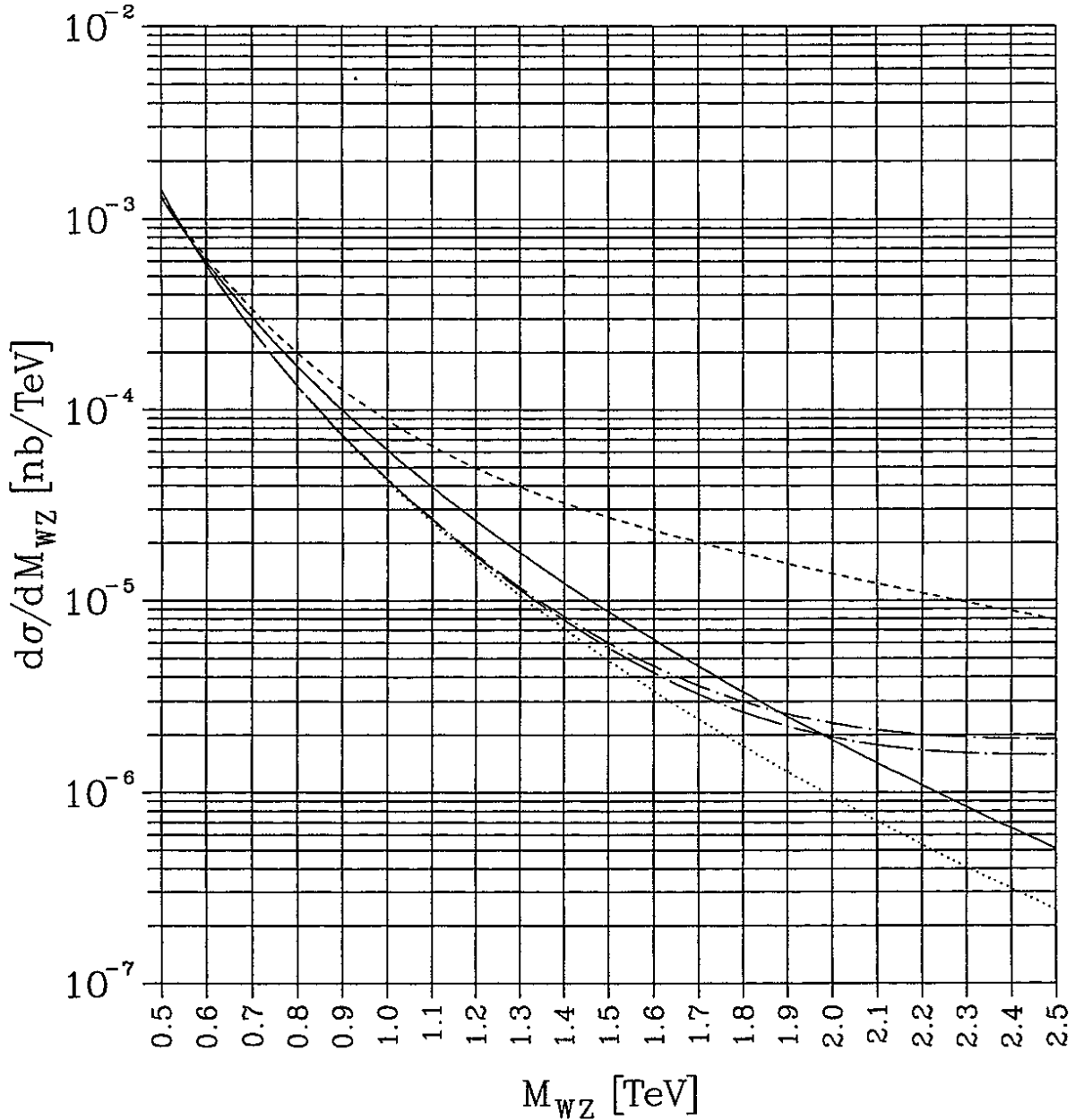Standard Model

via $q\bar{q}'$

via WV

Figure 6.19: The contributions from WV-scattering and from $q\bar{q}'$-annihilation to the cross-section for $pp \rightarrow WZX$ in the standard model as a function of M_{WZ}. A pseudorapidity-cut of $\eta = 2.5$ has been chosen.

$pp \to W^+ Z$ X, $\sqrt{s} = 14$ TeV, Y = 2
Parameters, Quark− and Vectorboson−
Distributions as in G. J. Gounaris et. al.

via q$\bar{\text{q}}'$, SM	via W^+V, SM
via q$\bar{\text{q}}'$, $\varepsilon_W = 0.01$	via W^+V, $\varepsilon_W = 0.01$
	via W^+V, $\varepsilon_W = -0.01$

Figure 6.20: The cross-section $d\sigma/dM_{WZ}(pp \to W^+ZX)$ as a function of M_{WZ} at $\sqrt{s} = 14$ TeV and $Y = 2$. All parameters have been chosen as in [41]. The high-energy approximation has been used.
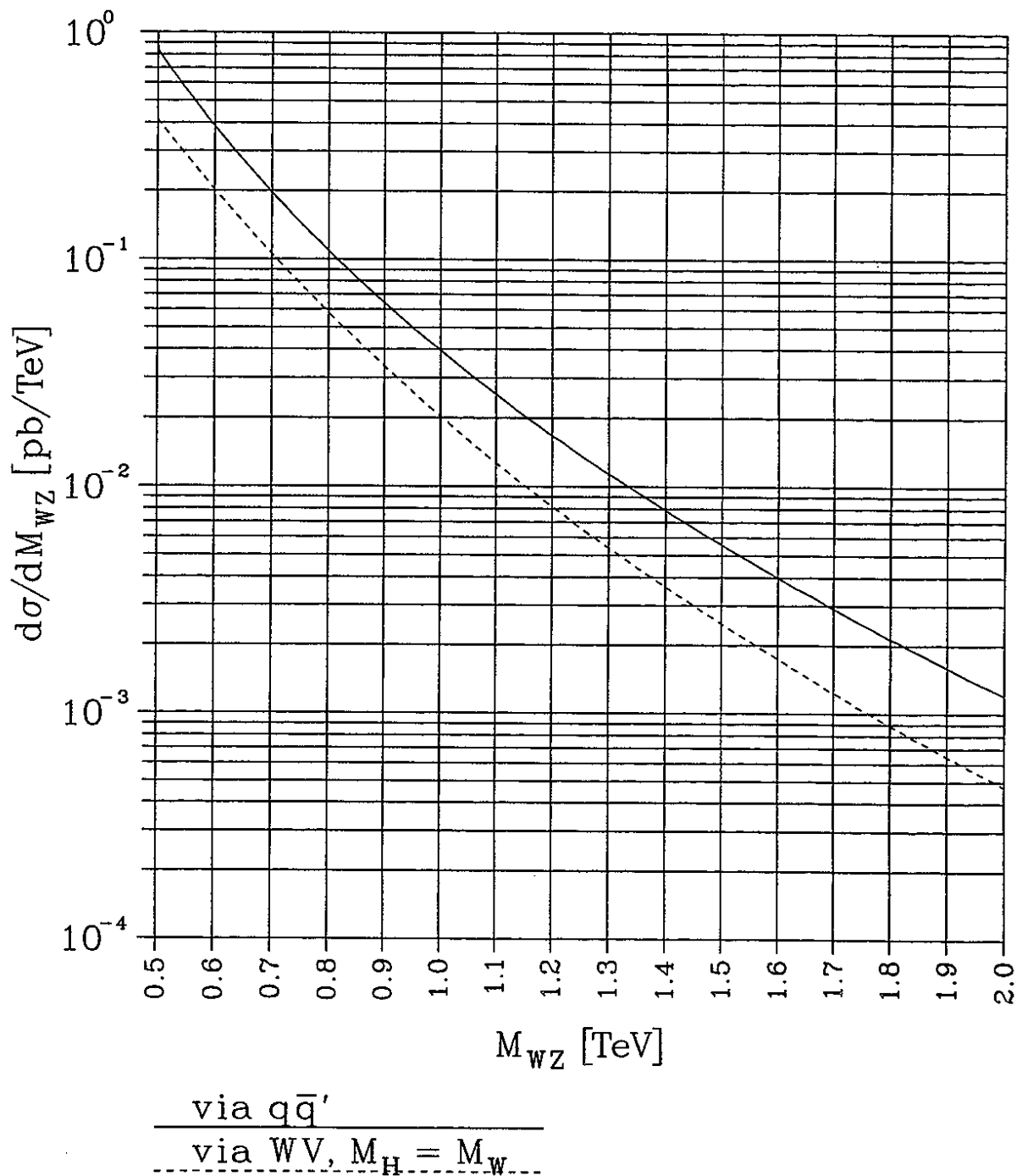
Figure 6.21: The cross-section $d\sigma/dM_{WZ}(pp \rightarrow WZX)$ as a function of M_{WZ} at $\sqrt{s} = 14$ TeV and $\eta = 1.5$. All parameters have been chosen as in [41].
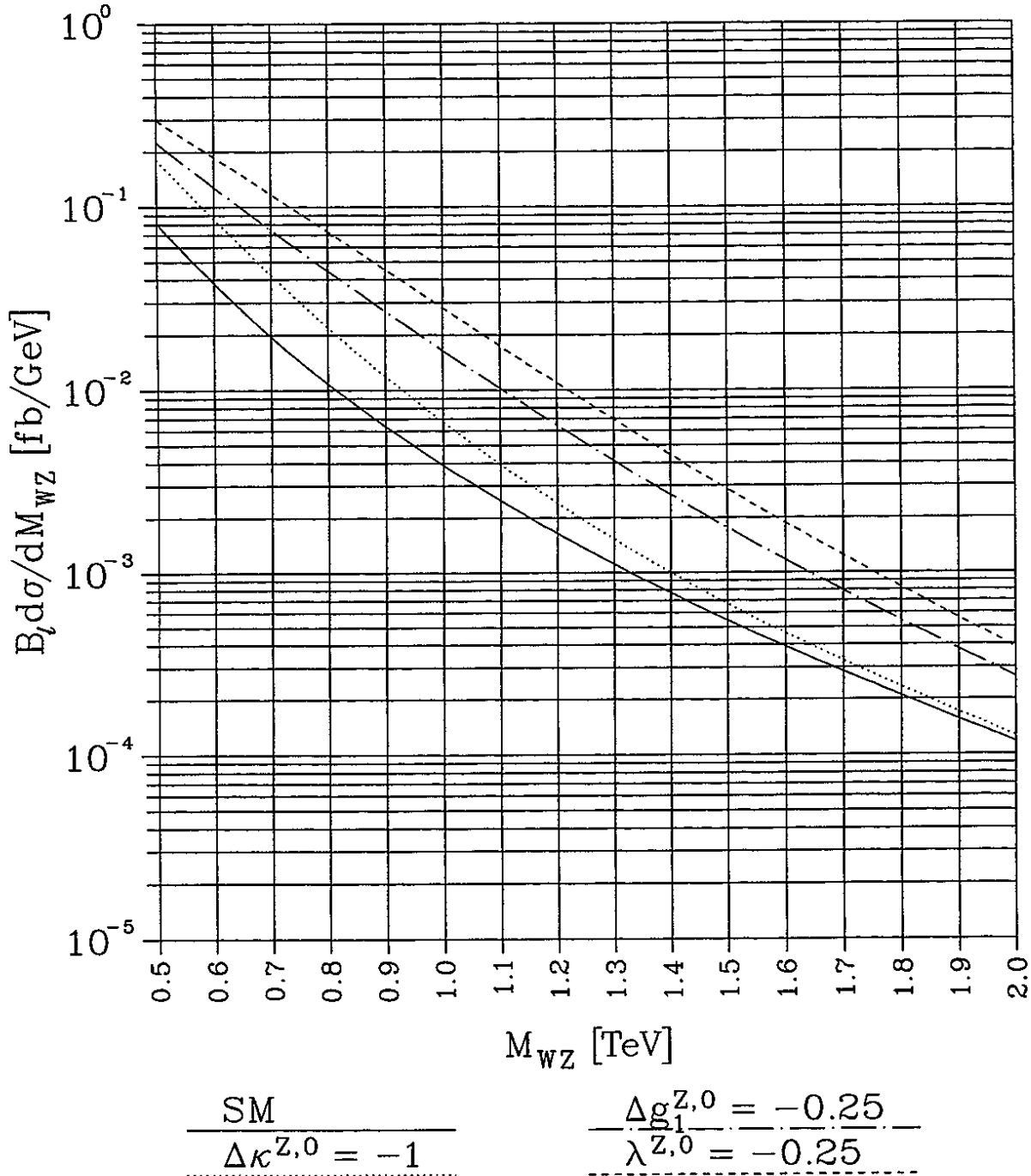
Figure 6.22: The cross-section for $d\sigma/dM_{WZ}(pp \to W^{+}ZX)$ as a function of M_{WZ} at $\sqrt{s} = 14$ TeV and $Y = 3$. All parameters have been chosen as in [27].

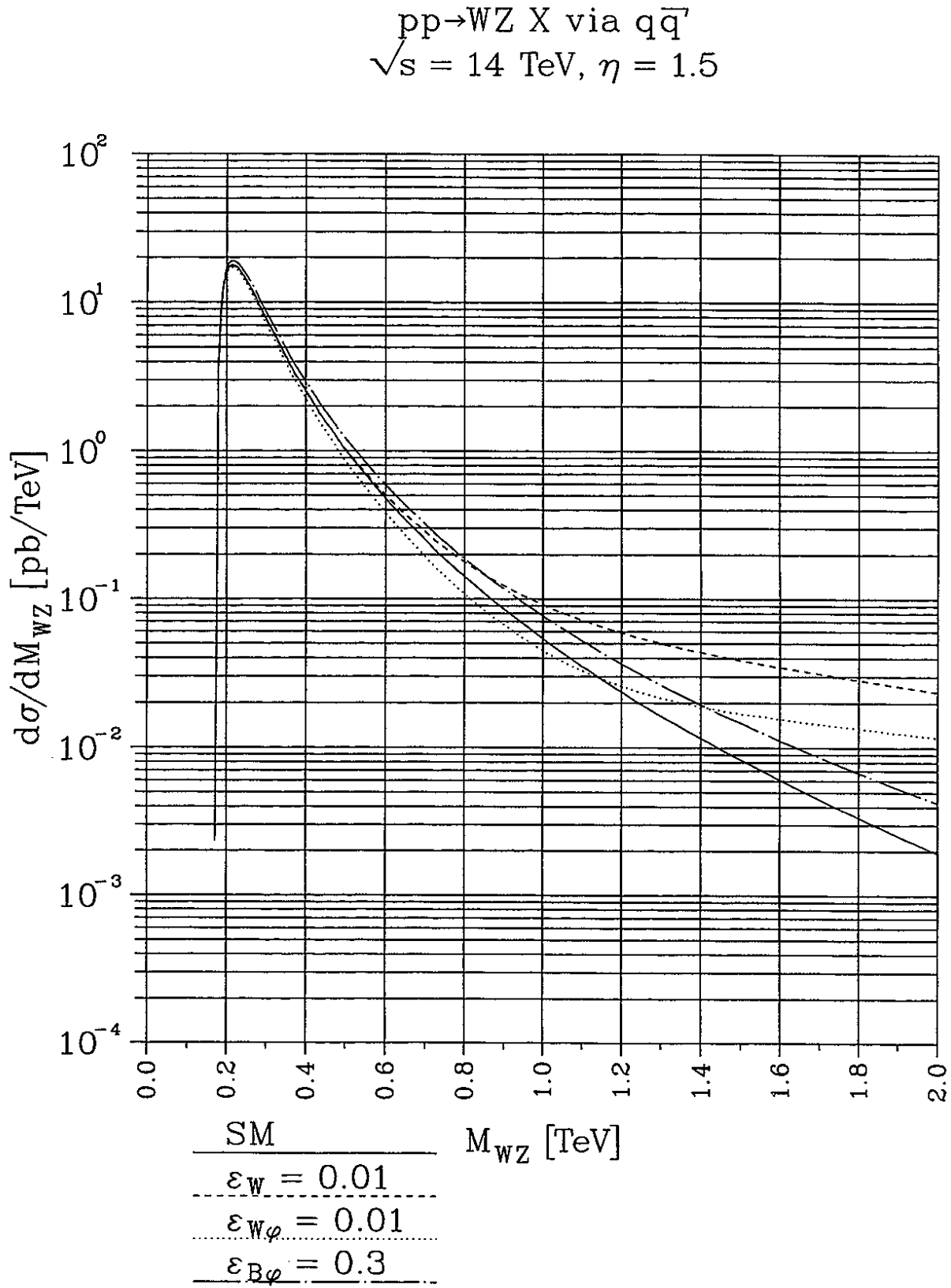Figure 6.23: The cross-section for $pp \to WZX$ via $q\bar{q}'$-annihilation for various positive values of the anomalous couplings as a function of M_{WZ}.

Figure 6.24: The cross-section for $pp \rightarrow WZX$ via $q\bar{q}'$-annihilation for various negative values of the anomalous couplings as a function of M_{WZ}.

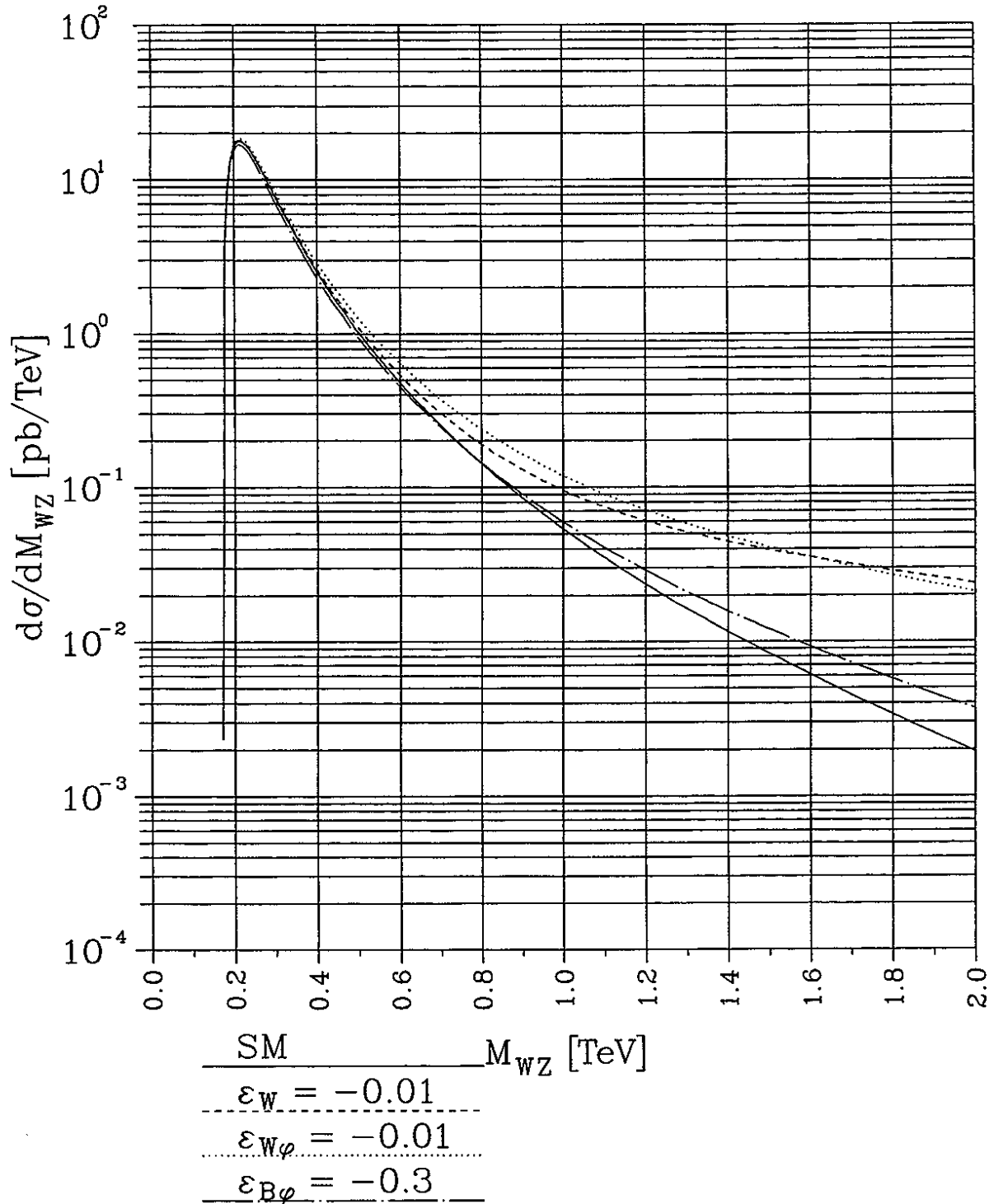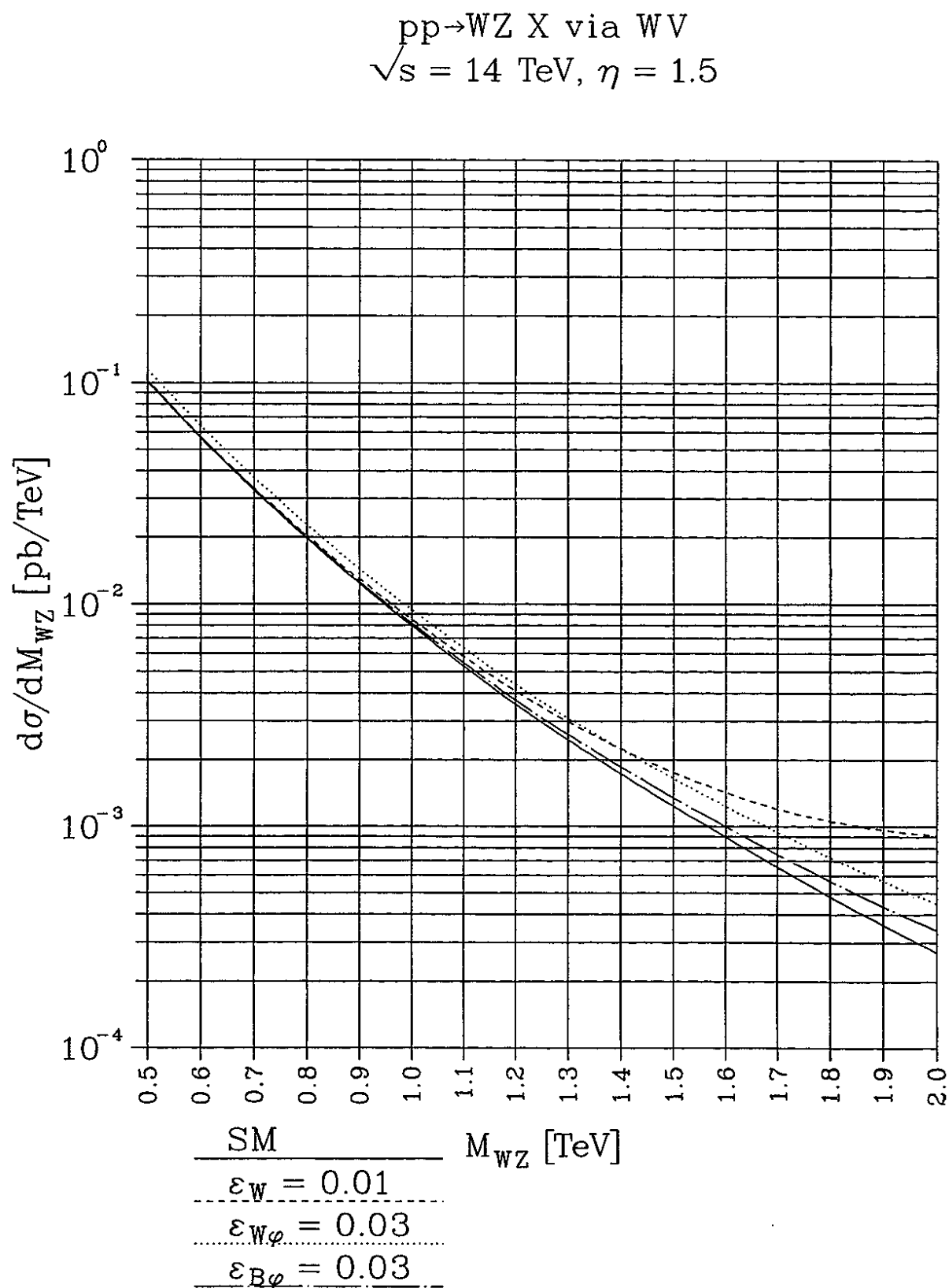Figure 6.25: The cross-section for $pp \rightarrow WZX$ via WV-scattering for various positive values of the anomalous couplings as a function of M_{WZ}.
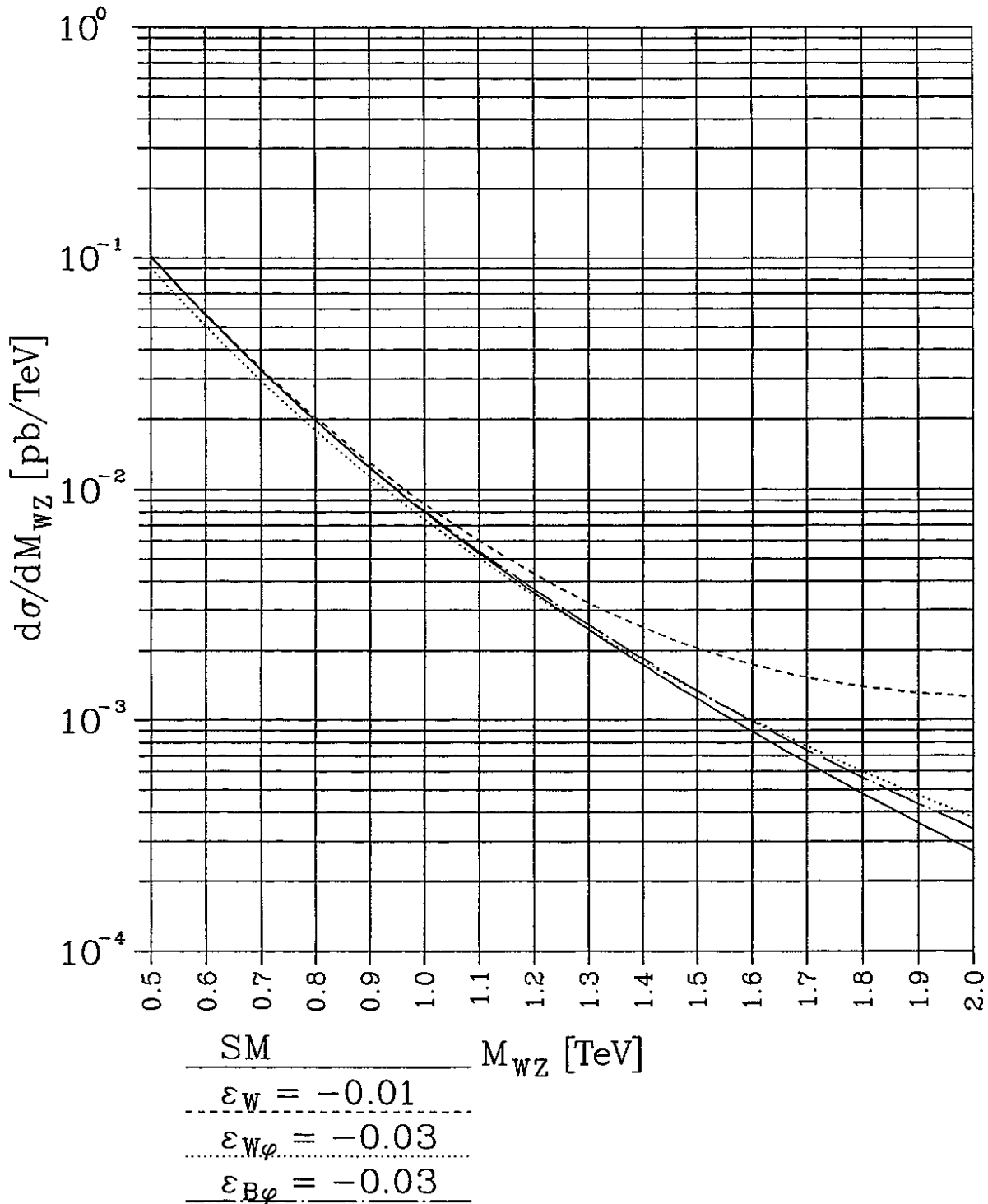
Figure 6.26: The cross-section for $pp \to WZX$ via WV-scattering for various negative values of the anomalous couplings as a function of M_{WZ}.

Chapter 7

Deriving Limits on Anomalous Couplings in an LHC Analysis

In this chapter we will derive observability limits for anomalous couplings in an LHC analysis of $pp \rightarrow WZX$. We will first discuss current experimental limits and then describe in some detail the method to derive sensitivity limits for the LHC experiment. The results will be compared with results obtained in the literature.

7.1 Current and Near-Future Experimental Limits

We discuss the current direct experimental limits on anomalous couplings and the limits which can be obtained in a near-future LEP 2 analysis.

Direct experimental limits have been so far obtained by the the CDF [8] and the D0 [9] collaborations. A review can be found in [11]. The clearest, most model-independent bound was obtained from a measurement of $W\gamma$-production in $p\bar{p}$-collisions at $\sqrt{s} = 1.8$ TeV. It concerns the two parameters $\Delta\kappa^{\gamma,0}$ and $\lambda^{\gamma,0}$. This measurement is independent of the parameters of the ZWW-coupling. The D0-collaboration [9] presents a two-parameter fit of these couplings to data, assuming a form-factor with $\Lambda_{FF} = 1.5$ TeV and $n = 2$. From this fit I read off the 95% CL limits for the couplings, allowing an arbitrary value for the respective other coupling,

$$-2.0 < \Delta\kappa^{\gamma,0} < 2.3,$$
$$-0.8 < \lambda^{\gamma,0} < 0.7 \,. \tag{7.1}$$

These experimental bounds have been obtained without any assumption on the respective other four parameters in (2.27). They translate into model-independent bounds for the parameters $\epsilon^0_{W\Phi} + \epsilon^0_{B\Phi}$ and ϵ^0_W,

$$-2.0 < \epsilon^0_{W\Phi} + \epsilon^0_{B\Phi} < 2.3 \,,$$
$$-0.8 < \epsilon^0_W < 0.7 \,. \tag{7.2}$$

I note that, considering the small collision energy of $\sqrt{s} = 1.8$ TeV, one would obtain nearly identical bounds for $\epsilon_{W\Phi} + \epsilon_{B\Phi}$ and ϵ_W, since the form factor is not much different from the value one. To give an example, one has $\epsilon_W = 0.81\epsilon^0_W$ for $M_{W\gamma} = 0.5$ TeV, which is already a rather large invariant mass for the $W\gamma$-pair in $\sqrt{s} = 1.8$ TeV collisions. Thus, we can write

$$-2.0 \lesssim \epsilon_{W\Phi} + \epsilon_{B\Phi} \lesssim 2.3 \,,$$

137

$$-0.8 \lesssim \epsilon_W \lesssim 0.7 \, . \tag{7.3}$$

Bounds on any other parameter have so far been obtained only with specific assumptions concerning the parameters which were not subjected to the fit. In [8], the data for W^+W^-- and WZ-production in $p\bar{p}$-collisions at $\sqrt{s} = 1.8$ TeV were analyzed. Assuming that the quadrupole couplings are zero, $\lambda^{\gamma,0} = \lambda^{Z,0} = 0$, and, in addition, assuming $\Delta\kappa^{\gamma,0} = 0$, a two-parameter fit with $\Lambda_{FF} = 1$ TeV and $n = 2$ was performed, leading to the 95% CL limits,

$$\begin{aligned} -1.3 &< \Delta g_1^{Z,0} < 1.5 \, , \\ -1.5 &< \Delta\kappa^{Z,0} < 1.6 \, . \end{aligned} \tag{7.4}$$

The bound on one of the parameters in (7.4) makes no assumption on the respective other parameter. Equivalently, expressed in terms of the parameters in (2.25), this fit assumed $y_\gamma^0 = y_Z^0 = 0$ and $x_\gamma^0 = 0$. Redrawing the two-dimensional confidence region in the δ_Z^0-x_Z^0-space I obtain the 95% CL bounds,

$$\begin{aligned} -2.5 &< \delta_Z^0 < 2.7 \, , \\ -4.0 &< x_Z^0 < 4.1 \, , \end{aligned} \tag{7.5}$$

where the respective other parameter is aribtrary. Expressed in terms of the parameters $\epsilon_W, \epsilon_{W\Phi}, \epsilon_{B\Phi}$, the same fit amounts to the assumption $\epsilon_W^0 = 0, \epsilon_{B\Phi}^0 = -\epsilon_{W\Phi}^0$. One is left with one free parameter, which can be taken to be $\epsilon_{W\Phi}^0$. This parameter is related to the fitted parameters by $\Delta g_1^{Z,0} = \epsilon_{W\Phi}^0/c_W^2$ and $\Delta\kappa^{Z,0} = \epsilon_{W\Phi}^0/c_W^2$, respectively. Therefore, the line $\Delta g_1^{Z,0} = \Delta\kappa^{Z,0}$ in the two-dimensional confidence region of $\Delta g_1^{Z,0}$ and $\Delta\kappa^{Z,0}$ represents the one-parameter model with $\epsilon_{W\Phi} \neq 0$. A bound on $\epsilon_{W\Phi}^0$ can be obtained by reading off the value of $\Delta g_1^{Z,0} = \Delta\kappa^{Z,0}$ at the intersections of this line with the border of the confidence region. In this way I obtain,

$$-0.7 < \epsilon_{W\Phi}^0 < 0.8 \quad (\epsilon_{B\Phi}^0 = -\epsilon_{W\Phi}^0, \quad \epsilon_W^0 = 0) \tag{7.6}$$

at 95% CL. Again, we can also write

$$-0.7 \lesssim \epsilon_{W\Phi} \lesssim 0.8 \, . \tag{7.7}$$

Equivalently, for $\epsilon_{B\Phi}^0$, we obtained the bound

$$-0.8 < \epsilon_{B\Phi}^0 < 0.7 \quad (\epsilon_{W\Phi}^0 = -\epsilon_{B\Phi}^0, \quad \epsilon_W^0 = 0) \, . \tag{7.8}$$

We present the results of another fit. Assuming $\lambda^{\gamma,0} = \lambda^{Z,0}$, $\Delta\kappa^{\gamma,0} = \Delta\kappa^{Z,0}$ and $\Delta g_1^{Z,0} = 0$, bounds on $\lambda^{Z,0}$ and $\Delta\kappa^{Z,0}$ have been obtained from the WW- and WZ-data in [8]. Assuming $\Lambda_{FF} = 1$ TeV and $n = 2$ these bounds are given by

$$\begin{aligned} -0.81 &< \lambda^{Z,0} < 0.84 \, , \\ -1.1 &< \Delta\kappa^{Z,0} < 1.3 \, . \end{aligned} \tag{7.9}$$

The two parameters show no correlation, i.e. they do not depend on the magnitude of the respective other parameter. From the bound on $\lambda^{Z,0}$, another bound on ϵ_W^0 can be obtained,

$$-0.81 < \epsilon_W^0 < 0.84 \quad \Leftrightarrow \quad -0.81 \lesssim \epsilon_W \lesssim 0.84 \, , \tag{7.10}$$

and the relations above imply $\epsilon_{W\Phi} = \epsilon_{B\Phi} = 0$ for this bound.

In summary, the current direct experimental bounds imply $|\epsilon_i^0| \lesssim 1$, where, however, only for ϵ_W^0 a model-independent bound has been derived, while the bounds on $\epsilon_{W\Phi}^0$ and $\epsilon_{B\Phi}^0$ assume certain relations among the anomalous couplings. Clearly, a confrontation of the general three-parameter model (2.46) with current data would give more model-independent bounds.

Dropping the form-factor assumption, the bounds on $\epsilon_W, \epsilon_{W\Phi}, \epsilon_{B\Phi}$, which could be obtained from present data, are nearly identical to those of the ϵ_i^0, and are thus given by

$$|\epsilon_i| \lesssim 1.$$

In the near future, an improvement of the bounds can be obtained by measurements at the CERN LEP 2 experiment [10, 11]. In this experiment, one plans to measure the cross section for $e^+e^- \to W^+W^-$ at scattering-energies of up to $\sqrt{s} = 190$ GeV. Fits to fictitious standard-model data have been performed and expected limits on the anomalous couplings have been derived. I quote the results of the first reference of [10], in which a fit to the three-parameter model (2.46) has been performed. The 95% CL limits for the parameters δ_Z, x_γ and y_γ have been derived assuming a luminosity of $\mathcal{L} = 500$ pb^{-1} and a scattering-energy of $\sqrt{s} = 190$ GeV. These limits translate into the following limits for $\epsilon_W, \epsilon_{W\Phi}$ and $\epsilon_{B\Phi}$,

$$
\begin{aligned}
-0.20 &< \epsilon_W < 0.24 \,, \\
-0.19 &< \epsilon_{W\Phi} < 0.13 \,, \qquad \text{LEP 2, \quad 95\% CL} \\
-0.35 &< \epsilon_{B\Phi} < 1.05 \,.
\end{aligned}
\tag{7.11}
$$

In deriving the limits (7.11), all three parameters were allowed to take on arbitrary values.

7.2 Analysis of Fictitious Data

We give a theoretical treatment on deriving observability limits. We want to determine to what extent fictitious data, which will be taken here equal to the standard model prediction, are consistent with theories which have non-zero anomalous couplings. This will lead us to determine upper and lower limits for the coupling parameters, in the range of which the true values for the coupling parameters lie with a given probability. The discussion here follows [92] and references therein.

For an analysis of this kind we have to define a quantity which describes a deviation from the standard model as a function of the anomalous couplings. We assume that there are M measured quantities $x_i, i = 1...M$,. In our case the x_i will be the number of WZ events predicted in the standard model occuring in different kinematical regions, $x_i = N_i(SM)$. The kinematical regions will be defined by dividing the distribution of the number of events over a certain kinematical variable, e.g. the invariant mass of the WZ-pair, into several intervals (bins). Then, M is the number of intervals, $M = N_b$. We further assume that the quantity x_i is the outcome of a measurement of a random variable with a Gaussian distribution, specified by a mean value $\hat{x}_i$ and a standard deviation σ_i. The mean value $\hat{x}_i$ is the true value of the measured quantity x_i, which in our case is the prediction of the theory as a function of the coupling parameters, $\hat{x}_i = N_i(\vec{\epsilon})$, where $\vec{\epsilon} = \epsilon_W, \epsilon_{W\Phi}, \epsilon_{B\Phi}$. We further assume that the number of events are Poisson-distributed so that their standard error is given by $\sigma_i = \sqrt{N_i}$.

The parameter χ^2, defined by

$$
\begin{aligned}
\chi^2 &\equiv \sum_{i=1}^{M} \frac{(x_i - \hat{x}_i)^2}{\sigma_i^2} \\
&= \chi^2(\vec{\epsilon}) = \sum_{i=1}^{N_b} \frac{(N_i(SM) - N_i(\vec{\epsilon}))^2}{N_i(\vec{\epsilon})},
\end{aligned}
\tag{7.12}
$$

quantifies the deviation of the measurement from the theory, assuming that the theory is correct. Here, the measurement is to be understood as being the combined measurement of all M quantities, thus, in our case, the measurement of the complete distribution of the number of events over the chosen kinematical variable, discretized by means of bins. The value of χ^2 directly tells us the number of standard deviations, n_σ, by which the measurement deviates from the theory,

$$
\chi^2 = n_\sigma^2.
\tag{7.13}
$$

The equations (7.12) and (7.13) give us the value of n_σ for any theory, represented by a point in the space of the parameters, and define for each value of n_σ a class of theories, represented by a (not necessarily continuous) region in this space (confidence region), in which the deviations from the measured values are less than n_σ. A subspace of the complete space can be defined by choosing a smaller number of anomalous couplings or even choosing only a single coupling parameter, whithout making assumptions on the magnitudes of the other parameters. One obtains the confidence region in the subspace by the (geometrical) projection of the complete confidence region on the subspace. The meaning of the projection is that the parameters which have been removed can take one arbitrary values.

The probability that the true values $\vec{\epsilon}$ lie inside the confidence region is given by the confindence level, $CL(n_\sigma, k) \equiv 1 - \alpha(n_\sigma, k)$, with

$$
\begin{aligned}
\alpha(n_\sigma, k) &= \int_{n_\sigma^2}^{\infty} f(z; k) dz, \\
f(z; k) &= \frac{z^{k/2-1} e^{-z/2}}{2^{k/2} \Gamma(k/2)},
\end{aligned}
\tag{7.14}
$$

where k is the dimension of the space or subspace. In projecting the confidence region onto a subspace the confidence level increases, since now one makes no statement about the magnitudes of the removed parameters anymore. Before the projection, these parameters were required to lie within the confidence region. Instead of the projection one can also consider the section (or cut) of the confidence region which is cut out by a particular subspace. The section is in general smaller than the projection and is the confidence region of a subclass of the general theory, namely of all those theories, in which the cut-away parameters have been fixed to a particular value. The confidence level for the section is the same as for the projection.

The form of the confidence region reveals information about the mutual influences of the effects of anomalous couplings, thus compensations or amplifications. Bulges in the hyper-area limiting a confidence region hint to compensations, inlets to amplifications.

The projection onto a two-dimensional subspace can be represented graphically (confidence area). We will make plots of such projections as well as of the corresponding

sections, in which one of the parameters has been set to its standard value. This we will do for $n_\sigma = 1$ and $n_\sigma = 2$. The probability that the true values of the parameters lie within the confidence area are $CL(1, 2) = 39.35\%$ for $n_\sigma = 1$ and $CL(2, 2) = 86.47\%$ for $n_\sigma = 2$. From the projection of the area on the parameter axes one obtains the limits for the single anomalous couplings (confidence interval). By this procedure, no assumptions are made about the magnitudes of the other couplings. The probability that a parameter lies within the confidence interval belonging to $n_\sigma = 1$ is $CL(1, 1) = 68.27\%$, while the probability that it lies within the 2σ interval is $CL(2, 1) = 95.45\%$.

7.3 Choice of Proper Kinematical Event-Regions for the Data-Analysis

More information can be obtained from the data if the data are appropriately devided into several event-regions. We discuss a suitable choice of event-regions for the detection of anomalous couplings in $pp \to WZX$.

7.3.1 Choice of Intervals in M_{WZ}

We want to divide the WZ phase-space into kinematical regions, which are appropriate for the analysis of the data concerning the search for anomalous couplings. As already mentioned, we expect that anomalous couplings manifest themselves particularly strongly at large invariant masses M_{WZ} of the WZ-pair. Therefore we investigate the sensitivity to anomalous couplings in different intervals of M_{WZ}. We note that the distribution over more than one variable, thus a multi-differential cross-section, is not a useful quantity to be considered here. The reason is that the number of expected events is too low for a corresponding analysis.

In the further discussion we will consider numbers of events instead of cross-sections. For the detection of a W- and Z-particle we are only going to count the leptonic decays, in which at least one charged lepton is among the decay products of each vector-boson. However, we are not going to consider decays into τ-leptons. We thus consider the decay channels $W^\pm \to e^\pm \nu_e$, $W^\pm \to \mu^\pm \nu_\mu$ (decay probability 10.7% each [92]) and $Z \to e^+ e^-$, $Z \to \mu^+ \mu^-$ (decay probability 3.37% each [92]). The probability of a WZ-pair decaying via these channels is thus $B_l = (2 \cdot 10.7\%) \cdot (2 \cdot 3.37\%) = 1.44\%$. We note that the hadronic decay channels are swamped by QCD background processes [15].

The number of events which one expects for a given cross-section σ is given by

$$N = \mathcal{L} B_l \sigma, \tag{7.15}$$

where $\mathcal{L}$ is the integrated luminosity of the experiment. For the LHC we will assume $\mathcal{L} = 10^5 \text{ pb}^{-1}$ [15].

We restrict ourselves in the discussion of this section to the parton-processes $q\bar{q}' \to WZ$. These yield both in the standard model and for anomalous couplings the dominant contribution to the cross-section for $pp \to WZX$. At first we are going to divide the events in such a way into intervals of M_{WZ} that there is a statistically significant number of events in each interval. In doing so we will take the standard predictions for our orientation. For a cut of $\eta = 1.5$ one expects less than one event above $M_{WZ} = 2$ TeV. The variation of the cut will be discussed in the next section. In the region 1 TeV $< M_{WZ} < 2$ TeV one

Table 7.1: Division of the phase space of the final state into M_{WZ}-intervals for the process $pp \to WZX$ via $q\bar{q}'$-annihilation at $\sqrt{s_{pp}} = 14$ TeV assuming an integrated luminosity of $\mathcal{L} = 10^5$ pb^{-1}.

Interval-	Interval Limits	Number of SM events		
Number	M_{WZ} [TeV]	$\eta=1$	$\eta=1.5$	$\eta=3$
1	1 - 2	6.1	19.8	127
2	0.8 - 1	7.9	25.8	175
3	0.7 - 0.8	8.4	27.4	188
4	0.6 - 0.7	15.4	50.4	348
5	0.5 - 0.6	31.5	102.2	698
6	0.4 - 0.5	74.5	237.4	1555

expects 20 events. We choose this region as the first interval. Until down to an invariant mass of $M_{WZ} = 0.4$ TeV we choose five more intervals, as shown in Table 7.1.

The intervals contain each more than 20 standard events at $\eta = 1.5$, where the number of events per interval increases with decreasing energy. In spite of the higher statistical significance of the lower-energy intervals, these intervals nevertheless exhibit a smaller sensitivity to anomalous couplings.

We note that it is expedient to discuss the sensitivity by means of sections at $\epsilon_{B\Phi} = 0$ instead of projections. This is because $\epsilon_{B\Phi}$ has only small effects and is eventually restricted in magnitude by its unitarity limits. To compare the sensitivity of different intervals it is therefore sufficient to discuss sections at $\epsilon_{B\Phi} = 0$.

Figure 7.1 shows the sections of 2σ confidence regions with the plane $\epsilon_{B\Phi} = 0$ for a pseudorapidity-cut of $\eta = 1.5$. Only a single interval at a time was used for the calculation of χ^2. The boundaries of the sections for the intervals 4,5 and 6 are not coherent and consist of an outer and an inner boundary. In the region beyond the outer boundary the number of events predicted in the anomalous model is more than two standard deviations greater than the number predicted in the standard model. In the region inside the inner boundary, in contrast, the anomalous model is by more than 2σ below the standard model. The reason for the deviation of the model to smaller values is the large, negative coefficient linear in $\epsilon_{W\Phi}$. With growing, positive $\epsilon_{W\Phi}$ or a growing magnitude of ϵ_W one leaves the inner region, since then the quadratic effects of $\epsilon_{W\Phi}$ and ϵ_W increase the cross-section again.

Had one considered projections instead of sections of confidence regions, there would be no inner region, since by choosing a sufficiently large value of $\epsilon_{B\Phi}$ one can always achieve that the cross-section in the inner region approaches the standard value. The inner regions therefore appear as cavities in the three-dimensional confidence region.

For the high-energy intervals 1, 2 and 3 an inner area does not exist, since the effects of the quadratic terms in $\epsilon_{W\Phi}$ are of the same order of magnitude as the linear ones already for small values of $\epsilon_{W\Phi}$.

Altogether one concludes from Figure 7.1 that the interval 1 alone already provides the bulk of the available information about anomalous couplings. By including further intervals, however, one can, via the linear effects of $\epsilon_{W\Phi}$, achieve a lowering of the upper bound for $\epsilon_{W\Phi}$. This is shown in Figure 7.2. We have now calculated χ^2 according to (7.12) as a sum over $N_b \geq 1$ intervals. The inner regions in Figure 7.1 manifest themselves

as inlets at positive $\epsilon_{W\Phi}$ in Figure 7.2. One recognizes that the bulk of the available sensitivity is seized if one restricts to the intervals 1 to 5, thus to the high-energy region of $M_{WZ} > 0.5$ TeV. In these intervals, there are altogether 226 events via $q\bar{q}'$-scattering in the standard model. In summary, the choice of the intervals 1 to 5 is reasonable.

7.3.2 Choice of the Cut η

An enlargement of the cut η leads to a worsening of the sensitivity. This is shown in Figure 7.3 for the cut $\eta = 3$. The figure is to be compared to Figure 7.2, for which $\eta = 1.5$ was chosen. Compared to $\eta = 1.5$ the confidence area considerably expanded. The reason for this is that the number of anomalous events is larger at greater transverse momenta. Choosing $\eta = 1$, the sensitivity can theoretically even be enlarged as compared to $\eta = 1.5$. This is shown in Figure 7.4. However, for $\eta = 1$ the number of events in the high-energy interval has decreased to $N = 6$, so that a statistical analysis becomes doubtful. In summary, the choice of $\eta = 1.5$ is reasonable.

Sections at $\varepsilon_{B\varphi} = 0$ through $\chi^2=4$ confidence region
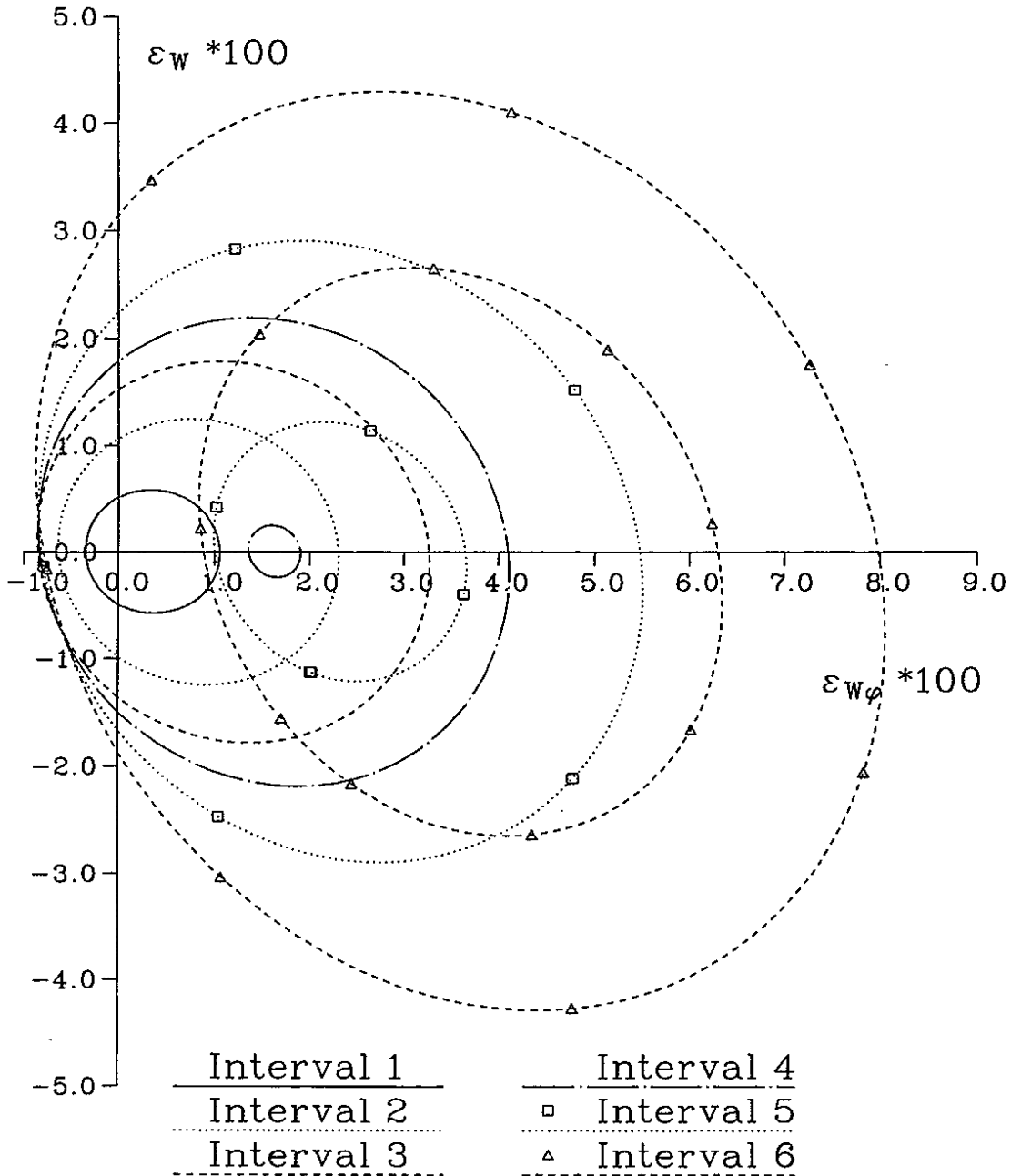pp $\rightarrow$ WZ X via q$\overline{q}'$, $\eta = 1.5$

Figure 7.1: Sensitivity of different intervals of M_{WZ}. Shown are the boundaries of the sections, which are obtained by the analysis of the data of a single interval at a time. The intervals have been defined in Table 7.1.

Sections at $\varepsilon_{B\varphi} = 0$ through $\chi^2 = 4$ confidence region
$pp \to WZ\,X$ via $q\bar{q}'$, $\eta = 1.5$

Figure 7.2: The sections of the 2σ confidence region with the plane $\epsilon_{B\Phi} = 0$ for a pseudorapidity-cut of $\eta = 1.5$. Different numbers of intervals over M_{WZ} have been taken into account in the calculation of χ^2.

Sections at $\varepsilon_{B\varphi} = 0$ through $\chi^2 = 4$ confidence region
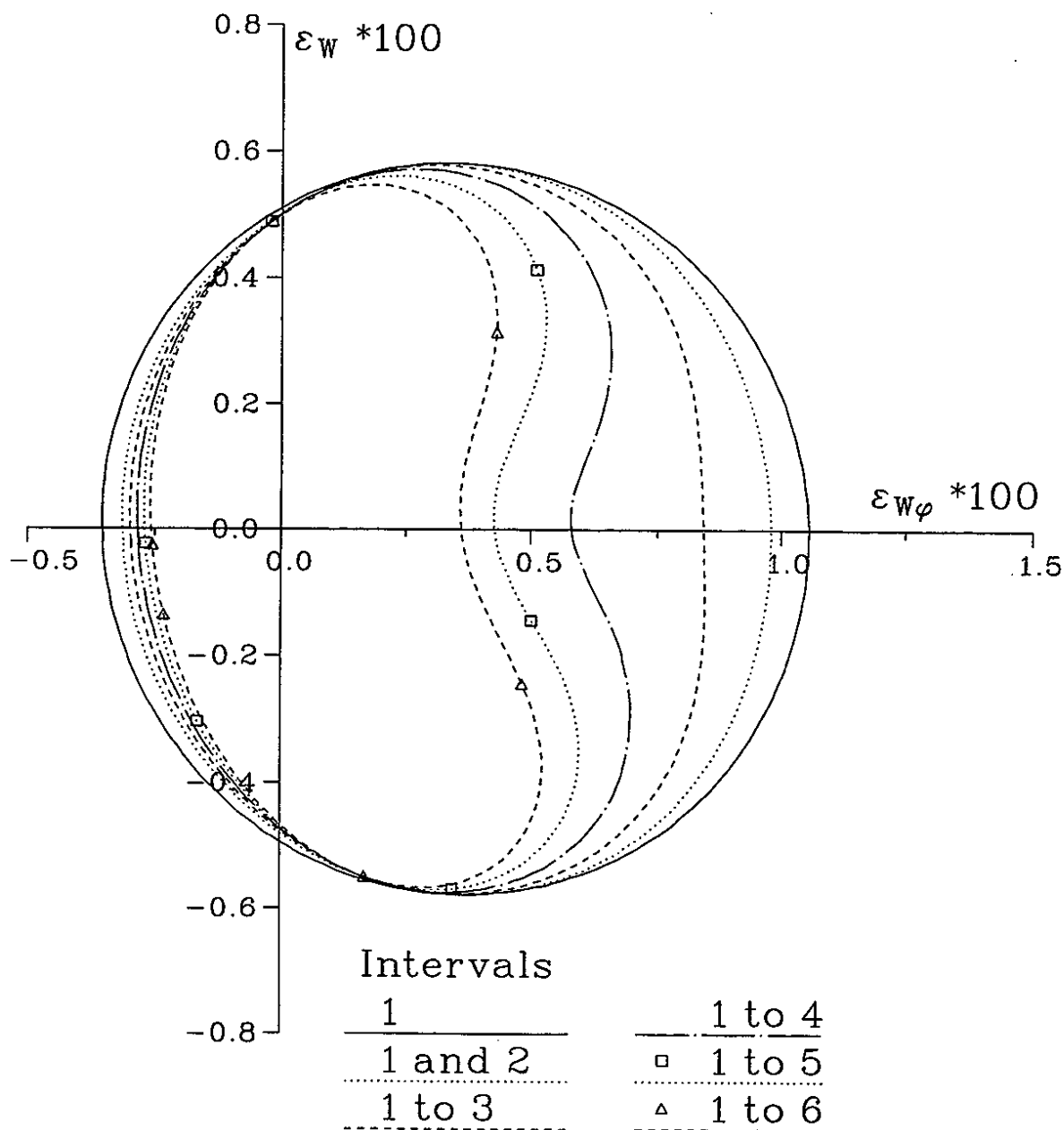pp → WZ X via q$\bar{q}'$, $\eta = 3$

Figure 7.3: The sections of the 2σ confidence region with the plane $\epsilon_{B\Phi} = 0$ for a pseudorapidity-cut of $\eta = 3$. Different numbers of intervals over M_{WZ} have been taken into account in the calculation of χ^2.

Sections at $\varepsilon_{B\varphi} = 0$ through $\chi^2=4$ confidence region
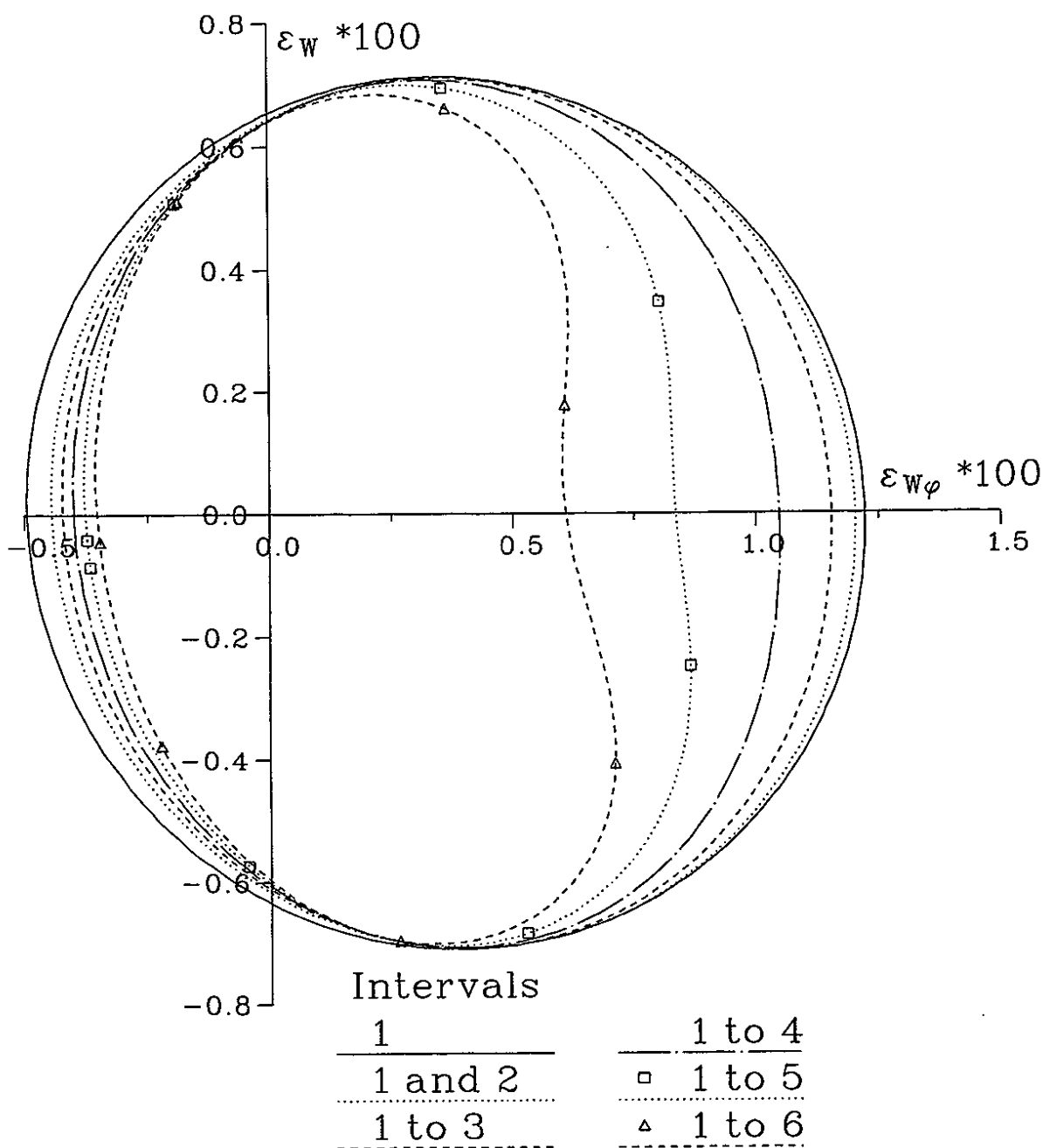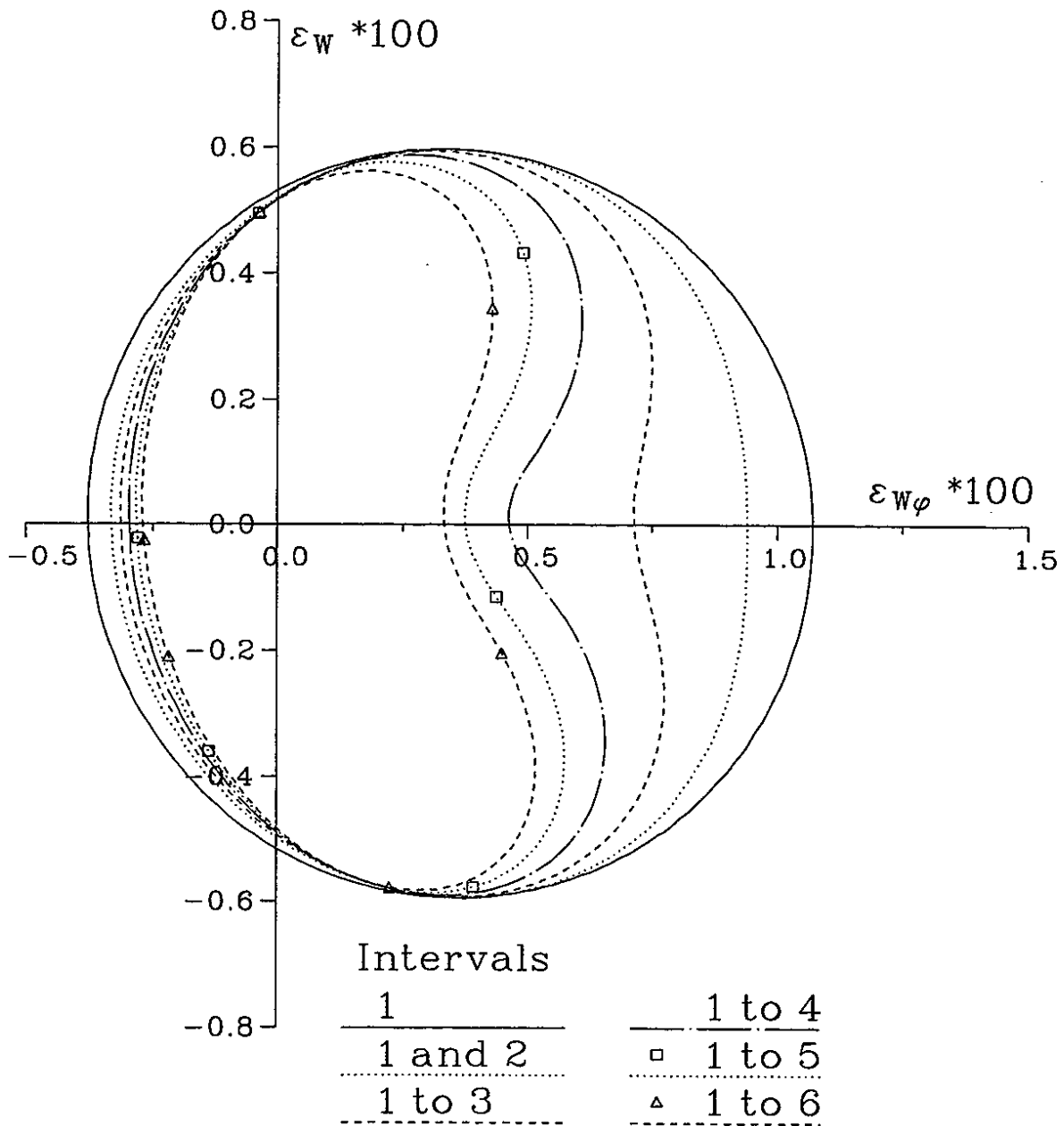pp $\to$ WZ X via $q\bar{q}'$, $\eta = 1$

Figure 7.4: The sections of the 2σ confidence region with the plane $\epsilon_{B\Phi} = 0$ for a pseudorapidity-cut of $\eta = 1$. Different numbers of intervals over M_{WZ} have been taken into account for the calculation of χ^2.

Interval	Coefficients N_j for number of events via $q\bar{q}'$									
	SM	$\hat{\epsilon}_W$	$\hat{\epsilon}_{W\Phi}$	$\hat{\epsilon}_{B\Phi}$	$\hat{\epsilon}_W^2$	$\hat{\epsilon}_{W\Phi}^2$	$\hat{\epsilon}_W\hat{\epsilon}_{W\Phi}$	$\hat{\epsilon}_W\hat{\epsilon}_{B\Phi}$	$\hat{\epsilon}_{W\Phi}\hat{\epsilon}_{B\Phi}$	$\hat{\epsilon}_{B\Phi}^2$
1	19.8	-0.76	-21.1	0.011	44.2	30.00	1.76	-0.153	-0.206	0.0096
2	25.8	-0.97	-14.2	0.014	11.7	8.47	1.09	-0.095	-0.123	0.0059
3	27.4	-1.01	-11.0	0.014	6.09	4.56	0.79	-0.069	-0.094	0.0044
4	50.4	-1.79	-15.6	0.025	6.10	4.78	1.05	-0.092	-0.125	0.0058
5	102.2	-3.42	-23.2	0.048	5.97	4.99	1.42	-0.124	-0.171	0.0080

Table 7.2: Coefficients N_j for anomalous couplings for $pp \to WZX$ via $q\bar{q}'$-annihilation in the 5 intervals defined in Table 7.1. The number of events in a given interval is obtained by multiplying the coefficient with the corresponding product of the couplings and subsequently summing over all terms. A rapidity-cut of $\eta = 1.5$ was applied.

7.4 Determination of Confidence Regions for Anomalous Couplings

We are now going to determine the confidence regions for anomalous couplings. This will establish the main result of our work. The true values of the parameters lie within these regions with definite probabilities. We assume that standard values will be actually measured.

The entire information about anomalous couplings can be expressed in terms of coefficients N_j for the anomalous couplings. To define the coefficients, the number of events $N(\vec{\epsilon})$ in each interval is written as a power series in the coupling parameters. For the production via $q\bar{q}'$-annihilation there are 9 coefficients plus the standard term. This is because the cross-section is quadratic in the couplings. We define the coefficients by writing the number of events as

$$
\begin{aligned}
N(\vec{\epsilon}) = &\; N_0 + N_1\hat{\epsilon}_W + N_2\hat{\epsilon}_{W\Phi} + N_3\hat{\epsilon}_{B\Phi} \\
&+ N_4\hat{\epsilon}_W^2 + N_5\hat{\epsilon}_{W\Phi}^2 + N_6\hat{\epsilon}_W\hat{\epsilon}_{W\Phi} + N_7\hat{\epsilon}_W\hat{\epsilon}_{B\Phi} + N_8\hat{\epsilon}_{W\Phi}\hat{\epsilon}_{B\Phi} + N_9\hat{\epsilon}_{B\Phi}^2. \quad (7.16)
\end{aligned}
$$

In (7.16),

$$
\hat{\epsilon}_W \equiv 100 \cdot \epsilon_W, \quad \hat{\epsilon}_{W\Phi} \equiv 100 \cdot \epsilon_{W\Phi}, \quad \hat{\epsilon}_{B\Phi} \equiv 100 \cdot \epsilon_{B\Phi}, \quad (7.17)
$$

are the coupling parameters and $N_j, j = 1...9$ are the coefficients for these couplings. The normalization of the couplings has been changed such that the coefficients for the parameters in (7.17) are of the order of magnitude $\mathcal{O}(10)$ or smaller. Table 7.2 shows the coefficients for the 5 intervals. The N_j have been calculated according to (5.43), (6.1) and (7.15).

Concerning the linear effects, those of $\hat{\epsilon}_{W\Phi}$ are dominant. As to the quadratic effects, the coefficients of $\hat{\epsilon}_W^2$ and $\hat{\epsilon}_{W\Phi}^2$ become large at large scattering energies. The effects of $\hat{\epsilon}_{B\Phi}$ are very small.

For the production via WV-scattering there are 34 coefficients for the anomalous couplings, as the amplitude itself is already quadratic in the couplings. Tables 7.3 and 7.4 show the coefficients N_j, multiplied with the factor 10^3, for the WZ- and $W\gamma$-processes for the intervall 1 as an example. As already discussed, the effects of anomalous couplings are largest in this interval. A Higgs boson mass of $M_H = 80$ GeV was chosen. The sum of

the two production mechanisms only amounts to 3 standard events in this interval. Concerning the anomalous terms, the coefficients are largest for the powers in which only $\hat{\epsilon}_W$ appears. An exception is the coefficient linear in $\hat{\epsilon}_{W\Phi}$, which is the largest linear coefficient. Another large coefficient is the one of $\hat{\epsilon}_W^2 \hat{\epsilon}_{W\Phi}^2$. If $\hat{\epsilon}_W$ is small, the effects of $\hat{\epsilon}_{W\Phi}$ and $\hat{\epsilon}_{B\Phi}$ can manifest themselves. In this case, also the coefficients of $\hat{\epsilon}_{W\Phi}^2$ and $\hat{\epsilon}_W^2 \hat{\epsilon}_{W\Phi}$ become important. For the $W\gamma$-scattering process, also the coefficients of $\hat{\epsilon}_{B\Phi}$, $\hat{\epsilon}_{W\Phi}\hat{\epsilon}_{B\Phi}$, $\hat{\epsilon}_{B\Phi}^2$, $\hat{\epsilon}_W\hat{\epsilon}_{W\Phi}^2$ and $\hat{\epsilon}_W\hat{\epsilon}_{W\Phi}\hat{\epsilon}_{B\Phi}$ are non-negligible in this case. All other coefficients are negligibly small.

The same coefficients, calculated within the high-energy approximation, are shown in the Tables 7.5 and 7.6. The large coefficients, those for $\hat{\epsilon}_{W\Phi}, \hat{\epsilon}_W^2, \hat{\epsilon}_W^3, \hat{\epsilon}_W^4, \hat{\epsilon}_W^2\hat{\epsilon}_{W\Phi}$, and the standard term deviate by less than 9% from the exact calculation. The coefficients which become important for small values of ϵ_W deviate by less than 25% from the exact value. An exception is the coefficient of $\hat{\epsilon}_{B\Phi}$ for the $W\gamma$-process, which deviates by 48%. This coefficient is determined by non-leading terms in the high-energy approximation.

Number of SM Events		
Interval	via WZ	via $W\gamma$
1	1.3	1.6
2	1.6	2.1
3	1.6	2.1
4	2.6	3.6
5	4.5	6.5

The Table to the left shows the number of standard events via WZ-scattering and via $W\gamma$-scattering in all intervals (no high-energy approximation). In the region 0.5 TeV $< M_{WZ} <$ 2 TeV there are 27.6 SM events via WV scattering, consisting of 11.7 events via WZ-scattering and 15.9 events via $W\gamma$-scattering, opposing 226 events via $q\bar{q}'$-annihilation.

The projections on the coordinate planes and the sections of the regions of constant χ^2, given by (7.12), can now be found. The Figures 7.5, 7.6 and 7.7 constitute the main result of our work. They show the projections of the $\chi^2 = 4$ (CL=86.5 %) and $\chi^2 = 1$ (CL=39.4 %) confidence regions onto the three coordinate planes in the space of anomalous couplings ($\epsilon_{B\Phi} = 0, \epsilon_W = 0, \epsilon_{W\Phi} = 0$). They also show the sections of the confidence regions with the planes. The sections are always inside the projections and are therefore not separately marked. Also shown are the unitarity limits for $\epsilon_{B\Phi}$, as given in 6.2.1. The analysis was based on the cross-section calculated as the sum of the $q\bar{q}'$- and WV-processes in the intervals 1 to 5. A cut of $\eta = 1.5$ was chosen and $M_H = 80$ GeV was taken. The figures show that the linear effects of $\epsilon_{W\Phi}$ manifest themselves in an inlet of the section of the confidence region on the positive $\epsilon_{W\Phi}$-axis. This leads to a bean-like form of the section. The effect is not present for the projections. Also, a correlation between the couplings $\epsilon_{W\Phi}$ and $\epsilon_{B\Phi}$ can be observed. The correlation between ϵ_W and $\epsilon_{W\Phi}$ or ϵ_W and $\epsilon_{B\Phi}$ is small.

The two-dimensional projection can be further projected onto the coordinate axes, from which one obtains the confidence intervals for the anomalous couplings. We only project the region which is inside the unitarity limits for $\epsilon_{B\Phi}$. This necessary restriction, however, only affects the upper bound on $\epsilon_{W\Phi}$. The confidence intervals are shown in Table 7.7. The table also shows the unitarity bound for $\epsilon_{B\Phi}$. The parameters lie with the given probability within the confidence intervals, if standard model values are measured. The respective other parameters can take on arbitrary values. Comparing with the current experimental limits discussed in 7.1 we conclude that an LHC analysis will allow to shrink the current confidence intervals by a factor of more than 100 for the couplings ϵ_W and $\epsilon_{W\Phi}$. The parameter $\epsilon_{B\Phi}$ can not be further constrained below its unitarity limits.

Coefficients $N_j \cdot 10^3$ for number of events via WZ in interval 1							
SM	$\hat{\epsilon}_W$	$\hat{\epsilon}_{W\Phi}$	$\hat{\epsilon}_{B\Phi}$				
1300	5	70	-8				
$\hat{\epsilon}_W^2$	$\hat{\epsilon}_{W\Phi}^2$	$\hat{\epsilon}_W\hat{\epsilon}_{W\Phi}$	$\hat{\epsilon}_W\hat{\epsilon}_{B\Phi}$	$\hat{\epsilon}_{W\Phi}\hat{\epsilon}_{B\Phi}$	$\hat{\epsilon}_{B\Phi}^2$		
236	19.2	-4.77	-1.20	1.35	1.68		
$\hat{\epsilon}_W^3$	$\hat{\epsilon}_W^2\hat{\epsilon}_{W\Phi}$	$\hat{\epsilon}_W\hat{\epsilon}_{W\Phi}^2$	$\hat{\epsilon}_{W\Phi}^3$	$\hat{\epsilon}_W^2\hat{\epsilon}_{B\Phi}$	$\hat{\epsilon}_W\hat{\epsilon}_{W\Phi}\hat{\epsilon}_{B\Phi}$	$\hat{\epsilon}_{W\Phi}^2\hat{\epsilon}_{B\Phi}$	$\hat{\epsilon}_W\hat{\epsilon}_{B\Phi}^2$
-95.6	27.8	-2.60	4.35	-0.84	-4.52	-0.32	-0.066
$\hat{\epsilon}_{W\Phi}\hat{\epsilon}_{B\Phi}^2$	$\hat{\epsilon}_{B\Phi}^3$						
0.040	0.009						
$\hat{\epsilon}_W^4$	$\hat{\epsilon}_W^2\hat{\epsilon}_{W\Phi}^2$	$\hat{\epsilon}_{W\Phi}^4$	$\hat{\epsilon}_W^3\hat{\epsilon}_{W\Phi}$	$\hat{\epsilon}_W\hat{\epsilon}_{W\Phi}^3$	$\hat{\epsilon}_W^3\hat{\epsilon}_{B\Phi}$	$\hat{\epsilon}_W^2\hat{\epsilon}_{W\Phi}\hat{\epsilon}_{B\Phi}$	$\hat{\epsilon}_W\hat{\epsilon}_{W\Phi}^2\hat{\epsilon}_{B\Phi}$
166	79.7	8.16	3.81	1.28	-0.0014	-0.486	-0.038
$\hat{\epsilon}_{W\Phi}^3\hat{\epsilon}_{B\Phi}$	$\hat{\epsilon}_W^2\hat{\epsilon}_{B\Phi}^2$	$\hat{\epsilon}_W\hat{\epsilon}_{W\Phi}\hat{\epsilon}_{B\Phi}^2$	$\hat{\epsilon}_{W\Phi}^2\hat{\epsilon}_{B\Phi}^2$	$\hat{\epsilon}_W\hat{\epsilon}_{B\Phi}^3$	$\hat{\epsilon}_{W\Phi}\hat{\epsilon}_{B\Phi}^3$	$\hat{\epsilon}_{B\Phi}^4$	
-0.010	0.023	0.014	0.0027	$4.9\cdot10^{-5}$	$-1.7\cdot10^{-4}$	$-2.5\cdot10^{-5}$	

Table 7.3: Coefficients N_j for anomalous couplings for the number of events for $pp \to WZX$ via the WZ-scattering mechanism in the interval 1, multiplied with the factor 10^3. A rapidity-cut of $\eta = 1.5$ and a Higgs boson mass of $M_H = 80$ GeV were chosen.

Coefficients $N_j \cdot 10^3$ for number of events via $W\gamma$ in interval 1							
SM	$\hat{\epsilon}_W$	$\hat{\epsilon}_{W\Phi}$	$\hat{\epsilon}_{B\Phi}$				
1600	-1	55	14				
$\hat{\epsilon}_W^2$	$\hat{\epsilon}_{W\Phi}^2$	$\hat{\epsilon}_W\hat{\epsilon}_{W\Phi}$	$\hat{\epsilon}_W\hat{\epsilon}_{B\Phi}$	$\hat{\epsilon}_{W\Phi}\hat{\epsilon}_{B\Phi}$	$\hat{\epsilon}_{B\Phi}^2$		
357	23.7	2.8	2.8	34.0	16.0		
$\hat{\epsilon}_W^3$	$\hat{\epsilon}_W^2\hat{\epsilon}_{W\Phi}$	$\hat{\epsilon}_W\hat{\epsilon}_{W\Phi}^2$	$\hat{\epsilon}_{W\Phi}^3$	$\hat{\epsilon}_W^2\hat{\epsilon}_{B\Phi}$	$\hat{\epsilon}_W\hat{\epsilon}_{W\Phi}\hat{\epsilon}_{B\Phi}$	$\hat{\epsilon}_{W\Phi}^2\hat{\epsilon}_{B\Phi}$	$\hat{\epsilon}_W\hat{\epsilon}_{B\Phi}^2$
-111	20.1	14.6	0.26	1.93	11.2	0.82	0.31
$\hat{\epsilon}_{W\Phi}\hat{\epsilon}_{B\Phi}^2$	$\hat{\epsilon}_{B\Phi}^3$						
0.12	-0.095						
$\hat{\epsilon}_W^4$	$\hat{\epsilon}_W^2\hat{\epsilon}_{W\Phi}^2$	$\hat{\epsilon}_{W\Phi}^4$	$\hat{\epsilon}_W^3\hat{\epsilon}_{W\Phi}$	$\hat{\epsilon}_W\hat{\epsilon}_{W\Phi}^3$	$\hat{\epsilon}_W^3\hat{\epsilon}_{B\Phi}$	$\hat{\epsilon}_W^2\hat{\epsilon}_{W\Phi}\hat{\epsilon}_{B\Phi}$	$\hat{\epsilon}_W\hat{\epsilon}_{W\Phi}^2\hat{\epsilon}_{B\Phi}$
227	70.6	0.0064	2.6	0.13	-0.64	0.12	0.084
$\hat{\epsilon}_{W\Phi}^3\hat{\epsilon}_{B\Phi}$	$\hat{\epsilon}_W^2\hat{\epsilon}_{B\Phi}^2$	$\hat{\epsilon}_W\hat{\epsilon}_{W\Phi}\hat{\epsilon}_{B\Phi}^2$	$\hat{\epsilon}_{W\Phi}^2\hat{\epsilon}_{B\Phi}^2$	$\hat{\epsilon}_W\hat{\epsilon}_{B\Phi}^3$	$\hat{\epsilon}_{W\Phi}\hat{\epsilon}_{B\Phi}^3$	$\hat{\epsilon}_{B\Phi}^4$	
-0.0054	0.57	-0.040	0.0065	$-2.2\cdot10^{-4}$	-0.0011	$-3.3\cdot10^{-4}$	

Table 7.4: Coefficients N_j for anomalous couplings for the number of events for $pp \to WZX$ via the $W\gamma$-scattering mechanism in the interval 1, multiplied with the factor 10^3. A rapidity-cut of $\eta = 1.5$ and a Higgs boson mass of $M_H = 80$ GeV were chosen.

High-energy approximation: Coefficients $N_j \cdot 10^3$ for events via WZ in interval 1					
SM	$\hat\epsilon_W$	$\hat\epsilon_{W\Phi}$	$\hat\epsilon_{B\Phi}$		
1390	7.3	66.4	-6.7		
$\hat\epsilon_W^2$	$\hat\epsilon_{W\Phi}^2$	$\hat\epsilon_W\hat\epsilon_{W\Phi}$	$\hat\epsilon_W\hat\epsilon_{B\Phi}$	$\hat\epsilon_{W\Phi}\hat\epsilon_{B\Phi}$	$\hat\epsilon_{B\Phi}^2$
243	18.8	-4.69	-2.60	1.39	1.46
$\hat\epsilon_W^3$	$\hat\epsilon_W^2\hat\epsilon_{W\Phi}$	$\hat\epsilon_W\hat\epsilon_{W\Phi}^2$	$\hat\epsilon_{W\Phi}^3$	$\hat\epsilon_W\hat\epsilon_{W\Phi}\hat\epsilon_{B\Phi}$	
-97.9	25.7	-5.13	5.58	-5.13	
$\hat\epsilon_W^4$	$\hat\epsilon_W^2\hat\epsilon_{W\Phi}^2$	$\hat\epsilon_{W\Phi}^4$			
169.3	78.3	7.97			

Table 7.5: Coefficients N_j for anomalous couplings for the number of events for $pp \to WZX$ via the WZ-scattering mechanism in the interval 1, multiplied by the factor 10^3. The high-energy approximation has been used to calculate the vector-boson scattering cross-section. A rapidity cut of $\eta = 1.5$ and a Higgs boson mass of $M_H = 80$ GeV were chosen.

High-energy approximation: Coefficients $N_j \cdot 10^3$ for events via $W\gamma$ in interval 1					
SM	$\hat\epsilon_W$	$\hat\epsilon_{W\Phi}$	$\hat\epsilon_{B\Phi}$		
1740	5.8	52.2	20.7		
$\hat\epsilon_W^2$	$\hat\epsilon_{W\Phi}^2$	$\hat\epsilon_W\hat\epsilon_{W\Phi}$	$\hat\epsilon_W\hat\epsilon_{B\Phi}$	$\hat\epsilon_{W\Phi}\hat\epsilon_{B\Phi}$	$\hat\epsilon_{B\Phi}^2$
362	24.9	5.88	7.00	28.9	14.8
$\hat\epsilon_W^3$	$\hat\epsilon_W^2\hat\epsilon_{W\Phi}$	$\hat\epsilon_W\hat\epsilon_{W\Phi}^2$	$\hat\epsilon_W\hat\epsilon_{W\Phi}\hat\epsilon_{B\Phi}$		
-113.5	15.1	13.3	13.3		
$\hat\epsilon_W^4$	$\hat\epsilon_W^2\hat\epsilon_{W\Phi}^2$				
230.7	69.1				

Table 7.6: Coefficients N_j for anomalous couplings for the number of events for $pp \to WZX$ via the $W\gamma$-scattering mechanism in the interval 1, multiplied by the factor 10^3. The high-energy approximation has been used to calculate the vector-boson scattering cross-section. A rapidity cut of $\eta = 1.5$ and a Higgs boson mass of $M_H = 80$ GeV were chosen.

$-0.0058 < \epsilon_W < 0.0057$, 95% CL	$-0.0042 < \epsilon_W < 0.0042$, 68% CL
$-0.0031 < \epsilon_{W\Phi} < 0.0078$, 95% CL	$-0.0017 < \epsilon_{W\Phi} < 0.0050$, 68% CL
$-0.079 < \epsilon_{B\Phi} < 0.079$	

Table 7.7: Confidence intervals for ϵ_W and $\epsilon_{W\Phi}$ from the LHC analysis of $pp \to WZX$ at $\sqrt{s} = 14$ TeV assuming a luminosity of $\mathcal{L} = 10^5$ pb^{-1} and that standard model predictions are actually measured. Also shown is the unitarity bound for $\epsilon_{B\Phi}$ for invariant masses of $M_{WZ} \le 2$ TeV.

$-0.037 < \epsilon_W^0 < 0.037$
$-0.015 < \epsilon_{W\Phi}^0 < 0.072$
$-1.5 < \epsilon_{B\Phi}^0 < 1.3$

Table 7.8: Confidence intervals for the anomalous couplings at 95% CL from the LHC analysis of $pp \rightarrow W^+ZX$ at $\sqrt{s} = 14$ TeV assuming a luminosity of $\mathcal{L} = 10^5$ pb^{-1} and that standard model predictions are actually measured. A form-factor with $\Lambda_{FF} = 1$ TeV and $n = 2$ was used.

Before drawing final conclusions, we compare our results with a calculation in [27]. In this calculation, a form-factor was used. We therefore repeat our derivation of the sensitivity limits with the following changes:

- A form-factor according to Eq. (6.14) with $\Lambda_{FF} = 1$ TeV and $n = 2$ is used.

- Only the $q\bar{q}'$-processes are taken into account.

- Only W^+Z-production is taken into account.

The same choices have been made in [27]. The remaining difference to the calculation of [27] is that there the p_T-distribution of the cross-section was used, while we are using the M_{WZ}-distribution. The choice of the cuts in the two calculations is also different. The Figures 7.8, 7.9 and 7.10 show the result of our modified calculation. They show the projections and sections of the $\chi^2 = 4$ and $\chi^2 = 1$ confidence regions in the different coordinate planes. The sections with $\chi^2 = 4$ in the $\epsilon_{B\Phi}^0 = 0$- and in the $\epsilon_W^0 = 0$-plane have an inner and an outer boundary. These sections thus have the form of a disc with a hole or of a ring. Apart from this new feature, the shape of the confidence regions is similar to the one of Figures 7.5, 7.6 and 7.7. Due to the use of a form-factor, the allowed region for the anomalous couplings has become larger. We note that the sections at $\chi^2 = 1$ in Figures 7.8 and 7.9 develop from the rings for $\chi^2 = 4$ in a way that the ring disconnects on the positive $\epsilon_{W\Phi}$-axis. The result is a sickle-shaped object. This shape is similar to the bean-like shape which one sees in Figures 7.5 and 7.6.

The confidence intervals are again obtained by projecting on the coordinate axis. The 95% CL ($\chi^2 = 4$) confidence intervals are shown in Table 7.8.

To compare with the results obtained in [27], we note that the confidence intervals for the parameters $\lambda^{Z,0}$ and $\Delta g_1^{Z,0}$ of (2.27) are directly and by multiplication with the factor $1/c_W^2$, respectively, given by the intervals for ϵ_W^0 und $\epsilon_{W\Phi}^0$. The confidence interval for the parameter $\Delta\kappa^{Z,0}$ from (2.27) can be obtained by projecting the confidence region in the $\epsilon_W^0 = 0$-plane onto the $\Delta\kappa^{Z,0}$-axis. This axis is also shown in Figure 7.9. The axis is at right angle to the line $\epsilon_{B\Phi}^0 \cdot 10 = 1/(10t_W^2)\epsilon_{W\Phi}^0 \cdot 100$, on which $\Delta\kappa^0$ is equal to zero. The axes deviates only by a small angle from the $\epsilon_{B\Phi}^0$-axis, so that we see that the limits on $\Delta\kappa^{Z,0}$ are essentially determined by those of $\epsilon_{B\Phi}^0$. Approximately, the limits on $\Delta\kappa^{Z,0}$ are those of $\epsilon_{B\Phi}^0$, multiplied with the factor $-t_W^2$.

The 95% CL confidence intervals for the parameters in (2.27) are shown in Table 7.9. The limits obtained in [27] are also shown in that table. Comparing the results, we see that the limits do not significantly deviate from each other, except for the upper limit on $\Delta\kappa^{Z,0}$.

confidence interval, 95% CL	for comparison [27]:
$-0.019 < \Delta g_1^{Z,0} < 0.093$	$-0.014 < \Delta g_1^{Z,0} < 0.082$
$-0.34 < \Delta \kappa^{Z,0} < 0.47$	$-0.34 < \Delta \kappa^{Z,0} < 0.17$
$-0.037 < \lambda^{Z,0} < 0.037$	$-0.036 < \lambda^{Z,0} < 0.038$

Table 7.9: Confidence intervals for the ZWW-couplings at 95% CL from the LHC analysis of $pp \rightarrow W^+ZX$ at $\sqrt{s} = 14$ TeV assuming a luminosity of of $\mathcal{L} = 10^5$ pb^{-1} and that standard predictions are actually measured. A form-factor of $\Lambda_{FF} = 1$ TeV and $n = 2$ was used. Also shown are the results of [27].

A possible explanation for this deviation is the following. As we have seen, the effects from $\Delta \kappa^{Z,0}$ are essentially those of $\epsilon_{B\Phi}^0$. The effects of $\epsilon_{B\Phi}^0$, however, are sub-leading terms in a high-energy approximation. They do not grow strongly with the energy, in contrast to the effects of the other couplings. Thus, one expects that the effects of $\epsilon_{B\Phi}^0$, in contrast to the other couplings, can best be seen near the threshold, where the experimental relative error, $1/\sqrt{N_j}$, N_j being the number of events in a particular interval, is small. In contrast to [27], we did not include this kinematical region in our analysis. Thus, our analysis can only give a less stringent bound on the parameter $\Delta \kappa^{Z,0}$ [1].

We conclude that one obtains only slightly different bounds on the couplings if either the M_{WZ}-distribution or the p_T-distribution is used. On the whole, the results we obtained have been confirmed by the comparison with [27].

Concluding this section, an LHC analysis of $pp \rightarrow WZX$ will allow to shrink the current experimental limits by a factor of more than 100 for ϵ_W and $\epsilon_{W\Phi}$, while the sensitivity to $\epsilon_{B\Phi}$ can not be improved beyond its unitarity bound. Further, anomalous couplings of an order of magnitude $\mathcal{O}(10^{-3}) \leq \epsilon_i \leq \mathcal{O}(10^{-2})$, which one derives from a dimensional analysis in the framework of an effective field theory, enter the domain of observability at the LHC.

---

[1] It has been recently noticed [29] that a more stringent bound on $\Delta \kappa^{\gamma,0}$ and $\Delta \kappa^{Z,0}$ can be obtained from a measurement of the cross-section for $pp \rightarrow W^+W^-X$ at the LHC. This is possible if a suitable cut or a jet veto is imposed in order to reduce the background from top quark pair production. In the process $q\bar{q} \rightarrow W^+W^-$, the effects of $\Delta \kappa^{V,0}$ are enhanced by a factor of $\hat{s}/M_W^2$, where $\hat{s}$ is the $q\bar{q}$ scattering-energy. This is in contrast to the corresponding production processes for WZ considered here or for $W\gamma$ pairs where such an enhancement is not present.

Projection of χ^2–surface and section at $\varepsilon_{B\varphi} = 0$.
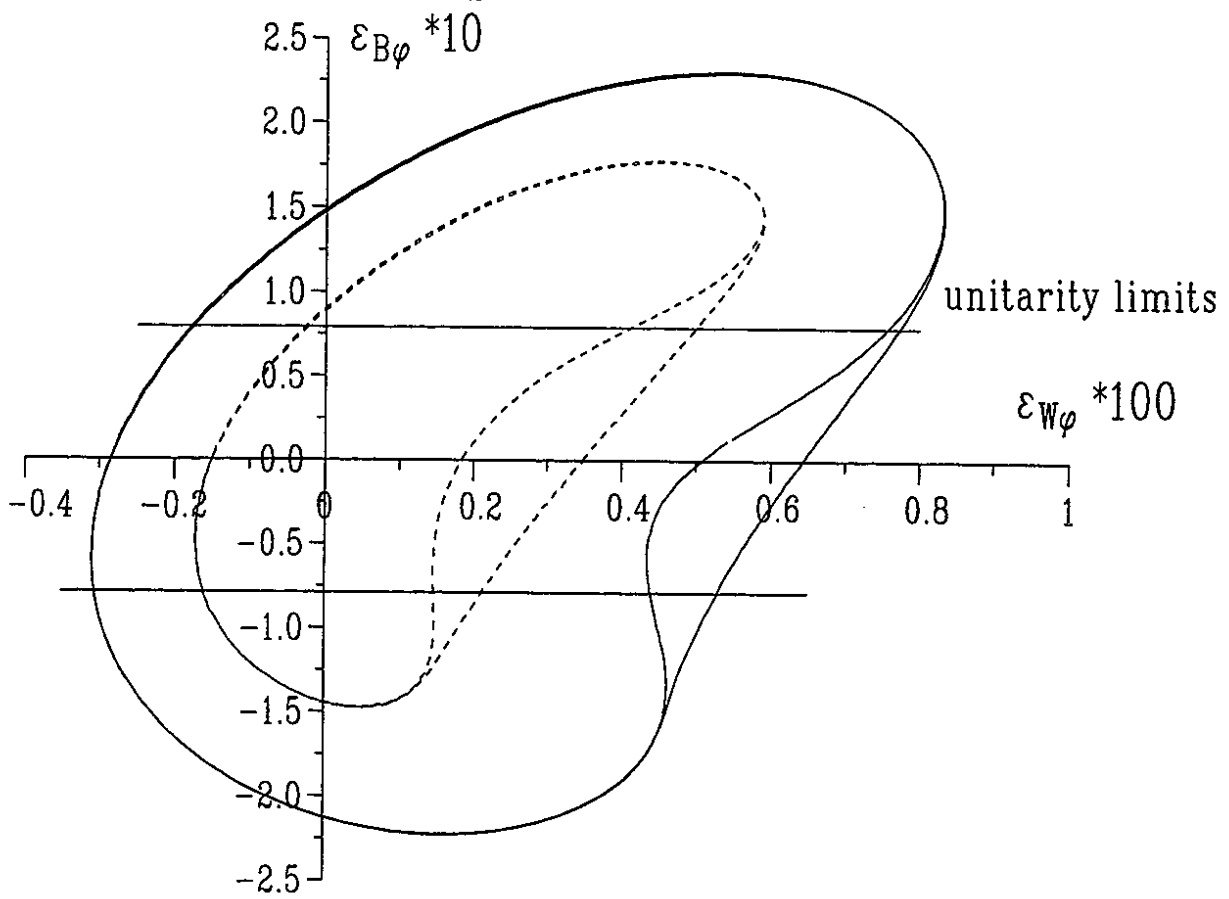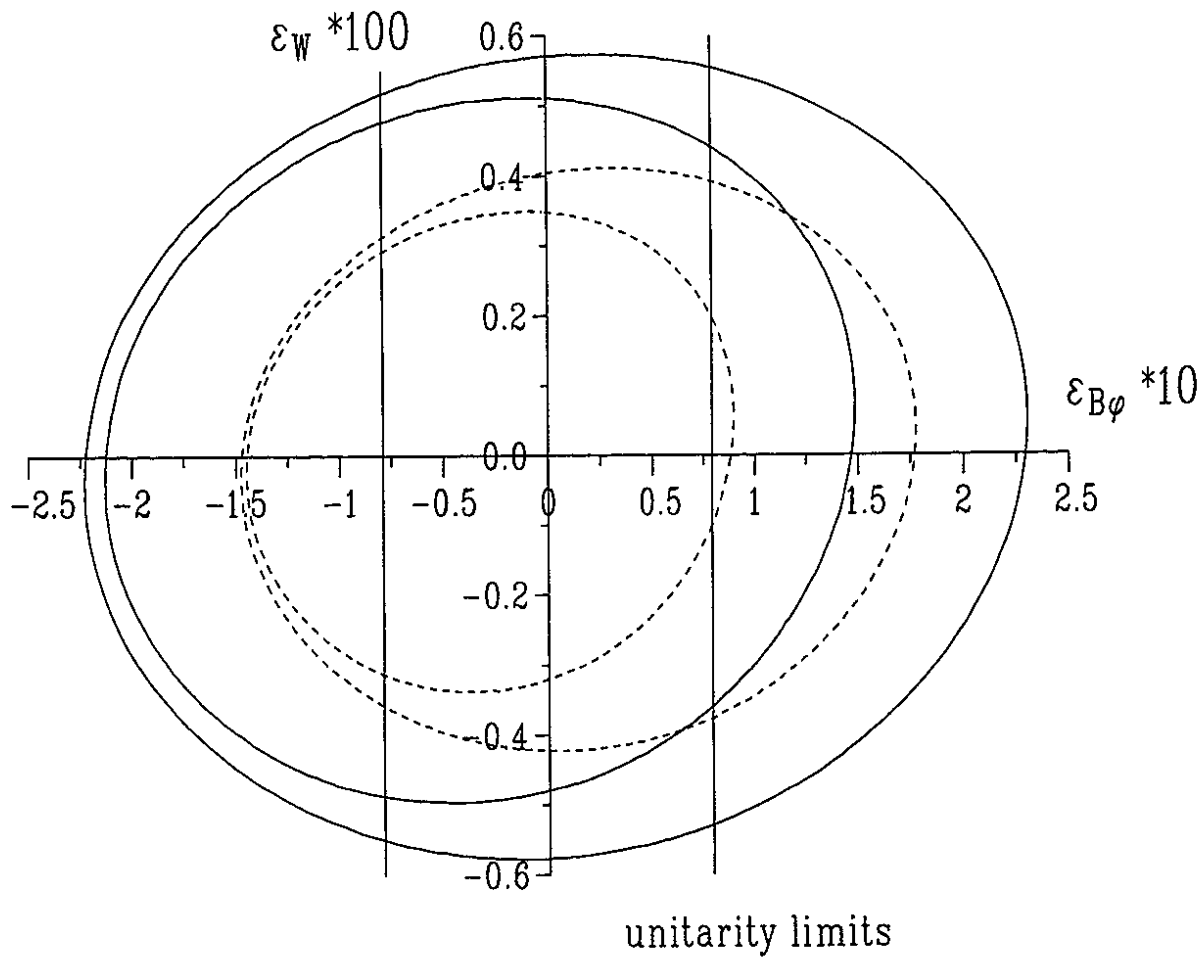3–parameter model for $q\bar{q}'$ and WV processes
$M_H = 80$ GeV
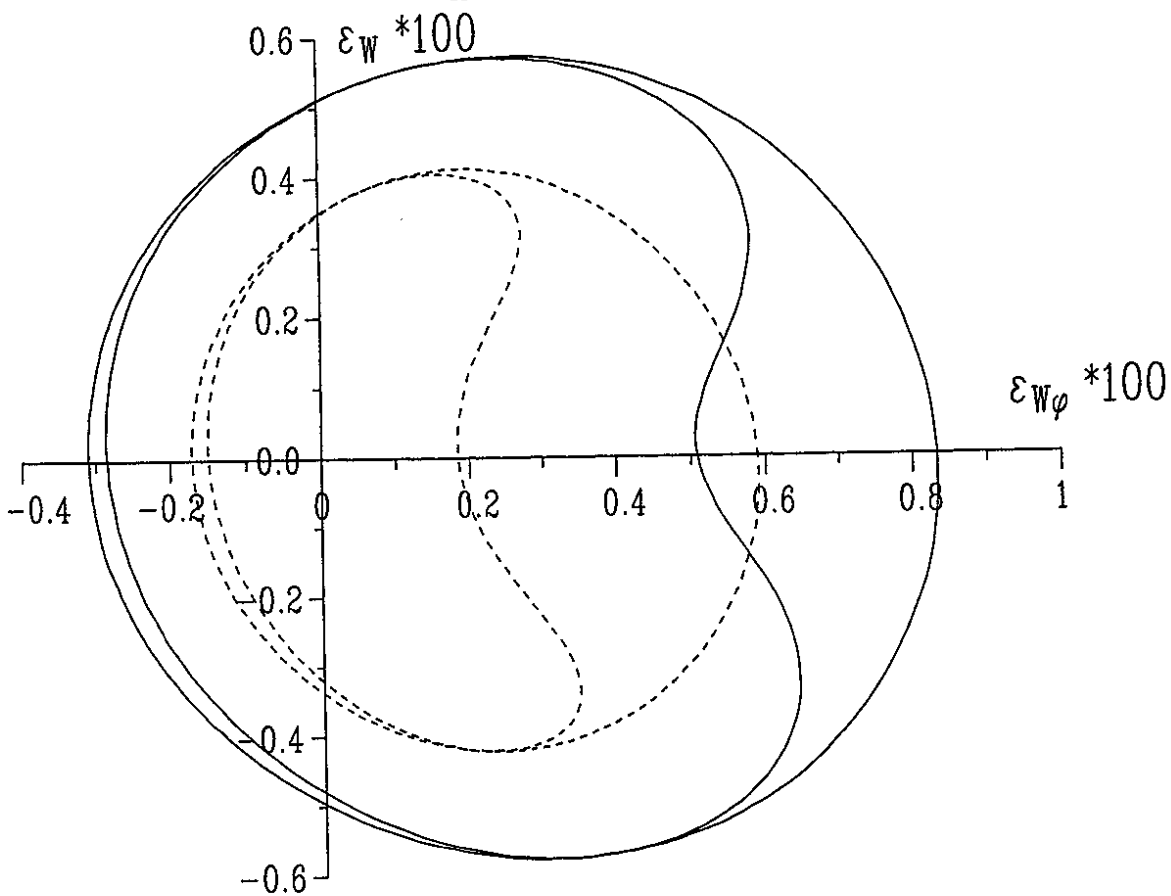
$$\frac{\chi^2 = 4}{\chi^2 = 1}$$

Figure 7.5: The projection of the $\chi^2 = 4$ and $\chi^2 = 1$ confidence regions on the plane $\epsilon_{B\Phi} = 0$ and the section of the regions with this plane.

Figure 7.6: The projection of the $\chi^2 = 4$ and $\chi^2 = 1$ confidence regions on the plane $\epsilon_W = 0$ and the sections of the regions with this plane.
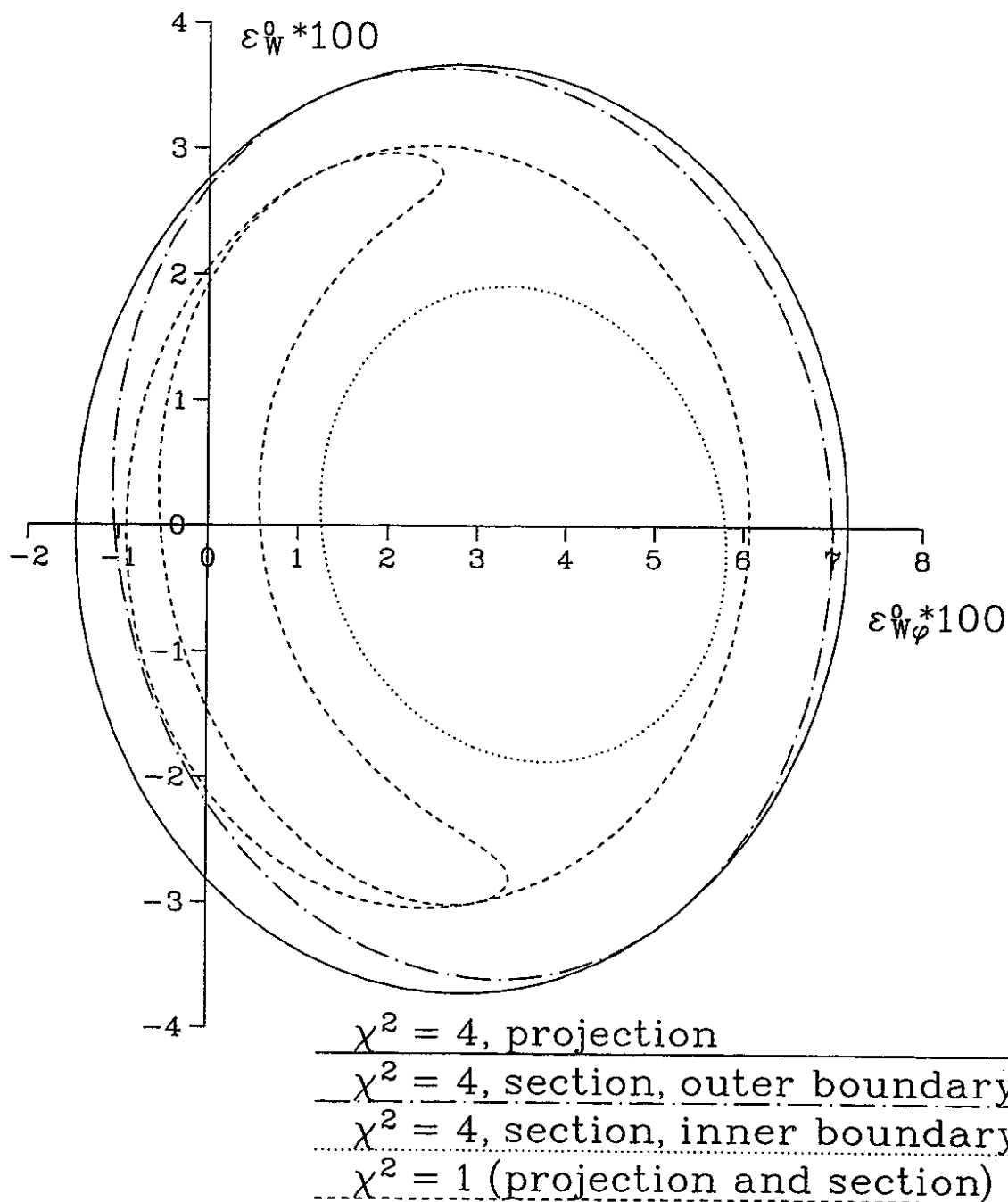
Figure 7.7: The projection of the $\chi^2 = 4$ and $\chi^2 = 1$ confidence regions on the plane $\epsilon_{W\Phi} = 0$ and the sections of the regions with this plane.

Figure 7.8: The projection of the $\chi^2 = 4$ and $\chi^2 = 1$ confidence regions on the plane $\epsilon^0_{B\Phi} = 0$ and the sections of the regions with this plane. As in [27], a form-factor was used.
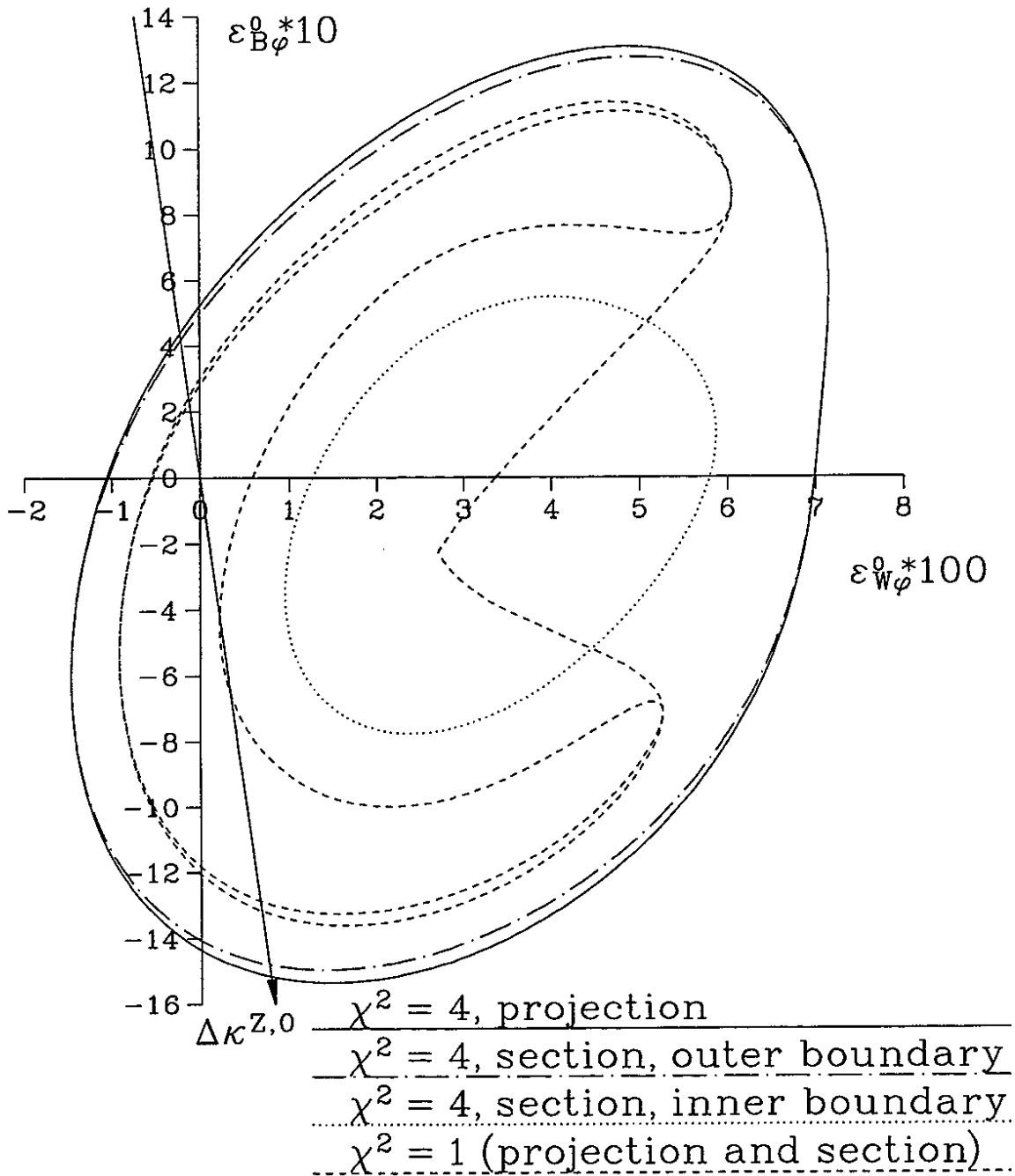
Figure 7.9: The projection of the $\chi^2 = 4$ and $\chi^2 = 1$ confidence regions on the plane $\epsilon_W^0 = 0$ and the sections of the regions with this plane. As in [27], a form-factor was used.
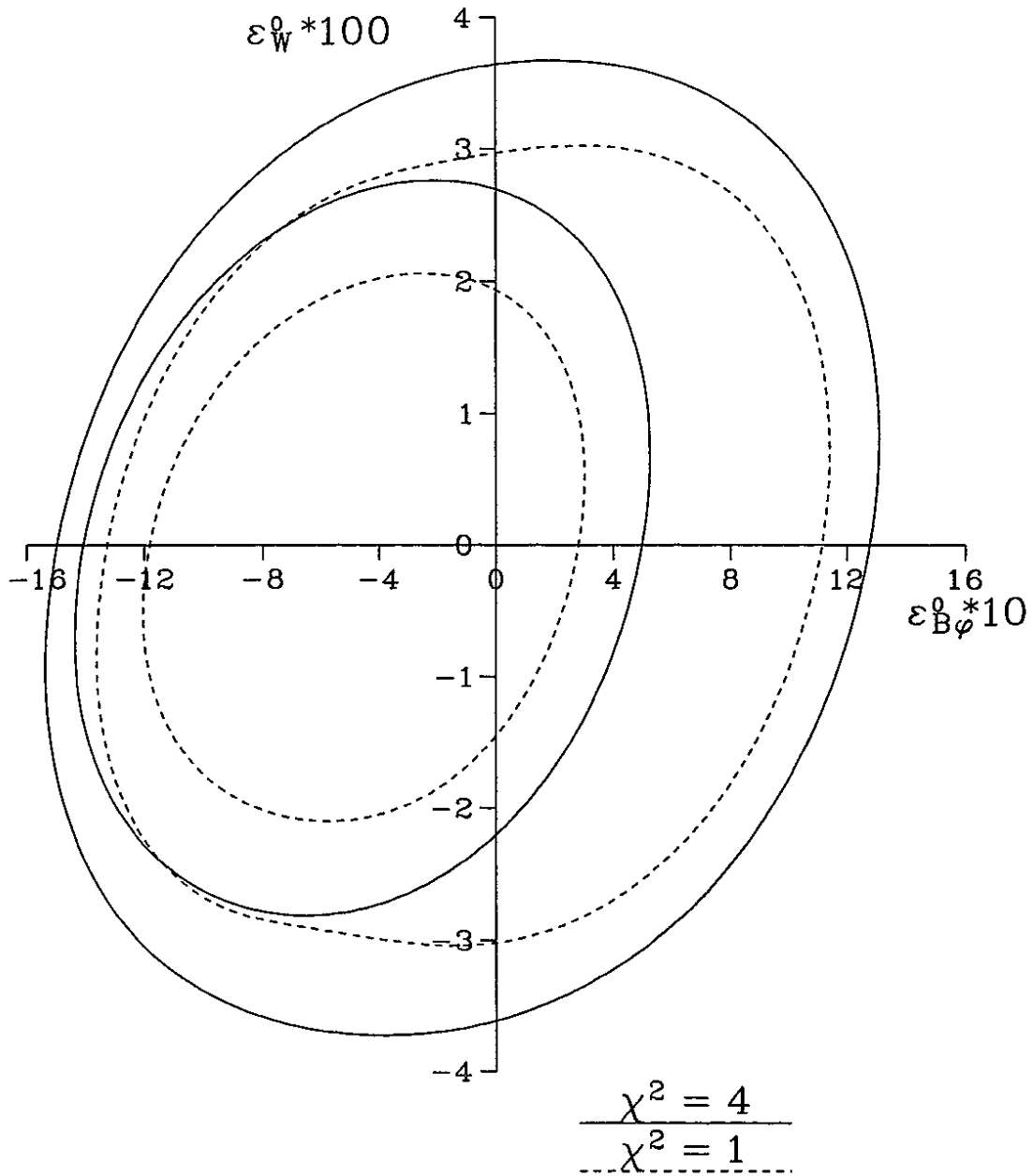
Figure 7.10: The projection of the $\chi^2 = 4$ and $\chi^2 = 1$ confidence regions on the plane $\epsilon^0_{W\Phi} = 0$ and the sections of the regions with this plane. As in [27], a form-factor was used.

7.5   Discussion of Errors

The calculated cross-sections and, as a consequence, to a smaller extent also the derived confidence intervals are subject to various theoretical errors, which will be briefly discussed in the following.

We first investigate the uncertainty due to the in principle unknown scale Q^2 of the parton-distributions. Figure 7.11 shows ratios of cross-sections for $pp \to ZZX$ proceeding via W^+W^--scattering as a function of M_{ZZ}. The quark-distributions of EHLQ [17] have been used. Three different curves are shown. The cross-section in the denominator always has $Q^2 = s_{qq}$. The cross-sections in the numerator have $Q^2 = s_{qq}/4$, $Q^2 = 4s_{qq}$ and $Q^2 = M_{WZ}^2$, respectively. In the high-energy region, $M_{ZZ} > 0.5$ TeV, the deviations of the ratios from the value one is less than 5% for all curves. Figure 7.12 shows ratios of cross-sections for $pp \to q\bar{q}' \to WZ$ as a function of M_{WZ}. The quark-distributions MRS(A) [82] were used. The cross-section in the denominator always has $Q^2 = s_{qq}$. In the numerator, $Q^2 = s_{qq}/4$ and $Q^2 = 4s_{qq}$ has been chosen for the two curves. The cross-section changes by less than 8%, if Q^2 is varied between $Q^2 = s_{qq}/4$ and $Q^2 = 4s_{qq}$. The maximum allowed value for Q^2 for the MRS(A) distributions is $Q^2 = 1.31$ TeV^2. If Q^2 becomes greater than this value, the maximum value was used, which leads to the discontinuities in the slope of the ratios. In summary, the uncertainty due to the choice of Q^2 induced to the cross section for $pp \to WZX$ is smaller than 5% for $M_{WZ} > 0.5$ TeV at $\sqrt{s} = 14$ TeV.

The use of different parametrizations of quark-distributions in the proton also leads to differing numerical results for the cross-sections. I have examined a number of available parton distribution functions differing in experimental input data and theoretical assumptions. These assumptions concern for example the choice of the renormalization scheme. Among the distributions I have examined were those of [82, 85, 90, 91], distributions of the package [93] and others. I find that the luminosities for finding a $q\bar{q}'$-pair in a proton pair vary by less than $\pm 25\%$ about a mean value at $\sqrt{s_{pp}} = 14$ TeV. This applies to the region 0.5 TeV $< \sqrt{s_{qq}} < 2.5$ TeV and all quark types. The same error will be induced to the cross-sections $pp \to V_3V_4X$. The uncertainty due to the parton distribution functions will improve with future measurements of structure functions at HERA.

The error due to the neglect of quark flavor-mixing is smaller than 1%.

As already mentioned in Chapter 3, $\mathcal{O}(\alpha_s)$ radiative corrections are to be added to the cross-sections. These corrections can amount to up to 70% of the Born cross-section [27]. As another consequence, the confidence intervals grow wider, as was also discussed in [27]. The interval limits grow by 30% or less in magnitude.

Higher order electroweak corrections have not yet been examined and might also give a non-negligible contribution.

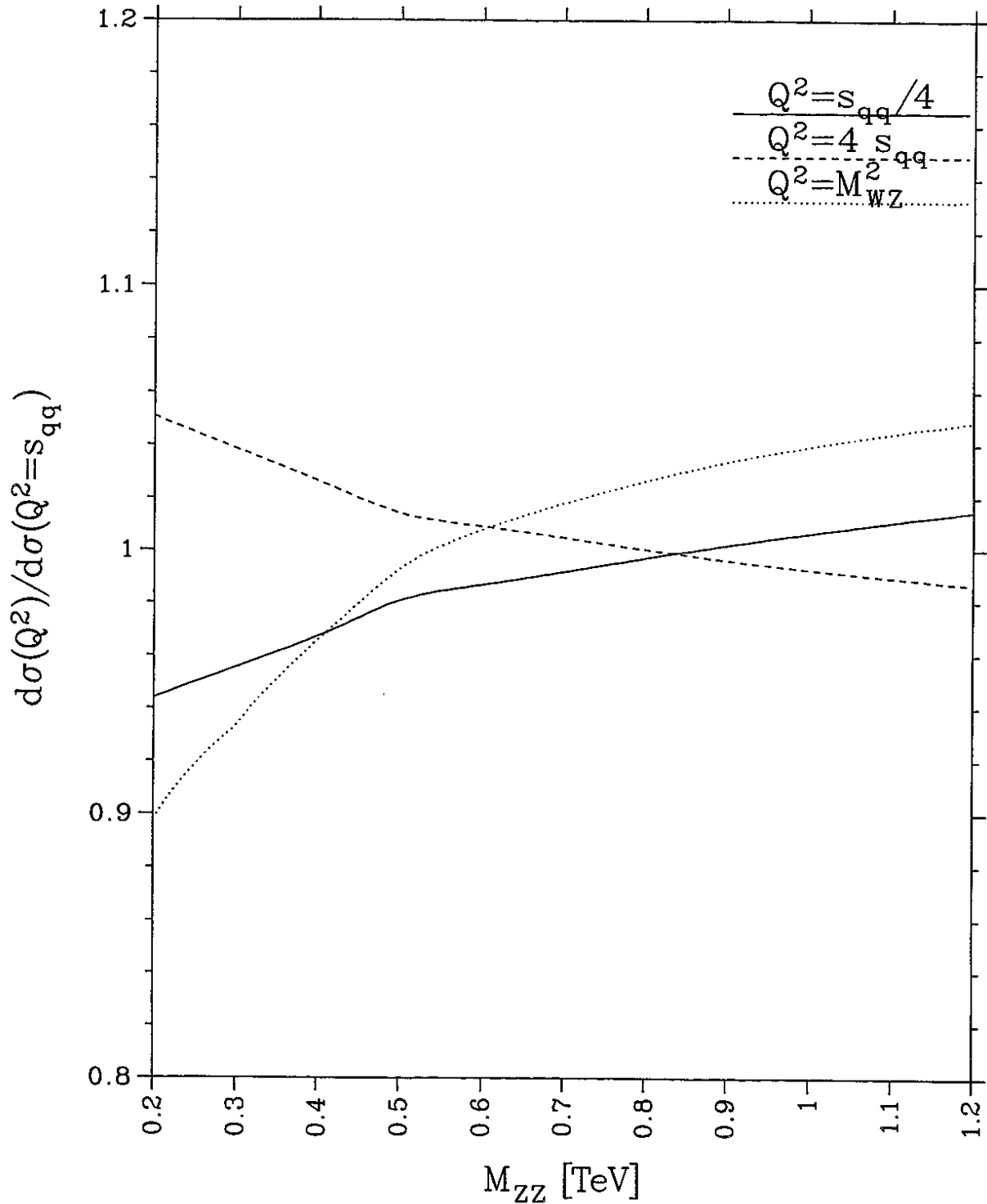Further, there are also other processes, in particular three- or four boson-production, which have not been considered here.

Figure 7.11: Ratios of cross-sections for $d\sigma(pp \to ZZX)$ via W^+W^--scattering with different values for Q^2 in the quark-distributions as a function of M_{ZZ}. A scattering energy of $\sqrt{s_{pp}} = 40$ TeV and a rapidity-cut of $Y = 1.5$ was chosen.
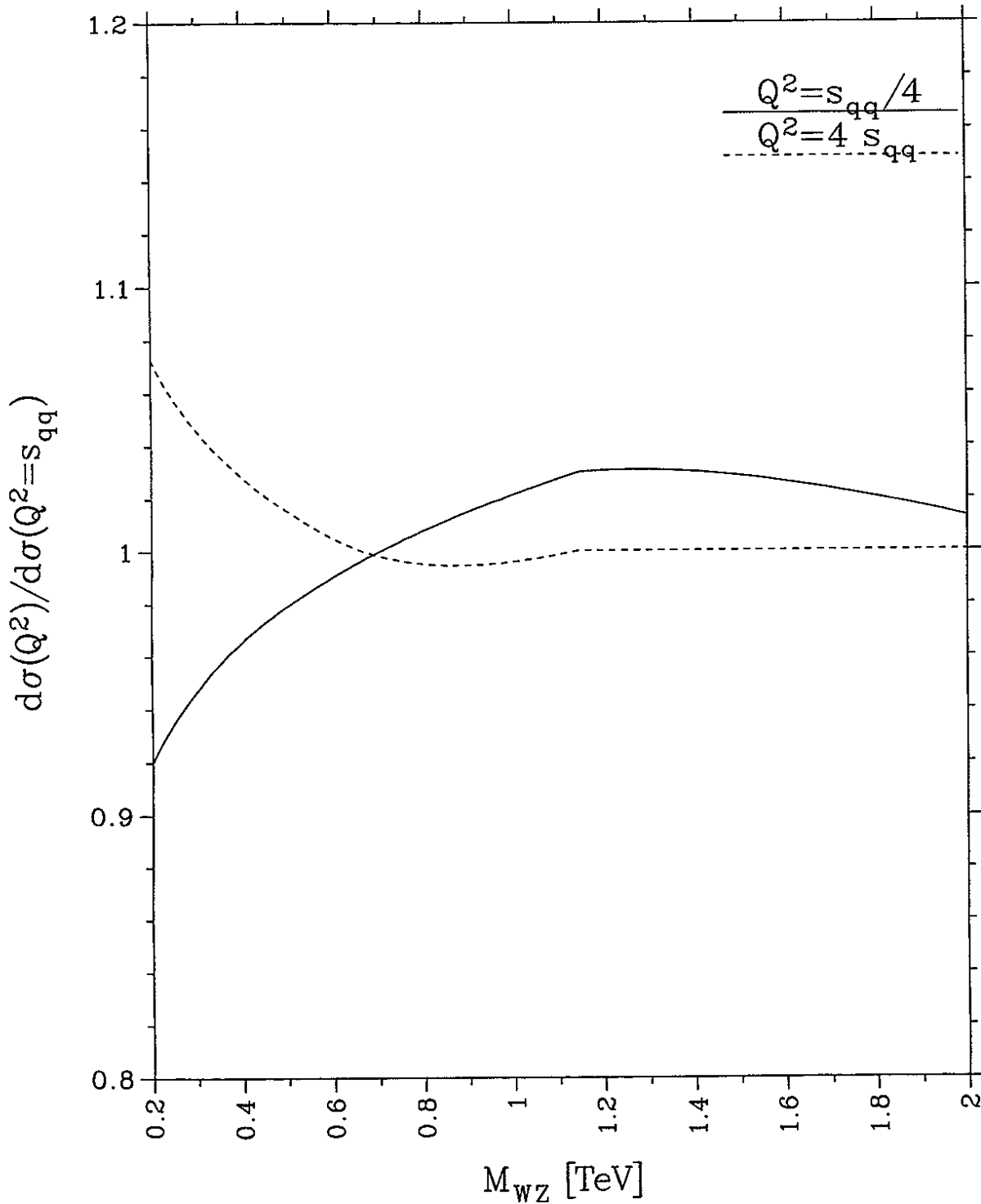
Figure 7.12: The ratio of differential cross-sections $d\sigma/dM_{WZ}$ for $pp \rightarrow q\bar{q}' \rightarrow WZ$ for various values of Q^2 as a function of the invariant mass M_{WZ}. In all cases, $Q^2 = s_{qq}$ has been chosen in the denominator.

Chapter 8

Conclusion

The observability of anomalous vector-boson self-couplings in high-energy proton-proton collisions has been examined.

A model with anomalous couplings was confronted to fictitious standard-model data for the process $pp \rightarrow WZ + X$ at a scattering-energy of $\sqrt{s_{pp}} = 14$ TeV and an integrated luminosity of $\mathcal{L} = 10^5$ pb^{-1}, corresponding to one year of running of the planned LHC machine. As a result of the analysis, the following 1σ- and 2σ-confidence intervals have been derived

-0.0058< ϵ_W <0.0057 , 95% CL	-0.0042< ϵ_W <0.0042 , 68% CL
-0.0031< $\epsilon_{W\Phi}$ <0.0078 , 95% CL	-0.0017< $\epsilon_{W\Phi}$ <0.0050 , 68% CL.

These bounds are smaller by a factor of more than 100 than the present direct experimental bounds on ϵ_W and $\epsilon_{W\Phi}$. The parameter $\epsilon_{B\Phi}$, in contrast, cannot be further constrained below its unitarity limits. Anomalous couplings of the order of magnitude $\epsilon_i \leq \mathcal{O}(10^{-2})$, which one derives from a dimensional analysis in the framework of an effective field theory, will enter the domain of observability at the LHC.

Of the different parton-subprocesses contributing to the cross-section for $pp \rightarrow WZ + X$, we included here the processes of quark-antiquark annihilation, $q\bar{q}' \rightarrow WZ$, and of $q_1 q_2 \rightarrow q_1' q_2' WZ$, where q_i, q_i' are quarks or antiquarks. The latter processes contain the vector-boson scattering processes, $WZ \rightarrow WZ$ and $W\gamma \rightarrow WZ$, as sub-processes. Previous derivations of observability limits did only include the contribution from $q\bar{q}' \rightarrow WZ$. It was known, however, that the cross-sections for the vector-boson scattering processes are significantly affected by the presence of anomalous couplings. We calculated the contribution from the processes $q_1 q_2 \rightarrow q_1' q_2' WZ$ within an effective vector-boson approximation (EVBA). This approximation is similar to the Weizsäcker-Williams approximation of photon-photon processes. In this approximation only the dominant diagrams containing vector-boson scattering are calculated while bremsstrahlung diagrams are neglected. The method of the EVBA is much easier to handle and physically more transparent than a complete perturbative calculation including all diagrams. We have presented an improved formulation of the effective vector-boson approximation applying to the generic processes of vector-boson scattering. Previous formulations of the EVBA were only applicable to processes in which longitudinally polarized intermediate vector-bosons play a dominant role. Using the improved formulation of the EVBA we have found that the contribution from the processes $q_1 q_2 \rightarrow q_1' q_2' WZ$ to the cross-section for $pp \rightarrow WZ + X$ amounts to 15% of the contribution from the $q\bar{q}' \rightarrow WZ$ processes. This result has been obtained in the standard model, using a rapidity cut of $Y = 2.5$ on the produced vector-bosons and

163

restricting to invariant masses of $M_{WZ} > 0.5$ TeV. In contrast, it was found in previous works in which existing formulations of the EVBA were used that the ratio of these contributions would be greater than 50%. Our result of 15%, however, is close to the result of a complete perturbative calculation, which includes the bremsstrahlung diagrams, in which the ratio was found to be 17%.

We have given an analytical expression for the cross-section for $q\bar{q}' \rightarrow WZ$ including the dependence on anomalous couplings. For the cross-sections for $WZ \rightarrow WZ$ and $W\gamma \rightarrow WZ$ we have given numerical results in the standard model and for anomalous couplings. We have further given approximate analytical forms for the cross-sections for all these processes including the effects of anomalous couplings. These forms are applicable if the scattering energy is large compared to the vector-boson masses. The validity of these approximations has been examined.

Concerning the sensitivity of the different subprocesses to anomalous couplings, we have found, in contrast to a naive expectation, that the anomalous couplings do not manifest themselves particularly strongly through the vector-boson scattering sub-processes. In fact, the $q\bar{q}'$-annihilation rate is affected more strongly by the presence of these couplings.

As far as the dependence of the cross-section for $pp \rightarrow WZ + X$ on the mass of the Higgs boson is concerned, we have evidenced that this cross-section is essentially unaffected if the mass of the Higgs boson is varied between $M_H = 100$ GeV and $M_H = 1$ TeV. This result is in contrast to the results for certain other processes $pp \rightarrow V_3 V_4 + X$, where $V_3 V_4$ is a different vector-boson pair.

Concerning our improved treatment of the effective vector-boson approximation, the approximations leading to this formulation have been discussed in detail and the improved formulation has been compared to existing ones. In the existing formulations, the cross-sections were described in terms of convolutions of vector-boson distribution-functions. In the improved formulation, expressions for vector-boson luminosities have to be used instead. Approximately, however, the vector-boson luminosities of the improved formulation can again be expressed as convolutions of vector-boson distribution-functions. The approximations which must be made on the improved formulation in order to obtain the formalism of convolutions result in an error of 10% to 20% in the cross-sections for $pp \rightarrow WZ + X$, depending on the invariant mass of the WZ-pair. We have thus extended the physically apparent formalism of vector-boson distribution-functions to the processes of vector-boson scattering. The distribution-functions derived in the approximation to the improved formulation are different from the distribution-functions derived in the existing formulations. We have compared the two versions of distribution-functions and discussed the observed failure of the existing version of the EVBA for the process $pp \rightarrow WZ + X$ in terms of the differences of the distribution-functions. Further, we have seen that the new feature, which plays a role in the vector-boson scattering processes but did not appear in previous applications of the EVBA (as far as these led to correct results), lies in the relative importance of the distribution-functions for transversely and longitudinally polarized intermediate vector-bosons. We have found that the transverse distribution-functions differ considerably in the existing formulations and in the improved formulation.

The improved EVBA has been further compared with results of complete perturbative calculations including bremsstrahlung diagrams. We have presented comparisons for the process $pp \rightarrow ZZ + X$. It was found that the two calculations deviate by only 10% if a rapidity-cut on the produced vector-bosons of $Y \leq 1.5$ is chosen.

As to the tasks which have not been attempted here we did not calculate γ, Z-interference terms. These terms are small but might not be completely negligible. They could be calculated with a straightforward extension of our formalism. Further, a more refined treatment of kinematical cuts could give a better simulation of an actual experimental situation. We also note that our prediction for the cross-section for $pp \rightarrow WZ + X$ could be improved by including radiative corrections and further processes on the quark-level. It is clear, however, that most of the mentioned improvements would result in a considerable complication of calculational techniques.

One advantage of this work is that fairly involved quantities have been calculated with a good degree of accuracy with easy-to-handle approximative formulae, which have been derived from complete expressions and passed the tests of comparison with complete calculations. These approximations (high-energy forms for cross-sections, vector-boson-distributions in hadrons, approximative treatment of cuts) can be used to quickly obtain reliable numerical estimates. Another useful result of this work is that it provides a careful examination of several calculations presented previously in the literature.

Appendix A

Expressions for Fivefold-Differential Luminosities for Vector-Boson Pairs

We derive expressions, in terms of which the five-fold differential luminosities, K_{pol}, Eq. (4.38), can be determined. These have been defined in terms of the helicity-tensors $C_j(m, m')$ and $S_j(m, m')$, defined in Eqs. (4.29) and (4.30). The helicity-tensors have been written in terms of the four-momenta l_j, l'_j of the fermions and the polarization-vectors $\epsilon_j(m)$ of the vector-bosons. We evaluate the four-momenta and polarization-vectors in the Breit systems of the vector-bosons, to be defined in the following.

A.1 Definition of Reference Frames

The four-momenta of the vector-boson V_j in their center-of-mass system, C, are given by

$$\left(k_1^C\right)^\mu = (k_0; 0, 0, K), \qquad \left(k_2^C\right)^\mu = (q_0; 0, 0, -K), \tag{A.1}$$

with $k_0 \equiv (\mathcal{W}^2 + k_1^2 - k_2^2)/2\mathcal{W}$ and $q_0 \equiv (\mathcal{W}^2 - k_1^2 + k_2^2)/2\mathcal{W}$. K has been defined in (4.53). For simplicity, we assume that the final state W produced via the two-boson process allows to specify the x- and y-axes of a coordinate system. If the state W decays into n particles with momenta w_i, we choose this system such that the y-component of one specific four-momentum, say w_s, of the set of the w_i vanishes and its x-component is non-negative.

We define two Breit systems, a system B_1 in which k_1 has only a non-vanishing z-component and $\vec{l}_2$ points in the negative z-direction, and a system B_2 in which k_2 has only a non-zero z-component and $\vec{k}_1$ points in the negative z-direction. The four-momenta in B_1 are

$$
\begin{aligned}
\left(l_1^{B_1}\right)^\mu &= \frac{\sqrt{-k_1^2}}{2}(c_h; -s_h \cos\varphi_1, -s_h \sin\varphi_1, 1), \\
\left(l_1'^{B_1}\right)^\mu &= \frac{\sqrt{-k_1^2}}{2}(c_h; -s_h \cos\varphi_1, -s_h \sin\varphi_1, -1), \\
\left(k_1^{B_1}\right)^\mu &= (0; 0, 0, \sqrt{-k_1^2}), \\
\left(l_2^{B_1}\right)^\mu &= \frac{\mu_X}{2\sqrt{-k_1^2}}(1; 0, 0, -1),
\end{aligned}
$$

166

$$p'^{\mu} \equiv p_W^{\mu} + l_2'^{\mu} = \frac{1}{2\sqrt{-k_1^2}}(\mu_X; 0, 0, -M_X^2 - k_1^2), \tag{A.2}$$

with

$$
\begin{aligned}
c_h &\equiv \frac{2s}{\mu_X} - 1, \\
s_h &\equiv \sqrt{c_h^2 - 1} = 2\frac{\sqrt{s}}{\mu_X}\sqrt{s - \mu_X},
\end{aligned} \tag{A.3}
$$

and μ_X as in (4.52). The overall azimuth of the system is defined by choosing the y-component of $k_2^{B_1}$ to be zero and its x-component non-negative, so that

$$\left(k_2^{B_1}\right)^{\mu} = \left(q_0'; \frac{\sqrt{-k_2^2}\beta}{\mu_X}, 0, -\frac{\nu}{\sqrt{-k_1^2}}\right), \tag{A.4}$$

with

$$
\begin{aligned}
q_0' &\equiv \frac{1}{\sqrt{-k_1^2}}\left(\nu - \frac{k_1^2 k_2^2}{\mu_X}\right), \\
\beta &\equiv \sqrt{\mu_X^2 - 2\nu\mu_X + k_1^2 k_2^2},
\end{aligned} \tag{A.5}
$$

and ν is defined as in (4.53).

The four-momenta in B_2 are given by

$$
\begin{aligned}
\left(l_2^{B_2}\right)^{\mu} &= \frac{\sqrt{-k_2^2}}{2}(c_h'; -s_h' \cos\varphi_2, -s_h' \sin\varphi_2, 1), \\
\left(l_2'^{B_2}\right)^{\mu} &= \frac{\sqrt{-k_2^2}}{2}(c_h'; -s_h' \cos\varphi_2, -s_h' \sin\varphi_2, -1), \\
\left(k_2^{B_2}\right)^{\mu} &= \left(0; 0, 0, \sqrt{-k_2^2}\right), \\
\left(k_1^{B_2}\right)^{\mu} &= \frac{1}{2\sqrt{-k_2^2}}(\kappa; 0, 0, -2\nu), \\
\left(p_W^{B_2}\right)^{\mu} &= \frac{1}{2\sqrt{-k_2^2}}(\kappa; 0, 0, -2\mathcal{W}\,q_0),
\end{aligned} \tag{A.6}
$$

with

$$
\begin{aligned}
c_h' &\equiv \frac{2}{\kappa}(\mu_X - \nu), \\
s_h' &\equiv \sqrt{(c_h')^2 - 1} = \frac{2\beta}{\kappa},
\end{aligned} \tag{A.7}
$$

and κ has been defined in (4.54). The overall azimuth of the system B_2 is defined by choosing the y-component of the same four-momentum w_s as employed in defining the system C equal to zero and its x-component non-negative.

A.2 Expressions for Polarization Vectors

The polarization vectors for the helicity eigenstates of the vector bosons V_j in the system C using the Jacob and Wick [94] phase conventions are given by

$$
\begin{aligned}
\left(\epsilon_1^C\right)^\mu(\pm) &= \frac{1}{\sqrt{2}}(0; \mp 1, -i, 0), \\
\left(\epsilon_1^C\right)^\mu(0) &= \frac{1}{\sqrt{-k_1^2}}(K; 0, 0, k_0), \\
\left(\epsilon_2^C\right)^\mu(\pm) &= \frac{1}{\sqrt{2}}(0; \pm 1, -i, 0), \\
\left(\epsilon_2^C\right)^\mu(0) &= \frac{1}{\sqrt{-k_2^2}}(-K; 0, 0, q_0).
\end{aligned}
\tag{A.8}
$$

By applying an appropriate coordinate transformation, the polarization vectors for V_1 in the system B_1 are found to be

$$
\begin{aligned}
\left(\epsilon_1^{B_1}\right)^\mu(\pm) &= \frac{1}{\sqrt{2}}e^{\mp i\varphi_2}\left(\mp\tilde{\sigma}; \mp\frac{\sqrt{-k_1^2}q_0'}{K\mathcal{W}}, -i, 0\right), \\
\left(\epsilon_1^{B_1}\right)^\mu(0) &= \frac{\sqrt{-k_1^2}}{K\mathcal{W}}\left(q_0'; \frac{\sqrt{-k_2^2}\beta}{\mu_X}, 0, 0\right),
\end{aligned}
\tag{A.9}
$$

with $\tilde{\sigma} = \sqrt{k_1^2 k_2^2}\beta/(\mu_X K\mathcal{W})$. Likewise, the polarization vectors for V_2 in B_2 are found to be

$$
\begin{aligned}
\left(\epsilon_2^{B_2}\right)^\mu(\pm) &= \frac{1}{\sqrt{2}}(0; \pm 1, i, 0), \\
\left(\epsilon_2^{B_2}\right)^\mu(0) &= (-1; 0, 0, 0).
\end{aligned}
\tag{A.10}
$$

A.3 Expressions for Helicity-Tensors

The epxressions for the helicity-tensors $\mathcal{C}_j(m, m')$ and $\mathcal{S}_j(m, m')$, given in Eqs. (4.29) and (4.30), can now be found by using the expressions (A.2) and (A.6) for the four-momenta and the expressions (A.9) and (A.10) for the polarization-vectors. The results are:

$$
\begin{aligned}
\mathcal{C}_1(++) &= -\frac{k_1^2}{4}\left[c_h^2 + 1 + \frac{4k_1^2 k_2^2\,\beta^2}{\mu_X^2\kappa^2}(c_h^2 + s_h^2\cos^2\varphi_1) \right. \\
&\quad \left. + \frac{8\,c_h\,s_h\sqrt{-k_1^2}\sqrt{-k_2^2}\,\beta}{\mu_X^2\kappa^2}(\nu\mu_X - k_1^2 k_2^2)\cos\varphi_1\right], \\
\mathcal{C}_1(00) &= -\frac{k_1^2}{2}\left[s_h^2 + \frac{4k_1^2 k_2^2\,\beta^2}{\mu_X^2\kappa^2}(c_h^2 + s_h^2\cos^2\varphi_1) \right. \\
&\quad \left. - \frac{8\,c_h\,s_h\sqrt{-k_1^2}\sqrt{-k_2^2}\,\beta}{\mu_X^2\kappa^2}(\nu\mu_X - k_1^2 k_2^2)\cos\varphi_1\right], \\
\mathcal{C}_1(+-) &= \frac{k_1^2}{2}\left[\frac{2k_1^2 k_2^2\,\beta^2}{\mu_X^2\kappa^2}(c_h^2 + s_h^2\cos^2\varphi_1) + s_h^2\left(\cos^2\varphi_1 - \frac{1}{2}\right)\right.
\end{aligned}
$$

$$+\frac{4\,c_h\,s_h\sqrt{-k_1^2}\sqrt{-k_2^2}\,\beta}{\mu_X^2\kappa^2}(\nu\mu_X-k_1^2k_2^2)\cos\varphi_1$$

$$-2\,i\frac{s_h}{\mu_X\kappa}(c_h\sqrt{-k_1^2}\sqrt{-k_2^2}\,\beta+s_h\,(\nu\mu_X-k_1^2k_2^2)\cos\varphi_1)\sin\varphi_1\Bigg],$$

$$\mathcal{C}_1(+0)\;=\;\frac{k_1^2}{\sqrt{2}}\Bigg[\frac{2\sqrt{-k_1^2}\sqrt{-k_2^2}\,\beta}{\mu_X^2\kappa^2}(\nu\mu_X-k_1^2k_2^2)(c_h^2+s_h^2\cos^2\varphi_1)$$

$$+\frac{2\,c_h\,s_h}{\mu_X^2\kappa^2}((\nu\mu_X-k_1^2k_2^2)^2+k_1^2k_2^2\,\beta^2)\cos\varphi_1$$

$$-i\frac{s_h}{\mu_X\kappa}(c_h(\nu\mu_X-k_1^2k_2^2)+s_h\,\sqrt{-k_1^2}\sqrt{-k_2^2}\,\beta\cos\varphi_1)\sin\varphi_1\Bigg],$$

$$\mathcal{S}_1(++)\;=\;-\frac{k_1^2}{2}\Bigg[2\,\frac{\nu\mu_X-k_1^2k_2^2}{\mu_X\kappa}\,c_h+2\,\frac{s_h\,\sqrt{-k_1^2}\sqrt{-k_2^2}\,\beta}{\mu_X\kappa}\cos\varphi_1\Bigg],$$

$$\mathcal{S}_1(+0)\;=\;\frac{k_1^2}{\sqrt{2}}\Bigg[\frac{c_h\,\sqrt{-k_1^2}\sqrt{k_2^2}\,\beta}{\mu_X\kappa}+\frac{s_h}{\mu_x\kappa}(\nu\mu_X-k_1^2k_2^2)\cos\varphi_1-i\frac{s_h}{2}\sin\varphi_1\Bigg]\;;\;\text{(A.11)}$$

$$\mathcal{C}_2(++)\;=\;-\frac{k_2^2}{4}\left((c_h')^2+1\right),$$

$$\mathcal{C}_2(00)\;=\;-\frac{k_2^2}{2}(s_h')^2,$$

$$\mathcal{C}_2(+-)\;=\;\frac{k_2^2}{4}(s_h')^2,$$

$$\mathcal{C}_2(+0)\;=\;\frac{k_2^2}{2\sqrt{2}}\,c_h'\,s_h',$$

$$\mathcal{S}_2(++)\;=\;-\frac{k_2^2}{2}c_h',$$

$$\mathcal{S}_2(+0)\;=\;\frac{k_2^2}{2\sqrt{2}}s_h'.\qquad\qquad\text{(A.12)}$$

Appendix B

High-Energy Formulae for
$WZ \to WZ$ and $W\gamma \to WZ$

We give expressions for the cross-sections for $WZ \to WZ$ and $W\gamma \to WZ$ in the high-energy approximation. For this purpose, we define the quantities G_{pol}, which are the squared helicity amplitudes integrated over the scattering angle $\cos\theta$,

$$G_{pol} \equiv \frac{1}{g^4} \int\limits_{-z_0}^{z_0} |\mathcal{M}_{pol}(\cos\theta)|^2 \, d\cos\theta, \tag{B.1}$$

where $g = e/s_W$ is the weak coupling constant and z_0 is an integration limit for $|\cos\theta|$. The indices pol denote the helicities of the particles $WV \to WZ$ (in this order) and $\mathcal{M}_{pol}$ is the scattering-amplitude. We further define the sums over the transverse helicity amplitudes,

$$\begin{aligned}
G^T_{++} &\equiv G_{++++,\text{leading}} + G_{+++-} + G_{++-+} + G_{++--}, \\
G^T_{+-} &\equiv G_{+--+,\text{leading}} + G_{+-+-} + G_{+-++} + G_{+----}.
\end{aligned} \tag{B.2}$$

The cross-sections for $WZ \to WZ$ are obtained in terms of the G_{pol} by the expressions,

$$\begin{aligned}
\sigma_{TT} &\equiv \frac{1}{2}(\sigma_{++} + \sigma_{+-}) \\
\sigma_{\overline{TT}} &\equiv \frac{1}{2}(\sigma_{++} - \sigma_{+-}),
\end{aligned} \tag{B.3}$$

with

$$\begin{aligned}
\sigma_{++} &= \frac{g^4}{32\pi s}\Big(G^T_{++} + G_{++++,\text{non-leading}} + G_{++00} \\
&\quad + G_{+++0} + G_{++-0} + G_{++0+} + G_{++0-}\Big) \\
\sigma_{+-} &= \frac{g^4}{32\pi s}\Big(G^T_{+-} + G_{+--+,\text{non-leading}} + G_{+-00} \\
&\quad + G_{+-+0} + G_{+--0} + G_{+-0+} + G_{+-0-}\Big), \\
\sigma_{TL} &= \frac{g^4}{32\pi s}\Big(G_{+00+} + G_{+00-} + G_{+0+0} + G_{+0-0} \\
&\quad + G_{+0++} + G_{+0+-} + G_{+0--} + G_{+0-+} + G_{+000}\Big) \\
\sigma_{LT} &= \frac{g^4}{32\pi s}\Big(G_{0++0} + G_{0+-0} + G_{0+0+} + G_{0+0-} \\
&\quad + G_{0+++} + G_{0++-} + G_{0+-+} + G_{0+--} + G_{0+00}\Big)
\end{aligned}$$

$$\sigma_{LL} = \frac{g^4}{32\pi s}\left(G_{0000} + 2G_{00++} + 2G_{00+-} + 2G_{000+} + 2G_{00+0}\right), \tag{B.4}$$

where s is the square of the scattering energy. Similarly, the cross-sections for $W\gamma \to WZ$ are obtained in terms of the corresponding G_{pol} by the relations

$$\sigma_{TT} \equiv \frac{1}{2}(\sigma_{++} + \sigma_{+-}) \tag{B.5}$$

with

$$
\begin{aligned}
\sigma_{++} &= \frac{g^4}{32\pi s}\frac{q}{p}\Big(G^T_{++} + G_{++++,\text{non-leading}} + G_{++00} \\
&\qquad + G_{+++0} + G_{++-0} + G_{++0+} + G_{++0-}\Big) \\
\sigma_{+-} &= \frac{g^4}{32\pi s}\frac{q}{p}\Big(G^T_{+-} + G_{+--+,\text{non-leading}} + G_{+-00} \\
&\qquad + G_{+-+0} + G_{+--0} + G_{+-0+} + G_{+-0-}\Big) \\
\sigma_{LT} &= \frac{g^4}{32\pi s}\frac{q}{p}\Big(G_{0++0} + G_{0+-0} + G_{0+0+} + G_{0+0-} \\
&\qquad + G_{0+++} + G_{0++-} + G_{0+-+} + G_{0+--} + G_{0+00}\Big). \tag{B.6}
\end{aligned}
$$

In (B.6), p and q are the magnitudes of the three-momenta of the vector-bosons in the initial and in the final state, respectively, evaluated in the center-of-mass system of the vector-bosons. They are given by

$$
\begin{aligned}
p &= \frac{\sqrt{s}}{2}\left(1 - \frac{M_W^2}{s}\right), \\
q &= \frac{\sqrt{s}}{2}\sqrt{1 - \frac{2}{s}(M_W^2 + M_Z^2) + \frac{1}{s^2}(M_W^2 - M_Z^2)^2}\ . \tag{B.7}
\end{aligned}
$$

Note that a cross-section $\sigma_{\overline{TT}}$ for the photon-process does not appear in our calculations. The reason is that the corresponding luminosity vanishes as the photon has no axial-vector coupling.

B.1 Formulae for $WZ \to WZ$

For the process $WZ \to WZ$ there are 25 different helicity amplitudes $\mathcal{M}_{pol}$, which can not be related to each other by discrete symmetries. Of these amplitudes, 15 have leading terms of the order $\mathcal{O}(s/4M_W^2)^0$, $\mathcal{O}(a_i)$ or $\mathcal{O}(a_i a_j)$,

$$a_i \equiv \frac{s}{4M_W^2}\epsilon_i, \tag{B.8}$$

$i, j = W, W\Phi, B\Phi$. Of these 15 terms, 6 only appear in the sums G^T_{++} and G^T_{+-}. In the following, we use the abbreviations

$$f_1 \equiv \frac{1}{1 - z_0^2}, \qquad \ln_1 \equiv \ln\left(\frac{1 + z_0}{1 - z_0}\right), \qquad r_H \equiv \frac{M_H^2}{M_W^2}, \tag{B.9}$$

and $t_W \equiv s_W/c_W$.

For a Higgs boson mass which is small against the scattering energy, $M_H^2 \ll s$, the expressions for the integrated squared amplitudes are given by

$$
\begin{aligned}
G_{++}^T &= 2c_W^4 \Big[16z_0 f_1 - 8a_W^2 (2\ln_1 - 7z_0 - z_0^3) - 8a_W^3 (3z_0 - \frac{7}{3}z_0^3) \\
&\quad + a_W^4 (9z_0 + \frac{46}{3}z_0^3 + \frac{z_0^5}{5}) \Big] \\
G_{+-}^T &= 2c_W^4 \Big[16z_0 f_1 - 16\ln_1 + 18z_0 + \frac{2}{3}z_0^3 + 2a_W^2 (7z_0 + \frac{5}{3}z_0^3) \\
&\quad + a_W^4 (9z_0 - \frac{2}{3}z_0^3 + \frac{z_0^5}{5}) \Big] \\
G_{\substack{++00 \\ 00++}} &= 2(a_{W\Phi} + a_{B\Phi})^2 s_W^2 t_W^2 z_0 + 2c_W^2 a_W^2 (1 - 4a_{W\Phi})^2 \frac{z_0^3}{3} \\
G_{\substack{+-00 \\ 00+-}} &= \frac{s_W^2 t_W^2}{2}(z_0 + \frac{z_0^3}{3t_W^4}) \\
G_{0+0+} &= \frac{c_W^4}{2}(1 - t_W^2)^4 z_0 \\
G_{0+0-} &= 2(1 - 2s_W^2)^2 (a_{W\Phi} - t_W^2 a_{B\Phi})^2 (z_0 + \frac{z_0^3}{3}) \\
G_{\substack{+00+ \\ 0++0}} &= 8c_W^2 z_0 f_1 - 2(1 - 2s_W^2)\ln_1 + \frac{z_0}{2c_W^2}(1 - 2s_W^2)^2 \\
G_{\substack{+00- \\ 0+-0}} &= \frac{c_W^2}{2}z_0 \Big((a_{W\Phi} + a_{B\Phi})t_W^2 - 3a_W - 6a_{W\Phi}a_W \Big)^2 \\
&\quad + \frac{z_0^3}{6}c_W^2 \Big[\Big((a_{W\Phi} + a_{B\Phi})t_W^2 + a_W - 4a_{W\Phi}a_W \Big)^2 \\
&\quad + 4 \Big((a_{W\Phi} + a_{B\Phi})t_W^2 - 3a_W - 6a_{W\Phi}a_W \Big) a_{W\Phi}a_W \Big] \\
&\quad + \frac{2}{5}z_0^5 a_{W\Phi}^2 a_W^2 c_W^2 \\
G_{+0+0} &= \frac{1}{2}z_0 \\
G_{+0-0} &= 2a_{W\Phi}^2 \Big(z_0 + \frac{z_0^3}{3} \Big) \\
G_{0000} &= 2z_0 f_1 - \frac{1}{2}\ln_1 (2 - r_H) + \frac{1}{8}z_0(9 - 2r_H + r_H^2) + \frac{1}{24}z_0^3 \\
&\quad + a_{W\Phi}(12\ln_1 - 15z_0 + 3r_H z_0 - z_0^3) \\
&\quad + a_{W\Phi}^2 \Big(-8\ln_1 + 43z_0 + 3r_H z_0 + \frac{z_0^3}{3}(25 - r_H) \Big) \\
&\quad + a_{W\Phi}^3 (36z_0 - 28z_0^3) \\
&\quad + a_{W\Phi}^4 (18z_0 + 20z_0^3 + 2\frac{z_0^5}{5}).
\end{aligned}
\tag{B.10}
$$

The non-leading terms for G_{++++} and G_{+--+} are given by

$$
\begin{aligned}
G_{++++,\text{non-leading}} &= 8c_W^2 \mu_W \Big[a_{W\Phi} \Big(8z_0 f_1 (2 - s_W^2) + t_W^2 (1 - 2s_W^2)\ln_1 \Big) \\
&\quad + a_{B\Phi} \Big(-8z_0 f_1 s_W^2 + t_W^2 (1 - 2s_W^2)\ln_1 \Big) \\
&\quad + a_W \Big((5 - 2s_W^2)\ln_1 - 2z_0(3 - s_W^2) \Big) \\
&\quad + s_W^2 t_W^2 (a_{W\Phi} + a_{B\Phi})^2 \ln_1 \\
&\quad + a_W(\ln_1 - 2z_0) \Big(a_W(3 - s_W^2) - 2a_{W\Phi}(2 - s_W^2) + 2a_{B\Phi}s_W^2 \Big) \Big]
\end{aligned}
$$

$$G_{+--+,\text{non-leading}} = 2c_W^2\mu_W\left\{2(16z_0f_1 - 16\ln_1 + 17z_0 + \frac{z_0^3}{3}) \cdot [a_{W\Phi}(2 - s_W^2) - a_{B\Phi}s_W^2]\right.$$

$$-(8\ln_1 - 14z_0 - \frac{2}{3}z_0^3)$$

$$\left.\cdot\left[2a_{W\Phi}(a_{W\Phi} + t_W^2 a_{B\Phi}) + \frac{1}{2}a_{W\Phi}\left(1 + \frac{1}{c_W^2}\right) + \frac{1}{2}t_W^2 a_{B\Phi}\right]\right\}, \quad (B.11)$$

where we introduced the variable

$$\mu_W \equiv \frac{4M_W^2}{s}. \quad (B.12)$$

Concerning the amplitudes which receive no leading contributions, the terms which are quartic in the couplings are given by

$$G_{\substack{+++0 \\ +0++}} = 4\mu_W c_W^2 a_W^2 (2a_{W\Phi} + a_W)^2 \left(z_0 - \frac{z_0^3}{3}\right)$$

$$G_{\substack{++-0 \\ +0--}} = \mu_W c_W^2 a_W^2 (a_{W\Phi} + a_W)^2 \left(9z_0 - \frac{8}{3}z_0^3 - \frac{z_0^5}{5}\right)$$

$$G_{\substack{++0+ \\ 0+++}} = 4\mu_W a_W^2 \left(c_W^2(a_{W\Phi} - t_W^2 a_{B\Phi}) + a_{W\Phi} + c_W^2 a_W\right)^2 \cdot \left(z_0 - \frac{z_0^3}{3}\right)$$

$$G_{\substack{++0- \\ 0+--}} = \mu_W a_W^2 (a_{W\Phi} + c_W^2 a_W)^2 \left(9z_0 - \frac{8}{3}z_0^3 - \frac{z_0^5}{5}\right)$$

$$G_{\substack{+--+0 \\ +0+-}} = \mu_W c_W^2 a_W^2 \left[(a_{W\Phi}^2 + a_W^2)\left(z_0 - \frac{z_0^5}{5}\right)\right.$$

$$\left.-2a_{W\Phi}a_W\left(z_0 - \frac{2}{3}z_0^3 + \frac{z_0^5}{5}\right)\right]$$

$$G_{\substack{+--0 \\ +0-+}} = 0$$
$$G_{\substack{+-0+ \\ 0++-}} = 0$$

$$G_{\substack{+-0- \\ 0+-+}} = \mu_W a_W^2 \left[4c_W^4(a_{W\Phi} - t_W^2 a_{B\Phi})^2 \left(z_0 - \frac{z_0^3}{3}\right)\right.$$

$$+(a_{W\Phi} + c_W^2 a_W)^2 \left(z_0 - \frac{z_0^5}{5}\right)$$

$$\left.-4c_W^2(a_{W\Phi} - t_W^2 a_{B\Phi})(a_{W\Phi} + c_W^2 a_W)\left(z_0 - \frac{z_0^3}{3}\right)\right]$$

$$G_{\substack{+000 \\ 00+0}} = \mu_W a_{W\Phi}^2 (a_W + a_{W\Phi})^2 \left(9z_0 - \frac{8}{3}z_0^3 - \frac{z_0^5}{5}\right)$$

$$G_{\substack{0+00 \\ 000+}} = \mu_W \frac{1}{c_W^2} a_{W\Phi}^2 (a_{W\Phi} + c_W^2 a_W)^2 \left(9z_0 - \frac{8}{3}z_0^3 - \frac{z_0^5}{5}\right). \quad (B.13)$$

B.2 Formulae for $W\gamma \to WZ$

For $W\gamma \to WZ$ there are 27 different amplitudes, out of which 14 have terms of the leading order $\mathcal{O}(s/M_W^2)^0$. Of these amplitudes, 8 only appear in the sums of the transverse amplitudes G_{++}^T and G_{+-}^T. Expressions for G_{++}^T and G_{+-}^T are obtained from the corresponding expressions for $WZ \to WZ$ by multiplication with the factor t_W^2. For the remaining polarizations, the integrated squared amplitudes are given by the expressions,

$$G_{++00} = 2s_W^2 \left(a_W^2(1 - 4a_{W\Phi}^2)\frac{z_0^3}{3} + (a_{W\Phi} + a_{B\Phi})^2 z_0\right)$$

$$G_{+-00} = \frac{s_W^2}{2}\left(z_0 + \frac{z_0^3}{3}\right)$$

$$G_{0+0+} = 2t_W^2(1 - 2s_W^2)^2 z_0$$

$$G_{0+0-} = 2t_W^2\left[a_{W\Phi}(\frac{3}{2} - 2s_W^2) + a_{B\Phi}(\frac{1}{2} - 2s_W^2)\right]^2\left(z_0 + \frac{z_0^3}{3}\right)$$

$$G_{0++0} = 2s_W^2\left(4z_0f_1 - 2\ln_1 + z_0\right)$$

$$\begin{aligned}
G_{0+-0} = \frac{s_W^2}{2}\Bigg[&(a_{W\Phi} + a_{B\Phi})^2\left(z_0 + \frac{z_0^3}{3}\right) + a_W^2\left(9z_0 + \frac{z_0^3}{3}\right)\\
&+(a_{W\Phi} + a_{B\Phi})a_W\left(6z_0 - \frac{2}{3}z_0^3\right)\\
&+2a_{W\Phi}a_W(a_{W\Phi} + a_{B\Phi})\left(6z_0 + \frac{2}{3}z_0^3\right)\\
&+2a_{W\Phi}a_W^2\left(18z_0 - \frac{10}{3}z_0^3\right)\\
&+2a_{W\Phi}^2a_W^2\left(18z_0 - \frac{4}{3}z_0^3 + \frac{2}{5}z_0^5\right)\Bigg].
\end{aligned} \tag{B.14}$$

The non-leading terms for G_{++++} und G_{+--+} have the following expressions,

$$\begin{aligned}
&G_{++++,\text{non-leading}}\\
= 8s_W^2\mu_W\Bigg[&a_{W\Phi}\left(4z_0f_1(3 - 2s_W^2) - \ln_1\left(\frac{1}{2} - 2s_W^2\right)\right)\\
&+a_{B\Phi}\left(4z_0f_1(1 - 2s_W^2) - \ln_1\left(\frac{1}{2} - 2s_W^2\right)\right)\\
&+a_W\left(\ln_1\left(\frac{7}{2} - 2s_W^2\right) - 2z_0(2 - s_W^2)\right)\\
&-s_W^2\ln_1(a_{W\Phi} + a_{B\Phi})^2\\
&+(\ln_1 - 2z_0)a_W\left(a_W(2 - s_W^2) - a_{W\Phi}(3 - 2s_W^2) - a_{B\Phi}(1 - 2s_W^2)\right)\Bigg]
\end{aligned}$$

$$\begin{aligned}
&G_{+--+,\text{non-leading}}\\
= 2s_W^2\mu_W\Bigg\{&a_{W\Phi}\Big[16z_0f_1(3 - 2s_W^2) - \ln_1(50 - 32s_W^2)\\
&+\frac{z_0}{2}(109 - 68s_W^2) + \frac{z_0^3}{3}(7 - 4s_W^2)\Big]\\
&+a_{B\Phi}\Big[32z_0f_1c_W^2 - \ln_1(22 - 32s_W^2)\\
&+\frac{z_0}{2}(35 - 68s_W^2) + \frac{z_0^3}{6}(1 - 4s_W^2)\Big]\\
&+a_{W\Phi}(a_{W\Phi} + a_{B\Phi})\left(8\ln_1 - 14z_0 - \frac{2}{3}z_0^3\right)\Bigg\}.
\end{aligned} \tag{B.15}$$

The amplitudes without leading contributions have the terms quartic in the couplings,

$$G_{+++0} = 4s_W^2\mu_W a_W^2(2a_{W\Phi} - a_W)^2\left(z_0 - \frac{z_0^3}{3}\right)$$

$$G_{++-0} = s_W^2\mu_W a_W^2(a_{W\Phi} + a_W)^2\left(9z_0 - \frac{8}{3}z_0^3 - \frac{z_0^5}{5}\right)$$

$$G_{++0+} = 4t_W^2\mu_W a_W^2\left[a_{W\Phi} + c_W^2a_W + c_W^2(a_{W\Phi} - t_W^2a_{B\Phi})\right]^2\left(z_0 - \frac{z_0^3}{3}\right)$$

$$G_{++0-} = t_W^2\mu_W a_W^2\left[c_W^4a_W^2\left(9z_0 - \frac{8}{3}z_0^3 - \frac{z_0^5}{5}\right)\right.$$

$$+12c_W^2 a_W (a_{W\Phi} - a_{B\Phi}) \left(z_0 - \frac{z_0^3}{3} \right)$$

$$+4(a_{W\Phi} - a_{B\Phi})^2 \left(z_0 - \frac{z_0^3}{3} \right) \Big]$$

$$G_{+-+0} = s_W^2 \mu_W a_W^2 \left[a_W^2 \left(z_0 - \frac{z_0^3}{3} \right) - 2 a_W a_{W\Phi} \left(z_0 - \frac{z_0^3}{3} \right) + a_{W\Phi}^2 \left(z_0 - \frac{z_0^5}{5} \right) \right]$$

$$G_{+--0} = 0$$

$$G_{+-0+} = 0$$

$$G_{+-0-} = s_W^2 c_W^2 \mu_W a_W^2 \left[a_W^2 \left(z_0 - \frac{z_0^5}{5} \right) - 4 a_W (a_{W\Phi} + a_{B\Phi}) \left(z_0 - \frac{z_0^3}{3} \right) \right.$$

$$\left. +4(a_{W\Phi} + a_{B\Phi})^2 \left(z_0 - \frac{z_0^3}{3} \right) \right]$$

$$G_{0+++} = 4 s_W^2 c_W^2 \mu_W a_W^2 (a_{W\Phi} + a_{B\Phi} + a_W)^2 \left(z_0 - \frac{z_0^3}{3} \right)$$

$$G_{0++-} = 0$$

$$G_{0+-+} = \mu_W t_W^2 a_W^2 \left[(a_{W\Phi} + c_W^2 a_W)^2 \left(z_0 - \frac{z_0^5}{5} \right) \right.$$

$$-4(a_{W\Phi} + c_W^2 a_W) c_W^2 (a_{W\Phi} - t_W^2 a_{B\Phi}) \left(z_0 - \frac{z_0^3}{3} \right)$$

$$\left. +4 c_W^2 (a_{W\Phi} - t_W^2 a_{B\Phi})^2 \left(z_0 - \frac{z_0^3}{3} \right) \right]$$

$$G_{0+--} = \mu_W t_W^2 a_W^2 \left[4(a_{B\Phi} + c_W^2 a_W)^2 \left(z_0 - \frac{z_0^3}{3} \right) \right.$$

$$\left. +4(a_{W\Phi} + c_W^2 a_W)(a_{B\Phi} + c_W^2 a_W) \left(z_0 - \frac{z_0^3}{3} \right) \right]$$

$$G_{0+00} = \mu_W s_W^2 a_{W\Phi}^2 a_W^2 \left(9 z_0 - \frac{8}{3} z_0^3 - \frac{2}{5} z_0^5 \right). \tag{B.16}$$

Bibliography

[1] S. L. Glashow, Nucl. Phys. **22**, 579 (1961);
S. Weinberg, Phys. Rev. Lett. **19**, 1364 (1967);
A. Salam, Proceedings of the 8th Nobel Symposium, p. 367, Stockholm (1968)

[2] P. W. Higgs, Phys. Lett. **12**, 132 (1964); Phys. Rev. Lett. **13**, 508 (1964); Phys. Rev. **145**, 1156 (1966)

[3] The UA2 collaboration: M. Banner et. al., Phys. Lett. **B122**, 476 (1983); P. Bagnaia et. al., Phys. Lett. **B129**, 130 (1983)

[4] The UA1 collaboration, G. Arnison et. al., Phys. Lett. **B122**, 103 (1983); Phys. Lett. **B126**, 398 (1983)

[5] The LEP collaborations and the LEP Electroweak Working Group, CERN/PPE/94-187, Nov. 1994, contributed to the 27th International Conference on High-Energy Physics, ICHEP 94, Glasgow, Scotland, UK, 20-27 Jul 1994

[6] T. Usher, representing the SLD collaboration, SLAC-PUB-95-6963, Oct. 1995, presented at the 9th Les Rencontres de Physique de la Valle d'Aoste: Results and Perspectives in Particle Physics, La Thuile, Italy, 5-11 Mar 1995

[7] The CDF-collaboration, F. Abe et. al., Phys. Rev. **D50**, 2966 (1994); Phys. Rev. Lett. **73**, 225 (1994)

[8] The CDF-collaboration, F. Abe et. al., Phys. Rev. Lett. **75**, 1017 (1995); Phys. Rev. Lett. **74**, 1941 (1995)

[9] The D0-collaboration, S. Abachi et. al., Phys. Rev. Lett. **75**, 1023, 1028 and 1034 (1995)

[10] M. Bilenky, J. L. Kneur, F. M. Renard and D. Schildknecht, Nucl. Phys. **B409**, 22 (1993);
P. Kalyniak, P. Madsen, N. Sinha and R. Sinha, Phys. Rev. **D48**, 5081 (1993);
C. G. Papadopoulos, Phys. Lett. **B333**, 202 (1994);
R. L. Sekulin, Phys. Lett. **B338**, 369 (1994)

[11] H. Aihara et. al., Summary of the Working Subgroup on Anomalous Gauge Boson Interactions of the DPF Long-Range Planning Study, to be published in "Electroweak Symmetry Breaking and Beyond the Standard Model", Editors T. Barklow, S. Dawson, H. Haber and J. Siegrist, LBL-37155, hep-ph/9503425, March 1995

[12] Proceedings of the European Committee for Future Accelerators (ECFA), ECFA 90-133, CERN 90-10 (1990), Editors: G. Jarlskog and D. Rein, Large Hadron Collider Workshop, Aachen, 4-9 Oct, 1990

[13] W. J. Stirling, R. Kleiss and S. D. Ellis, Phys. Lett. **B163**, 261 (1985);
J. Gunion, Z. Kunszt and M. Soldate, Phys. Lett. **B163**, 389 (1985);
J. Gunion and M. Soldate, Phys. Rev. **D34**, 826 (1986)

[14] F. Cavanna, D. Denegri and T. Rodrigo in [12], Vol. II, p. 329

[15] H. Kuijf et. al. in [12], Vol. II, p. 91

[16] R. W. Brown and K. Mikaelian, Phys. Rev. **D19**, 922 (1979);
R. W. Brown, D. Sahdev and K. Mikaelian, Phys. Rev. **D20**, 1164 (1979)

[17] E. Eichten et. al., Rev. Mod. Phys. **56**, 579 (1984)

[18] J. Cortes, K. Hagiwara and F. Herzog, Nucl. Phys. **B278**, 26 (1986)

[19] M. Kuroda, J. Maalampi, D. Schildknecht and K. H. Schwarzer, Nucl. Phys. **B284**, 271 (1987)

[20] D. Zeppenfeld and S. Willenbrock, Phys. Rev. **D37**, 1775 (1988)

[21] U. Baur, D. Zeppenfeld, Nucl. Phys. **308**, 127 (1988)

[22] G. L. Kane, J. Vidal and C. P. Yuan, Phys. Rev. **D39**, 2617 (1989)

[23] U. Baur and E. L. Berger, Phys. Rev. **D41**, 1476 (1990)

[24] A. Falk, M. Luke and E. H. Simmons, Nucl. Phys. **B365**, 523 (1991)

[25] J. Ohnemus, Phys. Rev. **D44**, 3477 (1991); Phys. Rev. **D50**, 1931 (1994)

[26] S. Frixione, Nucl. Phys. **B410**, 280 (1993)

[27] U. Baur, T. Han and J. Ohnemus, Phys. Rev. **D51**, 3389 (1995)

[28] K. R. Barger and M. H. Reno, Phys. Rev. **D51**, 90 (1995)

[29] U. Baur, T. Han and J. Ohnemus, Phys. Rev. **D53**, 1098 (1996)

[30] B. W. Lee, C. Quigg and H. Thacker, Phys. Rev. **D16**, 1519 (1977);
M. Veltman, Acta Phys. Pol. **B8**, 475 (1977)

[31] S. Dawson, Nucl. Phys. **B249**, 42 (1985)

[32] G. L. Kane, W. W. Repko and W. B. Rolnick, Phys. Lett. **B148**, 367 (1984)

[33] J. Lindfors, Z. Phys. **C28**, 427 (1985)

[34] E. Fermi, Z. Phys. **29**, 315 (1924);
C. F. von Weizsäcker, Z. Phys. **88**, 612 (1934);
E. Williams, Phys. Rev. **45**, 729 (1934)

[35] M. S. Chanowitz and M. K. Gaillard, Nucl. Phys. **B261**, 379 (1985)

[36] A. Dobado, M. Herrero and J. Terron, Z. Phys. **C50**, 465 (1991)

[37] J. Bagger, V. Barger, K. Cheung, J. Gunion, T. Han, G. A. Ladinsky, R. Rosenfeld and C.-P. Yuan, Phys. Rev. **D49**, 1246 (1994) and Phys. Rev. **D52** 3878 (1995)

[38] S. Gupta, J. Johnson, G. Ladinsky and W. W. Repko, Phys. Rev. **D53**, 4897 (1996)

[39] J. Bagger, S. Dawson and G. Valencia, Nucl. Phys. **B399**, 364 (1993)

[40] G. J. Gounaris and F. M. Renard, Z. Phys. **C59**, 143 (1993), err. p. 682

[41] G. J. Gounaris, J. Layssac and F. M. Renard, Z. Phys. **C62**, 139 (1994)

[42] W. A. Bardeen, R. Gastmans and B. Lautrup, Nucl. Phys. **B46**, 319 (1972);
K. J. F. Gaemers and G. J. Gounaris, Z. Phys. **C1**, 259 (1979)

[43] T. Appelquist and C. Bernard, Phys. Rev. **D22**, 200 (1980);
A. Longhitano, Nucl. Phys. **B188**, 118 (1981)

[44] W. Buchmüller and D. Wyler, Nucl. Phys. **B268**, 621 (1986);
C. N. Leung, S. T. Love and S. Rao, Z. Phys. **C31**, 433 (1986)

[45] M. Kuroda, F. M. Renard and D. Schildknecht, Phys. Lett. **B183**, 366 (1987)

[46] J. Maalampi, D. Schildknecht and K. H. Schwarzer, Phys. Lett. **B166**, 361 (1986)

[47] K. Hagiwara, R. Peccei, D. Zeppenfeld and K. Hikasa, Nucl. Phys. **B282**, 253 (1987)

[48] A. de Rújula, M. B. Gavela, P. Hernandez and E. Massó, Nucl. Phys. **B384**, 3 (1992)

[49] K. Hagiwara, S. Ishihara, R. Szalapski and D. Zeppenfeld, Phys. Lett. **B283**, 353 (1992) and Phys. Rev. **D48**, 2182 (1993)

[50] J.-M. Frère, J. M. Moreno, J. Orloff and M. Tytgat, Phys. Lett. **B292**, 348 (1992)

[51] G. J. Gounaris and F. M. Renard, Z. Phys. **C59**, 133 (1993)

[52] C. Grosse-Knetter, I. Kuss and D. Schildknecht, Z. Phys. **C60**, 375 (1993); Phys. Lett. **B358**, 87 (1995)

[53] C. Grosse-Knetter, Phys. Rev. **D49**, 6709 (1994)

[54] E.C.G. Stueckelberg, Helv. Phys. Acta **11**, 299 (1938);
T. Kunimasa and T. Goto, Prog. Theor. Phys. **37**, 452 (1967);
T. Sonoda and S.Y.Tsai, Prog. Theor. Phys. **71**, 878 (1984)

[55] C. Grosse-Knetter and R. Kögerler, Phys. Rev. **D48**, 2865 (1993)

[56] I. Kuss, Diploma Thesis, Universität Bielefeld, Nov 1993 and Phys. Rev. **D50**, 6713 (1994)

[57] R. P. Feynman, "Photon-Hadron Interactions", Benjamin, Reading, Mass. (1972)

[58] M. Böhm, A. Denner, T. Sack, W. Beenakker, F. A. Berends and H. Kuijf, Nucl. Phys. **B304**, 463 (1988);
J. Fleischer, F. Jegerlehner and M. Zrałek, Z. Phys. **C42**, 409 (1989)

[59] W. Beenakker, A. Denner, S. Dittmaier, R. Mertig and T. Sack, Nucl. Phys. **B410**, 245 (1993);
W. Beenakker, A. Denner, S. Dittmaier and R. Mertig, Phys. Lett. **B317**, 622 (1993)

[60] H. Spiesberger, Phys. Rev. **D52**, 4936 (1995)

[61] I. Kuss and H. Spiesberger, Phys. Rev. **D53**, 6078 (1996)

[62] G. L. Kane, Proceedings of the Conference "Physics of the XXIst century", Tucson, Arizona, Dec. 1983.

[63] A. Dobrovolskaia and V. Novikov, preprint LPTHE 93/14 (April 1993)

[64] G. Bonneau, M. Gourdin and F. Martin, Nucl. Phys. **B54**, 573 (1973);
G. Bonneau and F. Martin, Nucl. Phys. **B68**, 367 (1974)

[65] P. W. Johnson, F. I. Olness, and W.-K. Tung, Proc. of the 1986 Summer Study on Physics of the Superconducting Super Collider, Snowmass, CO, Jun 23 – Jul 11, 1986, p. 164;
P. W. Johnson, F. I. Olness, and W.-K. Tung, Phys. Rev. **D36**, 291 (1987)

[66] A. Abbasabadi, W. W. Repko, D. Dicus and R. Vega, Phys. Rev. **D38**, 2770 (1988);
A. Abbasabadi and W. W. Repko, Phys. Rev. **D36**, 289 (1987)

[67] R. M. Godbole and S. D. Rindani, Phys. Lett. **B190**, 192 (1987); Z. Phys. **C36**, 395 (1987)

[68] M. Capdequi Peyranére, J. Layssac, H. Leveque, G. Moultaka and F. M. Renard, Z. Phys. **C41**, 99 (1988)

[69] J. Lindfors, Z. Phys. **C35**, 355 (1987)

[70] M. Kuroda, F. M. Renard and D. Schildknecht, Z. Phys. **C40**, 575 (1988)

[71] M. J. Duncan, G. L. Kane, and W. W. Repko, Nucl. Phys. **B272**, 517 (1986);
A. Abbasabadi and W. Repko, Proc. of the 1986 Summer Study on Physics of the Superconducting Super Collider, Snowmass, CO, Jun 23 – Jul 11, 1986, p. 154;
M. C. Bento and C.-H. Llewellyn-Smith, Nucl. Phys. **B289**, 36 (1987)

[72] M. Chanowitz and M. K. Gaillard, Phys. Lett. **B142**, 85 (1984)

[73] A. Abbasabadi and W. W. Repko, Phys. Rev. **D50**, 5704 (1994);
B. Mele, Proc. of the Workshop on Physics at Future Accelerators, La Thuile and Geneva (1987), CERN 87-07

[74] S. Willenbrock and D. A. Dicus, Phys. Rev. **D34**, 155 (1986);
J. Lindfors, Z. Phys. **C33**, 385 (1987);
S. Dawson, G. L. Kane, C. P. Yuan and S. Willenbrock, Proc. of the 1986 Summer Study on Physics of the Superconducting Super Collider, Snowmass, CO, Jun 23 –

Jul 11, 1986, p. 235;
S. Dawson and S. Willenbrock, Nucl. Phys. **B284**, 449 (1987);
R. P. Kauffman, Phys. Rev. **D41**, 3343 (1990)

[75] R. Cahn, Nucl. Phys. **B255**, 341 (1985); Err. ibid. **B262**, 744 (1985);
J. F. Gunion, J. Kalinowski, A. Tofighi-Niaki, A. Abbasabadi, and W. Repko, Proc.
of the 1986 Summer Study on Physics of the Superconducting Super Collider, Snow-
mass, CO, Jun 23 – Jul 11, 1986, p. 156;
W. W. Repko and W.-K. Tung, ibid. p. 159;
J. P. Ralston and F. Olness, ibid. p. 191
D. A. Dicus and R. Vega, Phys. Rev. Lett. **57**, 1110 (1986);
G. Altarelli, B. Mele, F. Pitalli, Nucl. Phys. **B287**, 205 (1987);
D. A. Dicus, K. J. Kallianpur and S. D. Willenbrock, Phys. Lett. **B200**, 187 (1988)

[76] J. F. Gunion, J. Kalinowski and A. Tofighi-Niaki, Phys. Rev. Lett. **57**, 2351 (1986)

[77] A. Dicus, S. Wilson and R. Vega, Phys. Lett. **B192**, 231 (1987)

[78] R. M. Godbole and F. Olness, Int. J. Mod. Phys. **A2**, 1025 (1987)

[79] V. M. Budnev, I. F. Ginzburg, G. V. Meledin and V. G. Serbo, Phys. Rep. **15C**, 183
(1974);
N. S. Craigie, K. Hidaka, M. Jacob and F. M. Renard, Phys. Rep. **99**, 69 (1983)

[80] S. Cortese and R. Petronzio, Phys. Lett. **B276**, 203 (1992)

[81] Z. Kunszt and D. E. Soper, Nucl. Phys. **B296**, 253 (1988)

[82] A. D. Martin, R. G. Roberts and W. J. Stirling, Phys. Rev. **D50**, 6734 (1994)

[83] M. Glück, M. Stratmann and W. Vogelsang, Phys. Lett. **B343**, 399 (1995)

[84] U. Baur and E. Glover, Nucl. Phys. **B347**, 12 (1990)

[85] D. Duke and J. Owens, Phys. Rev. **D30**, 49 (1984)

[86] A. Abbasabadi and W. W. Repko, Phys. Rev. **D37**, 2668 (1988)

[87] U. Baur, T. Han and J. Ohnemus, Phys. Rev. Lett. **72**, 3941 (1994)

[88] G. J. Gounaris, J. Layssac, J. E. Paschalis and F. M. Renard, Z. Phys. **C66**, 619
(1995)

[89] G. J. Gounaris, J. Layssac and F. M. Renard, Phys. Lett. **B332**, 146 (1994)

[90] C. Bourrely, J. Soffer and P. Taxil, Phys. Rev. **D36**, 3373 (1987)

[91] A. D. Martin, R. G. Roberts and W. J. Stirling, Phys. Lett. **B306**, 145 (1993)

[92] The Particle Data Group, Phys. Rev. **D50**, 1173 (1994)

[93] K. Charchuła, Comp. Phys. Commun. **69**, 360 (1992)

[94] M. Jacob and G. C. Wick, Annals of Physics **7**, 404 (1959)

Lebenslauf

<u>Ingolf</u> Karl Kuss

14.09.1967	geboren in Osnabrück als Sohn von Richter am Amtsgericht Helmut Kuss und seiner Frau Magdalene, geb. Schierbaum
ab 1980	Besuch des Ratsgymnasiums Osnabrück
Mai 1987	Abitur mit den Leistungsfächern Mathematik und Physik, (Durchschnittsnote 1.2)
1987/88	Grundwehrdienst
1988-90	Studium der Physik an der Universität Osnabrück
9.8.1990	Diplomvorprüfung in Physik (Gesamtnote:,,sehr gut")
August 1990 bis August 1991	Studium der Physik an der Case Western Reserve University in Cleveland, Ohio, USA als Stipendiat der Fulbright-Stiftung; graduate studies in physics, Beteiligung an einem Forschungsprojekt bei Prof. Dr. R. W. Brown
22.8.1991	Master of Science in Physics, (Notendurchschnitt: 4.0 = ,,perfect")
Oktober 1991	Fortsetzung des Studiums der Physik an der Universität Osnabrück, Studiengang Diplom Physik
März 1992	Fortsetzung des Physikstudiums an der Universität Bielefeld, Diplomarbeit auf dem Gebiet der Elektroschwachen Wechselwirkungen der Elementarteilchen
15.11.1993	Diplom in Physik (Gesamtnote:,,ausgezeichnet")
seit 22.11.1993	Arbeit auf dem Gebiet der elektroschwachen Wechselwirkungen der Elementarteilchen an der Universität Bielefeld mit dem Ziel der Promotion, Stipendiat der Landesgraduiertenförderung des Landes Nordrhein-Westfalen (1.9.94 bis 31.12.95)
1.7.1996	Disputation und Bewertung der Promotion mit der Gesamtnote: ,,sehr gut"